THE UNIVERSITY
of EDINBURGH

Characterisation of macrophage iron metabolism in Interstitial Lung Disease.

Cecilia Isotta Boz

A thesis submitted for the degree of

Doctor of Philosophy

The University of Edinburgh

Centre of Inflammation Research

2022

Declaration

I declare that this thesis has been composed solely by myself and that it has not been submitted, in whole or in part, in any previous application for a degree. Except where states otherwise by reference or acknowledgment, the work prese ted is entirely my own.

Dedicated to Nonna Bianca

Acknowledgements

I would like to firstly thank my supervisors, Dr Nik Hirani, Prof Marc Vendrell and Dr Alison Mackinnon, for the opportunity to work on this project and for guiding me through the various hurdles that presented themselves on the way. Nik, thank you for the clinical guidance and your optimism throughout; Marc, thank you for being there at the lowest points and helping me build my confidence back when needed; Alison, thank you for the support in the lab and for being an inspirational woman in science. I would also like to thank Len (Dr Li Feng) for all the support as a daily supervisor in the lab and the help with the clinical samples: without you and your many skills my project would have simply not been possible. Thank you to Dr Ross Mills and Dr Duncan Humphries for teaching me and helping me with the protocols in the lab.

Thank you to all the patients, healthy volunteers, associated phlebotomists, research nurses and doctors, who have helped with the collection of the samples for this thesis. Also thanks to all the staff in the various facilities at the Bioquarter and at King's Buildings who have helped me with the machines and samples analysis. In particular thanks to the QMRI Flow facility – Shonna Johnston, Will Ramsay and Mari George. Thank you to everyone in W2.06 who has helped me through the years, especially Naomi in recent times for all the early mornings and long days during a very dark winter. Thank you to the Dynafluors group, present and past, for your support and friendly faces during frustrating times.

I can't extend enough thanks to the OPTIMA programme and all the students and staff involved throughout the years. The opportunities and experiences that we were offered have made this PhD particularly worthwhile. In particular, thanks to Dr Jean O'Donoghue: I will be forever grateful for the support and helpful discussions. Thank you also to the optimal 2017 cohort for being such a great bunch of science-driven women (+1), who enjoy a laugh, a drink and a chat.

I would like to thank all my Scotland-based friends for sticking around and making these past years unforgettable. Mairi, Philippe and Alex – thank you

for providing a safe space inside and outside the lab. I hope once all of this is over, we will be able to have a Sneaky celebration like we should have had back in 2018. Sam, thank you for all the video calls and honest conversations in the past couple of years, our laughter and stories have kept me going. Clara, Tom, Jo, Miru and everyone else, thank you for being an inspiration and great friends that I look up to. To all the cycling friends I have met through the years, I hope you know how important you have been for me. Eleanor and Mairi, thank you for all the laughter, adventures, gnarly shreds and associated falls. We have grown so much in the past few years, and I can't wait to see where our bikes will take us next. Thank you to Dan for providing a home, (mechanical) support and overall handling this three-year rollercoaster we have been on - a pandemic was not on the cards, but I am glad I spent it with you.

Thank you to my parents who have been my rocks and biggest supporters, listened to my frustration, encouraged me, and made sure I was okay. I will now write in Italian to address my family. Mamma, grazie per tutte le chiamate e tutte le volte che ti preoccupi di me. Essere distanti non è facile ma negli ultimi quattro anni ci siamo avvicinate molto e sei la persona su cui so di poter contare sempre. Papà, grazie per tutti i kudos (sia su Strava che nella vita reale) e per avermi incoraggiato a fare cose che non avrei mai creduto di poter fare. Non vedo l'ora di spingere i nostri limiti di nuovo insieme. Siete entrambi la mia più grande fonte di ispirazione, incoraggiamento e sostegno, grazie di tutto. Un ringraziamento anche a tutto il resto della mia famiglia, il nonno, le zie, gli zii e i cugini, che mi hanno sostenuto e incoraggiato a distanza, il vostro supporto è stato essenziale.

To all my friends back home who have known and supported me for a long time – thank you. Chiara, you are like a sister to me, and your support means so much I don't think I can really put it into words. Just thank you, and ti voglio bene. Chris, our friendship has developed a lot in the past few years, and I can't believe we were flatmates at the start of the PhD! Thank you for all the laughs and support in the past years, I love how I can be completely honest and spontaneous with you. Ale, Fabio, Gughi and everyone else in our little grooppone, thank you.

Abstract

Introduction

Interstitial lung disease (ILD) is used to describe a heterogeneous group of disorders, characterised by inflammation and fibrosis of the pulmonary interstitium. Previous work has shown alveolar macrophage (AM) CD71 expression, which is also known as the transferrin receptor 1 (Tfr1), was able to stratify lung fibrosis patients into progressors (CD71high) and non-progressors (CD71low), implying a role for iron metabolism in fibrotic ILDs. This led to the initial hypothesis that the labile iron in AM is associated with lung fibrosis and progression of disease.

The overall thesis aim was to investigate iron metabolism and ferroptosis pathways in relevant cell lines and bronchoalveolar lavage cells from patients with lung fibrosis.

Methods

Alveolar macrophages derived from bronchoalveolar lavages were assayed for iron through Prussian blue staining (Golde Score), ICP-MS and two fluorescent probes. The phenotype of alveolar macrophages was characterised through qPCR and flow cytometry. Clinical samples were derived from patients diagnosed with IPF, unclassifiable ILD (UNC) with or without fibrosis and unexplained cough with or without haemoptysis. Multiple regression analysis was performed to assess association of Golde score and other clinical variable on fibrosis and progression of disease in ILD. The BAL cell transcriptome, through RNAseq, was compared in patients with progressive versus non-progressive fibrotic ILD. Ferroptosis was assessed through RSL3 and ferrous ammonium sulphate (FAS) treatment in macrophages (RAW 264.7, THP1 and AM) and epithelial cells (HT29).

Results

Iron accumulation in AM was significantly increased in patients with fibrosis (IPF and UNC with fibrosis) compared to those without fibrosis. Higher levels of iron were shown to be associated with fibrosis and IPF diagnosis. Patients

with IPF had a comparatively higher level of the genes encoding the iron export protein ferroportin, and the iron transporter DMT1, compared to UNC with fibrosis patients, perhaps reflecting a cellular response to high iron content.

Higher Golde score was not associated with progression of ILD (defined as >10% decline in FVC over 12 months) and indeed high Golde score was associated with slightly lower risk of progression. RNAseq was performed on a cohort of progressors (N=4) and non-progressors (N=6). No differentially expressed genes (DEGs) were identified having a false-discovery rate (FDR)-adjusted P-value of <0.1. When a more relaxed threshold of unadjusted P<0.05 was considered, 215 genes were upregulated and 400 downregulated in progressors compared to non-progressors. None of the genes encoding the iron and macrophage polarisation proteins previously discussed were statistically different.

Due to the increased iron level of the alveolar macrophages of fibrotic ILD patients, their ability to undergo ferroptosis, an iron regulated form of cell death, was tested. The susceptibility of macrophages to ferroptosis was assessed using a murine macrophage cell line (RAW), and a human monocytic cell line differentiated to macrophages (THP-1), and compared to HT29, a human colon cancer cell line known to undergo ferroptosis. Macrophages were less sensitive to drugs that induce and rescue ferroptosis compared to HT29 cells. RAW and THP1 cells were however more sensitive to iron loading as shown by increased reactive oxygen species (ROS) compared to HT29. Limited study on alveolar macrophages, suggested similar results to THP1 when using pharmacological induction of ferroptosis. Iron-loading significantly reduced viability in all cell lines, but not proportionate to the ROS increase suggesting macrophages are relatively resistant to iron loading and ferroptosis.

Conclusions

In this single centre study, Golde score was independently associated with the presence of fibrosis in ILD. At the gene expression level, the phenotype of these cells was not significantly different between IPF, UNC with fibrosis and

UNC without fibrosis, but some differences were shown between the UNC with fibrosis and IPF groups when looking at the macrophage inflammatory phenotype. Golde score was not associated with disease progression and indeed higher Golde score was associated with a slightly lower risk of progression. BAL cell transcriptome of patients with progressive versus non-progressive fibrotic ILD was not significantly different but the sample size was small. Macrophages (RAW, THP1 and alveolar macrophages) were relatively insensitive to pharmacologically induced ferroptosis compared to an epithelial cell line (HT29). In contrast to HT29 cells, RSL3 induced significant apoptosis as well as ferroptosis in human macrophages. Macrophages produced a higher level of ROS upon iron-loading, but their viability was relatively maintained compared to the HT29 cell line. These findings suggest that macrophages were relatively insensitive to iron loading and was consistent with the observation that alveolar macrophages remain viable even if they have high iron levels. Future studies could elucidate whether iron loading in macrophages leads to a protective or injurious phenotype, thus leading to potential treatments.

Lay Summary

Interstitial Lung Disease (ILD) is an umbrella term for multiple diseases. The most common one is Idiopathic Pulmonary Fibrosis (IPF), a disease with no known cause that affects about 6000 people every year in the UK and leads to scarring of the lungs. It is a progressive disease which leads to a continuous worsening of the lungs. The average survival time is of 3-5 years and there are no drugs that can cure it. The available treatments are often not well tolerated and only some patients with specific characteristics can use them. ILDs are diagnosed through a multidisciplinary team that takes into consideration multiple clinical characteristics of the patient such as CT scans and lung washing, which involve collecting cells directly from the lungs. Sometimes a clear diagnosis cannot be made and therefore patients are given an unclassifiable disease diagnosis. However, the most important aspect of the disease is to determine if fibrosis is present or not, as this changes treatment options and survival.

Although we do not know what causes ILD, we know that an immune cell called macrophage plays a role in the development of disease. In this study, we found that the macrophages from lung washings from patients with fibrosis (scarring) contained more iron than patients without fibrosis. This high iron did not seem to be associated with gender, age or smoking so we think iron and fibrosis are directly linked. Although we tried to understand why this occurs, no clear cellular characteristics were identified.

Cells are usually very good at keeping a normal level of iron. When an iron accumulation occurs, cells die. We therefore hypothesised that the macrophages from the fibrotic patients are less sensitive to this form of cell death and therefore remain alive but malfunction, leading to scarring in the lungs. We compared these cells to other cells that are known to be sensitive to ferroptosis and determined that they are indeed less susceptible to this form of cell death. We do not know yet whether this leads to malfunctioning. Future work could focus on understanding why these cells are less sensitive to ferroptosis and what the effect is in the lungs of the patients.

Abbreviations

AEC	Alveolar Epithelial Cells
AM	Alveolar Macrophage
ASB	Asbestosis
BAL	Bronchoalveolar Lavage
BF	Bird fancier's lung
COP	Cryptogenic Organising Pneumonia (COP)
COPD	Chronic Obstructive Pulmonary Disease
CP	Ceruloplasmin
CPI	Composite Physiologic Index
DFO	Deferoxamine
DMT1	Divalent Metal Transporter 1
ECM	Extracellular Matrix
EMT	Epithelial-Mesenchymal Transition
ER	Endoplasmic Reticulum
FAS	Ferric Ammonium Sulphate
Fer-1	Ferrostatin 1
FIP-1	Fret Iron Probe 1
FPN	Ferroportin
FRET	Fluorescence Resonance Energy Transfer
FTH	Ferritin Heavy Chain
FTL	Ferritin Light Chain
FVC	Forced Vital Capacity
GAP	Gender Age Physiology Index
GO	Gene Ontology
GPX4	Glutathione Peroxidase 4
GSH	Glutathione (Reduced)
GSSG	Glutathione (Oxidised)
HIF	Hypoxia-Inducible Factor

Hmox1	Heme Oxygenase 1
HRCT	High Resolution Computed Tomography
ICP-MS	Ion-Coupled Plasma Mass Spectrometry
IIP	Idiopathic Interstitial Pneumonia
ILD	Interstitial Lung Disease
IM	Interstitial Macrophage
IPF	Idiopathic Pulmonary Fibrosis
IRE	Iron-Responsive Elements
IRP	Iron Regulatory Protein
LIP1	Liproxstatin 1
LOX	Lipoxygenase Enzymes
MDM	Monocyte-Derived Macrophages
MDT	Multidisciplinary Team
MMP	Matrix Metalloproteinases
NOAC	Novel Oral Anticoagulant
NSIP	Non-Specific Interstitial Pneumonia
PAI-1	Plasminogen Activator Inhibitor-1
PF-ILD	Non-IPF Progressive Fibrotic ILD
PFT	Pulmonary Function Test
PMA	Phorbol 12-Myristate-13-Acetate
PUFAs	Polyunsaturated Fatty Acids
qPCR	Quantitative Polymerase Chain Reaction
RA-ILD	Rheumatoid Arthritis ILD
RBC	Red Blood Cells
RB-ILD	Respiratory Bronchiolitis ILD
RCD	Regulated Cell Death
RIE	Royal Infirmary Edinburgh
ROS	Reactive Oxygen Species
RSL3	RAS-Selective Lethal

SNV	Single Nucleotide Variants
TBI	Transferrin Bound Iron
TCA	Tricarboxylic Acid
TfR1	Transferrin Receptor
TGF	Transforming Growth Factor
TLCO	Transfer factor for Carbon Monoxide
UIP	Usual Interstitial Pneumonia
UNC	Unclassifiable disease
uPA/tPA	Urokinase-Type/Tissue-Type Plasminogen Activator

Table of Contents

Chapter 1 - Introduction 1
1.1 Interstitial Lung Disease 1
1.2 Idiopathic Pulmonary Fibrosis (IPF) 4
1.2.1 Risk Factors 5
1.2.2 Presentation, Diagnosis and Treatments 5
1.2.3 Progression 6
1.2.4 Studying IPF through the murine bleomycin model 8
1.3 Cellular characterisation of IPF 9
1.3.1 Epithelial cells and fibroblasts 10
1.3.2 Macrophages 11
1.4 Iron metabolism 16
1.4.1 Systemic iron 17
1.4.2 Transferrin-dependent cellular iron metabolism 20
1.4.3 Transferrin-independent route 22
1.4.4 Regulation of iron metabolism 22
1.4.5 Iron metabolism disruption in lung disease 24
1.4.6 Iron detection 26
1.5 Ferroptosis 27
1.5.1 Glutamate metabolism inhibition causes ferroptosis. 31
1.5.2 Iron metabolism 32
1.5.3 Ferroptosis inhibitors 33
1.5.4 Detection of ferroptosis 35
1.5.5 Ferroptosis in lung disease 36
1.6 Hypothesis and aims 38
Chapter 2 - Materials and Methods 39
2.1 Ethical Approvals 39
2.2 Bronchoalveolar lavage procedure and processing 39
2.2.1 Cytospins 39
2.2.2 Alveolar macrophage culture 40
2.2.3 Gene expression quantification 40
2.3 Cell lines 42
2.3.1 HT29 43
2.3.2 THP1 43

2.3.3 RAW 264.7 44
2.4 Monocyte-derived macrophages 44
2.4.1 Isolation of human monocytes 44
2.4.2 Macrophage stimulation 46
2.5 Flow Cytometry 46
2.6 Iron quantification 47
2.6.1 Prussian Blue and the Golde Score 47
2.6.2 Staining fixed BAL cells for iron with TRX-Puro 48
2.6.3 Staining live BAL cells for iron with FIP1 51
2.6.4 Iron level assessment of BAL cells through ICP-MS 51
2.7 RNAseq 52
2.8 Ferroptosis assays 54
2.8.1 ROS Assay 54
2.8.2 Flow cytometry on the AttuneNxt for viability and CD71 staining 54
2.8.3 Prussian blue 56
2.8.4 GSH Assay 56
2.9 Statistical Analysis 57
Chapter 3 - Iron content in Alveolar Macrophages of IPF compared to non-fibrotic and fibrotic UNC disease. 58
3.1 Introduction 58
3.2 Results 62
3.2.1 Validation of iron detection methods in THP1 cells and patient BAL cells 62
3.2.2 Alveolar macrophages from IPF patients contain more iron compared to non-fibrotic unclassifiable disease. 65
3.2.3 Iron loading is independently associated with the presence of fibrosis. 68
3.2.4 Alveolar Macrophage M1/M2 gene expression in IPF, UNC with fibrosis and UNC no fibrosis 71
3.2.5 Alveolar macrophages from IPF patients have an iron exporting phenotype compared to UNC with fibrosis and with no fibrosis. 74
3.2.6 Iron regulatory genes and macrophage markers in healthy peripheral monocyte-derived macrophages (MDM) and IPF alveolar macrophages 76
3.3 Discussion 79
3.3.1 Choice of patients 79

3.3.2 Iron loading is a feature of IPF and is associated with fibrosis… 81
3.3.3 Alveolar Macrophage phenotype is similar between diseases ... 82
3.3.4 Alveolar macrophage phenotype is only partially mimicked by MDMs 86
3.3.5 Iron-loading association with fibrosis ... 87
3.4 Limitations ... 88
3.5 Conclusions ... 90
3.6 Appendix ... 91
3.6.1 Appendix 3.6.1 ... 91
3.6.2 Appendix 3.6.2 ... 92
3.6.3 Appendix 3.6.3 ... 94
Chapter 4 - The association of macrophage iron and disease progression ... 95
4.1 Introduction ... 95
4.2 Results ... 98
4.2.1 Iron loading is increased in non-progressive patients with fibrotic ILD ... 98
4.2.2 Lower iron loading is independently associated with greater progression in fibrotic ILD ... 100
4.2.3 RNAseq analysis of progressors vs non-progressors ... 101
4.3 Discussion ... 110
4.3.1 Macrophage and iron phenotype in progression ... 111
4.3.2 Transcriptome phenotype associated with progression ... 112
4.4 Limitations ... 114
4.5 Conclusions ... 115
4.6 Appendix ... 116
4.6.1 Appendix 4.6.1 ... 116
4.6.2 Appendix 4.6.2 ... 117
Chapter 5 - Ferroptosis in Macrophages ... 118
5.1 Introduction ... 118
5.2 Results ... 121
5.2.1 Macrophage-like cell lines are relatively resistant to RSL3 induction and rescue of ferroptosis compared with HT29 ... 121
5.2.2 RSL3 causes both apoptosis and ferroptosis in THP1 cell but not in HT29 or RAW cells ... 127

5.2.3 RSL3-induced ferroptosis leads to ROS increase at different timepoints and at different levels. 131
5.2.4 CD71 is not consistently expressed when ferroptosis is induced… 134
5.2.5 RSL3 treatment results in increased GSH in RAW cells 139
5.2.6 FAS treatment causes an increase in cell death (mostly ferroptosis) at all timepoints with or without RSL3 140
5.2.7 FAS treatment leads to an increase in ROS with and without RSL3 145
5.2.8 Viability following FAS treatment is rescued by LIP1 in HT29, but not in macrophages. 148
5.2.9 Expression of CD71 in RAW cells in response to iron is more pronounced compared to HT29 cells. 150
5.2.10 RSL3 causes a reduction in viability in alveolar macrophages at 24 hours 152
5.3 Discussion 153
5.3.1 Viability reduction through ferroptosis 154
5.3.2 Apoptosis and ferroptosis 156
5.3.3 GPX4-inhibition and ferroptosis 157
5.3.4 ROS and ferroptosis 158
5.3.5 CD71 and ferroptosis 160
5.3.6 Differences and similarities between RAW, THP1 and alveolar macs 161
5.3.7 RSL3 and iron-induced ferroptosis 163
5.4 Limitations 164
5.5 Conclusions 166
5.6 Appendix 167
5.6.1 Appendix 5.6.1 167
5.6.2 Appendix 5.6.2 168
5.6.3 Appendix 5.6.3 169
5.6.4 Appendix 5.6.4 171
5.6.5 Appendix 5.6.5 172
5.6.6 Appendix 5.6.6 175
Chapter 6 - Discussion and Conclusion 176
6.1 Summary 176
6.2 Iron and ILD 176
6.2.1 Iron detection methods 179

6.2.2 Ferroptosis and ILD..... 180
6.3 Future directions..... 182
Chapter 7 - References..... 184

List of Figures

Figure 1.2.1.1 - Axial and coronal images of high-resolution computed tomography (HRCT) showing Usual Interstitial Pneumonia (UIP) patterns. 2
Figure 1.2.1.2 - Survival curves for IPF, unclassifiable disease with fibrosis and unclassifiable disease without fibrosis. 4
Figure 1.3.2.1 - Roles of alveolar macrophages in the pathogenesis of IPF. 14
Figure 1.4.2.1 - Transferrin-dependent iron metabolism in cells. 20
Figure 1.4.5.1 - Kapler-Meier curve comparing survival of patients based on high and low CD71 expression dichotomised according to median CD71 expression by flow cytometry 25
Figure 1.4.6.1 - Key pathways leading to ferroptosis 29
Figure 3.1.1 - Structure of TRX-Puro, developed by Spangler et al., 2016. . 59
Figure 3.1.2 - FIP-1 structure and decrease in FRET following Fe^{2+} cleavage of the endoperoxide bond. 59
Figure 3.2.1.1 – Optimisation of Prussian Blue staining to detect iron in macrophages..... 62
Figure 3.2.1.2 – Optimisation of TRX-puro to detect iron in macrophages . 63
Figure 3.2.1.3 – Optimisation of FIP-1 to detect iron in macrophages 64
Figure 3.2.2.1 – Golde score of BAL derived alveolar macrophages in control groups that presented with or without haemoptysis, UNC with no fibrosis, UNC with fibrosis, IPF patients..... 67
Figure 3.2.2.2 – TRX-puro and FIP-1 assessment of iron levels in BAL-cells, ... 68
Figure 3.2.3.1 – Multiple Linear regression plots showing significant associations of clinical variables with prussian blue. 70
Figure 3.2.4.1 – Macrophage markers of gene expression measured through qPCR. 72
Figure 3.2.4.2 - Flow cytometry results assessing CD163 and CD206 levels in HLA-DR positive macrophages. 73
Figure 3.2.5.1 - Levels of gene expression measured through qPCR normalised to actin in the three different diseases. 75

Figure 3.2.6.1 – Macrophage markers for peripheral blood MDM from healthy volunteers. 76
Figure 3.2.6.2 - Iron markers for peripheral blood MDM from healthy volunteers..... 77
Figure 3.2.6.3 – Graphs comparing the phenotype of IPF derived alveolar macrophage with the phenotype of MDMs treated with IL10. 78
Figure 4.2.1.1 – Survival curves and Golde Score of the progressor and non-progressor cohorts 99
Figure 4.2.2.1 – Multiple logistic regression showing odds ration estimated for the association of clinical variables to progression. 101
Figure 4.2.3.1 - Volcano plot showing significant (-log10 transformed p-values) against magnitude (log2(fold change). 102
Figure 4.2.3.2 – Heatmap showing gene differences of progressors and non-progressors samples 103
Figure 4.2.3.3 – Bubble plot of enriched Reactome pathways with enrichment Z-score 105
Figure 4.2.3.4 - Bubble plot of enriched GO Terms with enrichment Z-score 107
Figure 4.2.3.5 – Box plots of relevant genes expression (log2 expression) 109
Figure 5.2.1.1 - Cell viability is not affected by LIP1 treatment over time in any of the cell lines..... 121
Figure 5.2.1.2 - Induction and rescue of ferroptosis in HT29 cells. 122
Figure 5.2.1.3 - Induction and rescue of ferroptosis in RAW cells..... 123
Figure 5.2.1.4 - Induction and rescue of ferroptosis in PMA-treated THP1 cells. 124
Figure 5.2.1.5 - Percentage change decrease in viability over time when RSL3 is added at different concentrations compared to media showing a greater reduction in viability (over 2 fold change). 125
Figure 5.2.1.6 - Prussian blue staining with HT29, RAW, THP1 treated with RSL3 at two different concentrations. 126
Figure 5.2.2.1 - Apoptosis level in RSL3 treated cells compared to media.. 127

Figure 5.2.2.2 - Flow plots for the cell lines showing AnxV-PI quadrants following treatment with either media or with RSL3 10μM at two different timepoints. 128
Figure 5.2.2.3 – Summary of the proportions of live, apoptotic and ferroptotic cells in HT29, RAW and THP1. 130
Figure 5.2.3.1 - ROS detection following RSL3 treatments. 131
Figure 5.2.3.2 - Fold change to untreated in ROS at the 2-hour timepoint for HT29, RAW and PMA-treated THP1 cells. 132
Figure 5.2.3.3 - ROS detection following RSL3 with LIP1 treatments. 133
Figure 5.2.3.4 – Baseline ROS levels are overall not significantly affected by the addition of LIP1 in HT29, RAW and THP1 cells. 134
Figure 5.2.4.1 - HT29 and CD71 expression. 135
Figure 5.2.4.2 – Timecourse of CD71 expression in HT29 cells 136
Figure 5.2.4.3 - RAW cells CD71 expression. 137
Figure 5.2.4.4 - Histograms representing fluorescence shift when the Fc block was added either with the antibody for 30 minutes or prior to the antibody for 10 minutes on ice. 138
Figure 5.2.5.1 – Quantification of GSH levels following two hours of RSL3 treatment in HT29 and RAW cells. 139
Figure 5.2.6.1 - Viability and apoptosis in cells treated with or without FAS. 141
Figure 5.2.6.2 – Percentage change in viability when iron is added compared to media in the three cell lines (4 hours). 142
Figure 5.2.6.3 – Proportion of viable (AnxV-PI-), apoptotic (AnxV+PI-) and ferroptotic (PI+) cells in HT29, RAW and THP1 cells treated with RSL3 143
Figure 5.2.6.4 - Viability in HT29, RAW and PMA-polarised THP1 for RSL3 5 μM treatment following incubation with media or iron (FAS 200μM), or both. 144
Figure 5.2.7.1 - ROS production following treatment with iron in different conditions, normalised to media with no iron 146

Figure 5.2.7.2 - ROS production at 2 and 4 hours in HT29, RAW or THP-1 cells were pre-treated with iron and then treated with different concentrations of RSL3 or media. 147
Figure 5.2.8.1 – Effect of LIP1 on iron loaded cells on normalised ROS production and viability respectively, for HT29, RAW and PMA-polarised THP1 compared to media with and without iron. 149
Figure 5.2.9.1 - Assessment of CD71 in HT29 cells. (..... 151
Figure 5.2.9.2 - CD71 expression in RAW cells following no iron (-FAS) or iron loading (+FAS). 152
Figure 5.2.10.1 – Summary of viable, apoptotic and ferroptotic BAL cells following RSL3 treatment at 2 hours and 24 hours..... 153

List of Tables

Table 1.2.1-1 - Classification guidelines for diagnosis of IPF and IIP. 3
Table 1.4.6-1 - Summary of the morphological and biochemical features with some inhibitors of ferroptosis, apoptosis and necrosis. 28
Table 2.2.3-1 - Pre-designed primers for gene of interest from Sigma-Aldrich 42
Table 2.5-2.4.2-1 - Antibodies used in flow cytometry 47
Table 3.2.2-1 - Clinical characteristics and BAL diferential cell counts the five groups of patients subsequenty assayed for Prussian Blue staining. 66
Table 3.2.3-1 - Summary of the parameter estimates of the variables, the percentage change of Golde Score and the relevant p values. 69
Table 4.2.1-1 - Patient demographics of progressors and non-progressors. No statistical differences were observed between the two groups (Mann-Whitney test) 98
Table 4.2.2-1 - Summary of the parameter estimates of the variables and the relevant p values. 100
Table 4.2.3-1 – Details of the top 10 Reactome pathways identified as significantly different in progressors compared to non-progressors.. .. 106
Table 4.2.3-2 – Details of the top 10 GO terms identified as significantly different in progressors compared to non-progressors. 108
Table 4.2.3-3 – Summary of fold changes and P-values of the genes of interest previously analysed 110
Table 5.3.7-1 – Table summarising the effect of the RSL3 and FAS treatments on the different cell lines. 163
Table 6.2.1-1 - Comparison between different methods of iron detection.. 180

Chapter 1 - Introduction

Interstitial Lung Disease (ILD) is used to describe a heterogeneous group of pulmonary disorders, characterised by inflammation and fibrosis of the pulmonary interstitium[1]. Under this umbrella term, idiopathic interstitial pneumonia (IIP) describes another cohort of diseases with unknown aetiology, where Idiopathic Pulmonary Fibrosis (IPF) is the most prevalent. One of the key cellular players in IPF is the alveolar macrophage. Different macrophage phenotypes have been implicated in the pathophysiology but mechanisms of injury (and repair) remain unclear[2]. Iron metabolism in macrophages, but also in specific organs, has been implicated in the pathogenesis of diseases such as neurodegenerative disorders, cancer and pulmonary diseases[3–5]. In particular, the concept of ferroptosis, an iron-dependent non-apoptotic form of regulated cell-death (RCD), has been shown to play both protective and injurious roles in various diseases[6–9], as well as some pulmonary disorders such as Chronic Obstructive Pulmonary Disease (COPD)[10]. This thesis aims to investigate the presence of iron in macrophages and the potential role of ferroptosis and iron metabolism in ILDs including IPF. In this chapter the clinical and cellular aspects of IPF with a focus on iron metabolism and ferroptosis are introduced.

1.1 Interstitial Lung Disease

Some ILDs are considered idiopathic and termed Idiopathic Interstitial Pneumonias (IIP). The most common interstitial pneumonia is usual interstitial pneumonia (UIP) and in its idiopathic form is equivalent to IPF. Other less common IIPs are non-specific interstitial pneumonia (NSIP), cryptogenic organising pneumonia (COP) and respiratory bronchiolitis-ILD (RB-ILD). A common differential diagnosis of IIPs is hypersensitivity pneumonitis. All ILDs should be diagnosed by specialist multidisciplinary teams (MDT) according to consensus guideline criteria. For IPF, the criteria have evolved over time and

are based on high-resolution computed tomography (HRCT) patterns and/or lung pathology if available (Figure 1.2.1.1)[11–14].

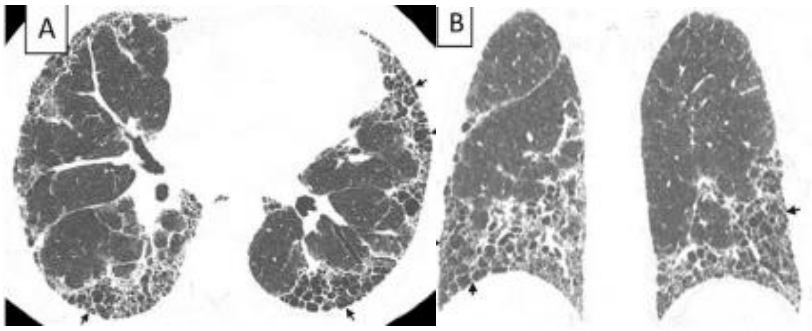

Figure 1.2.1.1 - Axial (A) and coronal (B) images of high-resolution computed tomography (HRCT) showing Usual Interstitial Pneumonia (UIP) patterns. (Adapted from the ATS/ERS/JRS/ALAT clinical practice guideline (2011)). Adapted with permission of the American Thoracic Society. Copyright © 2022 American Thoracic Society. All rights reserved. The American Journal of Respiratory and Critical Care Medicine is an official journal of the American Thoracic Society. Readers are encouraged to read the entire article for the correct context at https://www.ers-education.org/sdi/media/showMedia.aspx. The authors, editors, and The American Thoracic Society are not responsible for errors or omissions in adaptations.

'Definite' IPF and 'probable' IPF are accepted terms based on consensus criteria and in this thesis the term 'IPF' is applied to include subjects with definite or probable disease. Many idiopathic ILDs require a lung biopsy to make a confident diagnosis. However, this procedure has a 2% mortality risk and sometimes does not lead to a definitive diagnosis. Hence historically biopsy rates in Edinburgh and in the UK have been low. Bronchoalveolar lavage is a relatively safe procedure, and a differential cell count may aid diagnosis, but this may not be sufficient to provide a definite or confident diagnosis. Therefore most ILD centres including Edinburgh frequently make an MDT diagnosis of 'unclassifiable' (UNC) disease' where a diagnosis cannot be made with high confidence despite clinical, HRCT and if available histological data[12,15]. A summary of the key clinical presentations of these diseases, as defined through clinical classification per guidelines and per Royal Infirmary Edinburgh (RIE) are listed in Table 1.2.1-1.

Table 1.2.1-1 - Classification guidelines for diagnosis of IPF and IIP.

MDT Diagnosis	**HRCT and LUNG HISTOLOGY pattern***
Definite IPF^	Definite UIP pattern on HRCT OR probable UIP pattern on CT and a UIP, probable UIP or possible UIP pattern on lung biopsy
PROBABLE IPF^	Probable UIP, not biopsied
UNCLASSIFIABLE idiopathic ILD with fibrosis#	HCRT pattern indeterminate for UIP, fibrotic pattern, no alternative diagnosis made with confidence either with or without biopsy
UNCLASSIFIABLE idiopathic ILD without fibrosis#	As above but no fibrosis on biopsy and/or HRCT
***HRCT and biopsy patterns based on 2011/2018 ATS/ERS consensus guidelines ^Definite and Probable IPF grouped as 'IPF' in studies herein #Fibrosis based on HRCT traction bronchiectasis or honeycombing with or without volume loss and/or histological fibrosis according to expert pathologist**	

Regardless of the specific diagnosis, it is known that the presence of fibrosis on HRCT or biopsy has prognostic significance. In the Edinburgh ILD MDT, in addition to the diagnosis (IPF, NSIP, unclassifiable) all subjects are classified according to the presence or absence of fibrosis based on HRCT appearance that incudes honeycombing and/or traction bronchiectasis with or without volume loss. By definition all patients with IPF have fibrosis. Other interstitial pneumonia, including unclassifiable disease, may be either fibrotic or non-fibrotic.

Previous analysis from the Hirani lab (unpublished) (Figure 1.2.1.2), shows the survival of patients from diagnosis (first CT scan) with IPF, UNC with fibrosis and UNC no fibrosis (median survival 4.12, 7.26 and 9.86 years respectively). Therefore, investigating the mechanisms that drive fibrotic versus

inflammatory ILDs may be helpful in identifying novel biomarkers and therapies.

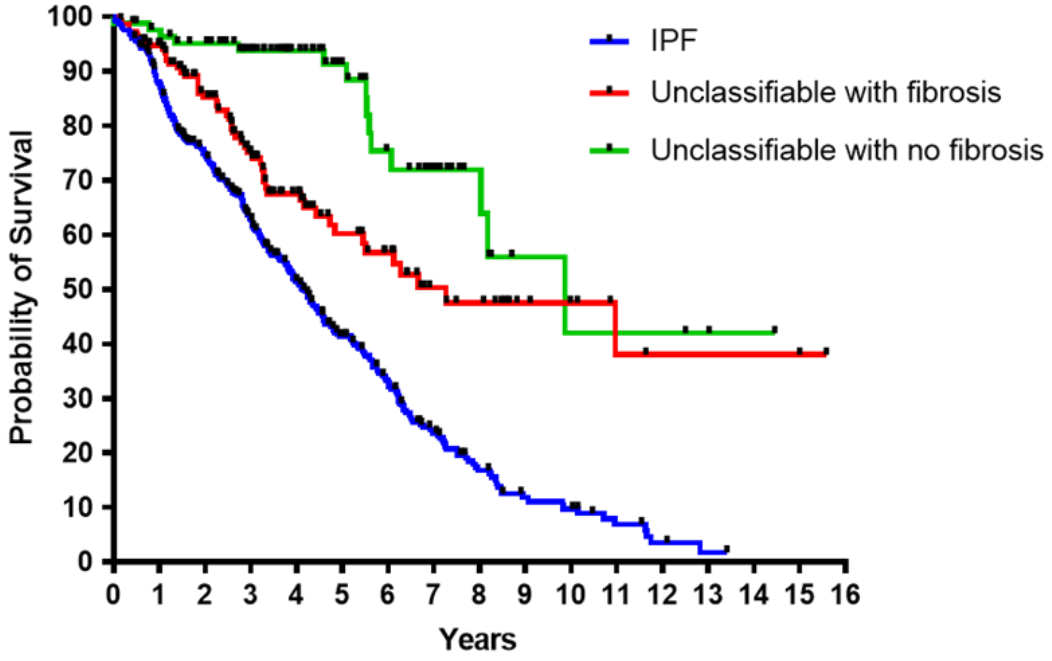

Figure 1.2.1.2 - Survival curves for IPF, unclassifiable disease with fibrosis and unclassifiable disease without fibrosis. Log-rank (Mantel-Cox) test shows a P value of <0.0001. IPF N=462; UNC with fibrosis N=155; UNC with no fibrosis N=85. IPF v UNC no fibrosis HR = 2.621 (CI 1.988 to 3.456, P<0.0001); UNC with fibrosis v UNC no fibrosis HR = 2.177 (CI 1.335 to 3.548, P=0.0018). UNC with fibrosis v IPF HR = 1.834 (CI 1.447 to 2.325, P<0.0001).

1.2 Idiopathic Pulmonary Fibrosis (IPF)

IPF is the most common fibrotic-ILD and it is a life-threatening, progressive disease. The median survival time is estimated to be of approximately 3-4 years and affects men (62 per 100,000) more than women (40 per 100,000). Deaths occur more often during winter, even when excluding infections. In the UK, in 2012, about 32,500 people had IPF and approximately 12 people for every 100,000 were diagnosed with the disease every year[16]. IPF outside of clinical trials, does not have well described rates of progression and the mechanisms that drive progression are unclear[14,15,17]. This progression is characterised by a deterioration of lung function and associated symptoms,

due to progressive worsening of gas exchange in the lung caused by fibrosis[17]. Fibrogenesis involves the continuous deposition of extracellular matrix (ECM) and collagen in the pulmonary interstitium by the coordinated efforts of fibroblasts and inflammatory stimuli.

1.2.1 Risk Factors

By definition IPF is of unknown cause. However risk factors for developing IPF include increased age (rare under 50yrs), male sex, smoking, environmental exposure to metal or wood dust and possibly microbial agents[17,18]. Additionally both genome-wide associated studies (GWAS) and deep sequencing have implicated single nucleotide variants (SNVs) of the mucin 5B gene (MUC5B), MUC5AC and AKAP13 as susceptibility genes for IPF[19,20,21].

1.2.2 Presentation, Diagnosis and Treatments

The diagnosis of IPF requires a multidisciplinary team, with specialist respiratory physicians, radiologists and pathologists and follows international guidelines[11,22]. The main symptoms are breathlessness, dry cough, general malaise and on examination, inspiratory lung crackles are a key feature[23]. However, these symptoms and signs are not exclusive to IPF, as they are associated to many ILDs. The first step for diagnosis is the exclusion of any known causes of ILD, such as environmental exposure (for example to asbestos causing asbestosis, or avian proteins, leading to bird fancier's lung), connective tissue disease (ILD associated to Rheumatoid Arthritis), or any drug toxicity. A pattern of definite or probable UIP, as defined in the 2018 guidelines, should then be identified on HRCT[11] (Figure 1.2.1.1). A probable or possible UIP pattern on HRCT may necessitate a lung biopsy to obtain a definite diagnosis. In large clinical trials, both definite and probable IPF subjects are eligible for recruitment, so most clinicians treat and manage both groups of patients in the same way.

Treatments to IPF are very limited. The only two pharmaceutical options for patients with IPF are Nintedanib and Pirfenidone, both acting as anti-fibrotic drugs, and the former has recently been licensed for non-IPF progressive-fibrotic ILD (PF-ILD). Nintedanib is a tyrosine kinase inhibitor which blocks

various growth factor receptors, such as PDGFR, VEGFR1/2 and fibroblast growth factor. These are involved in signalling pathways implicated in fibrosis progression, including fibroblast migration and ECM deposition. Pirfenidone leads to the inhibition of TGFβ1-stimulated collagen synthesis and downregulates pro-inflammatory cytokines such as TNFα. Additionally, it acts as a free-radical scavenger, therefore playing an additional antioxidant role[24,25]. Due to the relative non-specificity of these compounds and the multitudes of roles of kinases and TGFβ1-pathways, these drugs often lead to significant side effects. With both Pirfenidone and Nintedanib the most common and predominant adverse events identified in a real world study are of gastrointestinal nature but can mostly be effectively managed. With pirfenidone the most common side effect was appetite loss (17%), followed by nausea and vomiting (15%), but also lightsensitivity. With Nintedanib, 24% of patients experienced diarrhoea and 13% experienced nausea. In 19% of patients the drug was discontinued permanently[26].

Arguably, the main limiting factors to the development of new drugs for IPF (and other ILDs) are the unclear pathophysiology and the lack of a mouse model which shows progressive fibrotic lung disease.

1.2.3 Progression

IPF is a progressive lethal disease but the rate of progression in individuals is variable. Some patients progress faster than other, leading to worse prognosis. Other non-IPF fibrotic ILD, including unclassifiable ILD also show variable rates of progression. In a study looking at non-IPF fibrosing ILD, 25% of patients were identified as having a progressive phenotype, with rest progressing at a significantly lower rate[27].

1.2.3.1 Conventional Biomarkers

Prediction tools or scores have been shown to be useful in estimating prognosis in ILD. However, these are not widely used in routine clinical practice. For example the GAP score is a multidimensional prognostic staging system which takes into consideration gender, age and physiology through two pulmonary function tests (PFT): forced vital capacity (FVC) and diffusing

capacity of the lung for carbon monoxide (TLCO)[28]. The Composite Physiologic Index (CPI) is another model used to assess disease extent and predicting mortality as observed by computed tomography scans[29].

However, in the clinic a validated and widely used measure of progression is change in FVC over a 12-month period. Many studies have shown that a 10% or greater reduction in FVC over 12 months is associated with increased risk of death[13,30] and declining FVC is used as a primary outcome measure in most mid and late stage IPF clinical trials[31].

1.2.3.2 Novel diagnostic and prognostic biomarkers

Peripheral blood biomarkers have been identified to selectively identify IPF patients over controls and some markers have been shown to have prognostic abilities. For example CCL18 concentration was found to predict outcome, high levels of serum surfactant protein A and YKL-40 levels both predict early mortality and survival respectively[32–34]. Additionally, high levels of KL-6 and SP-D were also shown to be associated with a higher rate of progression[35,36]. In contrast, high levels of MMP-7 were shown to be negatively correlated with lung function and survival[37–39]. However currently biomarkers do not exhibit drug induced changes and are not robust enough to be used in clinical settings. Some studies have shown that telomere length is associated with poorer survival and some genetic mutations in genes related to telomere maintenance, such as TERT, have been identified in IPF patients[40–42]. In particular telomere-associated foci are increased in IPF and p16 expression is increased with disease severity[43]. Both these biomarkers are associated with cellular senescence, which has been shown to be associated with IPF. Indeed, key markers of senescence have been shown in both IPF lung tissue derived fibroblasts and epithelial cells, as well as in the bleomycin model[44–46]. More Both genetic and pharmacological elimination of senescent cells, was shown to restore lung elasticity and improve pulmonary function in the bleomycin model in both aged mice and at disease onset[43,47].

Thus some markers and molecular mechanisms have been shown to contribute to development or progression of the disease. These studies have

mostly been carried out on blood samples, but differences at the cellular level are unclear. A good animal model would be beneficial.

1.2.4 Studying IPF through the murine bleomycin model

To study IPF, the bleomycin-induced lung fibrosis rodent model is the most established and well characterised animal model[48–50]. Other models of pulmonary fibrosis involve the use of silica and radiation but are less well characterised, and to a certain extent, do not represent human disease as well[51]. Bleomycin was a clinically relevant anti-cancer chemotherapy drug which acts on oncogenic cells, by producing reactive oxygen species (ROS) in the presence of iron and oxygen, thus causing oxidative damage and inhibiting replication[52,53]**.** Side effects associated to this therapy were commonly seen in lungs, skin and mucous membranes, as the bleomycin-inactivating enzyme, bleomycin hydrolase, is found at very low levels in these tissues. Lung fibrosis is one of the better-known side effects of this drug. When bleomycin is instilled in murine lungs, either endo-tracheally, trans-orally, subcutaneously, intraperitoneally or intranasally, it causes lung injury through oxidative stress, leading to an inflammatory response and consequent fibrosis[49].

The initial acute injury, characterised by an influx of inflammatory cells leads to production and activation of pro-inflammatory cytokines and mediators, and occurs in the first week after instillation[50]. The following week is characterised by an increase in fibroproliferation and activation of collagen genes, assessed by myofibroblasts markers such as α-SMA. The third week is considered the “chronic stage” of fibrosis, where alveolar fibrosis becomes evident, with an increased deposition of ECM, peaking around day 28[50,54]. Although this is how IPF pathophysiology is now thought to occur - through a lung insult, albeit of unknown origin, possibly resulting in an inflammatory response and following aberrant repair causing fibrosis - the following phase in the bleomycin model does not represent human disease. Known as the resolution phase, the mice lungs show reduced inflammation and, in some reports, showed complete resolution of fibrosis as well[50,55]. Although this is useful to study the characteristics of fibrotic resolution, it remains controversial as other studies

do not observe a complete resolution even after 6 months. However, this seems to be somewhat related with the protocol of administration of bleomycin, thus varying concentrations and number of repeated insults[56–58].

This model therefore presents some limitations, such as this resolution pathway or the exogenous induction, whereas it occurs idiopathically in human. Nevertheless, most of the knowledge regarding the pathophysiology of IPF and the development of the current therapeutics used clinically, Pirfenidone and Nintedanib, were characterised through the bleomycin model.

1.3 Cellular characterisation of IPF

IPF is a complex disease involving a combination of aberrant processes and cellular pathways. Due to its unknown aetiology, it is unclear but unlikely that there is a single cell type that is responsible for the pathology, leading to a cascade of aberrant responses. The current paradigm of IPF pathophysiology is of epithelial injury (wounding) followed by an aberrant healing process. Historically IPF was treated with corticosteroid therapy, however a more recent randomised, double-blind, placebo-controlled (PANTHER) study, showed that using a combination of corticosteroids and azathioprine (an immunosuppressant) showed an increased risk of hospitalisation and death[59]. Thus the role of inflammation was uncertain[60].

The IPF lung is characterised by a pro-fibrotic environment, enriched with TGFβ and TNFα, stimulating and activating fibroblasts, and downregulated fibrinolytic pathways, such as reduction of collagenases. One of the key players implicated in this inflammatory phenotype are pulmonary macrophages, both alveolar and interstitial[61]. Indeed it was demonstrated that macrophages are involved with the production of TGFβ and with fibroblast collagen synthesis through the bleomycin model[62,63].

The accepted paradigm for IPF pathogenesis involves a repeated insult of unknown origin to the alveolar epithelium which becomes damaged, leading to aberrant repair pathways, characterised by resulting fibrosis. This involves ECM and collagen deposition, epithelial endoplasmic reticulum (ER) stress

and apoptosis in alveolar epithelial cells type II (AECII), and increased reactive oxygen species (ROS) production[64,65]. Although the cause of this erroneous repair is still unclear, different studies have tried to elucidate these mechanisms.

A simplified model of the processes involved with IPF pathogenesis therefore should include three main cell types recognised to be key: epithelial cells, fibroblasts and macrophages.

1.3.1 Epithelial cells and fibroblasts

Epithelial cells are thought to not only be the initially damaged cell type, leading to a vicious cycle of further injury and ROS production, but also involved in the production and activation of fibroblasts. Following initial injury to the AECII, these undergo either regulated cell-death through apoptosis, or begin a process called epithelial-mesenchymal transition (EMT), a still somewhat controversial mechanism as discussed later. Interestingly, through familial IPF studies, mutations in surfactant proteins were identified, which caused apoptosis and chronic injury to these cells through chronic ER stress[65,66].

Different single cell RNAseq (scRNAseq) studies, showed an increased proportion of airway epithelial cells and a decrease in alveolar epithelial cells[67,68]. Additionally, studies showed an indeterminate state of differentiation of these epithelial cells with aberrant activation of signalling pathways such as TGFβ and Hippo-Yap/Taz[68]. In a later study, this population was defined as an aberrant basaloid cell, as they express both epithelial and basal cells markers[67]. The latter population is normally key in lung development and represent a progenitor cell, able to differentiate in any type of airway cell during development. Interestingly, these cells were seen at the edge of myofibroblast foci, the areas of fibrosis remodelling, and were not seen in healthy controls or in COPD patients, thus being specific to IPF. Their intermediate phenotype suggests that they are undergoing EMT, as they have also lost the gatekeeper gene against EMT (mir-205)[67].

EMT and the location of these intermediate progenitor-like basal cells, suggests that the epithelial cells may become fibroblasts and play a direct role

in fibrosis. As aforementioned, this remains controversial due to contrasting lineage tracing studies. The high plasticity of these cells when cultured, leads to changes in phenotype, losing the specificity needed for these experiments. Animal studies have shown EMT occurring in vivo, and implicating the extracellular matrix mediators as a key regulator[69]. In a recent scRNAseq paper, fibroblasts involved in IPF are not a discrete population but are part of a continuum, thus do not transdifferentiate from a single population[67].

The same epithelial cells from IPF patients have been shown to preferentially undergo apoptosis over EMT when exposed in vitro to active TGFβ1[69]. Further studies in TGFβ Receptor 2 lung epithelial deficiency had an improved survival (compared to more apoptotic epithelial cells) and an overall decrease in the population of lung fibroblasts in murine models. This led to a protection from bleomycin-induced fibrosis[57].

Both apoptosis and EMT lead to recruitment of inflammatory cells such as macrophages, which initiate an inflammatory cascade leading to fibrosis. Fibroblast activation and fibrosis progression indeed occurs as a result of anti-inflammatory macrophages (which will discussed in the next section) activating the TGFβ/Smad2 signalling pathway. This creates a fibrotic niche which leads to the characteristic phenotype of IPF[65,70–74].

1.3.2 Macrophages

Macrophages are immunomodulatory cells which are present in all tissues and their roles range from host defence to tissue repair and remodelling. They are a heterogeneous cell population, which regulate processes ranging from infection to fibrosis. Pulmonary macrophages can be alveolar (AM), positioned in the airways, or interstitial macrophages (IM), located in the parenchymal tissue of the lungs[75]. The latter are mostly monocyte-derived and play key roles in lung immune homeostasis, for example through the production of the cytokine IL10. Different populations of IM are being identified which may play a role in disease[76].

Alveolar macrophages are the main inflammatory cell in the lungs of IPF patients and can be collected through bronchoalveolar lavages (BALs) in

patients, a procedure routinely carried out at the RIE. This makes them an interesting and useful cell that can be studied to understand IPF further and will therefore be the focus herein.

AMs are initially differentiated from foetal monocytes and then are mostly maintained by self-renewal[77,78]. They play a dual role of developing inflammation to fight disease, but also limiting inflammation caused by infections, thus protecting the tissue[79,80]. Evidence shows that this regulation may involve AM recognition of pulmonary epithelial cell death, which fits well with the current paradigm of IPF pathogenesis as discussed previously[81]. These multiple roles and the fact that they are of foetal origin, also implies an underlying plasticity of this cell population.

This plasticity was initially dichotomously stratified as pro-inflammatory (M1) – involved with injury and death - and anti-inflammatory (M2) – characterised by dysregulated repair pathways - macrophages, representing a simplistic but useful method of characterisation[82,83]. The M2 group was then expanded to encompass different anti-inflammatory phenotypes, namely M2a, M2b and M2c. These have different inducers, IL4 or IL10, different functions, such as Th2 responses, allergy or immunoregulation, and different levels of protein expression. Therefore, different heterogeneous cohorts of macrophages can be thought to play a role in different diseases. Further characterisation, through scRNAseq has identified further heterogeneity with a spectrum of immunomodulatory macrophages and will be discussed later. These and previous studies helped understanding the role of macrophages in the pathogenesis of IPF.

The pathogenesis of IPF is thought to involve an aberrant response by macrophages, with a production of TGFβ and consequent collagen synthesis, leading to fibrosis[62]. This is thought to involve anti-inflammatory (M2-like) AM, which activation leads to acute exacerbations of IPF[84]. Acute exacerbations are defined as an unexplained worsening or development of dyspnoea and/or consolidation of a UIP pattern on HRCT, while excluding infections[85,86]. In particular high levels of the mannose receptor Mrc1 (CD206) and increased

production of cytokines such as TGFβ, CCL18 and IL8 are all characteristics of this macrophage phenotype and also correlate to worse clinical parameters of IPF[87]. M2-like macrophages are also involved in the ECM remodelling through a mannose receptor-dependent pathway which degrades collagen through secretion of metalloproteinases[88,89]. Another receptor, CD163, which is upregulated by IL10 and involved in scavenging haptoglobin-hemoglobin complexes from plasma, has been implicated in worse IPF prognosis in combination with CD204[90–92]. These environmental stimuli therefore have been shown to affect the polarisation and function of these cells at different stages of disease. Conversely, in IPF, macrophages with an M1-like pro-inflammatory phenotype, characterised by high CD80 and CD86, are less abundant. They have however been shown to be expressed at higher levels in the excessive insults, characterised by a pro-inflammatory environment, of acute pneumonia. This might be linked as well to respiratory infections, to which M1-like macrophages would react to[93,94]. AM have been shown to acquire these receptors (CD80 and CD86) as a result of early or late acute rejection episodes. These receptors are often co-stimulated and are part of the pro-inflammatory axis. Most recently, inhibition of these receptors by a drug that blocks co-stimulation (abatacept), has been shown to antagonise the excessive pro-inflammatory response observed in COVID-19, highlighting their involvement with these key M1-roles[95].

The characterisation of this population may aid in not only understanding the disease further, but also identifying possible therapeutic targets. A graphical summary of the known role of macrophages in promoting pathogenesis of IPF is shown in Figure 1.3.2.1.

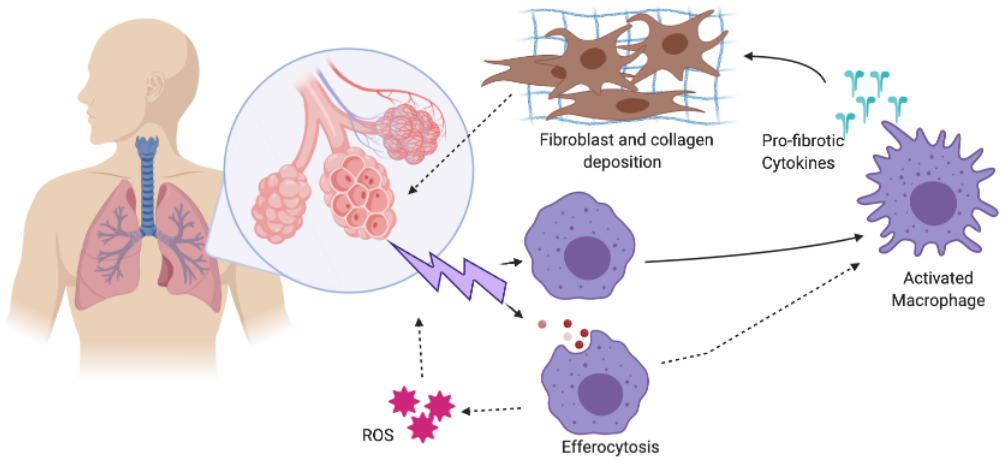

Figure 1.3.2.1 - Roles of alveolar macrophages in the pathogenesis of IPF. Following alveolar epithelial injury, alveolar macrophages become activated and lead to the activation of fibroblasts and collagen deposition as a result of the production of pro-fibrotic cytokines such as TGFβ. Macrophages also can carry out efferocytosis, phagocytosis of apoptotic bodies, and erythrophagocytosis, phagocytosis of red blood cells which may result following injury. This process, which has been shown to be decreased in IPF AMs, may increase iron accumulation intracellularly and may cause increase in reactive oxygen species production. This may also affect the response of macrophages to injury, leading to aberrant wound response with increased fibrosis. Figure made with Biorender.com.

Macrophages involved with lung injury and fibrosis in the murine bleomycin model, were identified and characterised through flow cytometry[96]. This study confirmed the plasticity of the macrophages involved, as the markers expression changed throughout the different phases of the bleomycin model (previously discussed)[96]. Moreover, through genetic lineage tracing systems and genetic deletion, it was identified that monocyte-derived AM seem to contribute to fibrosis more, compared to tissue resident AM[97]. In a monocyte/macrophage depletion model of pulmonary fibrosis, it was shown that this led to a reduced collagen deposition and consequent reduced inflammatory phenotype[63]. Additionally studies such as Aran et al., (2019) aforementioned[98], identified transitional macrophages which localised to activated fibroblasts and were necessary for their migration and proliferation during fibrosis. Concurrently of their role as drivers of fibrosis, macrophages have also been identified as having a resolution-promoting role during the late resolution stage in the bleomycin model[99]. However, limitations of using these murine models need to be considered when assessing its translation to human disease.

Efferocytosis is another key role of macrophages and as aforementioned, apoptotic cell recognition resulting phagocytosis, may be a key mechanism of the immunoregulation in pulmonary fibrosis. In other fibrotic syndromes, it has been shown that alveolar epithelial cell (AEC) dysfunction and apoptosis underlies the pathogenesis of fibrosis through the recruitment of TGFβ-producing macrophages, and changes in this, affect the susceptibility to fibrosis[100]. TGFβ then stimulates fibroblasts activation and collagen deposition, thus promoting fibrosis further[101,102]. An interesting study in small cohorts of patients showed that efferocytosis in alveolar macrophages is significantly lower in IPF compared to other interstitial pneumonias. This could also contribute to the pathogenesis of disease as the lack of clearance of apoptotic bodies is likely to create a pro-inflammatory environment, leading to further injury[103]. IL37, a protein expressed both in AECs and AMs, has been shown to inhibit oxidative-stress induced cell death in AECs and to downregulate the TGFβ pathway in murine and in vitro work by promoting autophagy[104]. IL37 administration also significantly decreased inflammatory infiltration and collagen deposition, thus fibrosis, in the bleomycin model[105]. The expression of this protein was also shown to be reduced in IPF patients' AECs and AMs, compared to healthy controls[104]. The protective role that this cytokine seems to have on lung fibrosis could be therefore linked to the reduced AEC death and aberrant macrophages, thus highlighting a possible therapeutic strategy.

Recent work has generated a single-cell atlas of pulmonary fibrosis patients-derived AM compared to controls. This identified four macrophage clusters of which one was associated with homeostatic tissue-resident AMs and was enriched in the healthy donor population, and the others were distinctively associated with disease and pro-fibrotic mechanisms. They also observed no differences in clustering in patients with IPF compared to other pulmonary fibrosis diseases, such as hypersensitivity pneumonitis and systemic sclerosis-associated ILD, but this was attributed to current computational approaches limitations[106]. Another study using single-cell sequencing in a bleomycin model showed a disease associated subgroup with a transitional gene expression profile, which phenotype was in between monocyte-derived

macrophage and the AM. These macrophages during fibrogenesis localise to fibroblasts and their deletion led to decreased total lung collagen and specific fibroblasts[98].

In a mouse model that develops fatal chronic pulmonary fibrosis, early loss of vascular integrity was identified which resulted in microinjuries[107]. Macrophages were observed to clear the lung space from the extravasated red blood cells in a process called erythrophagocytosis, thus accumulating iron. These microinjuries led to the deposition of fibrin, thus playing a role in fibrosis. No assessment of TGFβ was carried out, and therefore it is not clear if these macrophages play a role in fibrin deposition through the production of TGFβ. Although some IPF patients have been shown to have pulmonary vascular lesions, it is not determined whether this has an effect[108].

Whether patients with IPF are more prone to, or the repeated epithelial damage leads to these microinjuries, thus leading to the accumulation of iron in macrophages and aberrant healing, remains unclear[107]. Interestingly when looking at IPF patients, it was found that CD163, the haemoglobin-haptoglobin complex scavenger receptor, was significantly more expressed in AM of IPF patients, compared to age-matched healthy controls[99]. It is unclear why this receptor is upregulated in IPF, but its role in the uptake of haemoglobin from the alveolar space could be linked to the microhaemorrhages and to dysregulated iron metabolism in macrophages. Other studies, discussed in further sections, have shown an involvement of dysregulated iron metabolism in lung disease pathogenesis[5,109]. These, together with other observations from our lab about iron mediators in IPF patients' alveolar macrophages, suggest a role of these two components in the pathogenesis of IPF.

1.4 Iron metabolism

Iron metabolism has been suggested to play an important role in alveolar macrophages of IPF patients[110–112]. In recent years the effect of iron on the polarisation of macrophages and its effect on the pathogenesis of disease has been focus of study. During infections, thus in a pro-inflammatory state,

macrophages show changes in gene expression, favouring iron sequestration in the case of extracellular pathogens, limiting the iron resources available to be used for proliferation. An opposite phenotype is observed in the case of intracellular pathogens, with a reduced heme-iron content. Additionally, the production of ROS by macrophages is also used by macrophages to directly target pathogens in phagolysosomes[113,114]. In some in vitro studies, iron accumulation in macrophages has been shown to impair bacterial killing[115]. Conversely, an M2-like phenotype similar to the macrophages in IPF, has been shown to have a more iron-recycling phenotype, with high ferroportin, the only known gate for iron to exit the cell, and downregulation of ferritin, the iron storage protein[116,117]. Iron metabolism is a complex, but well-studied and thoroughly reviewed mechanism with a multiplicity of players involved. It is continuously used by living organisms in multiple processes, ranging from oxygen transport and respiration, to DNA synthesis, to electron transport through Fe-S clusters and activation of a plethora of enzymes[118,119]. The cellular and systemic handling of iron is hereby discussed.

1.4.1 Systemic iron

Systemically, iron is mostly found bound to haemoglobin in red blood cells (RBC) (or erythrocytes), which are thought to represent nearly 85% of all our cells. In a healthy steady state 20-25mg/day of iron is needed to regenerate this cellular pool in the bone marrow[120]. However, dietary iron absorption by the intestine only accounts for about 1-2mg of iron, and overall there is a loss of iron mostly associated with desquamation and menstrual bleeding[121]. This occurs through the divalent metal transporter 1 (DMT1) on the apical membrane, identified in 1997 as DCT1[122]. The uptake (through DMT1) and iron passage through enterocytes is stimulated transcriptionally by the hypoxia-inducible factor 2α (HIF2α).

The export of iron is negatively controlled by hepcidin, a hormone secreted by hepatocytes following detection of elevated levels of circulating iron or inflammatory mediators. An increase in hepcidin expression was observed, both in human and mouse, concurrently with an increase in iron levels;

consequent genetic mouse models, showed severe iron overload when hepcidin was deleted, and iron deficiency in over-expression models[123–128]. Hepcidin binds directly to ferroportin (FPN1), which is the only cellular efflux protein for ionic iron on the basolateral membrane of enterocytes (and all other cells), leading to its internalisation and degradation[129].

Enterocytic export through ferroportin, requires oxidation of Fe^{2+} to Fe^{3+} for loading onto transferrin. In the intestine this is carried out by hephaestin, a multicopper oxidase homologue of ceruloplasmin (CP), a ferroxidase used for the same purpose ubiquitously[130–132]. Once iron enters the bloodstream, it is oxidised, and two iron ions are bound to transferrin (Tf) or act as the central cation of haemoglobin and other heme-containing proteins. This dampens its possible pro-oxidative role, mostly defined by the production of reactive oxygen species (ROS) via Fenton chemistry, thus activating damaging pathways in the bloodstream and beyond[133].

In turn hepcidin is controlled by the *hfe* gene and the HFE protein is mostly found in hepatocytes. HFE competes with transferrin-bound iron (TBI) for binding to the same site of the transferrin receptor (TfR1), involved in the uptake of TBI in all cells. Transferrin however has a much higher affinity for TfR1, compared to Apo-Tf, its iron-free form. The competition between the HFE and Tf therefore depends on the latter's occupancy by iron. In the presence of low iron, thus in the presence of Apo-Tf, HFE binds to Tfr1. In high iron, TBI displaces HFE from TfR1, and the latter interacts with TfR2, a liver specific homolog of TfR1. This forms a signalling complex involved with the upregulation of hepcidin, thus with the inactivation of ferroportin and consequent decreased iron absorption and accumulation of iron in macrophages[134,135]. Mutations in *hfe* leading to improper activation of hepcidin, results in physiological low levels of HFE expression[135]. Consequently, ferroportin is not inactivated, thus causing an increased iron absorption by enterocytes and release into circulation by macrophages. This causes a clinically relevant pathology, hemochromatosis, where cells and organs present with iron overload[135]. Ferroportin global knockouts develop embryonic lethality, and the selective inactivation has shown iron accumulation

in enterocytes, hepatocytes and macrophages. These experiments highlight the importance of ferroportin in some clinically relevant diseases, such as hemochromatosis, and patients with autosomal dominant ferroportin disease[136]. Variants in the *hfe* gene, but not TfR2 or ferroportin, were identified in IPF patients compared to a control population. This variant did not correlate to iron accumulation or overall lipid peroxidation, but labile iron-dependent ROS generation was significantly greater in the IPF patients carrying this genetic characteristic[137].

Since the levels of dietary iron absorption are so low, but the demand for iron is comparatively high, iron recycling is essential for maintaining appropriate levels of iron systemically. This is mostly carried out by red pulp macrophages in the spleen, which are supported in high levels of iron by liver macrophages, Kupffer cells[138]. However, macrophages present in other organs, such as alveolar and interstitial macrophages in the lungs, can also recycle iron from their organs due to extravasation following injury or during inflammation[107,139].

Senescent erythrocytes are identified by macrophages and phagocytosed, through a process called erythrophagocytosis. Here heme oxygenase 1 (Hmox1), the heme catabolism enzyme, plays a key role in releasing the iron from the protoporphyrin ring present in heme. Mouse models where Hmox1 is knocked out, lose recycling ability and suffer from anaemia and other iron deficiency complications[140]. From this stage, the iron is either stored within the cell bound to ferritin, thus lowering iron concentration in the serum and preventing iron overload, or it exits the cell through ferroportin, which as aforementioned, is associated with the ferroxidase ceruloplasmin[128,132].

If this mechanism is disrupted at any stage it can lead to diseases associated with either iron overload, such as haemochromatosis, or iron deficiency such as anaemia.

1.4.2 Transferrin-dependent cellular iron metabolism

Generally, iron is tightly regulated and controlled by a plethora of proteins. The principal iron-route into the cell is through transferrin and its receptor, Tfr1 (or CD71). A graphical summary of the pathway is shown in Figure 1.4.2.1. This receptor's transcription is activated in iron-deprived cells by hypoxia-inducible factors (HIF2α) and its mRNA is transcriptionally regulated by Iron Regulatory Proteins IRP1 and IRP2[141,142].

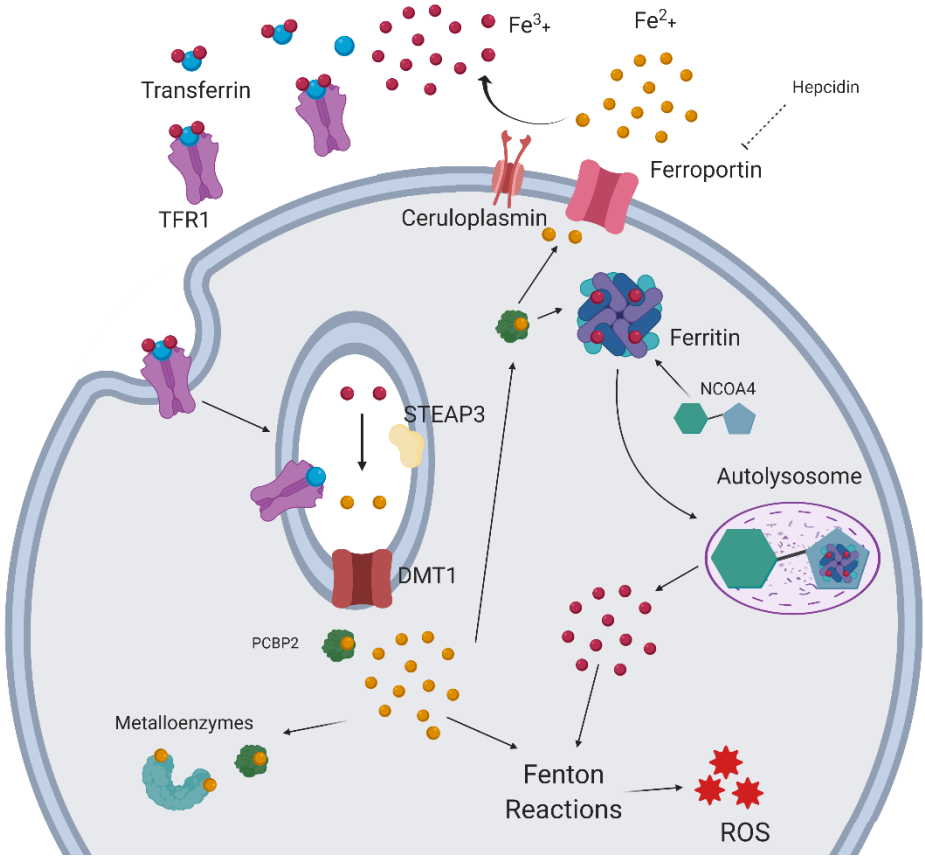

Figure 1.4.2.1 - Transferrin-dependent iron metabolism in cells. Two ions of Fe^{3+} bind transferrin, which then binds the transferrin receptor. This is internalised by the cell in an endosome, where the low pH dissociates the iron from transferrin and through STEAP3 it is reduced to Fe^{2}. Iron(II) exits the endosome through DMT1 into the cytoplasm, where it forms the labile iron pool. The cargo protein PCBP2 can take it to metalloproteins and enzymes that require iron to function or to ferritin, where it is stored, or to ferroportin, which leads to its exit from the cell. Ferroportin, which expression is regulated by hepcidin, is closely associated to ceruloplasmin, a ferroxidase that leads to the oxidation back to Fe^{3+} outside the cell. If the iron needs to be stored intracellularly, the multimeric protein ferritin assembles. If the cell needs more iron ferritin is targeted to the lysosome by NCOA4, leading to ferritinophagy and release of iron. Free iron in the cell can cause Reactive Oxygen Species (ROS) development as a result of Fenton reactions.

Apo-transferrin (Apo-Tf) binds two ions of Fe^{3+} and it is up taken by the cell in its differric form (Tf) bound to the high-affinity transferrin receptor (Tfr1), through clathrin-dependent endocytosis requiring the adaptor protein AP2[143]. Accumulating evidence from spontaneous mutations and mouse models, shows the involvement of vesicular trafficking protein complexes such as EXOC6, part of the exocyst, or SNX3, as key players in this recycling mechanism[144–146]. Once within the endosome, the lower pH triggers conformational changes in both Tfr1 and Tf, leading to release of iron[147]. The Fe^{3+} ions are reduced to Fe^{2+} by STEAP, a metalloreductase[148]. Here DMT1, previously mentioned as an enterocytic apical membrane protein, plays a key role as the iron transfer protein from the endosome to the cytosol. Tfr1 and Apo-Tf are recycled back to the membrane. Fe^{2+} in the cytosol forms the labile iron pool, which, if not tightly regulated leads to reactive oxygen species, cellular damage and ferroptosis. PCBP1 and PCBP2 are chaperone proteins identified to deliver iron to metalloenzymes and to the iron storage protein ferritin[149–151]. Ferritin is a multimeric protein with 24 subunits of heavy (FTH1) and light (FTL) chains, which ratio depends on the state of inflammation and infection. Fe^{2+} binds to FTH in the ferroxidase centre. Iron is oxidised to Fe^{3+}, migrates and, with the aid of the FTL, it nucleates forming the iron core[152].

Depending on the levels of intra- and extra-cellular iron, ferritin can be degraded through a mechanism called ferritinophagy. This is mediated by NCOA4, a cargo receptor, which interacts selectively with FTH1, leading to the delivery of ferritin to the lysosome via autophagosomes[153,154]. From here the iron returns to form the labile iron pool and it can be used by the cell accordingly.

If iron needs to be exported from the cell, PCBP2 alone carries it to ferroportin, the only known iron exit protein[155]. As aforementioned, FPN is tightly regulated by hepcidin expression, binding to which leads to its internalisation and degradation[129]. Recent studies in cell lines have shown that treatment with iron, thus provoking iron overload, leads to a decrease in TfR1 molecules at the cell surface and increased transferrin endocytic rate. TfR1 was

endocytosed independently of Tf, thus identifying an additional post-translational control to prevent iron overload[156].

1.4.3 Transferrin-independent route

The transferrin receptor is required for erythropoiesis and neurologic development. Embryos with a complete Tfr1 knockout develop organs normally, but develop a lethal phenotype at day 12.5 associated with anaemia[157]. These early studies, reinforced by consequent ones where Tfr1 was preferentially disrupted in selected organs, supported the notion of transferrin-independent routes of iron uptake. ZIP14, a zinc transporter was identified as a possible candidate and studies in cardiomyocytes and neuronal cells implicated calcium channels in this as well[130,158,159].

Another route that occurs exclusively in monocytes and macrophages, is through CD163, a haemoglobin-haptoglobin scavenger receptor. Following intravascular haemolysis due to injury or inflammation, haemoglobin binds to acute phase protein haptoglobin (Hb-Hp). From here CD163 mediates the endocytosis of the complexes inside the macrophage, where the haemoglobin is cleared. Interestingly, the inflammatory interleukin IL6 upregulates this receptor and haptoglobin expression, as well as HMOX1, key for haemoglobin degradation[160]. IL10, an anti-inflammatory cytokine, is also produced as a result of Hb-Hp binding. Its binding has therefore been shown to skew the polarisation of the macrophage population and high levels of CD163 (and CD204) positive macrophages have been associated with the clinical course of IPF[90,161]. This highlights the importance of iron metabolism for the expression and characterisation of macrophages in an inflammatory context.

1.4.4 Regulation of iron metabolism

Systemically iron metabolism, as mentioned before, is regulated by hepcidin, a hormone produced by the liver, which binds to ferroportin and leads to its degradation. Hepcidin itself has been shown to be regulated only at the transcriptional level. Its expression is inhibited by anaemia and hypoxia; and stimulated by iron loading and inflammation[162]. It is regulated by the BMP/SMAD signalling pathway and IL6, an important inflammatory cytokine,

can regulate it through the JAK1/2-STAT3 pathway[163,164]. This is reviewed by Schmidt (2015)[128].

The tight regulation of iron metabolism in a cellular context is regulated post transcriptionally by iron regulatory protein 1 and 2 (IRP1 and IRP2). Through insights from murine models, the two proteins have been found to be largely redundant, but at least one is essential. Indeed a full knockout murine model is not viable, but $Irp1^{-/-}$ mice develop polycythemia and pulmonary hypertension, while $Irp2^{-/-}$ mice present with microcytic anaemia and iron overload of selected organs[165]. These iron-responsive RNA-binding proteins bind to a conserved cis-regulatory hairpin structure, known as iron-responsive elements (IREs). This is present in the untranslated region (UTR) of the target mRNA of proteins involved in iron uptake, export and storage. IRPs are iron-sulphur proteins which lose one of their iron ions when there are low iron levels in the cells. This leads to increased affinity to the IREs in the target mRNA. Depending on what end of the mRNA it binds to, it leads to either translational control if bound on the 5' UTR IRE, or to mRNA stability control, if bound to the 3' UTR IRE. In the case of TfR1 and DMT1, the IRP binds to the 3' UTR IRE, where it leads to increased translation and thus increased iron intracellularly. Conversely, in the case of ferritin and ferroportin, IRP binds to the 5' UTR and inhibits translation, thus reducing levels of these storage and export proteins. When the iron starts to increase intracellularly, an iron ion is incorporated in the IRP and it loses its affinity to the mRNA, thus reducing its stability or translational control, and reversing the prior mechanism[130,166].

IRE and IRP defects have been causatively linked to clinically relevant human disorders, such as sideroblastic-like anaemia with iron overload[167]. GWAS studies have also implicated mutations in the IRPs genes to be associated with diseases like Chronic Obstructive Pulmonary Disease (COPD), lung cancer and Alzheimer's disease[168–170]. Interestingly IRP can also be activated by other factors, such as oxidative stress, as initially demonstrated in vitro, by causing disassembly of the Fe/S clusters[171].

1.4.5 Iron metabolism disruption in lung disease

Alveolar macrophages have been shown to accumulate iron intracellularly in IPF when compared to healthy controls and this was also observed in murine pulmonary fibrosis models[110,172,173]. A recent study showed, through knockout mouse models, that this accumulation plays a key role in both the pathogenesis of pulmonary fibrosis and the lung function decline[174]. However, in human disease, it is unclear whether this is due to dysfunctional alveolar macrophages, or due to microhaemorrhages/microinjuries leading to release of excessive erythrocytes in the lung space and consequent erythrophagocytosis, or a combination of both. Nevertheless, it implies a dysregulated iron metabolism which is likely to lead to excessive ROS production, possibly causing further inflammation and injury through a pro-inflammatory phenotype[110].

Recent studies have shown seemingly different results when observing expression levels of the transferrin receptor (CD71 or TfR1), the gate for transferrin-bound iron into the cell, on AM in the IPF lung. Allden et al. (2019), showed an increase in proportion of AM lacking CD71 ($CD71^-$) in IPF patients compared to healthy controls. These CD71- AMs had impaired phagocytosis and transferrin uptake abilities, even if the transferrin concentration in BAL fluid was increased. A higher proportion of CD71 negative macrophages were also independently associated with worse survival[112]. These macrophages also showed a pro-fibrotic phenotype with high levels of metalloproteinases (MMP2, MMP8), vascular endothelial growth factor (VEGF) and other mediators that can increase the activation of TGFβ. It is however unclear if these low expressing CD71 macrophages are recently recruited, immature, monocyte-derived AM which have been shown to persist in the fibrotic lung[97]. More sophisticated scRNAseq studies may be able to show the origin and persistence of these macrophages over the progression of disease, if using a murine model. However, in murine bleomycin-induced pulmonary fibrosis studies, an increase in $CD71^+$ AM was observed, and this was suppressed by the use of an iron chelator, DFO (deferoxamine)[174]. This may highlight significant differences between human disease and the bleomycin model,

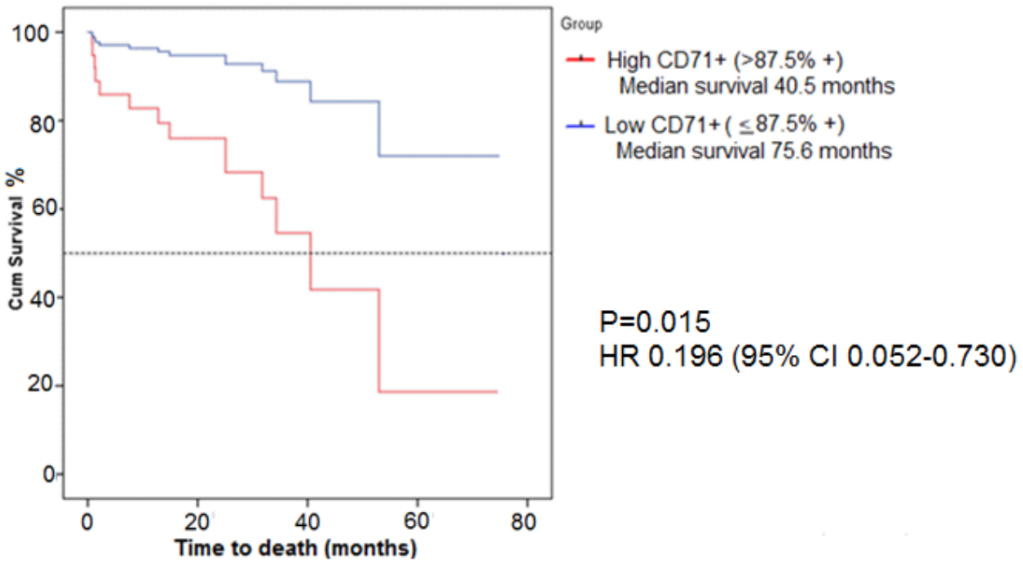

Figure 1.4.5.1 - Kapler-Meier curve comparing survival of patients based on high and low CD71 expression dichotomised according to median CD71 expression by flow cytometry. Lisa Nicol data (unpublished)

limiting its use in understanding progression of disease. Previous unpublished work from the Hirani lab identified CD71 through flow cytometry on BAL-derived alveolar macrophages of IPF patients as a prognostic marker for progressors and non-progressors (Figure 1.4.5.1)[175]. Patients with a higher expression of CD71 had a worse survival compared to low CD71 expression, thus supporting the murine study[174] previously discussed and not the one based on IPF patients[112]. These differences could be down to the gating strategy used in each study. Indeed, the resident pulmonary monocyte-like cells (rPMLC), previously characterised by a $CD14^{+}CD16^{+}$ phenotype[176], are excluded from this CD71 characterisation by our lab. Additionally, CD71 negative cells may just not have been considered in the other studies.

A study comparing IPF patients with controls, identified a significant increase in macrophage iron accumulation and iron-dependent ROS in the BAL fluid and cells of the fibrotic patients. This iron dysregulation was then also associated with an allelic variant of HFE[137]. As described earlier, HFE is an iron-induced gene, which can cause hemochromatosis, a disease of iron accumulation.

Therefore, increasing evidence implicates dysregulated iron metabolism, with an accumulation of iron in alveolar macrophages, in pulmonary fibrotic

disease. This dysregulated iron accumulation may lead to an increased ROS production in alveolar macrophages and in the pulmonary interstitium. This may consequently lead to an aberrant wound response due to dysfunctional macrophages, but also to an increase in injury due to the increased oxidative stress. Recent studies have started implicating ferroptosis, a form of iron-dependent cell death, in diseases ranging from cancers to other pulmonary disorders such as asthma and COPD. Elucidating the role of this pathway in pulmonary fibrosis may be of help in understanding its progression and pathogenesis.

1.4.6 Iron detection

The level of iron in cells can be assessed in different ways through iron-sensitive probes, immunohistochemical stains such as Prussian blue, and through analytical methods such as Ion-Coupled Plasma Mass Spectrometry (ICP-MS).

Many iron-sensitive probes have been developed over the years but have various limitations in different cell types, according to the basal iron levels and proliferation of the cells[177]. Two probes will be discussed here as they were available through collaborations. TRX-puro is a highly selective reactivity-based probe which involves the intracellular unmasking of puromycin following a Fenton-type reaction with Fe^{2+}. Puromycin can then be detected and imaged with high throughput microscopy[178]. FRET Iron Probe 1 (FIP-1) is a reactivity based Fe^{2+} -sensitive fluorescent probe. FIP1 links two fluorophores through an Fe^{2+}-cleavable endoperoxide bond. This bond is broken when the probe interacts with Fe^{2+}, leading to a decrease in fluorescence resonance energy transfer (FRET) and to a significant excitation of fluorescein. This can be detected through imaging, flow cytometry, or as plate reader assessment[179].

A long established method of detecting iron is Prussian blue, a histochemical stain that detects Fe^{3+}. Hydrochloric acid splits iron from any proteins (including ferritin) and this allows potassium ferrocyanide to combine with ferric iron, forming ferric ferrocyanide, or Prussian blue. The levels of iron are then assessed through a semiquantitative method termed Golde Score, which

involves visually assessing cells based on blue colour intensity and an average score, between 0 and 400, allocated[180].

Finally, ICP-MS is an analytical method to detect trace levels of metal ions, such as iron. This is carried out by full decomposition of the sample into its elements through addition of pure Nitric Acid and subsequent ionisation and detection. Fe56, the most common iron isotope, is then detected and normalised accordingly.

As part of this study, these four methods of detection are compared and discussed further in the context of alveolar macrophages.

1.5 Ferroptosis

Ferroptosis is an iron-dependent form of nonapoptotic regulated cell death[181]. It was identified following the characterisation of two small molecules, erastin and RSL3, that were defined as RAS-selective lethal (RSL) compounds, as they were shown to be selectively lethal to oncogenic RAS mutant cell lines[181]. This family of small GTPases are mutated in 30% of all cancers and therefore were thought to be a possible oncogenic treatment target[182]. Dixon et al., (2012) hypothesised that erastin and RSL3 caused a distinct form of cell death compared to apoptosis, necrosis and other forms of well characterised regulated cell death[181]. Ferroptosis shows different biochemical, morphological, and genetic features, and over time this has been further characterised. A summary of the changes in morphology and biochemical features, compared to other form of cell deaths, is shown in Table 1.4.6-1.

Ferroptosis remains a relatively new pathway with many unclear mechanisms, especially in relation to disease pathogenesis. Recent evidence has implicated ferroptosis in respiratory diseases, such as asthma, as described in the next section.

Cellular metabolism, redox, iron homeostasis and various signalling pathways all impinge on ferroptosis. A summary of the ferroptosis KEGG pathway, representing lipid peroxidation, iron, and glutamate metabolism, is shown in Figure 1.4.6.1.

Table 1.4.6-1 - Summary of the morphological and biochemical features with some inhibitors of ferroptosis, apoptosis and necrosis. Adapted from Cao and Dixon (2016) and Li et al., (2020)[183,184]

	Morphological Features	**Biochemical Features**	**Inhibitors**
Ferroptosis	• Small mitochondria • Higher mitochondrial membrane densities • Cell swelling	• Iron accumulation • Lipid peroxidation • Protein upregulation – TFRC, ACSL4	• Lipophilic antioxidants (e.g. Ferrostatin 1) • Iron chelators (e.g. DFO)
Apoptosis	• Reduction of cell and nucleus size • Nuclear fragmentation (chromatin condensation) • Apoptotic bodies	• DNA fragmentation • Caspase and endonuclease activation	• Caspase inhibitors
Necrosis	• Plasma membrane permeabilisation • Generalised swelling	• Drop in ATP levels • Death ligand (e.g. Fas, TNFα) binding to TNF receptor in caspase-inhibited cells	• Necrostatins

Iron-dependent lethal accumulation of reactive oxygen species (ROS) can be considered one of the major aspects of ferroptosis known thus far. Particularly relevant to ferroptosis is lipid peroxidation, which involves ROS-induced damage to polyunsaturated fatty acids (PUFAs). This ROS production is promoted by iron and its ability to change between its Fe^{2+} and Fe^{3+} forms. When Fe^{2+} reacts with hydrogen peroxide it becomes Fe^{3+} through Fenton reactions and produces a hydroxyl radical and a hydroxyl. On the other hand, when Fe^{3+} reacts with hydrogen peroxide, it becomes Fe^{2+} and forms

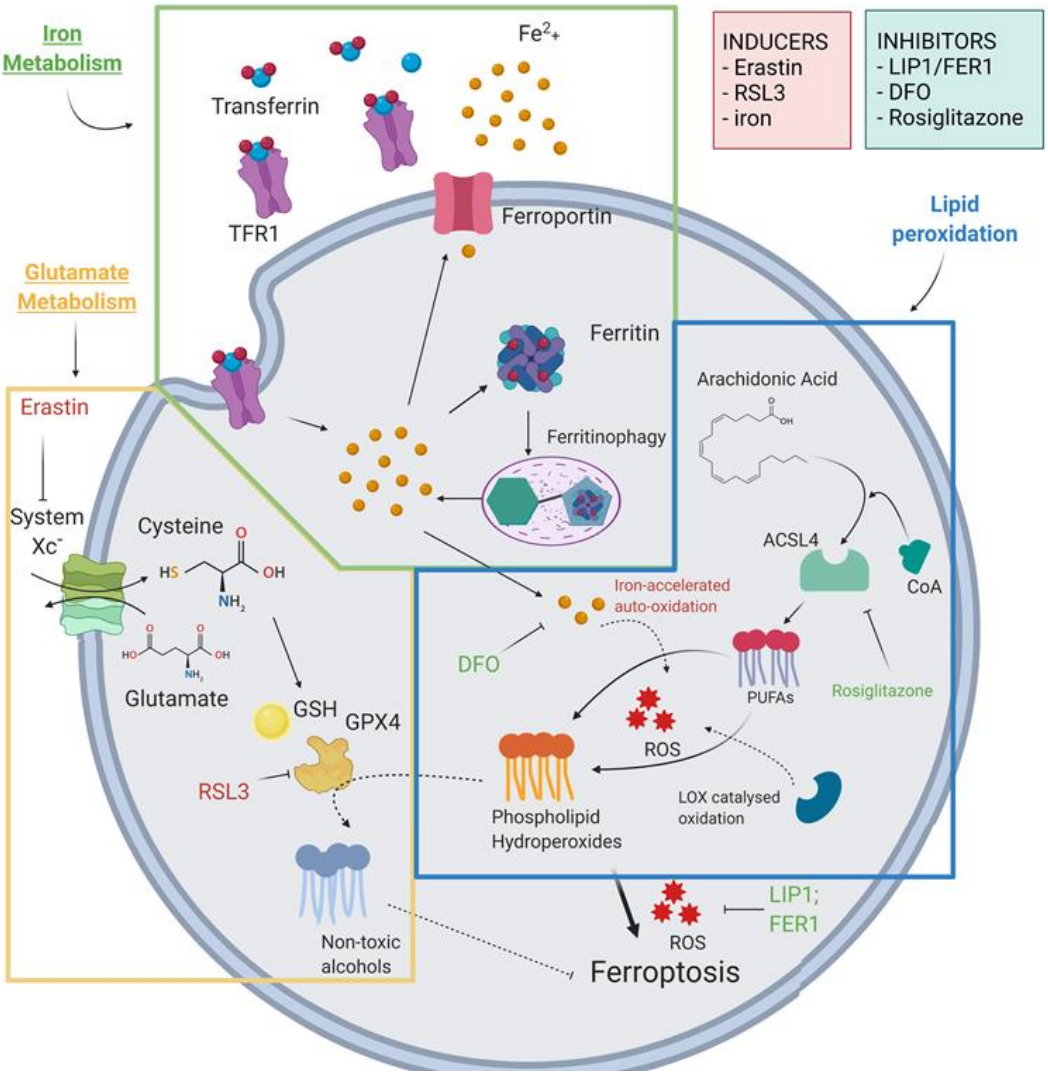

Figure 1.4.6.1 - Key pathways leading to ferroptosis which are described in text. Lipid peroxidation is the main hallmark of ferroptosis where PUFAs become phospholipid hydroperoxide as a result of ROS which are either catalysed through iron-dependent Fenton Reactions or LOX-catalysed oxidation. Both of these auto-oxidations are fuelled directly or indirectly by iron and its metabolism. In contrast glutamate metabolism dampens ferroptosis through GPX4 which transforms the damaging hydroperoxides into non-toxic alcohols. If something occurs leading to impaired glutamate metabolism, this protective effect is lost and ferroptosis occurs.

hydroperoxyl and a proton, through a reaction called Haber-Weiss (Equation 1). Whether this ROS accumulation leads to consequent signalling pathways or leads to the breakdown of the phospholipid-rich plasma membrane causing death, remains unclear. This iron-dependent peroxidation is dampened by known proteins, such as GPX4 which will be discussed further in the next section, but also through iron chelation, for example with deferoxamine (DFO), and other drugs and compounds, such as Ferrostatin-1 (Fer-1), Liproxstatin 1 (LIP1) and other radical-trapping antioxidants.

$$Fe^{3+} + O_2^{\cdot -} \leftrightarrow Fe^{2+} + O_2$$

$$Fe^{2+} + H_2O_2 \longrightarrow Fe^{3+} + HO^{\cdot} + OH^{-} \quad (Fenton\ reaction)$$

$$O_2^{\cdot -} + H_2O_2 \leftrightarrow O_2 + HO^{\cdot} + OH^{-} \quad (Haber-Weiss\ reaction)$$

Equation 1. Fenton and Haber-Weiss reaction which involve iron and the development of reactive oxygen species.

Another key player in the peroxidation of PUFAs is the lipoxygenase enzymes (LOX) family. In particular ALOX15, arachidonic acid being its most prominent substrate, can drive ferroptosis. Although it remains unclear which other members of the LOX family are important for ferroptosis, double-knockout studies have suggested that multiple LOX enzymes fuel this peroxidation[185–187]. In turn, LOX enzymes, which contains a Fe^{3+}-containing active site, is regulated by the control of iron availability by the phosphorylase kinase G2 (PHKG2)[188].

The generation of phospholipid peroxides also depends on the initial availability of the substrate. It consists of polyunsaturated fatty acids (PUFAs), which are much more reactive than monosaturated and unsaturated fatty acids. Through knockout studies, ACSL4 was identified as essential to influence the lipid composition leading to ferroptosis, and in certain models even predictive of sensitivity to ferroptosis[189]. Indeed, it is responsible for the esterification of CoA to free fatty acids, in particular arachidonic acid, thus consequently activating fatty acid oxidation or lipid biosynthesis[189].

1.5.1 Glutamate metabolism inhibition causes ferroptosis.

Ferroptosis was initially identified as a result of an inhibition through the compound erastin of the so-called System Xc^- a disulphide-linked heterodimer composed of SLC7A11 and SLC3A2 acting as a cysteine/glutamate antiporter[190]. This leads to cysteine starvation and thus depletion of the intracellular pools of glutathione in both its reduced form, GSH, and oxidised form, GSSG. One of the key roles of glutathione is as an anti-oxidant and the ratio between its reduced and oxidised form is often used to measure cellular oxidative stress[191,192]. GSH is key for the correct functioning of the essential phospholipid hydroperoxidase, glutathione peroxidase 4 (GPX4). GPX4 normally suppresses the synthesis of phospholipid hydroperoxides by converting them to non-toxic alcohols[193,194]. Therefore, if GSH is depleted there is an increase in reactive oxygen species (ROS), which is likely to induce cell death, assessed by triggering serum-dependent necrosis[195].

However, GPX4 inhibition, both indirectly by System Xc^- inhibition through erastin, or through direct GPX4 inhibitors such as RSL3 and consequent accumulation of lipid peroxides, is not sufficient to cause ferroptosis[190,196]. Indeed, it has been shown that lipid peroxidation is strictly regulated by multiple players, such as iron and iron-related proteins, as previously discussed.

When the antiporter is blocked by erastin, not only does it cause the cell to be starved of cysteine, but it also leads to an accumulation of glutamine. L-glutamine specifically was found to be linked to ferroptosis[195]. Being the most abundant amino acid in the body, it plays multiple roles and acts as an important carbon source for the tricarboxylic acid (TCA) cycle within the mitochondria, following glutaminolysis[195,197]. As a result many enzymes involved in this degradation, such as glutaminase2, have been shown to play important roles in ferroptosis, particularly in cancer where ferroptotic cell death is a protective mechanism through tumour suppression, regulated by p53[198]. Moreover, L-glutamine degradation plays an important role in lipid biosynthesis, through the citrate pyruvate cycle, providing CoA to ACSL4[181,199,]. This latter enzyme helps channel arachidonic acid and adrenic

acid to this oxidisable pool, preferentially used in ferroptosis[189,200]. Mitochondria are therefore implicated in ferroptosis and are thought to play a pivotal role particularly in cysteine-deprivation-induced ferroptosis.

Additionally, ferroptosis can be identified through morphological changes in mitochondria. Indeed following erastin-induced ferroptosis mitochondria appear to have an increased membrane density, volume reduction and increased mitochondrial potential, distinguishable from other forms of cell death[181,199]. Erastin also inhibited cellular GPX enzymes through GSH depletion, their substrate derived from cysteine[201,202].

RSL3 is able to inactivate GPX4 directly, via alkylation of the catalytic selenocysteine[203]. A reduction of GSH was not observed in these studies, suggesting that it is not linked to the deprivation of cysteine or changes in the System Xc^-. Other studies, however, have implicated the importance of iron in this lethality. Indeed, iron chelators such as DFO were able to significantly inhibit RSL3 activity. Moreover, the intrinsic signalling following RSL3 treatment was shown to upregulate TfR1, while downregulating FTH1 and FTL, thus increasing the labile iron pool within the cell[196].

1.5.2 Iron metabolism

As the name suggests, ferroptosis was initially identified as dependent on iron accumulation and its metabolism. It was later clarified that it is often iron-dependent lipoxygenases (LOX) that initiate ferroptosis by causing lipid peroxidation, and the labile iron pool acts as fuel for the resulting lipid peroxides, thus fuelling these oxidative species production through Fenton reactions[204,205]. However other proteins involved in iron metabolism, described previously, have been shown to play a role in ferroptosis.

Recently, TfR1 (or CD71) has been identified as one of the key markers of ferroptosis and fluorescent antibodies have been used to selectively stain this mechanism over other forms of regulated cell death[206]. Interestingly, it was noticed that TfR1 seems to accumulate over time on the cell surface of ferroptotic cells, but its mRNA levels, measured through qPCR, remain unchanged. Since the autophagic pathway involved in the internalisation of the

receptor was shown to be working correctly, it was hypothesised that this accumulation was related to altered iron metabolism and a possible positive feedback loop between ferroptosis and iron uptake[206]. The role of altered iron metabolism' proteins in ferroptosis still needs to be understood. Therefore, whether the accumulation of iron in AM discussed above may be linked to the increased levels of TfR1 on the surface due to ferroptosis is yet to be studied.

Ferritin levels have been shown to indicate sensitivity to ferroptosis, as high levels of ferritin lead to a lower level of free iron, thus less oxidative stress. Conversely, ferritinophagy has been shown to promote ferroptosis through the consequent increase of LIP[207,208]. Nevertheless, a recent study has identified another method to limit ferroptosis by exporting ferritin-bound iron out of the cells through exosomes, promoted by a protein called Prominin2. This increased resistance to ferroptosis was observed in mammary epithelial and breast cancer cells, where following a pro-ferroptotic stimulus, the gene of interest was increased[209]. Whether this applies to other cell types and in vivo needs to be observed.

IRPs have also been shown to be activated by oxidative stress, as initially demonstrated in vitro, by causing disassembly of the Fe/S clusters[171]. Recently a cancer drug called dihydroartemisinin (DAT) was shown to sensitise cancer cells to ferroptosis as a result of increased iron intracellularly and impinging on IRP/IRE-controlled iron homeostasis[210]. However, the role of ROS in this context was not discussed or assessed. Another study assessed levels of both mRNA and protein expression of TfR1 during pharmacological induction of ferroptosis, and only found an increase over time of TfR1 protein, but no change in TfR1 mRNA. Whether this is due to increased translation – possibly by the stabilisation of the TfR1 IRE by IRP - or decreased degradation of the protein, remains unclear[206].

1.5.3 Ferroptosis inhibitors

There are two main classes of known ferroptosis inhibitors: radical trapping antioxidants (RTA) and lipoxygenase inhibitors.

RTAs are used to reduce the accumulation of ROS by breaking the autoxidation chain reaction. The main natural RTA is Vitamin E which possesses the greatest biological activity in vitro and has been shown to suppress ferroptosis. In some genetic studies, where GPX4 was knocked-out in murine endothelial cells, these did not function correctly if the mouse was fed a low vitamin E diet[211]; in another study Vitamin E supplementation was able to restore antiviral and antiparasitic T cell responses[212]. Liproxstatins and ferrostatins were identified through high-throughput screening following RSL3 and erastin ferroptosis induction, respectively. Although they also have some lipoxygenase inhibitor functions, their ability to slow lipid hydroperoxides accumulation was shown to be associated with their RTA ability. Although they were shown to react approximately 10-fold more slowly than vitamin E with peroxyl radicals, they were significantly more reactive in lipid bilayers, thus explaining the higher potency for ferroptosis inhibition[213]. The highest potency is thought to be associated with their transformation to nitroxides, another class of potent RTAs[214,215]. In this thesis project, ferroptosis was induced with RSL3 and therefore liproxstatin-1 (LIP1) was used.

ACSL4 inhibitors on the other hand work by inhibiting this enzyme, which as discussed previously is involved in the preferential oxidisation of arachidonic and adrenic acid rich phospholipids, by enriching cellular membranes with these fatty acids. ACSL4-deficient cells were also shown to be less sensitive to GPX4 inhibition induced ferroptosis[189]. Administration of ACSL4 inhibitor Rosiglitazone before ischaemia was also shown to reduce the ferroptotic damage in lung ischemia-reperfusion injury[216]. Another recent study showed a similar effect with the same inhibitor but in a model of murine stroke, where it was shown to promote neurological function[217].

Iron chelators are also considered ferroptosis inhibitors as they block the iron-dependent increase of ROS by either removing iron from the labile iron pool, or directly removing iron ions from the active site of enzymes such as ALOX, thus inactivating them. They have been shown to block ferroptosis both in vitro and in vivo through these different mechanisms[181]. In a model of spinal cord

injury, it was suggested that deferoxamine (DFO), an iron chelator, can promote repair spinal cord injury[218].

1.5.4 Detection of ferroptosis

There is no single marker for ferroptosis. In the literature detection of ferroptosis is carried out through confirming two or more biomarkers' changes, following induction or inhibition of ferroptosis. Chen et al., 2021 have summarised the key biomarkers of ferroptosis in a review, but below is a further summary of some of the most relevant ones that can be used to detect ferroptosis in vitro[219].

Reactive oxygen species (ROS) increase, which then results in lipid oxidation, is one of the main hallmarks of ferroptosis. To measure ROS fluorescent probes like H_2DCFDA or C11-bodipy can be used and can be detected either through a plate reader or flow-cytometry, or through high-throughput imaging. Readily available lipid peroxidation kits (such as the MDA kit) can be used to assess the resultant oxidation of lipid following ferroptosis induction.

The other main hallmark of this regulated form of cell death is, indeed, reduction of viability. This can be assessed in some cell types through an MTT assay; however, this is not always possible for some cell types that have low metabolism rate. Propidium Iodide staining assessed through flow cytometry is more accurate and can be used in conjunction with AnnexinV to exclude that the cell death observed is apoptosis.

Accumulation of iron is another key hallmark following ferroptosis induction. This can be measured through Prussian blue, iron-sensitive probes and ion-coupled plasma mass spectrometry, methods discussed in a previous section.

GPX4 inhibition through RSL3 has been shown to lead to a decreased protein levels of this enzyme through Western Blot, which are rescued if liproxstatin-1 is used as well[220]. Its activity can be detected through commercially available kits either measuring its decreased activity, or by measuring the substrate levels (glutathione – GSH). Some experimental evidence showed that GSH

levels are not as affected with RSL3 as with erastin, which leads to cysteine starvation, thus inhibiting the synthesis of GSH indirectly[203].

Finally, CD71 has been recently shown to be a marker of ferroptosis and therefore raised levels of this iron-related receptors are associated with ferroptosis induction[206].

As aforementioned, these markers are often used in combination to assess ferroptosis. Additionally, correct controls considering induction and inhibition of this pathway need to be clearly used to assess whether the cells are undergoing this form of regulated cell death.

1.5.5 Ferroptosis in lung disease

Ferroptosis has recently been implicated in the pathogenesis of lung diseases, however the role it plays in ILD remains unclear.

In a study using a radiation-induced lung fibrosis model, it was shown that ferroptosis inhibitor liproxstatin-1 alleviated fibrosis by reducing collagen deposition in lung tissue. This was shown to occur through downregulation of TGF-β1 by the inhibitor activating the Nrf2 pathway, thus reducing ROS production[221].

Another study suggested that cigarette smoke induced epithelial cell ferroptosis in a model of COPD through GPX4 modulation as seen in the genetic mouse models. This group observed an increase in NCOA4, a selective cargo receptor for ferritinophagy, leading to release of free iron and increase lipid peroxidation during cigarette smoke exposure[10]. They observed the increase in NCOA4 in COPD lung tissues compared to control and negatively correlated it with lung function, supporting a link between ferritinophagy and prognosis. This is in contrast with other studies that showed degradation of ferritin promotes ferroptosis[207].

In asthma, an iron-loading phenotype was observed in BAL cells and decreased non-heme bound iron levels in the BAL fluid and this was correlated with severity of disease[5]. Moreover, they found that both TFR1 and DMT1 were elevated in airways and negatively correlated with lung function, thus

confirming this iron accumulation phenotype. However, this study did not investigate ROS levels, thus the role of ferroptosis and asthma remains unclear. Nevertheless, evidence from bronchoscopic brushing of patients with controlled asthma showed co-localisation of a scaffolding protein which was found to regulate ferroptosis, PEBP1, with a type of lipoxygenase, ALOX15, which together leads to the generation of lipid peroxidation[205].

It is unclear whether ferroptosis acts as a protective mechanism in lung disease or leads to further injury through the activation of pro-inflammatory pathways. ROS-induced damage is one of the critical inflammatory events in many diseases, such as fibrosis, and it is also one of the major triggers of ferroptosis. However, ferroptosis being a regulated-form of cell death, may be involved with the disposal of this ROS-producing dysfunctional cells. Whether this is then managed correctly by the tissue, dampening further damage from these oxidative species or whether it causes a pro-inflammatory cascade remains unclear. Studies have shown that both iron and ROS are increased in IPF compared to controls[172,222]. Whether ferroptosis is impaired in IPF is one of the questions that this thesis attempts to answer.

1.6 Hypothesis and aims

The main goal of this study was to further understand and characterise the role of iron metabolism and ferroptosis in alveolar macrophages of fibrotic ILD patients and to elucidate its potential role in progression and pathogenesis of disease.

The overarching hypothesis is that iron accumulates in AM of fibrotic lungs, but these cells are resistant to ferroptosis and therefore remain viable and acquire a pro-fibrotic phenotype.

The main three hypotheses in this study are:

1. Iron accumulates in alveolar macrophages of fibrotic ILD patients.
2. Iron regulatory pathways are altered in alveolar macrophages of progressive ILD.
3. Macrophages are resistant to ferroptosis compared to other cells.

Chapter 2 - Materials and Methods

2.1 Ethical Approvals

The study is part of the Edinburgh Lung Fibrosis Molecular Endotyping (ELFMEN) study (which is registered (NCT04016181) and has been approved by University of Edinburgh/NHS Ethics Committee (REC 17/ES/0075). All patients that participated in this study had been fully informed and consented.

The phlebotomy of healthy volunteers was approved by the Lothian Local Research Ethics committee AMREC Reference number 20-HV-069. Volunteers gave full informed consent to participate.

2.2 Bronchoalveolar lavage procedure and processing

Bronchoalveolar lavage was collected by a standardised clinical protocol. Briefly 160- 240ml saline was instilled into the right middle lobe in 40ml aliquots and aspirated via suction. BAL fluid was transferred to a sterile Teflon pot and kept on ice and processed within 2 hours of collection. The fluid was strained through a CorningTM 40um cell strainer, collected into 50ml BD falcon tubes and centrifuged for 10mins at 400x*g* at 4^{o}C. The total volume was recorded, and the cells counted using a Chemometec nucleocounter. If the fluid was blood-tinged, red blood cells were lysed by resuspending cells in 2ml of Biolegend Red Blood Cell Lysis buffer for 10 minutes at room temperature. DPBS without Magnesium or Calcium (DPBS-/- ; Gibco, 14190250) was then added to wash the cells. The wash was performed with a centrifugation at *400g* for 10 minutes. The cells were resuspended in IMDM w/o phenol red (GIBCO, Ref: 21056-023) at appropriate concentration (5x10^{6}/ml). The cellular yield varied between patients but was on average 16.5x10^{6} cells.

2.2.1 Cytospins

Cytospins were carried out with 1x10^{5} cells per slide (10 slides total) with a ThermoScientific Shandon Cytospin 4 at *300g* for 3 minutes. Cells were fixed with methanol (VWR Chemicals). The slides were left to air dry. One slide for each patient was used for differential counting and stained with the Wright's stain technique involving eosin and methylene blue dyes. Over 200 cells were

then counted and differentiated it according to morphology. Some slides were also stained for Prussian blue as described below.

2.2.2 Alveolar macrophage culture

Cells were plated in a standard 24 well plate (flat bottom with low evaporation lid, tissue culture treated, polystyrene) at $5x10^5$ cells per well and left to adhere for 1 hour in IMDM w/o phenol red. The supernatant was then removed, and the cells washed with DPBS -/- through pipetting, to ensure non-adherent cells were removed.

2.2.3 Gene expression quantification

For gene expression assessment cells (at least $1x10^6$ cells depending on availability) were prepared as alveolar macrophage culture protocol (above). The RNA isolation step below was then performed within the wells.

2.2.3.1 RNA isolation

Surfaces and instruments were cleaned and sprayed with RNAzap (RNaseZap™ RNase Decontamination Solution; Catalog number: AM9780). If cells were used, an appropriate volume of β-mercaptoethanol (β-ME – 2-Mercaptoethanol (M3148-100ml), Sigma LifeSciences) was added to RLT buffer from a QIAGEN RNeasy mini kit (10μl of β-ME to 1ml of RLT) (Cat No./ID: 74106 - QIAGEN). The solution was directly added to the culture well and pipetted to ensure lysis of cells. The same volume of 70% ethanol was added to the well, given a quick mix and the whole volume loaded onto RNA columns from the kit. The columns were then spun for 30 seconds at 10'000 RPM. The volume collected at the bottom was discarded and 700μl of RW1 wash buffer added back to the column, followed by a centrifugation for 30 seconds at 10'000 RPM. The collected liquid was discarded and 500μl of RPE buffer (which contains 70% ethanol) added back to the column, to fix the RNA to the column. Following a spin at 30secs at 10'000 RPM and removal of solution from column, the previous step with RPE was repeated and the column spun at 10'000 for 2 minutes. The bottom tube was emptied, and the column spun for another 2 minutes with no solution added to ensure complete removal of ethanol. The bottom tube was discarded, and the column placed in

a clean collection tube or Eppendorf. A small amount of RNase free water was decanted to ensure no contaminations and 30μl of it was added to column. A spin for 30 seconds at 10'000 RPM was carried out, the bottom tube closed, labelled and placed on ice and the column discarded. The sample containing the RNA was taken immediately to the ThermoFisher Nanodrop™ 2000 and RNA concentration measured at 260/280. The machine was blanked with 2μl RNase water ensuring the correct settings; then 2μl of RNA sample was added and both concentration and quality recorded. The RNA was then placed back on ice if cDNA synthesis was carried out immediately after or frozen on dry ice, stored at -20°C overnight and then brought to -80°C.

2.2.3.2 cDNA synthesis

The QIAGEN QuantiTect Reverse Transcription Kit (ID: 205311, QIAGEN) was used to make cDNA from 1μg of RNA. The quantity was calculated from the nanodrop readings and the volume made up to 12μl with RNase-free water in a 200μl Eppendorf. If 1μg was not present in the sample, 12μl of RNA was used directly. The buffers were defrosted on ice and 2μl of gDNA wipeout buffer added to the tube. Using a C1000 Touch™ Thermal Cycler an initial incubation at 42°C (lid temperature of 110°C) for 5 minutes was carried out. A master mix was created with 1μl of RT, 4μl of Quantiscript RT buffer and 1μl RT primer mix per sample. Following the previous incubation, 6μl of master mix was added to the 200μl Eppendorf and the PCR machine set to the following cycle: 42°C for 30 minutes, 95°C for 3 minutes and 4°C infinite time. The cDNA was then stored at -20°C.

2.2.3.3 qPCR

The cDNA was diluted 1:10 in nuclease-free water (to 20μl of cDNA, 180μl of nuclease-free water). Using genes of interest and β-actin as a housekeeping gene, primer-containing master mixes were prepared. These contained 5μl of SYBR green (which contains buffer, dNTPs, thermostable DNA polymerase and the SYBR green dye) (SYBR® Green PCR Master Mix Ref:4309155, Applied Biosystems by ThermoFisher Scientific) and 1μl of primer of gene of interest (0.5μl forward and 0.5μl reverse primer (Pre-designed primers from

Sigma-Aldrich)). Primers of interest are shown in the table below (Table 2.2.3-1) . In a 384 well plate, 6μl of primer mix was added, followed by 4μl of diluted cDNA. Once completed the plate was securely sealed with a microamp optical adhesion film and spun at 200G for 2 minutes to ensure removal of air bubbles. Using the ABI7900 384-well qPCR machine the program was set to SYBR green detection and a dissociation stage added to the cycles. The Ct values were transferred to an excel file and average between duplicates calculated. The -dCt was then calculated by subtracting the Ct of the gene of interest from the housekeeping gene (Actin-β) Ct. The gene expression was then calculated as the 2^{-dCT}.

Table 2.2.3-1 - Pre-designed primers for gene of interest from Sigma-Aldrich

Primer	Code	Sequence
ACTB	SY190821288-018; SY190821288-017	5'-ATGATCTGGGTCATCTTCTC; 5'-GACGACATGGAGAAAATCTG
MRC1	SY180833543-093; SY180833543-094;	5' -AAATTTGAGGGCAGTGAAA-G; 5'-GGATTTGGAGTTTATCTGG-TAG
CD163	SY190719392-016; SY190719392-015	5'-TCCTTCTGGAATAGATTGGGG; 5'-AGTCTGCTCACGATACATAG
CD80	SY180828760 – 044; SY180828760 - 045	5'-AGGAGGAATGAGAGATTGA-G 5'-AGACCTTCAGATCTTTTCAGC
CD86	SY180828760-046; SY180828760-047	5'-CCCACTGAATTTTGTGTACC; 5'-CTCTAGAGCATAGTAATCA-CAC
FTH1	SY180438804-059; SY180438804-060;	5'-CAGGATATCAAGAAACCAG-AC; 5'-AGTTCCAGTAGTGACTGAT-TC
SLC11A2	SY180438804-064; SY180438804-065	5'-GACTTGACTAAGGCAGAATG; 5'GAGTATGTTACAGTGAAAC-CC
SLC40	SY180438804-062; SY180438804-061	5'-GTTGTAGTAGGAGACCCATC; 5'-AAAGATACTGAGCCAAAACC
TFRC	SY190108094-024; SY190108094-025	5'-AAGATTCAGGTCAAAGACA; 5'-CTTACTATACGCCACATAA-CC

2.3 Cell lines

Three different cell lines were cultured for different experiments. All cells were routinely tested for mycoplasma infection.

2.3.1 HT29

HT29 is a human cell line with epithelial morphology, derived from colorectal carcinoma (ATCC HTB-38). They were cultured in DMEM (DMEM + 4.5g/L D-Glucose, 0.11g/l Sodium Pyruvate, Ref: 21969-035, Gibco) with 10% FBS (Fetal Bovine Serum, Ref:35-015-CV, Corning), 1% L-Glutamine (L-glutamine 200mM; Ref: 25030-024, Gibco) and 1% Pen/Strep (Penicillin Stremptomycin; Ref:15140-122, Gibco). They were passaged every 2-3 days according to confluency. To do so the supernatant was first discarded from the flask (T-75, Corning® 75cm² U-Shaped Canted Neck Cell Culture Flask with Vent Cap, number: 430641U). DPBS was added to cover the bottom of the flask and wash the cells. Following a couple of agitations of the flask with DPBS, this was discarded and 10ml of trypsin (0.05% Trypsin-EDTA, Ref:25300-054, Gibco) added. The flask was then placed in the incubator for 5 minutes (37°C; 5% CO_2). The cells were then inspected under the microscope to observe any detachment. The flask was vigorously hit with a hand to ensure resuspension. Trypsin was then neutralised by addition of 10ml of full media (DMEM with FBS, L-glutamine and Pen/Strep as above). The cells were then centrifuged at 300*g* for 5 minutes and resuspended in 10ml of media. 2ml of cell in suspension was added to 18 ml of media inside a new sterile flask.

2.3.2 THP1

THP1 is a human monocytic cell line, derived from acute monocytic leukaemia (ATCC TIB-202). They were cultured in RPMI (RPMI Medium 1640, Ref: 31870-025, Gibco) with 10% FBS (Fetal Bovine Serum, Ref:35-015-CV, Corning), 1% L-Glutamine (L-glutamine 200mM; Ref: 25030-024, Gibco) and 1% Pen/Strep (Penicillin Stremptomycin; Ref:15140-122, Gibco). They were passaged every 4 days according to confluency. To do so the cells in suspension were transferred from the flask (T-75, Corning® 75cm² U-Shaped Canted Neck Cell Culture Flask with Vent Cap, number: 430641U) to a 50ml BD Falcon Tube and spun down at 300*g* for 5 minutes. The supernatant was then discarded, and cells resuspended in 10ml of fresh complete media. 2ml of cells were added to 23ml of full media in a new sterile flask.

For experiments, THP1 were differentiated from monocyte to macrophage by resuspending the monocytes in a 100nM solution of PMA (Phrobol 12-myristate 13-acetate, P8139y, Sigma) in full RPMI media for 24 hours. The cells acquired an elongated morphology. All THP1 cells used in this thesis have been differentiated by PMA.

2.3.3 RAW 264.7

RAW 264.7 is a mouse macrophage cell line, derived from Abelson murine leukemia virus-induced tumour (ATCC TIB-71). They were cultured in RPMI (RPMI Medium 1640, Ref: 31870-025, Gibco) with 10% FBS (Fetal Bovine Serum, Ref:35-015-CV, Corning), 1% L-Glutamine (L-glutamine 200mM; Ref: 25030-024, Gibco) and 1% Pen/Strep (Penicillin Stremptomycin; Ref:15140-122, Gibco). They were passaged every 4 days according to confluency. To do so the supernatants from the flask (T-75, Corning® 75cm² U-Shaped Canted Neck Cell Culture Flask with Vent Cap, number: 430641U) were discarded and 10ml of fresh full media was added. The cells were then scraped from the bottom of the flask and collected in a 50ml BD Falcon Tube and spun down at *300g* for 5 minutes. The supernatant was then discarded, and cells resuspended in 10ml of fresh complete media. 2ml of cells were added to 18ml of full media in a new sterile flask.

2.4 Monocyte-derived macrophages

2.4.1 Isolation of human monocytes

Whole blood (40ml) from a healthy donor was collected into a falcon tube with 4ml of 3.8% sodium citrate to prevent coagulation. The blood was then centrifuged (350*g*, 20 minutes, 0 brake and 1 acceleration) to separate platelet rich plasma – which was collected and stored in glass vials with calcium chloride at 37°C - from the cells at the bottom. To the bottom layer 6ml of 6% dextran (T500, 5510 0500 8007) was added per 50ml and topped up to 50ml with 0.9% sodium chloride (UKF7124, Gibco Life Technologies). The erythrocytes were allowed to sediment for 20 minutes and the top layer containing the rest of the cells was collected, without disturbing the buffy coat layer, in a separate tube. This was then topped up with sodium chloride and

centrifuged (350*g*, 6 minutes, full acceleration, full brake) to form pellet. A Percoll (GE Healthcare) gradient is prepared by adding 3mls of 10X PBS to 27ml of Percoll to create Percoll stock. The 81% layer was prepared with 8.1 ml of Percoll stock and making it up to 10ml with PBS; the 68% layer was prepared with 6.8ml of Percoll stock and making it up to 10ml with PBS; the 55% layer was prepared with 6.8ml of Percoll stock and making it up to 10ml with PBS. They were then layered by taking 4ml of 81% Percoll and adding 3ml delicately in a 15ml BD Falcon tube. The next 68% Percoll gradient (3ml) was added delicately on top of the 81% layer by using a needle or a strippette, ensuring no disturbance or mixing occurred with the layer below. Once the cells were spun down, the supernatant was discarded, and the pellet gently flicked and resuspended by adding 3ml of the 55% Percoll gradient and mixing delicately. The final layer was then delicately added on top of the 68% gradient, ensuring no mixing. The cells on the gradient were then centrifuged at 720G for 20 minutes (no brake, no acceleration). This ensures separation of PBMC, neutrophils and red blood cells. The PBMCs were collected, washed with DPBS w/o Mg,Ca (Gibco) and further purification to monocytes was carried out using a Pan Monocyte Isolation Kit (Miltenyi Biotec). Cells were resuspended in 4µl of macs buffer (20ml of DPBS with 80µl EDTA (Sigma-Aldrich, E8008) and 100µl of autologous serum) per 10^7 total cells. 10µl of FcR Blocking Reagent per 10^7 total cells is added, followed by 10µl of Biotin-Antibody Cocktail per 10^7 total cells. It was then mixed well and incubated in the fridge for 5 minutes. 30µl of macs buffer was added per 10^7 total cells and then 20µl of Anti-Biotin MicroBeads per 10^7 total cells. This was mixed well and incubated for 10 minutes in the fridge. LS positive selection columns (Order No: 130-042-401; Miltenyibiotec) were used on a MidiMACS™ Separator (Order No: 130-042-302). The column was positioned on the magnetic field of the separator and 3ml of Macs buffer added to it to prime it. Once the buffer run through it was discarded and a fresh 15ml falcon tube positioned underneath. The cell suspension was added onto the column and the flow-through collected. This represents the enriched monocyte fraction. The column was then washed 3 times with 3ml Macs buffer and the flow

through collected with the cells. The cells were then spun down at *300g* for 5 minutes and resuspended in full media (IMDM (Lot: 12440053), with 10% FBS (Fetal Bovine Serum, Ref:35-015-CV, Corning), 1% L-Glutamine (L-glutamine 200mM; Ref: 25030-024, Gibco) and 1% Pen/Strep (Penicillin Stremptomycin; Ref:15140-122, Gibco).

2.4.2 Macrophage stimulation

The purified monocytes were then plated in low adherence 24 well plates – $0.5x10^6$ per well – and treated with MCSF or GMCSF (R&D, 216-MC/CF) at a concentration of 100ng/ml. The cells were cultured for 5 days. On day 5 the supernatant was removed and then treated with IL4 (20ng/ml; R&D, 204-IL) and IL10 (20ng/ml; R&D, 217-IL) or IFNγ (50ng/ml; Abcam, ab192085) and LPS (100ng/ml; Sigma) for another 2 days. Following stimulation, the cells were then used for different applications, such as qPCR or flow cytometry, described below.

2.5 Flow Cytometry

Cells were collected, washed with Gibco DPBS and resuspended accordingly in FACS buffer (Gibco DPBS with 0.5% BSA (Bovine Serum Albumin, No:A8806, SigmaAldrich). If the cells were adherent they were detached depending on the cell type: HT29 were left for 5 minutes in trypsin (0.05% Trypsin-EDTA, Ref:25300-054, Gibco) in the incubator at 37°C (5% CO_2); THP1 and primary macrophages for 10 minutes in trypsin in the incubator at 37°C (5% CO_2); RAW were resuspended by vigorous pipetting. The stained sample had $2x10^6$ cells, $2x10^5$ for single stain or isotype and $5x10^5$ for unstained, all resuspended in 50µl of FACS buffer. 2.5µl of Fc Receptor Blocking Solution (Human TruStain FcX) was added to each tube and incubated for 10 minutes at 4°C. 1µl of relevant antibodies or isotypes was added to each tube and incubated for 30 minutes at 4°C. Antibodies used are shown in Table 2.5-1 below. Cells were washed with DPBS (*400g* 4°C). They were then resuspended in 500µl of FACS lyse solution (Biolegend RBC Lysis/Fixation solution diluted 1:10 with deionised water) and incubated for 10 minutes at room temperature. The FACS lyse was washed off with FACS

buffer and the samples centrifuged at 1200 RPM for 5 minutes. The samples were then resuspended in 250μl of FACS lyse and stored in the dark at 4°C until flow cytometry processing. Samples were analysed within 24 hours. Prior to analysis, the cells were washed with DPBS at 1200 RPM for 5 minutes and resuspended in 300μl of FACS buffer. The samples were processed on the BD LSRFortessa™ Cell Analyzer and analysed on FlowJo v10, where compensation was carried out on either single stains or on Invitrogen™ UltraComp eBeads™ Plus Compensation Beads. Gating strategy was initially carried out by selecting for cells (excluding debris), and then by selecting singlets (SSC-FSC plot). Details of each gating strategy is shown in relevant chapters.

Table 2.5-2.4.2-1 - Antibodies used in flow cytometry

Antibody/Isotype	Clones	Brand
Alexa Fluor 700 anti-human HLA-DR	Clone: L243; Isotype: Mouse IgG2α,k	BioLegend
APC Anti-human CD71	Clone: CY1G4; Mouse IgG2α K	BioLegend
APC Mouse IgG2a, K isotype control	Clone: MOPC-173	BioLegend
APC anti-human CD163	Clone: GHI/61	BioLegend
PE anti-human CD206 (MMR)	Clone 15-2	BioLegend
APC/Cy7 anti-human CD163	Clone GHI/61	BioLegend
APC/Cyanine7 Mouse IgG1, κ Isotype	Clone: MOPC-21	Biolegend
APC Anti-mouse CD71	Clone RI7217 Isotype: Rat IgG2α K	BioLegend

2.6 Iron quantification

2.6.1 Prussian Blue and the Golde Score

Cytospins were placed in a deionized water soaked sequenza rack and adherence ensured. Two washes with deionized water were performed and a

working solution of Prussian blue (Abcam Iron Stain Kit) was prepared. Equal parts of 2% hydrochloric acid and potassium ferrocyanide solution. 120μl of working solution was added to each slide for 1 hour at room temperature. The slides were then washed three times for 5 minutes with 120μl of deionised water. Using the nuclear fast red solution provided in the kit, the slides were counterstained for 5 minutes and then washed three times with deionised water. The slides were allowed to air dry for 20 minutes and then a coverslip was mounted with DPX (SigmaAldrich, 44581). The slides were then imaged on Invitrogen™ EVOS™ XL Digital Inverted Brightfield and Phase Contrast Microscope and analysed with ImageJ. The Golde Score was calculated according to Golde et al[180]. For BAL cells, alveolar macrophages were identified based on nuclear morphology and size. Approximately 300 cells per slide were counted and scored according to the scoring system below. The weighted score of the cells, was divided by the total number of cells and multiplied by 100, to calculate the Golde Score for 100 cells, with 0 being the minimum score and 400 being the maximum.

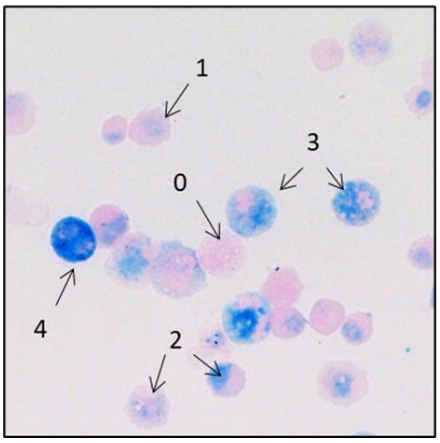

Score per cell

0 = no blue colour,

1 = faint blue staining in cytoplasm,

2 = dense blue colour in minor portion of cytoplasm or medium colour intensity throughout cell,

3 = deep blue staining in most of cytoplasm,

4 = cell filled with haemosiderin;

$$Golde\ Score = \frac{Weighted\ Score}{Total\ N\ of\ cells}\ x\ 100$$

where Weighted Score is the number of cells with the above score times the score itself, and $N > 300$ cells

2.6.2 Staining fixed BAL cells for iron with TRX-Puro

Cells were plated in a 96 well clear, flat bottom, black plate and treated with deferoxamine (DFO – 250μM) (iron chelator) (Deferoxamine Mesylate, Ab120727, Abcam) or ferric ammonium sulphate (FAS – 200μM) (Ammonium Iron(II) sulphate hexahydrate, ACS reagent, Code:423721000) accordingly. Trx-puro or puromycin (positive control) (Puromycin Dihydrochloride, A1113803, ThermoFisher) were added at 1μM to selected wells and incubated at 37°C for 4 hours. Wells were then washed twice with DPBS and once with

DPBS with 0.1% triton (Triton ® X-100; Sigma Ultra, SigmaAldrich). Anti-puromycin antibody (1:500 – Anti-puromycin, clone 12D10 mouse monoclonal, EMD Millipore Corp) in 10% FBS (Fetal Bovine Serum, Ref:35-015-CV, Corning) in DPBS with 0.1% Triton was added for 30 minutes at 37°C. It was then washed off with the DPBS with 0.1% Triton and then stained with anti-mouse secondary (1:200) (Goat anti-Mouse IgG (H+L) Cross-Adsorbed Secondary Antibody, Alexa Fluor 568, ThermoFisher Scientific), Hoechst (10μg/ml – Hoechst 33342 20mM Prod#62248, Thermo Scientific) and HCS CellMask™ Green Stain (1:10000 – Ref: H32714, Invitrogen by ThermoFisher Scientific) in 10% FBS in DBPS with 0.1% triton for 30 minutes at 37°C. The cells were then washed with DPBS and stored in DPBS at 4°C. The plate was then processed with the PerkinElmer High Content Imaging System Operetta and analysed with the companion software Columbus following the protocol hereby described

Through the Columbus software, specific features can be selected and either excluded or included for assessment. Through the next steps, cells were selected based on their nuclei and cytoplasm, and TRX-Puro fluorescent intensity assessed solely in the cytoplasm.

1. 13 non-consecutive fields were selected per well - Hoechst (blue), Cell Mask (green), TRX-Puro (red)

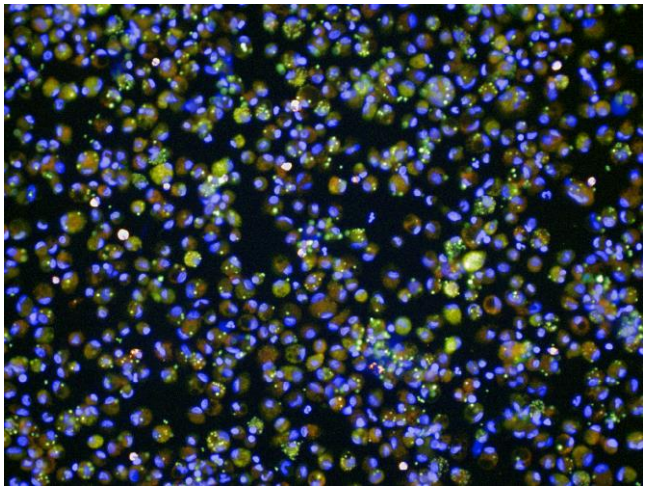

2. Nuclei selected based on Hoechst

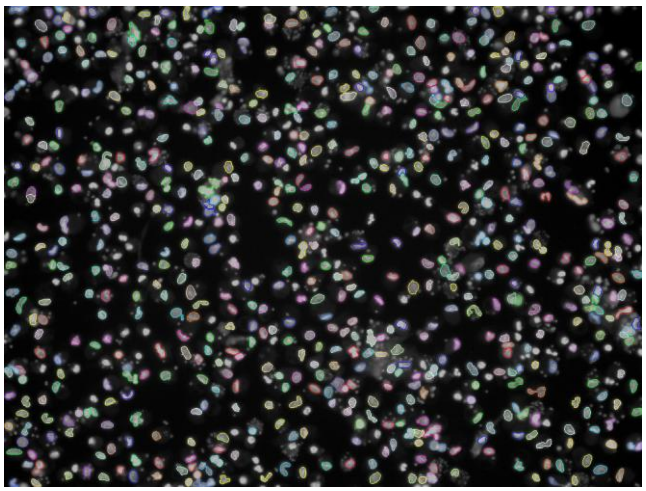

3. Exclude nuclei with intensity of >14000 and nuclei roundedness (>0.7)

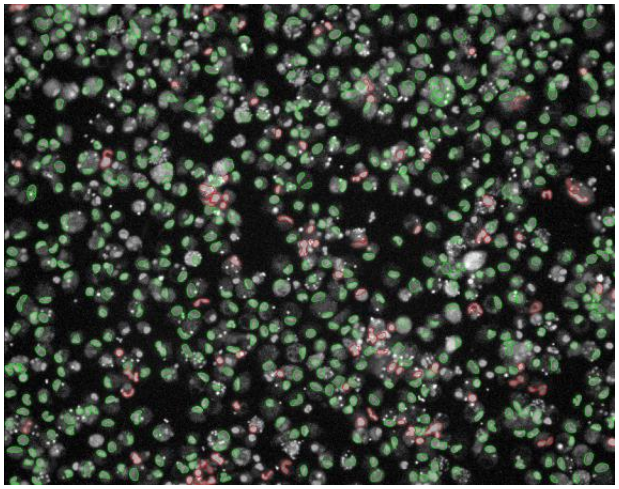

4. Selected cytoplasm with AF488 (excluding intensities >2000)

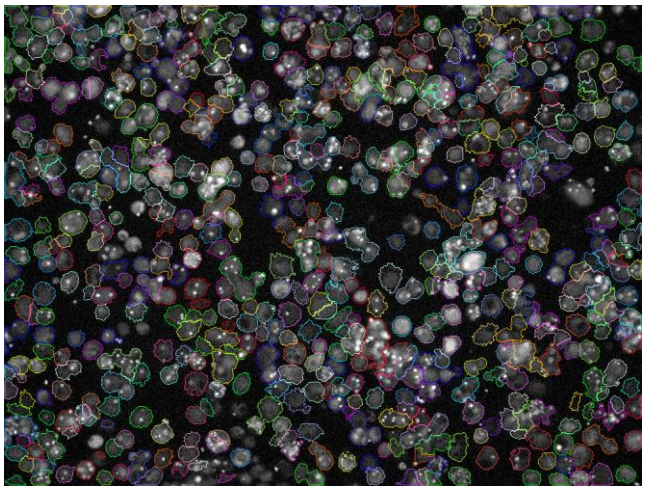

5. Calculate AF568 fluorescence intensity of cytoplasm (cell – nucleus)

2.6.3 Staining live BAL cells for iron with FIP1

Following processing, BAL cells were washed with DPBS without magnesium and calcium (Gibco, 14190250). They were then incubated in phenol red-free IMDM + 0.2% BSA, Pen/Strep (Penicillin Streptomycin; Ref:15140-122, Gibco) and L-glutamine (L-glutamine 200mM; Ref: 25030-024, Gibco) for 45 minutes to select for macrophages by adhesion and washed to remove non-adherent cells. This was carried out in black imaging plates (Tissue Culture treated microplate, black, µClear, with lid. (Greiner Bio-One Inc.; 655090) IMDM was added and incubated overnight. For chelation experiments the cells were incubated overnight in 240µM DFO (deferoxamine) (Deferoxamine Mesylate, Ab120727, Abcam). Fe^{2+} supplementation experiments through the addition of 200µM of FAS (Ammonium Iron(II) sulphate hexahydrate, ACS reagent, Code:423721000) were incubated for 90 minutes. Cells were washed twice with DPBS and FIP1 (1µM) was incubated with the cells for 30 minutes at 37°C. Cells were either imaged directly on a Leica Confocal SP5 Microscope on an 8-well plate or analysed on the 5LSR Fortessa flow cytometer, at emission of 515nm. For flow cytometry the cells were removed from the wells by adding a 2mM EDTA solution (with 0.1% BSA in DPBS -/- and left on ice for 10 minutes, prior to resuspension in DPBS -/-. DAPI (1:1000) was added as a live stain and cells were immediately analysed.

FIP1 activation was tested previously with 10µM and 100µM FAS at 37°C over time in a 96well plate on a plate reader (Cytation3 Imaging Reader, Biotek) at 515 and 556nm. FIP1 was added to the wells containing the two different concentrations of iron (FAS) and immediately imaged over 90 minutes.

2.6.4 Iron level assessment of BAL cells through ICP-MS

ICP-MS is a mass spectrometry method used to detect trace levels of ions. It uses inductively coupled plasma to ionise the samples and then detected. Cells were resuspended in 250µl of pure Nitric Acid and were processed by Dr Lorna Eades at the Mass Spectrometry facility in King's Buildings. The samples were left to sit for about 30 minutes and then they were sonicated for

1 minute and let to sit for another minute to ensure that all iron was in suspension. The samples were then spun down and 100µl removed. This was then diluted with 2.9ml of further acid to increase the counts detected by the ICP-MS. The counts were then averaged per $1x10^6$ cells.

2.7 RNAseq

Total RNA was extracted from 4 Progressors and 6 Non-Progressor using RNeasy mini columns. Full demographics in relevant chapter (Chapter 4). Progressors were defined as the patients who had a greater than or equal to 10% decline in lung function (FVC) or death within 12 months from BAL. The non-progressors were the patients who had less than 10% change in their FVC in 12 months. Libraries were prepared using Illumina Ribo-Zero and then the RNA converted into sequencing-ready libraries for Illumina sequencing systems using TruSeq Stranded by Oxford Genomics Centre.

The analysis was carried out by FIOS Genomics. The quality of the sequencing reads was assessed using FastQC. Reads were aligned to human transcriptome build GRCh38 using STAR aligner and the number of mapped read-pairs were counted based on the GENCODE v36 annotation. Outliers were excluded if they failed 2 or more of the 4 objective statistical tests. A summary of the sample's alignment showing the percentage count of the input read-pairs that either mapped uniquely to the genome (% Uniquely mapped), mapped more than once to the genome (% Multimapped) or did not map to the genome (% Unmapped), are shown in Figure 2.7.1A. Figure 2.7.1B shows the summary of percentage of read-pairs that mapped uniquely to the genome either by mapping unambiguously to a single gene (% gene), or mapped to more than one gene (% ambiguous) or did not overlap any gene models in the genome annotation (% no features).

For the association tests, the subset filtered raw data of the ten samples of interest were processed by normalising the count data using trimmed mean of M-values normalisation. To facilitate investigation of overlapping changes in gene expression across the contrasts, a relaxed statistical threshold of unadjusted $P < 0.05$ was selected to identify differentially expressed genes

(DEGs). The results show unadjusted P-value threshold meaning that the proportion of potentially false discoveries are not accounted for. Functional enrichment analysis was performed in order to identify Reactome pathways (www.reactome.org) or Gene Ontology (GO) terms that were enriched in differentially expressed genes (DEGs). Significant enriched genes were identified as over-represented in the Reactome or in the Gene Ontology terms through a conditional hypergeometric test with a P<0.05. This test allows to identify the enriched genes even if the child-terms are removed, thus assessing for a loss in enrichment independently.

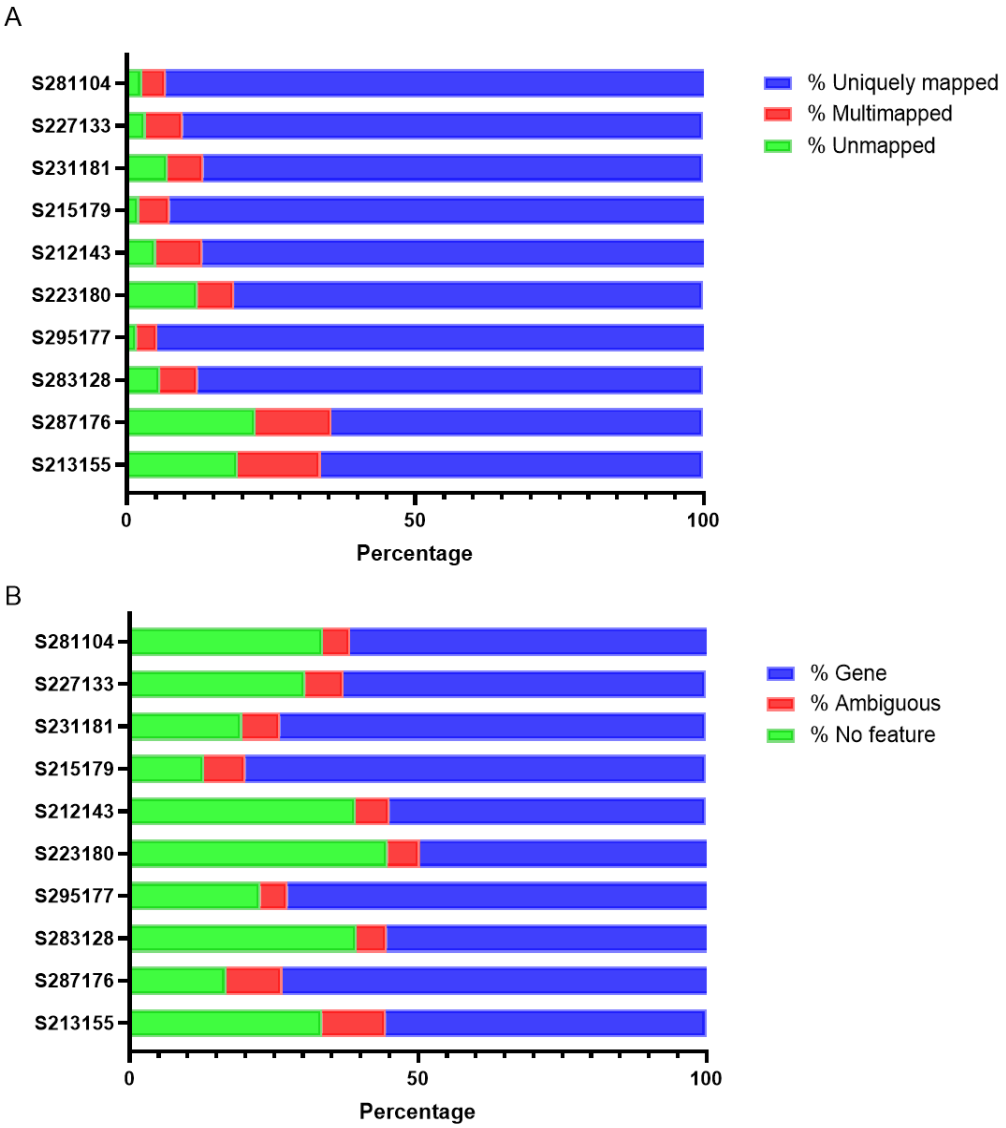

Figure 2.7.1 – Summary of (A) alignment to human transcriptome GRCh38 using STAR aligner and (B) mapping of the pair reads to GENCODE v36 annotation.

2.8 Ferroptosis assays

Cells were plated in sterile flat 96 well plates (96 well cell culture plate, flat bottom with low evaporation lid, tissue culture treated, polystyrene) (RAW and HT29 – $2x10^4$ cells, THP1 with PMA (Phorbol 12-myristate 13-acetate, P8139, Sigma) (100ng/ml) $5x10^4$) overnight in duplicates. The cells were then washed with DPBS and in some experiments they were pre-treated with FAS at 100µM for 2 hours in the incubator (37°C; 5% CO2). Ferroptosis was then induced with RSL3 (Merck Life Sciences, SML2234-5Mg) in DMEM for HT29 cells (DMEM + 4.5g/L D-Glucose, 0.11g/l Sodium Pyruvate, Ref: 21969-035, Gibxco) or RPMI for RAW/THP1 cells (RPMI Medium 1640, Ref: 31870-025, Gibco) for different lengths of time (2, 4, 6, 12, 18, 24 hours) and at different concentrations (10 µM; 5 µM; 1µM). Liproxstatin 1 (LIP1) (Merck Life Sciences, SML1414-5MG) was also used as a ferroptosis inhibitor in some conditions at 1µM.

2.8.1 ROS Assay

Reactive oxygen species were measured through DCFDA (2'7' Dichlorofluorescein Diacetate) (Sigma-Aldrich, Lot 287810). The cells were treated with iron, RSL3 or LIP1 (concentrations and times as above) and then washed with PBS. DCFDA (20µM) and added to relevant wells for 30 minutes at 37°C. Without washing, the cells were read with the Cytation 3 Imaging reader with excitation/emission 485/535nm.

2.8.2 Flow cytometry on the AttuneNxt for viability and CD71 staining

Following induction of ferroptosis as described above, the plates were centrifuged at *400g* for 4 minutes at 4°C to collect all cells. The supernatants were discarded, and cells washed with PBS. Following another centrifugation at *400g* for 4 minutes at 4°C, RAW cells were pipetted up and down to ensure resuspension of cells and then transferred to a round bottom 96 well plate. For HT29 and PMA-polarised THP-1, 50µl of trypsin (0.05% Trypsin-EDTA, Ref:25300-054, Gibco), which had been warmed up to 37°C, was added to each well and left in the incubator for 5 and 10 minutes respectively. Following

this incubation, 50µl of media (DMEM for HT29, RPMI for THP1) with 10% FBS was added to each well to neutralise the trypsin and pipetting up and down was carried out to ensure cells were in suspension. At this stage cells, were transferred to a new round bottom 96 well plate and spun down. The cells were then washed with DPBS (*400g* for 4 minutes) and stained as explained below. The cells were analysed on the Attune flow cytometer.

2.8.2.1 Viability assay with AnxV/PI

Following this wash, cells were resuspended in 100µl of Annexin V (Annexin V, Alexa Fluor™ 647 conjugate, Ref: A23204, Invitrogen by ThermoFisher Scientific; or Annexin-V-FLUOS; Ref:11828681001, Roche Diagnostics GMbH) solution (1:500 dilution in HBSS (Hanks' Balanced Salt Solution+$CaCl_2$+$MgCl_2$; Ref:14025-050; Gibco) with 0.3% $CaCl_2$ (Calcium Chloride, Code: 21097, SigmaUltra, Sigma). The cells were stained for 20 minutes on ice in the dark. Just prior to flow cytometry, 0.5µl of PI (Propidium Iodide Solution, PC code: 1002957359, SigmaAldrich) was added to each well (except AnxV single stain and unstained samples). The Attune Flowcytometer plate function was used to analyse all wells. The analysis was carried out through FlowJo v10 through quadrants. Any PI^+ cell (both $AnxV^-PI^+$ and $AnxV^+PI^+$) were considered late-stage death cells, $AnxV^+PI^-$ cells were considered apoptotic and the double negative population ($AnxV^-PI^-$) was considered live.

2.8.2.2 CD71 staining

Following the previous explained wash, HT29s and RAWs were resuspended in 50µl of DPBS with 1:200 CD71 (APC) antibody or relevant isotype (for information about antibody see Table 2.5-2.4.2-1). Cells were stained for 30minutes on ice in the dark, then washed with DPBS and fixed in 50µl of lysis buffer (1x RBX Lysis/Fixation solution (Cat. No. 422401 Biolegend UK)) for 10 minutes in the dark. The cells were then spun down at *400g* for 4 minutes at 4°C, resuspended in fresh lysis buffer and kept at 4°C in the dark until flow cytometry. Prior to analysis cells were centrifuged and resuspended in DPBS.

2.8.3 Prussian blue

To assess whether any changes in iron were detectable through Prussian blue staining following ferroptosis induction, the cells were treated with relevant treatments as above and then fixed with methanol in the wells for 10 minutes at room temperature. The methanol was then removed, and the wells were left to air dry. Two washes of deionized water were performed and working solution of Prussian blue was prepared according to manual (Abcam Iron Stain Kit): equal parts of 2% hydrochloric acid and potassium ferrocyanide solution. 50µl of the working solution was added to each well and incubated at room temperature for 1 hour. The solution was then removed, and the wells washed with deionised water. 50µl of nuclear fast red solution was added to each well and stained for 5 minutes at room temperature. The wells were then washed with deionised water and left to air dry. They were then imaged on the Invitrogen™ EVOS™ XL Digital Inverted Brightfield and Phase Contrast Microscope and analysed with ImageJ. The Golde Score was calculated as described in section 2.6.1.

2.8.4 GSH Assay

The cells were treated with RSL3, iron or LIP1 and then lifted from the well as described previously. At least $1x10^6$ cells per condition were used. They were collected in eppendorfs and washed with ice cold DPBS (No Ca, No Mg) and analysed according to the ThermoFisher (Invitrogen™) Scientific Glutathione Colorimetric Detection Kit (EIAGSHC). The cells were resuspended in 250µl 5% SSA (1g of aqueous 5-sulfo-salicylic acid dehydrate to 20ml of distilled H_2O. The samples were frozen on dry ice and stored at -20°C. The cells were lysed by vigorous vortexing or by freeze-thaw cycling. They were then incubated at 4°C for 10 minutes, and then centrifuged at 14000G for 10 minutes at 4°C. The supernatants were collected for analysis. The cell lysate samples were diluted by adding 4 volumes of assay buffer and then diluted 1:4 with sample diluent (5% SSA diluted 1:5 in assay buffer).

Standards were prepared in eppendorfs labelled 1 to 6 for a concentration range of 25 µM to 0µM of GSH.

The colorimetric detection reagent was prepared according to instructions with the detection reagent concentrate and assay buffer and depending on number of samples.

The reaction mixture was also prepared according to instructions with NADPH concentrate, Glutathione Reductase Concentrate and Assay buffer. Samples and standards were added to a 96 well plate in excess. With a multichannel 50µl of standards or samples were transferred to new 96 well plate in duplicates. Using a multichannel and another 96-well plate 25µl of colorimetric detection reagent were added to each well containing the samples or standards. Finally, 25µl of the reaction mixture was added to each sample and standard well in the same way. The sides of the plate were tapped to ensure mixing. The plate was then incubated for 20 minutes at room temperature and then the absorbance was read on the plate reader at 405nm. A standard curve was generated from the standards with a four-parameter algorithm and the concentrations for unknown samples derived taking into account dilution.

2.9 Statistical Analysis

Data are presented as mean ± SD unless otherwise stated. Statistical analysis was performed with GraphPad Prism v9 (GraphPad Software, La Jolla, CA, USA). Data were tested for normality and analysis carried out accordingly using one-way ANOVA with Tukey's Multiple Comparison Test, or student t-test, or two-way ANOVA as indicated. Statistical significance was taken at $p \leq 0.05$. Multiple linear regression and multiple logistic regression analysis were carried out with Graphpad Prism v9 as well and are described in more detail in relevant chapters. Sample size for experiments with clinical samples were based on number of available samples and not based on power calculations. Statistical advice was given by Alex Przybylski and Margaret Horne (Statistician, Usher Institute, University of Edinburgh).

Chapter 3 - Iron content in Alveolar Macrophages of IPF compared to non-fibrotic and fibrotic UNC disease.

3.1 Introduction

The presence of iron in alveolar macrophages in interstitial lung disease has not been comprehensively studied. A previous study in IPF patients showed iron accumulation and speculated possible occult pulmonary haemorrhage[172]. Another study in IPF showed increased iron loading and a likely-associated "unrestrained" activation pattern in alveolar macrophages[110]. In this chapter, iron load in macrophages was assessed in patients with IPF, other fibrotic unclassifiable (UNC) and non-fibrotic UNC disease, as determined by a multidisciplinary team (MDT) at diagnosis. A multiple linear regression analysis was performed to determine the association of iron loading with clinical variables (presence of fibrosis, age, sex, smoking etc).

Iron was primarily assessed with the Golde Score[180], an established semi-quantitative measure of iron through Prussian blue staining (see methods). Alveolar macrophages in BAL cytospins were identified based on classical morphology. Although this semiquantitative score is now nearly 50 years old, it is still commonly used in the literature, due to its simplicity and applicability in historical fixed samples[110,137,172,173]. This technique was also compared to three more recent techniques that are more suited to non-fixed or live cells: ICP-MS, TRX-Puro, a reactivity-based probe that can detect Fe^{2+}, and FIP-1, a fluorescent probe sensitive to Fe^{2+}[179,223].

Inductively Coupled Plasma Mass Spectrometry (ICP-MS) can be used to measure elements at trace levels[224]. The technology involves full decomposition of the sample into its core elements and subsequent ionisation and detection. To assess iron in the clinical samples, unfixed $1x10^6$ BAL cells were diluted in nitric acid and the abundance of Fe^{56}, the most common isotope of iron, was detected through ICP-MS.

TRX-Puro (kindly provided by Dr Adam Renslo, UCSF) (Figure 3.1.1) is a highly selective reactivity-based probe which reacts with intracellular labile Fe^{2+} [223]. Probe reaction with iron, leads to a dose-dependent unmasking of intracellular puromycin that can be detected by immunochemistry and thereby acts as an indirect measurement of iron. Stained fixed cells were assessed by a high-throughput imaging microscope (Operetta CLS High-Content Analysis System, PerkinElmer).

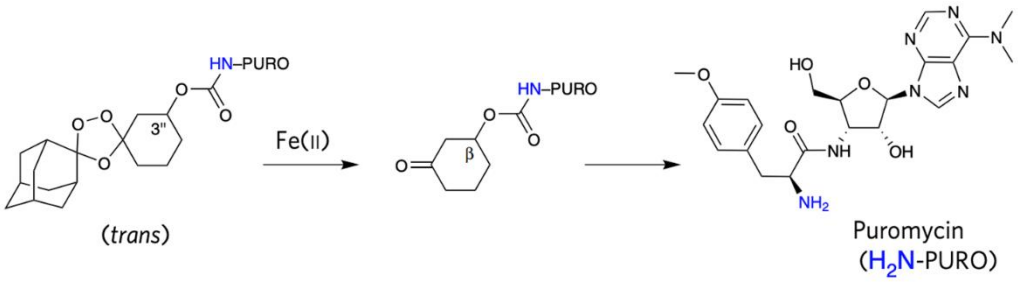

Figure 3.1.1 - Structure of TRX-Puro, developed by Spangler et al., 2016. When iron is detected by this probe, the trioxolane ring is fragmented and the ketone intermediate is formed. Puromycin is therefore exposed (through a spontaneous retro-Michael reaction) and it can be detected by immunohistochemistry.

TRX-puro provides a snapshot of iron levels in live cells before fixation, but cannot be used to assess iron changes in live cells. The FRET Iron Probe 1 (FIP-1, kindly provided by Dr Chang, UC Berkeley) is a reactivity based probe which links two fluorophores through an Fe^{2+}-cleavable endoperoxide bond[179]. Cleavage leads to a decrease in fluorescence resonance energy transfer (FRET) from the fluorescein to Cy3, by splitting them apart and increasing the

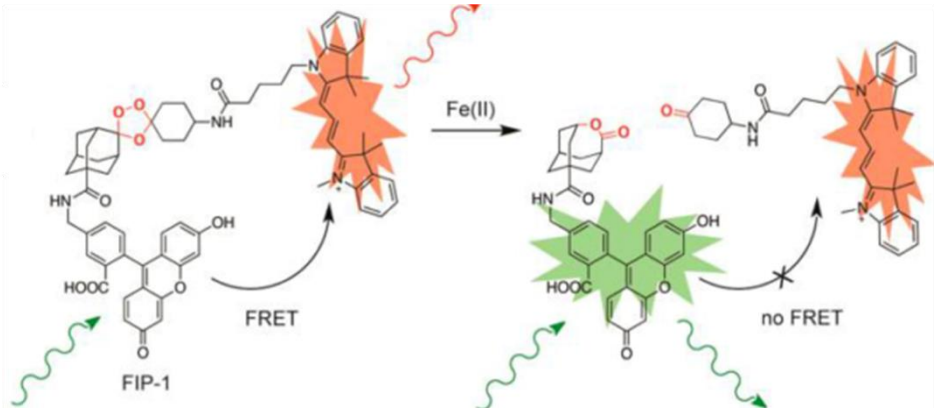

Figure 3.1.2 - FIP-1 structure and decrease in FRET following Fe^{2+} cleavage of the endoperoxide bond.

emission from the fluorescein (Figure 3.1.2). This can be used in live cells and therefore can assess the dynamic changes in cellular iron.

Macrophages play an important role in inflammatory responses and fibrosis in lung disease[225]. Both classically (M1-like) and alternatively activated macrophages (M2-like) are present in the lungs and play important roles in maintaining homeostasis. The latter are thought to be directly implicated in aberrant wound healing[226]. Anti-inflammatory M2-like and pro-inflammatory M1-like macrophages exist on a phenotypic spectrum, displaying a combination of receptors dependent on the cytokines present that conventionally are used to describe phenotype[83,227,228]. CD206 is known to be expressed on alveolar macrophages, especially in an alternatively activated context[229]. CD163, another M2-like phenotype associated receptor, has also been implicated in worse IPF prognosis, and interestingly plays a role in iron metabolism[91,92,230]. IL10, together with IL4, have been shown to polarise macrophages towards anti-inflammatory phenotype, favouring high CD163 and epithelial repair through further production of IL10[231,232]. Many other markers for alternatively activated macrophages have been identified, such as CCL18, CCL7, CCL22, CD204, but were not prioritised in this study. CD80 and CD86 on the other hand are two prototypical M1-like pro-inflammatory markers and they have been shown to play a role in the excessive initially pro-inflammatory insult in models of acute pneumonia[93,94].

Macrophages have been shown to handle iron differently depending on polarisation state[116,233]. M1-like macrophages have been shown to favour a phenotype with low ferroportin, the sole protein known to export iron from the cell, and high ferritin, the iron storing protein[116]. This implies an iron sequestration phenotype, thus concealing it from pathogens which would use iron to replicate. In contrast, M2-like macrophages tend to have an iron-recycling phenotype, characterised by high ferroportin and low ferritin[116]. Therefore, the study of alveolar macrophage iron loading and phenotype may provide insights into the pathogenesis of lung fibrosis.

Aims and Hypothesis

The overarching aim of this chapter was to determine iron content in alveolar macrophages in patients with fibrotic and non-fibrotic ILD.

Aim 1 – To determine iron loading in macrophages of patients with IPF, UNC with fibrosis and UNC without fibrosis through Prussian blue staining

Hypothesis 1 – Iron loading is a feature of fibrotic lung disease.

Aim 2 – To determine the role of clinical variables including age, smoking and sex in iron loading.

Hypothesis 2 – Iron loading is associated with the presence of fibrosis independently other clinical variables.

Aim 3 – To characterise macrophage polarisation and iron phenotypes in different ILDs.

Hypothesis 3 – There are distinct alveolar macrophage phenotypes that are associated with IPF, UNC with fibrosis and UNC without fibrosis

Aim 4 – To optimise an in vitro monocyte-derived macrophage model mimicking IPF patient-derived alveolar macrophages

Hypothesis 4 – A M2-like polarisation is able to mimic IPF patients' derived alveolar macrophages

3.2 Results

3.2.1 Validation of iron detection methods in THP1 cells and patient BAL cells

To initially validate the Prussian blue stain and the scoring system, THP1 cells were differentiated with PMA and treated with different concentrations of iron (FAS) and then quantified (Figure 3.2.1.1A-B). This showed that Prussian blue

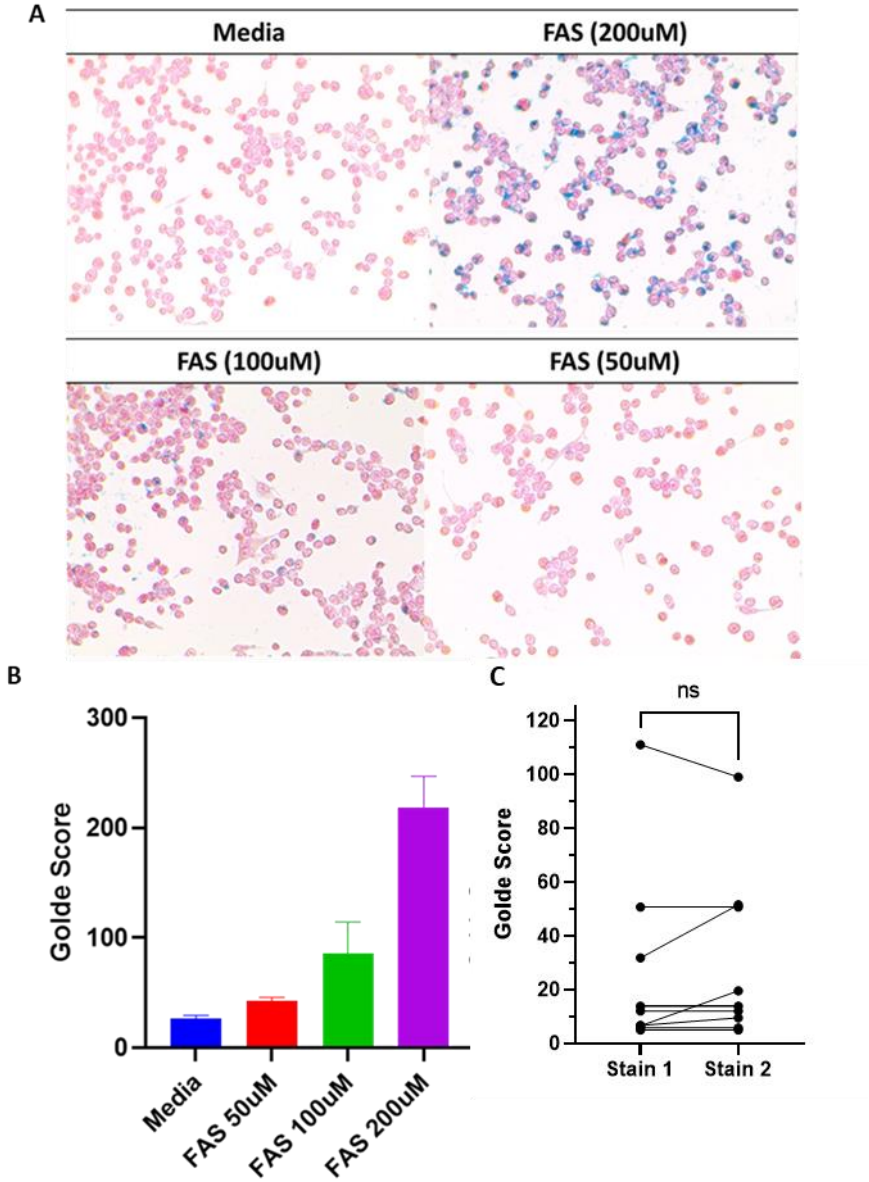

Figure 3.2.1.1 – (A) Prussian blue staining on PMA-differentiated THP1 cells with different concentrations of FAS and (B) Iron quantification by Golde score. (C) Two separate cytospins from n=9 patients were stained for Prussian blue and their Golde Score calculated. This was carried out blind. They were tested for normality and a Wilcoxon test was performed on Graphpad Prism. No statistically significant difference was observed between the two Golde Score measurements (P=0.437).

was able to stain iron at different concentrations and the Golde Score correctly used to assess these.

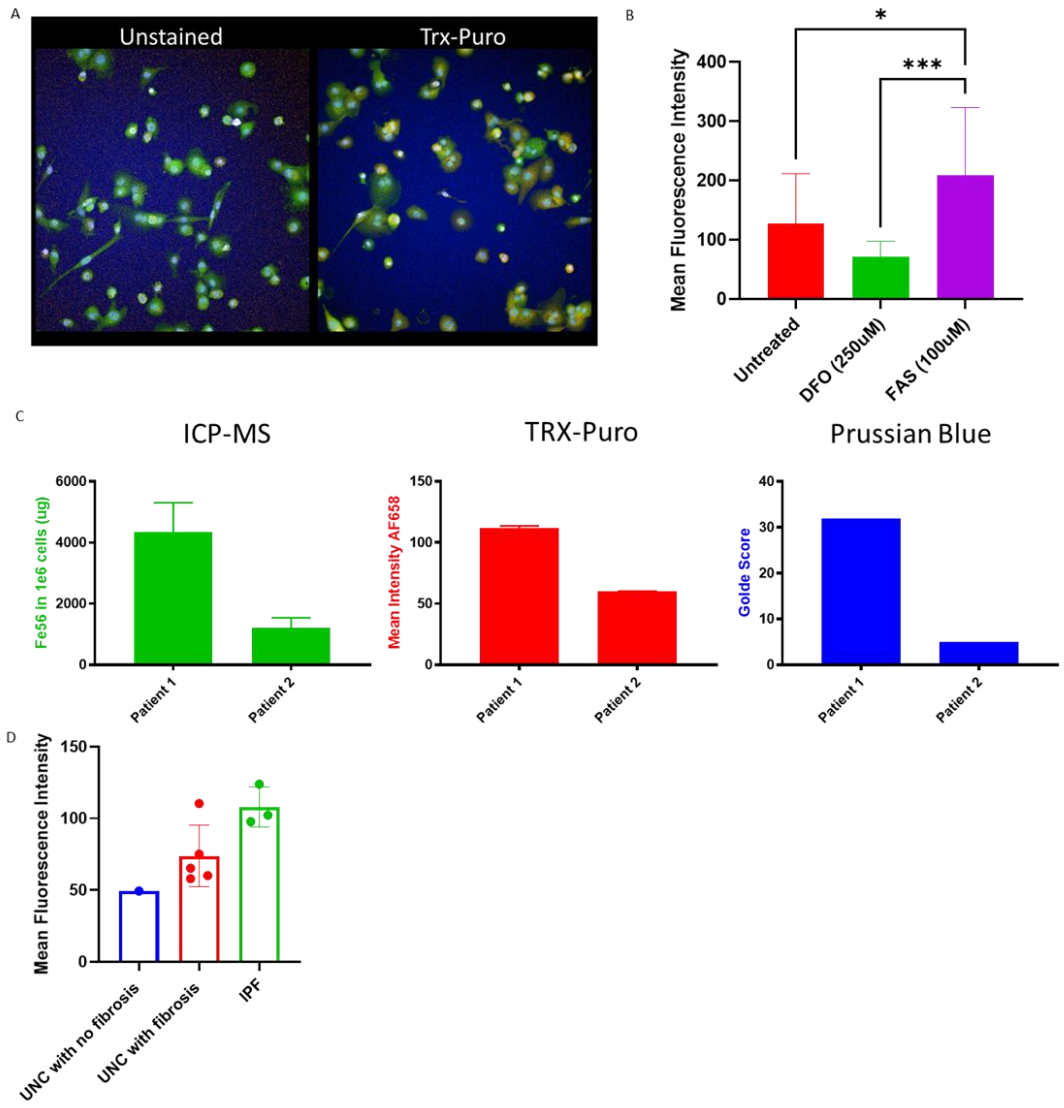

*Figure 3.2.1.2 – (A) Imaging of TRX-puro on PMA-differentiated IL10 polarised THP1 showing cell mask and Hoechst staining (green and blue respectively) and anti-puromycin staining in red. (B) Mean fluorescence intensity of AF658 anti-puromycin antibody on PMA-differentiated IL10 polarised THP1 following TRX-puro incubation. Following addition of 100uM Ferric Ammonium Sulphate, the mean fluorescence intensity was increased significantly both compared to untreated cells and to cells treated with iron chelator. Different concentrations of FAS give a concentration-dependent response. There is no statistically significant difference between the untreated sample and the iron chelated one. Samples were tested for normality with a Shapiro-Wilk test and a Kruskal-Wallis test was performed. * p<0.05, ** p<0.01, *** p<0.001. Error bars = SD. (C) Comparison of three different methods assessing iron levels (ICP-MS, TRX puro and Prussian blue), between two patients. All three techniques showed a higher level of iron in Patient 1 compared to Patient 2.*

To assess intra-observer variation in Golde Score derived from these stains on the patient's cytospins, two slides from the same patients (n=9) were

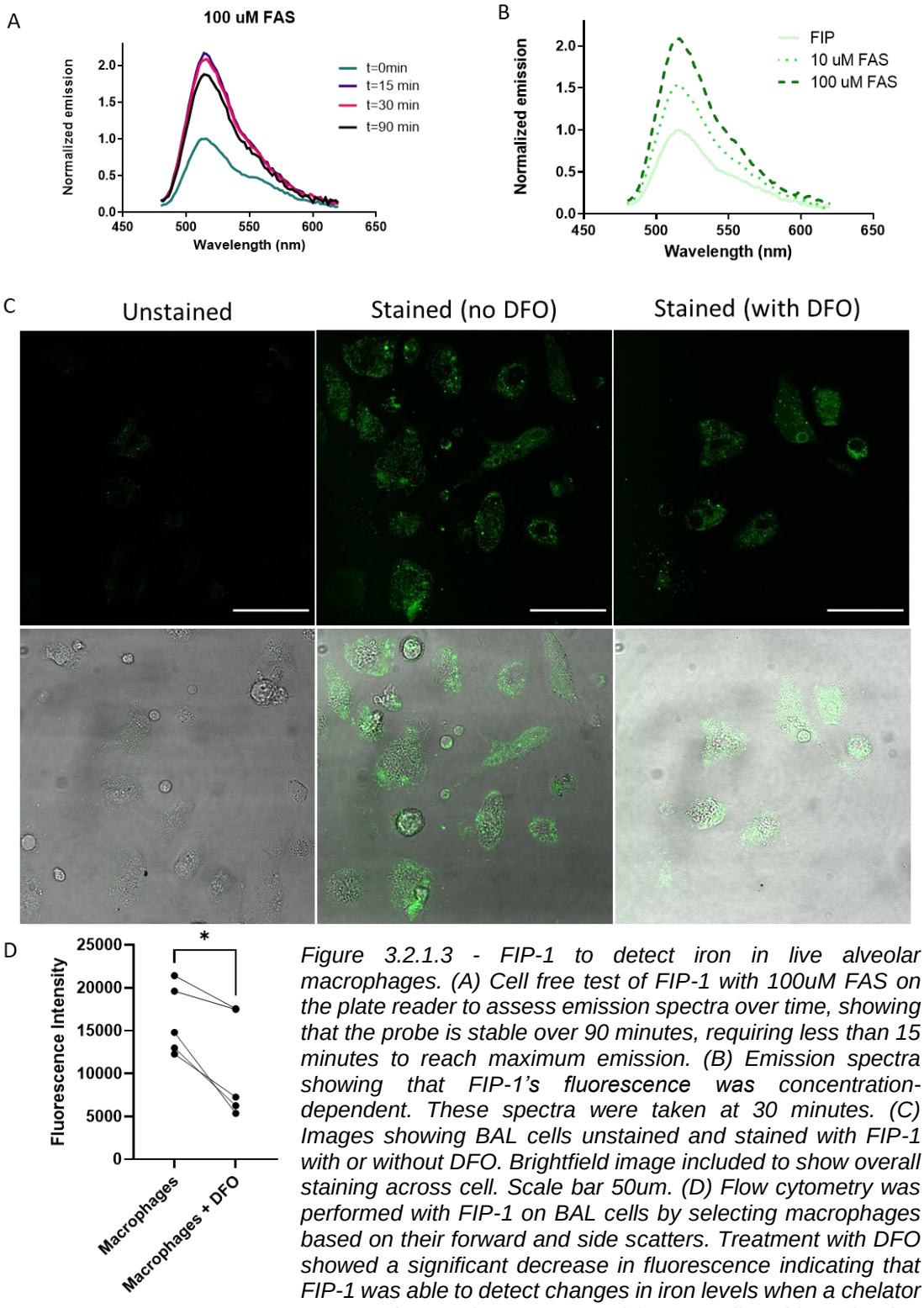

*Figure 3.2.1.3 - FIP-1 to detect iron in live alveolar macrophages. (A) Cell free test of FIP-1 with 100uM FAS on the plate reader to assess emission spectra over time, showing that the probe is stable over 90 minutes, requiring less than 15 minutes to reach maximum emission. (B) Emission spectra showing that FIP-1's fluorescence was concentration-dependent. These spectra were taken at 30 minutes. (C) Images showing BAL cells unstained and stained with FIP-1 with or without DFO. Brightfield image included to show overall staining across cell. Scale bar 50um. (D) Flow cytometry was performed with FIP-1 on BAL cells by selecting macrophages based on their forward and side scatters. Treatment with DFO showed a significant decrease in fluorescence indicating that FIP-1 was able to detect changes in iron levels when a chelator was used. Samples were tested for normality with a Shapiro-Wilk test and a Paired T-test was performed. * p<0.05, ** p<0.01, *** p<0.001. Error bars = SEM.*

stained and counted on different days. The samples were blinded for diagnosis. No statistically significant difference was observed between the two stains (Figure 3.2.1.1C).

Another method to detect iron, the TRX-puro probe, was used on PMA-differentiated THP1 cells (Figure 3.2.1.2A). The full protocol used for analysis is shown in the methods section. The cells were treated with an iron chelator, deferoxamine and exogenous iron (FAS). Although the difference with the addition of DFO was not significant compared to untreated, when comparing the iron treated cells the mean fluorescence intensity was significantly higher than both the untreated and DFO treated cells (Figure 3.2.1.2B). Two ILD patients (Patient 1 with IPF and Patient 2 with UNC with fibrosis) were tested across Prussian blue, TRX-puro and ICP-MS. Across the three different methods a similar pattern is maintained, with patient 2 having a lower level of iron compared to patient 1 (Figure 3.2.1.2C).

To overcome some limitations of TRX-puro, such as the use on fixed samples, the iron-specific fluorescent probe FIP-1 was tested. The probe was tested cell-free with either FAS at 10uM or 100uM. The change in spectral emission was assessed over 90 minutes and normalised to blank. The FIP-1 probe was rapid, stable over time (Figure 3.2.1.3A) and could discern between the concentrations of FAS (Figure 3.2.1.3B).

The probe was also tested on alveolar macrophages from patients in the presence or absence of the iron chelator DFO. Figure 3.2.1.3C shows that FIP-1 entered the cells, but no striking visual change was observed with DFO treatment. When repeating the experiments on BAL derived macrophages through flow cytometry, a significant change was observed when DFO was added compared to no treatment (Figure 3.2.1.3D)

3.2.2 Alveolar macrophages from IPF patients contain more iron compared to non-fibrotic unclassifiable disease.

A cohort of archived patient cytospins was identified across five diagnostic groups and their bronchoalveolar lavage cells stained with Prussian blue. The five groups of patients were those with unexplained chronic cough without

haemoptysis, unexplained chronic cough with haemoptysis, UNC with no fibrosis, UNC with fibrosis and IPF. Patient with unexplained cough by definition had normal chest CT images and normal lung function. Further information on the diagnosis of the UNC patients is shown in Appendix 3.6.1.

Table 3.2.2-1 - Clinical characteristics and BAL diferential cell counts the five groups of patients subsequenty assayed for Prussian Blue staining. Statistical differences are discussed in Appendix 3.6.2.

	Controls with haemoptysis	**Controls with no haemoptysis**	**UNC with no fibrosis**	**UNC with fibrosis**	**IPF**
N	6	3	18	35	40
Age (mean±SD)	59.83 ±10.83	59.67 ±7.02	63.50 ±10.62	70.74 ±7.68	71.82 ±9.21
Sex (M/F)	4/2	2/1	10/7	21/14	25/15
BMI (mean±SD)	32.75 ±6.19	36.00 ±2.83	29.47 ±5.86	27.18 ±4.59	29.17 ±5.79
Current/Ex/ Never smoker	3/3/0	0/3/0	4/9/4	8/15/12	14/19/7
Anticoagulant (Y/N)	3/6	0/3	2/16	3/32	2/38
Haemoptysis (Y/N)	6/6	0/3	0/18	0/35	0/40
Macrophage (%)	90.00 ±6.75	69.00 ±19.08	84.67 ±14.43	88.46 ±10.82	76.58 ±20.20
Neutrophils (%)	4.83 ±3.60	16.00 ±18.52	4.78 ±5.77	6.09 ±9.56	14.58 ±17.57
Lymphocytes (%)	10.17 ±16.95	3.00 ±3.00	7.17 ±9.75	3.20 ±3.10	4.48 ±3.84
Eosinophils (%)	0.50 ±0.84	0.67 ±0.57	3.05 ±4.69	2.14 ±3.05	3.40 ±4.82

The demographics and the differential counting of BALs of these patients are in Table 3.2.2-1. Since occult haemorrhage is speculated to be associated with increased macrophage iron, the proportion of patients prescribed anticoagulants at the time BAL may be relevant and shown in Table 3.2.2-1. Anticoagulant drug treatment was defined as warfarin, novel oral anticoagulants (NOACs), therapeutic dose heparin or clopidogrel for at least 1

month prior to BAL. Patients were required to stop anticoagulation at least 72 hours prior to BAL as per local BAL guidelines.

At least 70% of cells on patient cytospins were macrophages (Table 3.2.2-1). Non-macrophage cells were not counted, although they were observed to stain for iron. Statistical analysis and graphs comparing the different groups are shown in Appendix 3.6.2.

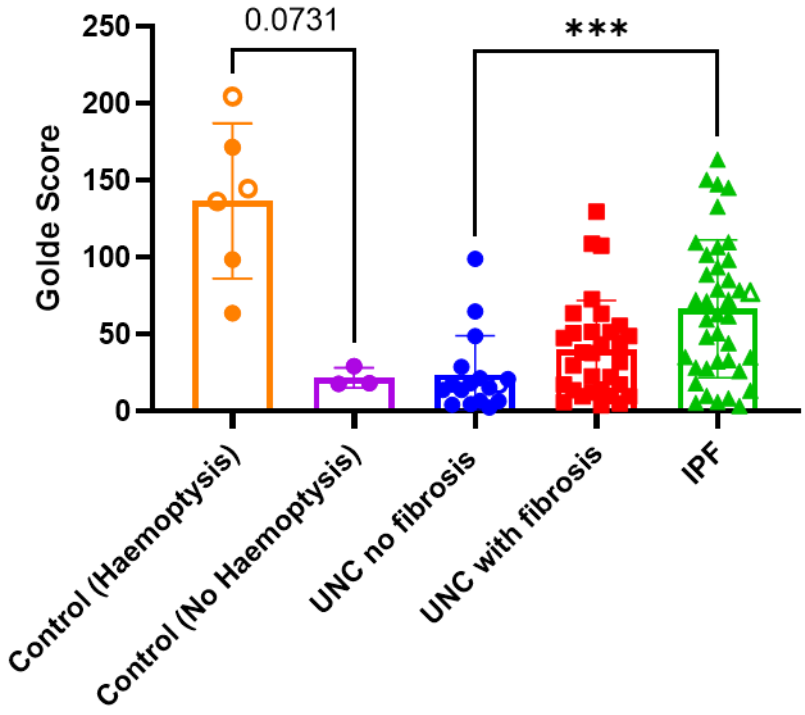

*Figure 3.2.2.1 – Golde score of BAL derived alveolar macrophages in control groups that presented with or without haemoptysis, UNC with no fibrosis, UNC with fibrosis, IPF patients Open labels indicate patients on anticoagulants. Data were tested for normality with a Shapiro-Wilk test and a Kruskal-Wallis test was performed with Dunn's multiple comparisons between the disease groups and the more relevant control with no haemoptysis. * p<0.05, ** p<0.01, *** p<0.001. Error bars = SD.*

Patients with unexplained cough with haemoptysis had a trending higher (P=0.0731) Golde Score compared those with unexplained cough without haemoptysis (Mean ± SD: 136.4 ± 50.44 vs 21.74 ± 6.56) (3.2.2.1A). The Golde score from the ILD patient groups also did not significantly differ from the control group with no haemoptysis. This lack of statistical significance is likely to be associated with the limited number of patients in the no haemoptysis group

Alveolar macrophages from IPF patients contain a significant higher amount of iron compared to macrophages of patients with UNC with no fibrosis (Mean ± SD: 66.62 ± 44.84 vs 23.81 ± 25.25 p= 0.0006). There was no significant difference between UNC with fibrosis and UNC with no fibrosis (Mean ± SD: 40.01 ± 32.00, P= 0.2612) or with IPF (P=0.0572). Only 7 ILD patients across all groups received anticoagulants.

To support the Prussian blue scoring data on BAL macrophages, both TRX-puro (Figure 3.2.2.2A) and the FIP-1 probe (Figure 3.2.2.2B) were tested in available cohorts of patients. No statistical analysis could be carried out in either technique, but both showed similar trends as Prussian blue: IPF patients having the highest level of iron compared to UNC with fibrosis and no fibrosis.

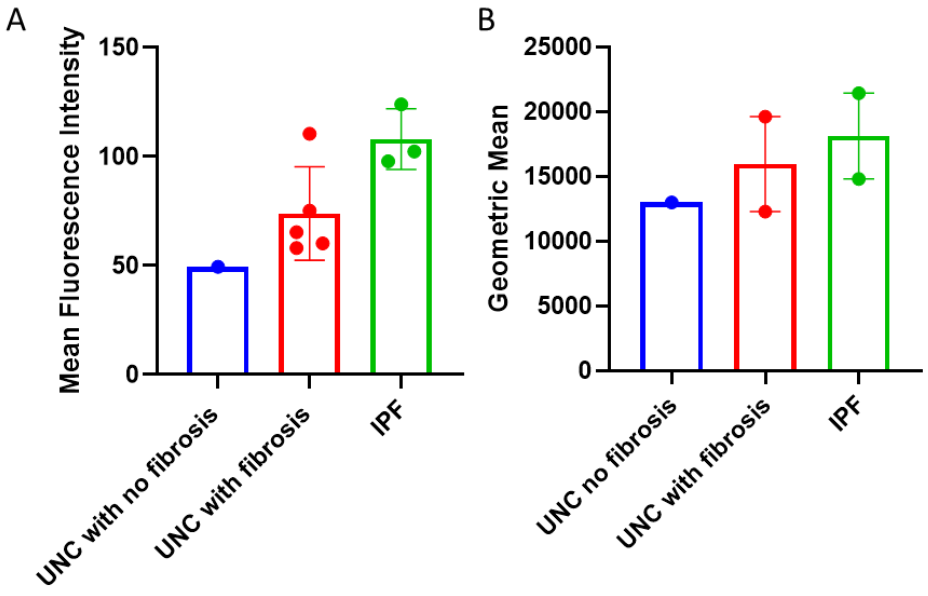

Figure 3.2.2.2 – (A) TRX-puro and (B) FIP-1 assessment of iron levels in BAL-cells, showing a similar trend compared to Prussian blue. No statistical analysis was carried out due to the limited number of patients assessed in the diagnostic groups.

3.2.3 Iron loading is independently associated with the presence of fibrosis.

To determine whether Golde Score is associated with fibrosis, independent of other plausibly relevant patient variables, a multiple linear regression analysis was performed on the data sets. The model used was:

$$Golde\ Score \sim Intercept\ +\ IIPvsIPF\ +\ Fibrosis\ +\ BMI$$
$$+\ Age\ at\ time\ of\ BAL\ +\ \%\ predicted\ VC\ at\ time\ of\ BAL$$
$$+\ sex + smoking\ (3cat) +\ \%\ macrophages + anticoagulants$$

However, because Golde score was not normally distributed, the score was log-transformed, and a log-level regression model was constructed as follows:

$$log_2(Golde\ score)$$
$$= \beta_0(Intercept) +\ \beta_1(IIPvsIPF) +\ \beta_2(Fibrosis) +\ \beta_3(BMI)$$
$$+\ \beta_4(Age\ at\ time\ of\ BAL) +\ \beta_5(\%pred\ VC\ at\ time\ of\ BAL)$$
$$+\ \beta_6(sex) + \beta_7\ (Smoking\ (3cat)\ [3]) +\ \beta_8\ (Smoking\ (3cat)\ [2])$$
$$+\ \beta_9(\%\ macrophages) + \beta_{10}(anticoagulants)$$

$$where\ \beta_n\ is\ the\ estimate\ calculated\ by\ the\ model\ and\ raised\ to\ the\ e$$

Table 3.2.3-1 - Summary of the parameter estimates of the variables, the percentage change of Golde Score and the relevant p values.

Variable	*Estimate*	*95% CI*	*Fold change* (2^{β_1})	*P value*	*P value summary*
UNC vs IPF[1]	0.92	0.17 to 1.66	1.89	0.02	*
Fibrosis [1]	1.19	0.21 to 2.16	2.28	0.02	*
BMI	0.02	-0.04 to 0.08	1.02	0.45	ns
Age	-0.02	-0.06 to 0.02	0.99	0.34	ns
%Pred FVC	0.02	-0.01 to 0.03	1.01	0.06	ns
Sex [0]	-0.06	-0.73 to 0.61	0.96	0.86	ns
Smoking (Never)	-0.20	-1.05 to 0.66	0.87	0.65	ns
Smoking (Current)	-0.27	-1.04 to 0.50	0.83	0.49	ns
%Macrophages	0.82	-1.20 to 2.83	1.76	0.42	ns
Anticoagulants [1]	-0.65	-1.87 to 0.56	0.64	0.29	ns

Table 3.2.3-1 shows the details of the estimates and P-values of this model, graphically shown in the accompanying forest plot (Figure 3.2.3.1B). Figure 3.2.3.1A shows the residual plot of the predicted Golde score, showing a random scattering, thus validating the model.

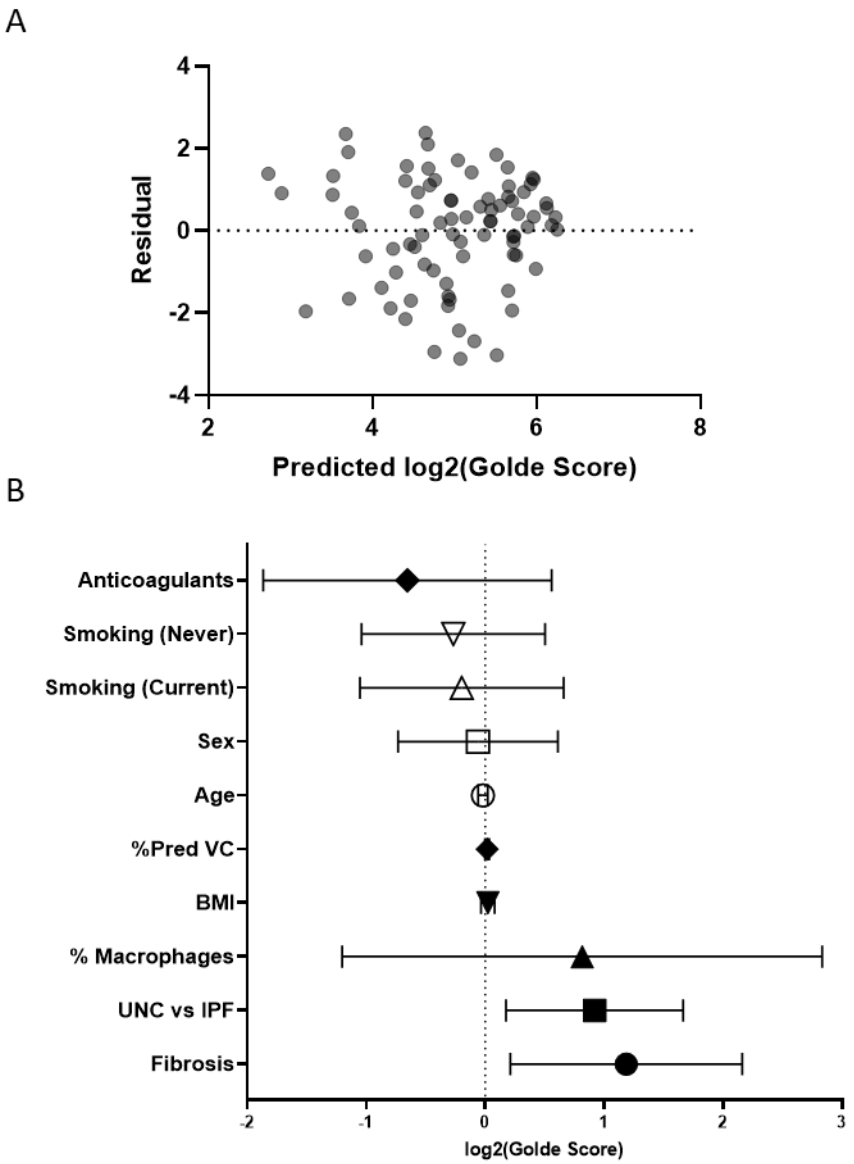

Figure 3.2.3.1 - (A) Residual plot showing points being randomly scattered around the x-axis. This showed that a multiple linear regression model was appropriate for this set of data. (B) Forest plots showing the estimates and 95% confidence intervals of the variables considered in this model. Fibrosis and IPF diagnosis were the only variables that are significantly associated with changes in Prussian blue.

Of the variables tested, the presence of fibrosis had the largest significant association with log Golde score, with a 2.3 fold-change increase. The diagnosis of IPF over UNC (fibrotic and non-fibrotic) was also shown to have

a significant association with increased Golde Score, (1.9 fold-change). Age, sex, smoking status, % predicted FVC or BMI were not associated with Golde score. This result suggests that presence of fibrosis is associated with iron loading independently of other plausible patient variables.

3.2.4 Alveolar Macrophage M1/M2 gene expression in IPF, UNC with fibrosis and UNC no fibrosis

The alveolar macrophage phenotypes from the different patient groups were assessed by qPCR. BAL macrophages were selected by adhesion. The four genes assessed were CD80 (Figure 3.2.4.1A) and CD86 (Figure 3.2.4.1B), receptors associated with a pro-inflammatory M1-like macrophage, and CD206 (Figure 3.2.4.1C) and CD163 (Figure 3.2.4.1D), representing a more anti-inflammatory M2-like macrophage. The results suggest that UNC with fibrosis and IPF may be different based on this small selection of cell receptor transcripts.

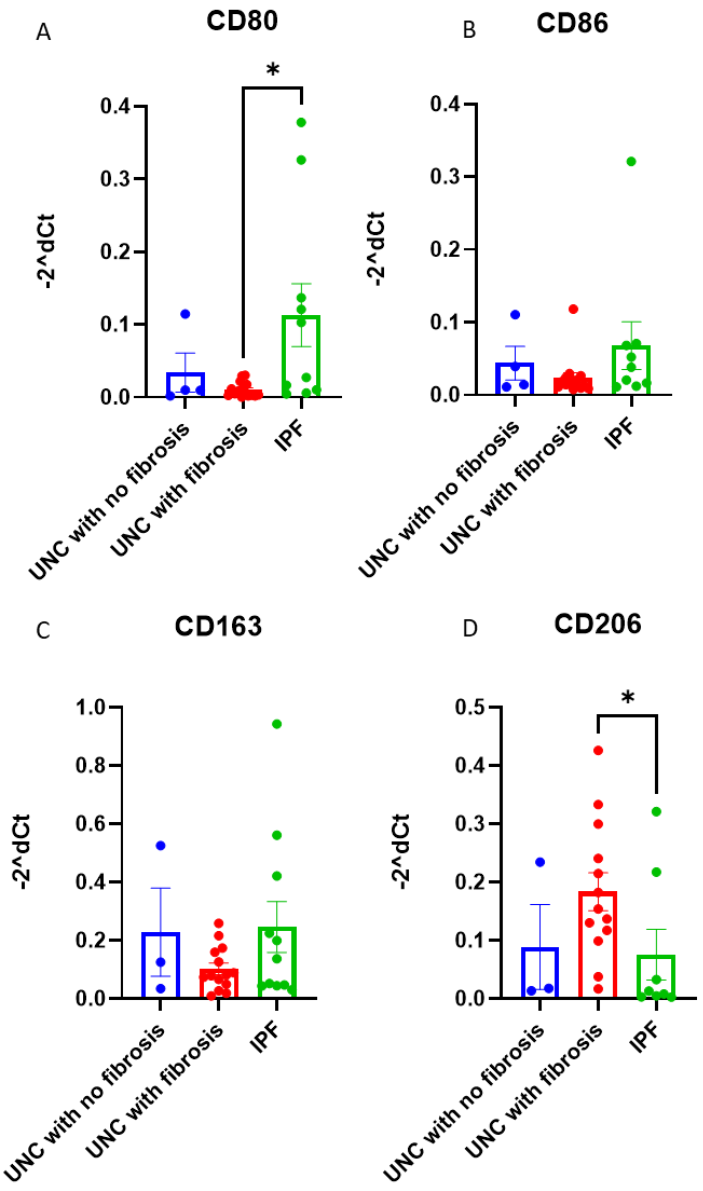

*Figure 3.2.4.1 – Levels of gene expression measured through qPCR normalised to actin in the three different diseases. In the first-row markers of a pro-inflammatory phenotype are shown: CD80 (A) was significantly higher in IPF compared to UNC with no fibrosis; CD86 gene expression was not different between diseases (B). In the second-row anti-inflammatory markers, CD163 (C) and CD206 (D) were shown and do not show statistically significant differences between diseases. Samples were tested for normality with a Shapiro-Wilk test and a Kruskal-Wallis test was performed. * p<0.05, ** p<0.01, *** p<0.001. Error bars = SEM. UNC with no fibrosis: N=4; UNC with fibrosis N=13; IPF N=8.*

Flow cytometry characterisation was also carried out. Figure 3.2.4.2A-C shows the histograms comparing unstained, stained and isotype of single cells. Although there was no unspecific staining observed for the CD206 isotype (Figure 3.2.4.2C), some was present with the CD163 isotype (Figure 3.2.4.2A),

suggesting the antibody was binding non-specifically. The geometric mean of these antibodies was assessed on single HLA-DR positive cells (gating strategy in Appendix 3.6.3). Although no statistical analysis was performed due to the limited numbers of patients in the UNC with no fibrosis group, qualitatively there was no difference in CD163 (Figure 3.2.4.2B) or CD206 expression (Figure 3.2.4.2D). However, the trend observed in the qPCR results (Figure 3.2.4.2C-D) was confirmed for CD163, where IPF had the

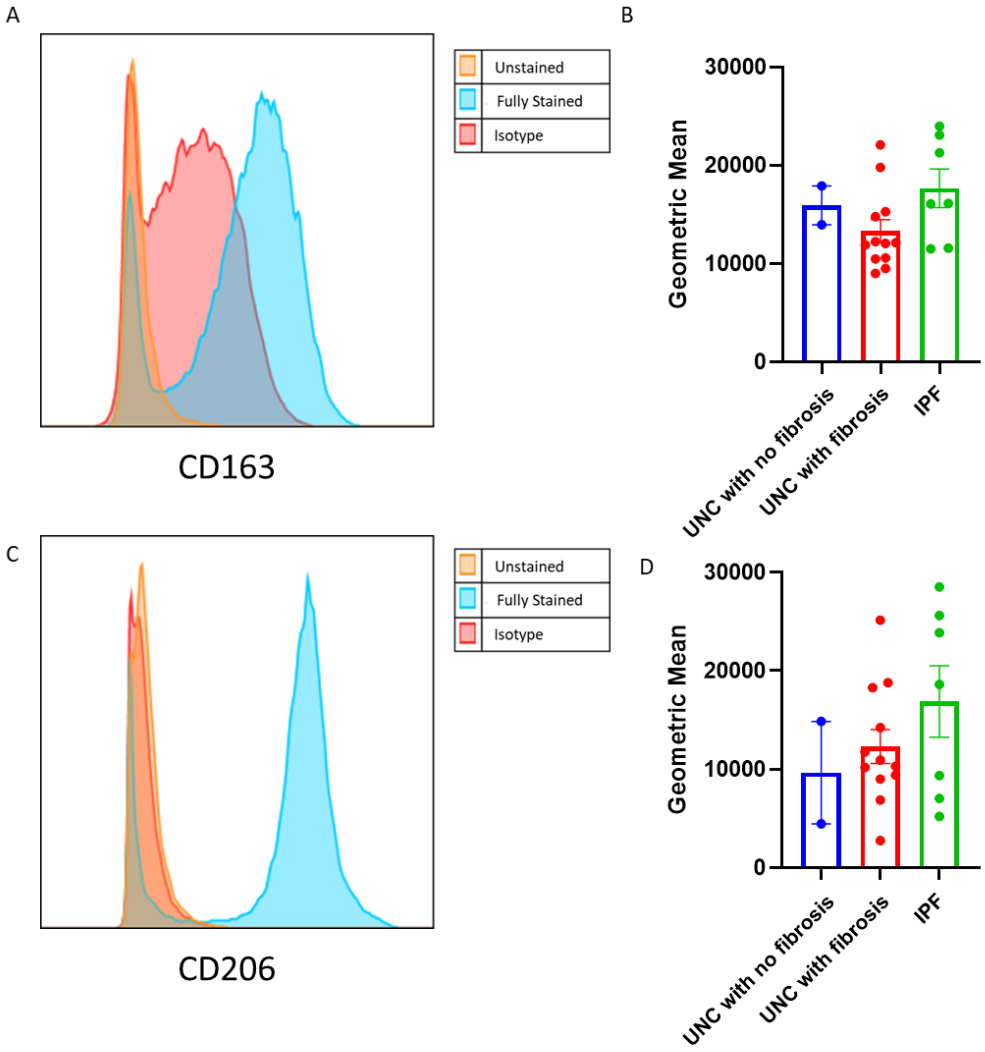

Figure 3.2.4.2 - Flow cytometry results assessing CD163 and CD206 levels in HLA-DR positive macrophages. (A) Histogram plot showing some unspecific binding for the isotype antibody used for CD163. (B) Geometric mean for the CD163 antibody on HLA-DR positive cells was assessed. (C) Histogram plots showing no unspecific binding for the CD206 isotype. (D) Geometric mean for the CD206 antibody on HLA-DR positive cells was assessed. No statistical analysis was performed due to the limited numbers of samples. UNC with no fibrosis: N=2; UNC with fibrosis N=12; IPF N=7.

highest levels of expression, followed by UNC with no fibrosis and UNC with fibrosis. On the other hand, CD206 was the highest in the IPF patient group through flow, compared to the UNC with fibrosis group when assessed through qPCR.

Although not conclusive, this data suggests that IPF may have an increased pro-inflammatory (CD80) phenotype with, in contrast to UNC with fibrosis having a more anti-inflammatory (CD206) phenotype.

3.2.5 Alveolar macrophages from IPF patients have an iron exporting phenotype compared to UNC with fibrosis and with no fibrosis.

A selection of iron receptors, previously discussed in the introduction, were assessed through qPCR on the adherent cells retrieved from BALs. There was no significant difference in level of mRNA expression of the Ferritin Heavy Chain 1 (*fth1*) (Figure 3.2.5.1A) or transferrin receptor 1 (Tfr1 - *tfrc*) (Figure 3.2.5.1B). FTh1, an iron storage protein, showed no differences between diagnosis, with IPF having a slightly higher mean. Conversely IPF patients had a low level of the transferrin receptor mRNA. There were some statistically significant differences between IPF and UNC with fibrosis when looking at the divalent metal transporter 1 (DMT1 – *slc11*) (Figure 3.2.5.1C) and the only known cellular outward gate for iron, ferroportin (FPN - *slc*40) (Figure 3.2.5.1D). These are both significantly higher in IPF compared to UNC with fibrosis and not-significantly higher than UNC with no fibrosis. These data whilst not conclusive suggest that alveolar macrophages from IPF patients may have an ‘iron export’ phenotype. The subtle increase in ferritin may also be part of this mechanism, as it may be storing the increased cellular iron.

However, these hypotheses would need to be tested by functional studies and other methods of assessment. This will be discussed further in the discussion.

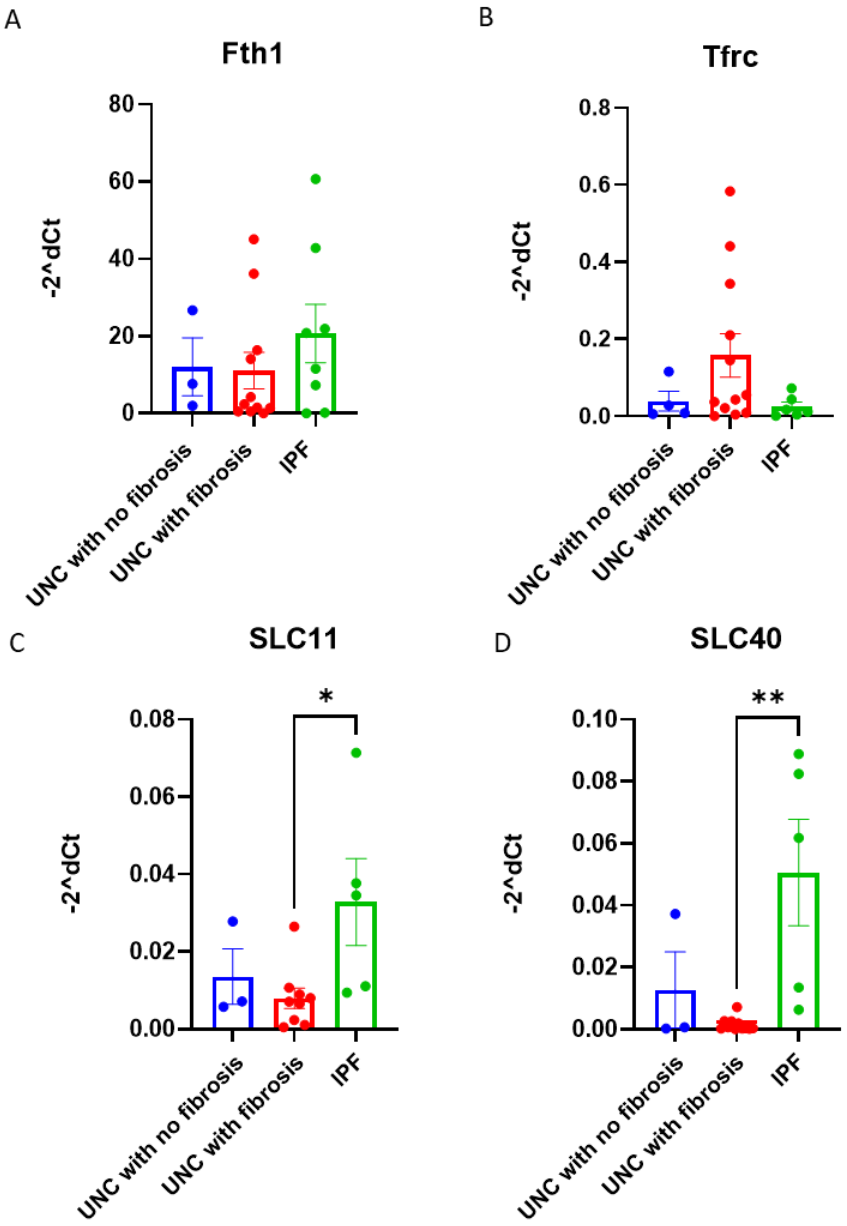

*Figure 3.2.5.1 - Levels of gene expression measured through qPCR normalised to actin in the three different diseases. (A) Ferritin heavy chain levels showing no significant differences between the three diseases, with IPF patients having the highest level. (B) Transferrin receptor levels showing no significant differences between diseases, with UNC with fibrosis having the highest level. (C) SLC11, or DMT1, levels showing a significant difference between IPF and UNC with fibrosis. (D) SLC40, or ferroportin, levels showing a significant difference between IPF and UNC with fibrosis. Samples were tested for normality with a Shapiro-Wilk test and a Kruskal-Wallis test was performed. * p<0.05, ** p<0.01, *** p<0.001. Error bars = SEM. UNC with no fibrosis: N=3; UNC with fibrosis N=13; IPF N=5/8*

3.2.6 Iron regulatory genes and macrophage markers in healthy peripheral monocyte-derived macrophages (MDM) and IPF alveolar macrophages

Due to the limited availability of patient alveolar macrophages due to the Covid-19 pandemic, healthy human peripheral blood monocytes were polarised with GM-CSF and LPS+IFNγ or M-CSF and IL4 and/or IL10 to derive macrophages, in order to optimise a more relevant model. The latter cytokines are known to generate M2-like polarisation that more closely resembles IPF

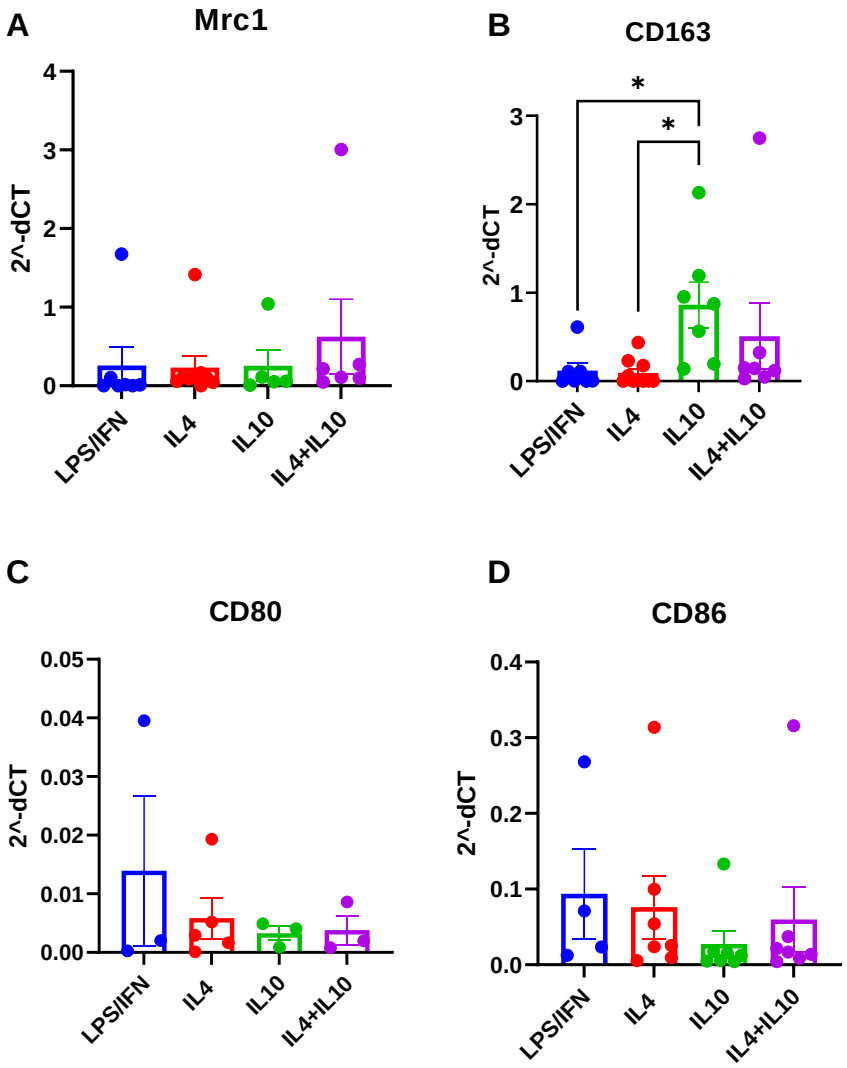

*Figure 3.2.6.1 – Peripheral blood MDM from healthy volunteers. qPCR results normalised to actin. (A) Mrc1 was not significantly different in any of the treatments (B) CD163 was significantly increased in IL10 compared to IL4. (C) CD80 and (D) CD86 were not significantly different between treatments. Samples were tested for normality with a Shapiro-Wilk test and a Kruskal-Wallis test was performed. * p<0.05, ** p<0.01, *** p<0.001. Error bars = SEM. N=7*

alveolar macrophages. This is in contrast LPS+IFNγ normally associated with a more pro-inflammatory M1-like phenotype. Although CD206 (Mrc1) (Figure 3.2.6.1A) is not statistically different between the groups, CD163 (Figure 3.2.6.1B) is significantly increased in IL10, compared to IL4 and LPS/IFN. The results suggests that IL10 drives this increase as IL4 levels are not significantly

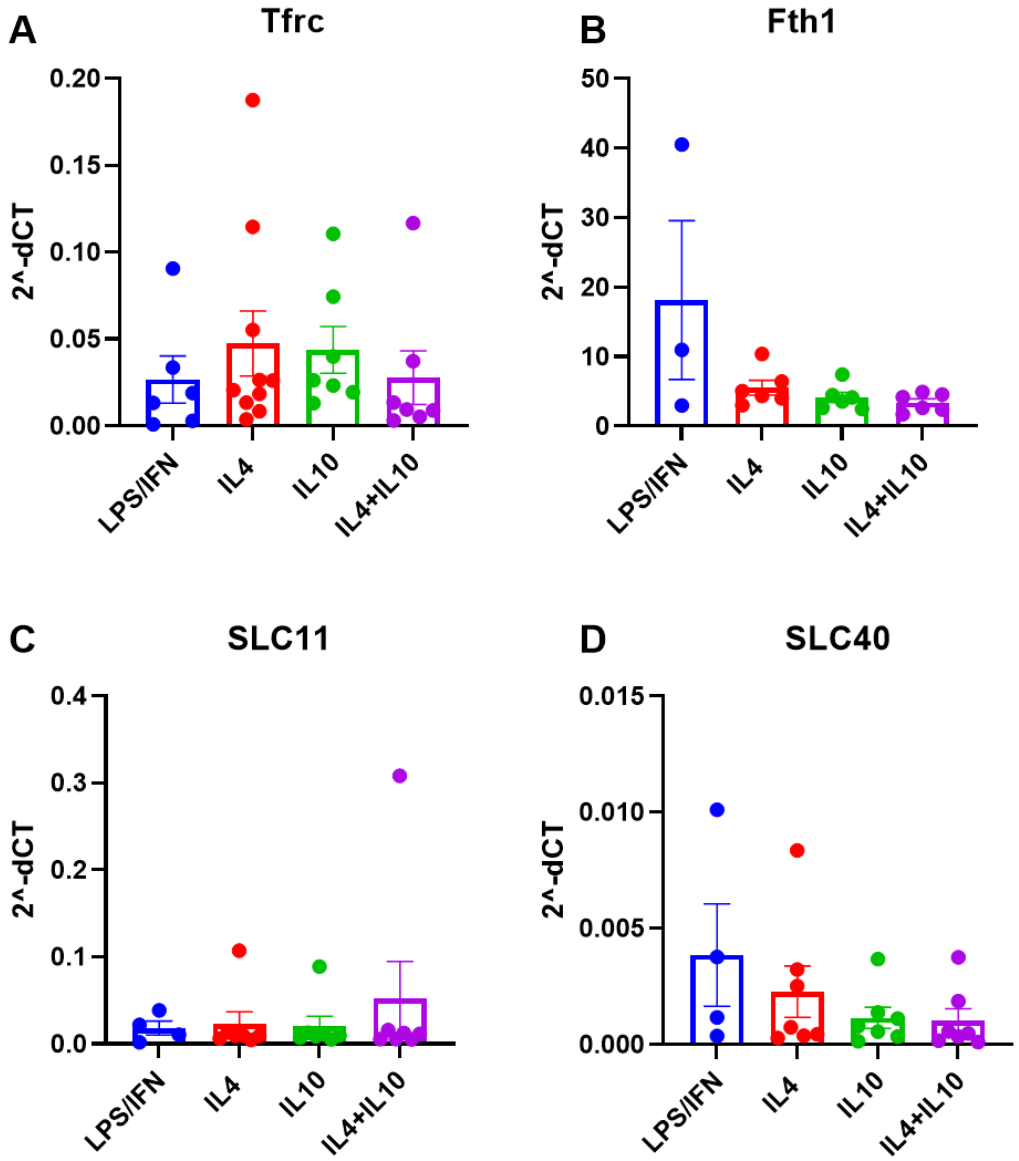

*Figure 3.2.6.2 - Peripheral blood MDM from healthy volunteers. qPCR results normalised to actin and MCSF/GMCSF. (A) FTH1 was not significantly different between groups but showed a trend for being higher in LPS+IFNy. (B) Tfrc was not significantly different between groups. (C) SLC11 (DMT1) was not significantly different between groups but showed a trend for being higher in the M1-like group. (D) SLC40 (ferroportin) was not significantly different between groups but show a trend for being higher in the M1-like group. Samples were tested for normality with a Shapiro-Wilk test and a Kruskal-Wallis test was performed. * p<0.05, ** p<0.01, *** p<0.001. Error bars = SEM. N=8*

different from LPS+IFN. CD80 and CD86 (Figure 3.2.6.1C-D) are considered M1-like markers but no significant differences could be observed between the different cytokine-treated groups. A trend for these two receptors being higher in the LPS+IFNy group was observed.

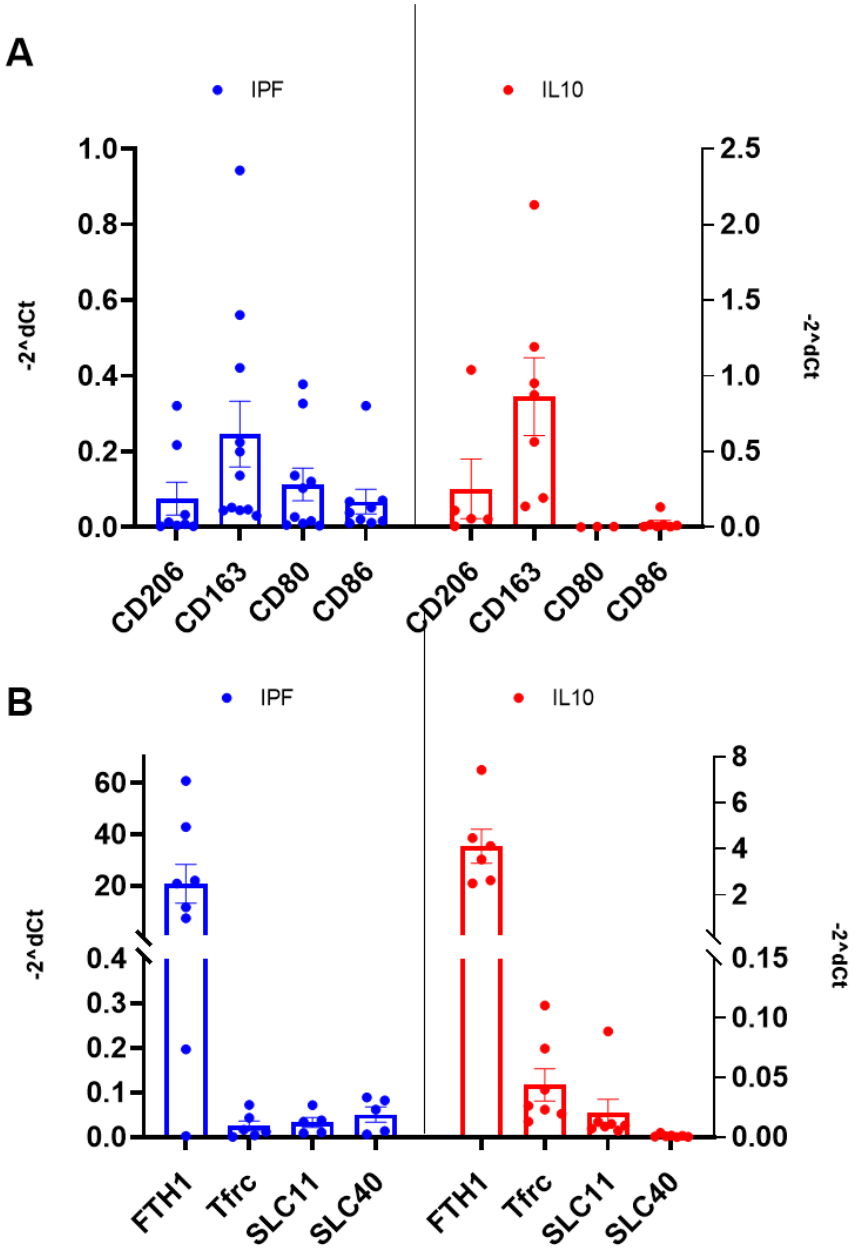

Figure 3.2.6.3 – Graphs comparing the phenotype of IPF derived alveolar macrophages (blue) with the phenotype of MDMs treated with IL10 (red). (A) M1/M2 markers showed similar trends in both cells, with CD163 being higher compared to the other receptors gene expression. (B) The iron phenotype in MDMs resembled the IPF alveolar macrophages. Both MDMs and AMs had a high level of FTH1 gene expression. Error bars = SEM.

Gene expression of iron receptors showed a non-significant increase in FTH (Figure 3.2.6.2A), with M1-like polarised cells. However no significant differences were observed in any of the iron genes (Figure 3.2.6.2)

IL10 treatment of MDM appeared to induce a polarisation state that most resembled IPF alveolar macrophages. Overall, IL10-polarised monocyte-derived macrophages show a similar macrophage-phenotype and a similar iron phenotype to patient derived alveolar macrophages. The M1/M2 markers (Figure 3.2.6.3A) show in both the in vitro model and the primary macrophages an increase in CD163 compared to the other markers which remain low. The iron protein gene expression followed a similar pattern in both IPF and IL10 polarised macrophages, with ferritin expression (FTH1) being increased in both (Figure 3.2.6.3B).

3.3 Discussion

Iron loading has previously been observed in IPF[137,172,174]. The overarching aim of this chapter has been to address whether alveolar macrophage iron content was increased in IPF and other fibrotic disease compared with non-fibrotic ILD. Additionally, the clinical characteristics including anticoagulation and presence of haemoptysis were assessed to discriminate whether these differences influenced iron loading.

3.3.1 Choice of patients

Although the primary aim was to measure alveolar macrophage iron in patients with fibrotic ILD versus non-fibrotic ILD, ideally age and sex match controls healthy controls would be included in these studies. The control patients in this study were restricted to small numbers and have unexplained chronic cough with or without haemoptysis. The final clinical diagnosis of patients with cough with haemoptysis was bleeding from the bronchial tree due to cough-induced trauma. The observation that the alveolar macrophages of these patients, particularly those on anticoagulants, had amongst the highest Golde scores suggests that blood in the alveolar space, via the bronchial tree or directly via the lung parenchyma, may be one of the mechanisms that could increase

macrophage iron content. This is likely to be linked to erythrophagocytosis by the alveolar macrophages. Whether this microinjuries is what happens in the IPF group as well, remains unclear, especially as the control patients are not seen to then progress into a fibrotic ILD phenotype. Moreover, the inflammation present in the lungs of the control group is probably of acute and pro-inflammatory nature, in contrast to the more chronic and anti-inflammatory one in the ILD cohorts. Overall, these groups of control patients are not significantly different from the disease groups. The lack of statistical difference, especially in the no haemoptysis group, is likely to be linked to the small number of patients assessed in this group. This kind of characterisation within the control group in comparison with the ILD groups had never been carried out before.

All patients with ILD were diagnosed according to a local MDT that used consensus guideline criteria. Patients with IPF were either definite or probable IPF based on MDT consensus. The diagnosis of unclassifiable ILD was based on an MDT decision that patients had idiopathic disease, did not meet criteria to make a single confident diagnosis but rather had a differential diagnosis that included at least two diseases (Appendix 3.6.1). Patients with suspected idiopathic unclassifiable disease are more likely to undergo a BAL for clinical reasons compared to patients that are confidently diagnosed with alternative ILDs (e.g. asbestosis, hypersensitivity pneumonitis due to known antigens, connective-tissue disease associated ILD etc). BAL samples for patients with alternative ILDs were available but in far fewer numbers than unclassifiable cases and therefore not studied. None of the patients with ILD had haemoptysis at the time of BAL suggesting overt bleeding was not the cause of high Golde score. Micro-alveolar haemorrhage is a potential mechanism that would increase alveolar macrophage iron, but Golde score was not associated with the presence of anticoagulant treatment in patients with ILD. Although this suggests this is not the primary mechanism, it does not exclude it.

3.3.2 Iron loading is a feature of IPF and is associated with fibrosis.

Prussian blue staining was used to assess iron levels of BAL derived macrophages. This was then quantified by Golde Score, a semi-quantitative method to detect labile iron inside cells, which involves a manual qualitative assessment of the intensity of blue stain within the cells. This specific technique has been previously used in clinical studies and can be said to be the gold standard for semi-quantitative intracellular iron assay[110,173]. It can therefore be used as a reliable and robust measurement of iron, especially when fresh samples are not available. Other techniques are used in the literature, and some were optimised in samples in this study[179,223]. Choice of iron detection method will be further discussed in Chapter 6.

The Prussian blue results showed that IPF macrophages had a statistically significantly higher level of iron compared to UNC with no fibrosis. The UNC with fibrosis patient tended to have lower Golde scores than IPF but higher than UNC without fibrosis. The differences between these groups were however not significant. These trends were confirmed by TRX-puro and FIP-1 assessment.

A multiple linear regression showed that the diagnosis of IPF and the presence of fibrosis were both independently associated with higher Golde score. The presence of fibrosis or an IPF diagnosis was associated with a 2.3-fold increase and the diagnosis of IPF was associated with a 1.9-fold increase in Golde score respectively.

Iron loading in macrophages has previously been observed in IPF patients through Golde Score. The range of Golde Score was similar to the one observed in this study, with IPF patients having an average score of approximately 70 and these studies did not identify an association with relevant variables, such as smoking and age[110,172]. This is in contrast to studies showing iron accumulation in epithelial lining fluid of the lung and ferritin increase in alveolar macrophages being associated with smoking[234,235]. No study had previously shown the relationship between iron loading in

macrophages and presence of fibrosis while comparing ILDs. Some studies using murine models of iron accumulation and pulmonary fibrosis, showed increased iron in lung tissue either through tissue homogenisation and commercially available iron assay or Prussian blue on fixed tissue slices. In the latter observations, iron staining was mainly associated with macrophages, with some evidence of loading in airway epithelium[111,236].

A study showed that *hfe* allelic variants were more common in IPF patients over controls; their macrophage iron loading and iron-dependent ROS production were significantly increased compared to controls[137]. *hfe* is a gene that is involved in homeostatic iron regulation and is mutated in haemochromatosis, a hereditary disease of iron overload[237,238]. The patients often have a gene polymorphism in *hfe* or other mutations in other iron genes[239]. These patients have an increased iron loading and present with liver fibrosis, but not with lung fibrosis[239,240]. This is likely to be associated to the liver's role in iron metabolism. Indeed, hepcidin and associated proteins, such as HFE, are mostly produced by the liver and play an important role in iron homeostasis.

HFE-deficient mice however showed an increased in iron levels in the lungs and this was associated with increased airway fibrosis and reduced lung function, independently of substantial changes in inflammatory response[111]. The bleomycin model was also shown to lead to iron loading in lung tissue, which was associated with macrophage iron loading[111]. In another study, increased lung iron overload did not exacerbate fibrosis in the bleomycin model when fibrosis was assessed as whole lung[236]. Although iron loading is involved in fibrosis, the effects that it has on its cause remain unclear.

3.3.3 Alveolar Macrophage phenotype is similar between diseases

The different iron loading in these alveolar cells could also be linked to the macrophages being phenotypically different between diseases. Indeed increased iron in IPF alveolar macrophages has been shown to be associated with a pro-inflammatory and tissue remodelling phenotype[110]. To assess

macrophage phenotype in the three disease groups, some key macrophage and iron-related receptors were assayed by qPCR and/or flow cytometry.

The gene expression of some common pro-inflammatory (CD80 and CD86) and anti-inflammatory (CD206 and CD163) receptors showed only some differences, CD80 being significantly higher in IPF compared to UNC with fibrosis and the opposite for CD206, which is significantly higher in UNC with fibrosis in contrast to IPF. No differences were observed with the UNC with no fibrosis group which is associated to the standard deviation of the results and the small sample number. For each disease indeed there is a large variance and some outliers. Interestingly these outliers are not the same patients across receptors, suggesting that these results are showing the extent of the heterogeneity in these samples. Flow cytometry was attempted to confirm this data but the limited number of data and some unspecific staining with the CD163 antibody, made it inconclusive. Additionally, the flow cytometry trends observed between the IPF and UNC with fibrosis group, are also inconsistent with the ones observed through qPCR. Western blots for these receptors may have helped clarifying this relationship, but it could also be linked to post-transcriptional changes affecting translation.

Although the alveolar space in pulmonary fibrosis is often associated with an M2-like anti-inflammatory phenotype, the increase in CD80 expression in IPF patients compared to UNC with fibrosis is striking. This could be linked to the two outliers present. However, three distinct populations seem to be identified within the IPF group. One with very low CD80 expression similar to the UNC groups, and the other two groups having medium or high expression. CD80 is a co-stimulatory molecule known for its role in T cells activation and B cell activity[241] and is considered a prototypical M1-like receptor. This could suggest that these three subgroups may have had different pro-inflammatory insults which affected their phenotype, potentially affecting pathology.

CD206 and CD163 are important receptors involved in the anti-inflammatory phenotype of macrophages. Interestingly CD163 is a monocyte-macrophage specific receptor involved in the removal of haemoglobin-haptoglobin

complexes during intravascular hemolysis[160,242]. Although no significant change between diseases was observed, it could have been interesting to test this receptor in the control patient's group. Due to their coughing, haemolysis is likely to have occurred in their lungs leading to an upregulation of CD163 in their alveolar macrophages. This was not possible as they are historical samples which have been frozen and no other control BALs were performed. A more readily available MDMs model was attempted for this reason and will be discussed further in the next section.

Phagocytosis assays could have been carried out to test effective functional changes between alveolar macrophages of the different diseases. However, these cells (especially in contrast with their interstitial counterpart) have been shown to have overall poor phagocytic activity and therefore no or very small differences may have been observed[75]. To complete this inflammatory phenotype analysis, cytokines could have also been assessed both at the gene expression through qPCR or at the protein level, through ELISA's and Western Blots. Cytokines like IL10, CCL18, TNFα or IL-1β are produced by alveolar macrophages and could have been measured both at the cellular level but also in the BAL fluid[32,75,84,96,110,243,244]. This would have had to be normalised to the number of cells or to the total volume collected.

To elucidate the macrophage phenotype further, their iron proteins were assessed. The only two proteins that changed significantly between UNC with fibrosis and IPF were SLC11 (or DMT1) and SLC40 (or ferroportin). This may suggest a more iron exporting phenotype of the IPF macrophages compared to UNC with fibrosis. However, these results may be skewed by the outliers present, but also by the very low levels observed. For both genes indeed the values observed were below 0.1 units in all cases, meaning that the levels in these cells may be low. The levels of FTH1 (ferritin heavy chain) are conversely very high, but not significantly different between diseases. The range of results observed and the fact that the outliers are not always the same patients, seem to suggest like for the macrophage markers, that this is a patient and cell specific characteristic.

This iron-exporting phenotype is in contrast to the high CD80 and low CD206 in IPF patients compared with the UNC with fibrosis group. Macrophages with a pro-inflammatory M1-like phenotype have indeed been shown to have a more iron storage phenotype to decrease iron available to pathogens, with high ferritin but low ferroportin (SLC40). Interestingly the transferrin receptor gene is not significantly changed across diseases, although a trend, once again driven by the outliers, suggests a higher level of expression in the UNC with fibrosis group compared to the IPF group. Flow cytometry data would have established whether this is true at the protein level as well, but some issues with the CD71 antibody (discussed further in Chapter 5) and then lack of new samples availability limited this.

Handling of iron metabolism could be tested by using iron chelators and exogenous iron. Some optimisation using FAS as a source of exogenous iron are discussed in Chapter 5 in macrophages from cell lines. This chapter will focus on ferroptosis, an iron-mediated form of cell death, and whether macrophages are susceptible to it.

The macrophage characterisation observed in this study has mostly demonstrated differences between UNC with fibrosis and IPF, but not with UNC with no fibrosis. This is in contrast with the iron loading results where UNC with fibrosis acted as an intermediate between the two other diseases. This highlights how both the small number of UNC with no fibrosis samples and the incomplete characterisation of these macrophages may skew the results significantly. To assess the effect of the gene expression on iron loading, thus, to understand why no difference was observed, a multiple linear regression analysis was attempted. This was to understand how the Golde Score would have changed based on the changes in genes. However due to the limited number of patients with qPCR data, this model was not possible and a very low degrees of freedom was achieved. A full gene expression assessment, such as RNAseq, may have elucidated this further and helped understanding the differences observed between datasets.

Rate of proliferation of the alveolar macrophages may have an impact on iron loading and should be tested. Indeed high-proliferating cells require more labile iron and this has been studied thoroughly within cancer and its therapeutic options[245–248]. Whether the iron loading is linked to a high proliferating rate of the alveolar macrophages is not something that was explored within this project. Markers like Ki67 or BrdU could have been used to determine this possible correlation. Interestingly, the transferrin receptor (CD71) has been shown to correlate with Ki67 (in cancer and T cells) and therefore act as a proliferation marker, highlighting further the link between the two[249,250].

3.3.4 Alveolar macrophage phenotype is only partially mimicked by MDMs

Due to the limited availability of the patient's alveolar macrophage samples, an in vitro monocyte-derived macrophage model (MDMs) was developed using blood from healthy volunteers. The monocytes were then plated and treated with cytokines that are known to polarise their phenotype.

An M1- and M2-like phenotype were induced in this in vitro model by using either LPS+IFNγ or IL4 and IL10, singularly or in combination, respectively. Although no significant differences were observed across all the genes observed, CD163 was significantly higher in the IL10 treatment group compared to both LPS+IFNγ and IL4. The lack of differences observed for CD80 and CD86 is likely associated with the limited number of samples in the M1-like group and the high variation observed. When comparing these phenotypes with what was observed at the RNA level in IPF patients, IL10 treatment showed the most similar trends compared to the primary alveolar macrophages. This is especially characterized by an increased CD163 level compared to the other proteins.

The iron proteins previously discussed in the context of the alveolar macrophages were tested for this model as well. The groups were not significantly different for any of these proteins' expression. Previous studies had shown that M1-like phenotypes are normally associated with an iron

storing phenotype, in contrast with an iron recycling phenotype in M2-like polarised cells[116]. The iron phenotype observed in IPF patients is somewhat replicated in IL10-polarised MDMs, with high CD163 and high FTH1. The high level of ferritin observed in IPF is likely to be associated with the high level of iron as discussed previously. However, the ferritin level of IPF patients was not significantly different compared to UNC with no fibrosis patients that have significantly lower levels of iron as shown through Prussian blue. Thus, the high ferritin level may be associated to disease in different, unclear ways.

3.3.5 Iron-loading association with fibrosis

It is unclear why the macrophages have an increased iron loading and how this leads to the development of fibrosis.

The macrophages may be dysfunctional and release pro-fibrogenic cytokines, increasing the probability of fibrosis. Experiments testing the effect of selectively chelating macrophage' iron loading, and assessing their functional cytokine release, may explain this relationship further. The use of an iron chelator, has been previously shown to lead to a reduction in ROS from alveolar macrophages with a pro-fibrotic phenotype[110]. In a murine study, using a chelator like DFO or Deferiprone in vivo, prevented renal interstitial fibrosis caused by unilateral ureteral obstruction. The transferrin receptor expression was lower, while DMT1, ferroportin and ferritin were increased. Additionally, macrophage infiltration was also reduced compared to control[251].

Iron-laden macrophages have been identified in multiple conditions that have occult-pulmonary haemorrhage and vascular abnormalities, such as patients with diffuse alveolar damage or pulmonary veno-occlusive disease, and some of these have been associated with IPF[108,173,252]. The Golde score observed in the alveolar macrophages of the control patients with haemoptysis suggests that presence of erythrocytes in the alveolar space is associated with iron loading. As aforementioned, the control patients are not seen to progress into fibrosis and therefore further underlying differences that may be associated with macrophage phenotype should be assessed. Nevertheless, possible vascular damage may lead to erythrophagocytosis by the macrophages as

previously discussed. This could lead to a skewing of their phenotype, which could result in pro-fibrotic chemokines being released[233]. The cytokine level in the BAL fluid of both groups may aid in this characterisation.

3.4 Limitations

There are a number of limitations with these studies.

The absence of healthy age and sex match controls is a limitation. However, the inclusion of patients without ILD and with unexplained chronic cough with haemoptysis is novel and informative. Additionally, age and sex do not appear to be associated with Golde score. The overall sample size is small especially the control patients with chronic cough. Patients were allocated as fibrotic and non-fibrotic ILD based on expert radiology assessment at MDT but the amount of fibrosis was not quantified. Blinded intra-observer Golde score was consistent but ideally Golde scores should be assigned by at least 2 observers and inter-observer variation measured.

The identification and selection of alveolar macrophages varied between experiments. In BAL cytospins, macrophages were identified through morphology. For fresh alveolar macrophages used in TRX-puro and some Prussian blue experiments, cells were positively selected by adhesion. For the FIP-1 studies, macrophages were selected based on FACS through conventional forward and side scatter properties. For ICP-MS studies, bulk-cell frozen pellets (i.e. all BAL cells) were used. Further studies should aim to consistently sort alveolar macrophages if possible.

All ILD patients that were included in the study by definition were fit enough to undergo BAL, which exclude patients with the most severe disease. Study of ILD subgroups e.g. asbestosis or Rheumatoid Arthritis ILD would be informative to address if highest Golde scores are most likely in IPF rather than other fibrotic ILDs.

When assessing the macrophage phenotype only small and inconclusive differences were observed. Similarly, when looking at iron specific proteins, small but significant differences suggest that IPF-derived macrophages may

have a more iron exporting phenotype compared to the other two diagnosis. However, both these conclusions would gain from an increased sample number and for other assessments of these proteins. This could be done through flow cytometry or western blots to assess these levels. Other functional assays for macrophages, such as phagocytosis ones, may have helped identifying other differences between these macrophages.

Attempts were carried out to characterise other proteins involved in cellular iron metabolism that have been identified as key in the literature, such as heme oxygenase 1 (HMOX-1), ceruloplasmin (CP) or NCOA4, but these were not successful[233,253]. Aside from expanding the characterisation of the proteins on these cells, functional iron-related assays might have clarified these inconsistencies and furthered the understanding of iron metabolism. Chapter 5 will introduce the topic of ferroptosis and how that is influenced by the iron metabolism of these cells and how it may aid in characterising these cells further. Other assays that could have been carried out are the assessment of free labile iron in the BAL fluid or plasma through ICP-MS or commercial assays, or the assessment of other soluble markers like transferrin and the transferrin receptor, ferritin or CD163. Additionally, these experiments would be supported further by cytokine assessments in both the supernatant following alveolar macrophage culturing, but also in the BAL fluid directly.

Development of an in vitro MDMs model to mimic the patient samples was attempted for this reason. However, its optimisation was limited to RNA levels and the model was not able to mimic fully IPF patients' alveolar macrophage phenotypes. Addition of exogenous iron, through ferric ammonium sulphate, could have attempted to mimic the iron loading observed in IPF patients. However, very small and limited gene expression differences were observed between diseases and therefore this MDM model could have been used, following further characterisation, for ILD patients in general, rather than IPF alone. This limits its use in the context of substituting primary alveolar macrophages.

3.5 Conclusions

This chapter demonstrated an increased iron loading in alveolar macrophages of IPF patients compared to patients with an unclassifiable disease with no fibrosis. Further analysis showed that this increase in iron is significantly associated with the presence of fibrosis and with an IPF diagnosis over an UNC one. The alveolar macrophages phenotype was different between disease, but further validation and characterisation is needed. Finally in control patients that had underlying unexplained cough, the alveolar macrophages of the group with haemoptysis showed increased iron levels, especially if treated with anti-coagulants.

3.6 Appendix

3.6.1 Appendix 3.6.1

Out of the 52 patients that were defined as UNC (both with and without fibrosis), the multi-disciplinary diagnostic team (MDT) had a greater than 70% confidence for two or more pathological entities for 17 of them. Out of this group 15 were thought to possibly have either NonSpecific Interstitial Pneumonia (NSIP) or hypersensitivity pneumonitis (HP), and 2 of them either NSIP or Desquamative interstitial pneumonia (DIP). The other 36 patients in the UNC group were defined as unclassifiable on CT as the MDT had less than 70% confidence in the disease being subacute interstitial pneumonia (SIP), Cryptogenic organising pneumonia (COP), Usual Interstitial Pneumonia (UIP), HP or sarcoidosis.

3.6.2 Appendix 3.6.2

Clinical characteristics for the patients and the control groups used in the Prussian blue study. The UNC with no fibrosis group is significantly younger compared to IPF (A). However, there are no differences in BMI and predicted FVC percentage at time of BAL between the groups (B and C). The differential counting from the BAL-derived cells, show that IPF has a significant less macrophages compared to UNC with fibrosis (D), No statistically significant differences are shown between the three diseases and the controls for neutrophils, lymphocytes and eosinophils, which present at very low levels. This confirms the macrophagic nature of these diseases. Samples were tested for normality with a Shapiro-Wilk test and a Kruskal-Wallis test was performed, with multiple comparisons between the no haemoptysis control group and the disease groups. (* $p<0.05$, ** $p<0.01$, *** $p<0.001$). Error bars = SD; Con with Haemoptysis N=6; Control with no haemoptysis N=3; UNC with no fibrosis N=18; UNC with fibrosis N=35; IPF N=40).

When the control group is separated into the group that had haemoptysis and the one that didn’t no statistically significant difference is observed between the two groups or the other pathological groups

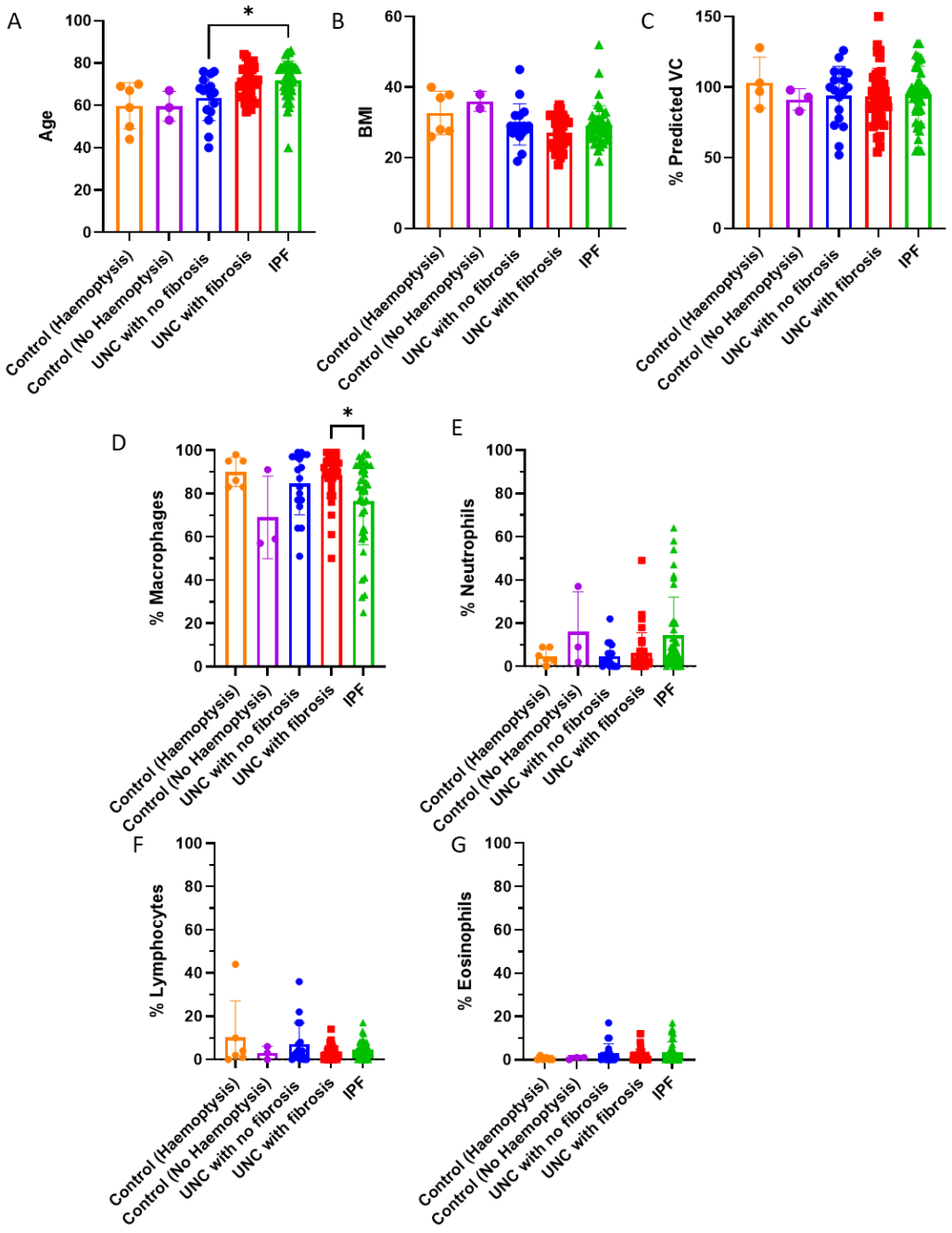
A
Age
100
80
60
40
20
0
*
B
BMI
60
40
20
0
C
% Predicted VC
150
100
50
0
D
% Macrophages
100
80
60
40
20
0
*
E
% Neutrophils
100
80
60
40
20
0
F
% Lymphocytes
100
80
60
40
20
0
G
% Eosinophils
100
80
60
40
20
0
Control (Haemoptysis)
Control (No Haemoptysis)
UNC with no fibrosis
UNC with fibrosis
IPF

3.6.3 Appendix 3.6.3

Single cells were selected from all cells following exclusion of debris (A-B). HLA-DR gating shown correctly identifying larger cells, thus the macrophages, and not the monocyte or other cells (C). Histogram for isotype control (red) compared to fully stained (blue) and unstained (orange) shown as well (D).

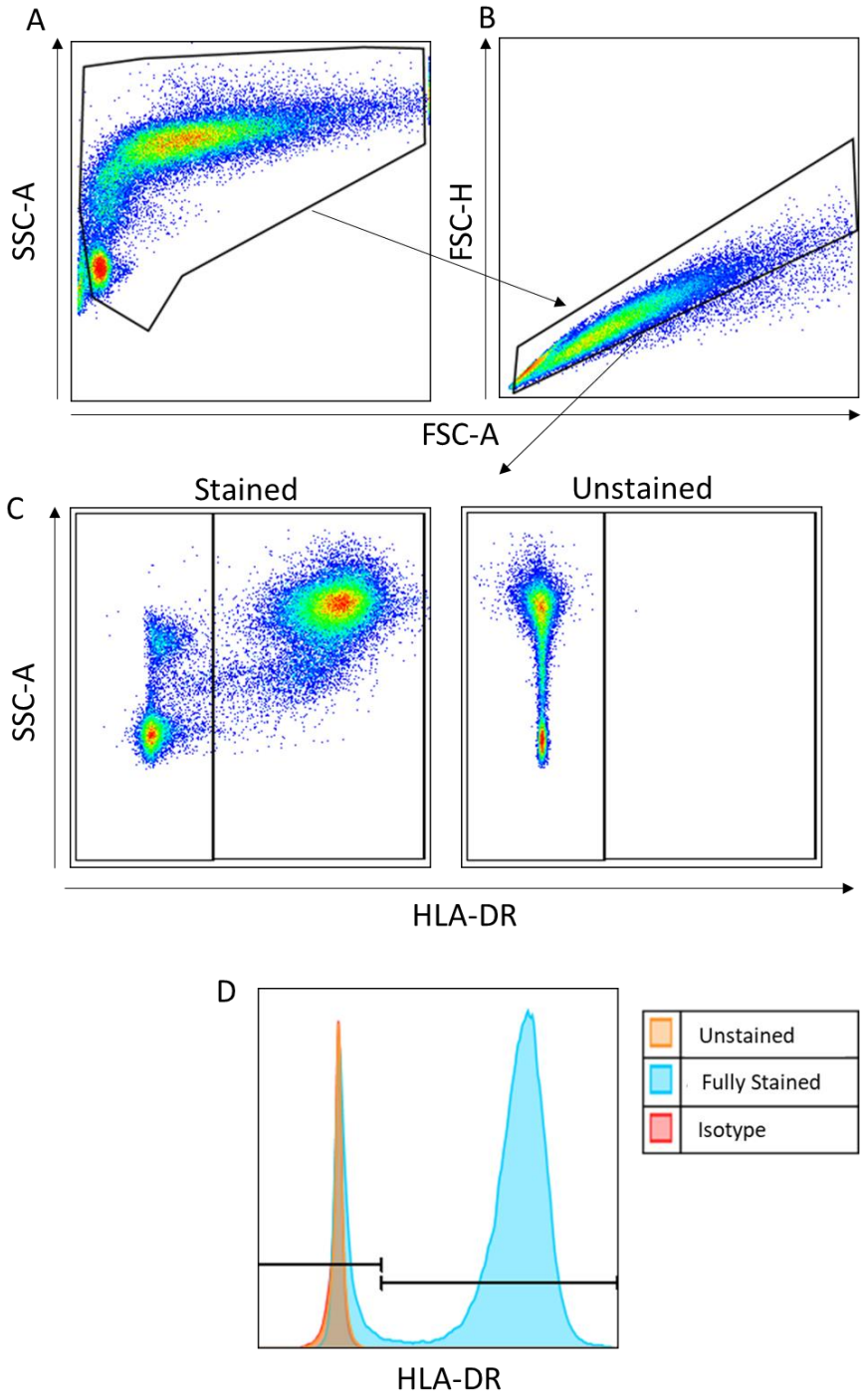

Chapter 4 - The association of macrophage iron and disease progression

4.1 Introduction

Although IPF is most commonly associated with disease progression, other fibrotic ILDs also show progression and the concept of progressive fibrotic ILD (PF-ILD) is now established in clinical practice[254] . Progression can be defined in various ways but change in lung function measurements are routinely used in the clinic. Patients in this study were stratified according to relative change forced vital capacity (FVC) or death over 12 months. If there was ≥10% reduction in FVC or death within a year of BAL, the patient was classified as a 'progressor'.

It is not yet known if the molecular mechanisms that drive progression are the same across IPF and other PF-ILDs. Studies carried out in Hirani lab by Dr Lisa Nicol (published in abstract form[175]) showed that alveolar macrophages CD71 (transferrin receptor) expression through flow cytometry, is associated with disease progression in patients with IPF with high $CD71^{+}$ expression (dichotomised according to the median) leading to worse survival compared to having a low $CD71^{+}$ expression (Figure 1.4.5.1). This suggests a role of iron and macrophages in the progression of disease. The importance of CD71 in this context has been shown by other groups in murine and patient samples[111,112]. In a murine study using the bleomycin model, increased iron was observed and associated with small airway fibrosis and decline in lung function[111]. Allden et al., (2019) showed the proportion of CD71 positive alveolar macrophages were higher in IPF patients than controls, but higher CD71 negative macrophages, which exhibit impaired iron-uptake, were associated with worse survival[112]. CD71 negative cells were not specifically analysed by Nicol et al. Thus CD71 expressing macrophages are abundant in lung fibrosis and iron content in these cells is associated with fibrosis. The association between fibrotic disease progression, macrophage CD71 expression (the main gate for iron-uptake into the cell) and macrophage-iron

content, is not certain. Additionally, the role of iron-regulatory pathways and fibrosis progression is not known.

To understand these relationships further, multiple logistic regression was performed to identify the association between progression and Golde score and other clinical variables known to be associated with progression in fibrotic ILD (IPF or unclassifiable ILD). Moreover, to interrogate the association between the macrophage phenotype and progression, the transcriptome of BAL cell pellets of patients with fibrotic ILD, grouped into progressor versus non-progressors, was analysed. The RNAseq data was analysed by FiosGenomics as described in the methods and materials chapter.

Aims and Hypothesis

The overarching aim of this chapter was to characterise the association between disease progression in fibrotic ILD (IPF and unclassifiable fibrotic ILD) and macrophage iron content and BAL cell transcriptome, particularly iron-regulatory pathways in patients with progressive and non-progressive fibrotic ILD:

Aim 1 – To determine iron content (Golde score) in alveolar macrophages of patients with progressive versus non-progressive ILD

Hypothesis 1 – Patients with progressive fibrosis have higher Golde score than those with non-progressive disease.

Aim 2 – To determine the effect of Golde score and other clinical variables including age, smoking, lung function and sex on progression.

Hypothesis 2 – Golde score independently associated with disease progression

Aim 3 – To characterise BAL cell transcriptome of progressive and non-progressive fibrotic ILD

Hypothesis 3 – The BAL cell iron-regulatory pathway transcriptome is significantly different in progressive disease versus non-progressive disease

4.2 Results

4.2.1 Iron loading is increased in non-progressive patients with fibrotic ILD

In the previous chapter it was established that iron content was higher in the alveolar macrophages of fibrotic versus non-fibrotic patients. Patients with fibrotic ILD (IPF and unclassifiable fibrotic ILD) were allocated into progressors and non-progressors groups according to lung function decline or death. These two groups had a significantly different percentage predicted FVC at time of BAL (Table 4.2.1-1 and Appendix 4.6.1).

Table 4.2.1-1 - Patient demographics of progressors and non-progressors. No statistical differences were observed between the two groups (Mann-Whitney test)

	Non-progressors	Progressors	P value	P value summary
N (UNC with fib/IPF)	47 (22/26)	28 (14/14)		
Age (mean±SD)	70.20±7.99	73.57±6.52	0.08	ns
SEX (males/Females)	15/26	8/15		
BMI	28.66±4.49	29.01±6.59	0.97	ns
Death within 12 months of BAL	0	4		
Current/Ex/Never smoker	12/18/11	6/11/6		
Macrophage (%)	82.67 (±18.93%)	82.18 (±15.23%)	0.37	ns
Neutrophils (%)	10.29 (±16.23%)	9.86 (±12.69%)	0.30	ns
Lymphocytes (%)	3.71 (±3.29%)	4.89 (±4.99%)	0.55	ns
Eosinophils (%)	8.89 (±4.34%)	2.25 (±3.46%)	0.89	ns
% Predicted FVC at BAL	97.40 (±17.05%)	87.81 (±22.54%)	0.04	*

Kaplan-Meier survival curves were constructed and showed the median survival in progressors was of 5.57 years compared to 6.12 years for non-progressors (HR=2.804; 95% CI 1.206 to 6.520; P=0.0003) (Figure 4.2.1.1A). The curves remained significantly different if the 4 patients that died within 12

months were excluded (HR=1.878; 95% CI 0.747 to 4.719; P=0.03) (Appendix 4.6.2). Survival was determined from date of first relevant CT and date of death or census date (31/12/19).

Contrary to the hypothesis, the Golde score was significantly higher in the alveolar macrophages of non-progressors compared to progressors (Mean Golde Score 59.62 ± 43.00 versus 38.71 ± 34.57) (Figure 4.2.1.1B).

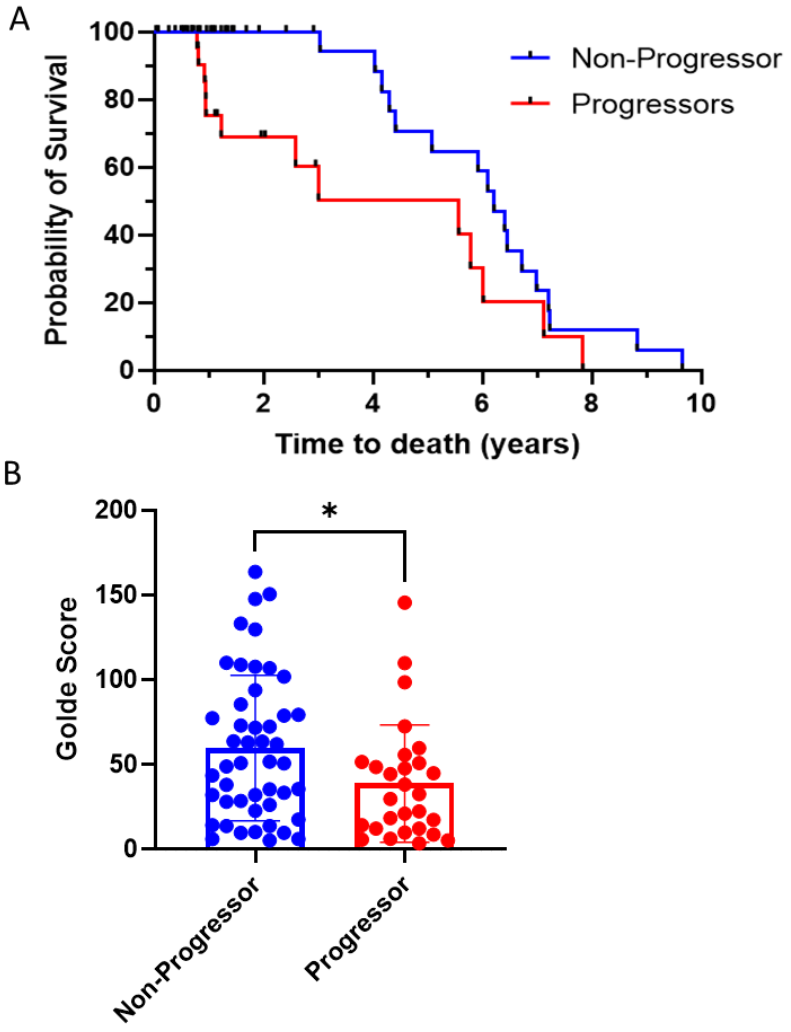

*Figure 4.2.1.1 – (A) Survival curves of the progressor and non-progressor cohorts, considering diagnosis date as start and 31/12/2019 as the census date. Median survival non-progressors = 6.12 years; progressors = 5.58 years). Log-rank (Mantel-Cox) test HR=2.804; 95% CI of ratio 1.206 to 6.520; P=0.0166; (B) Alveolar macrophages of non-progressors had significantly higher Golde scores compared to progressors. Samples were tested for normality with a Shapiro-Wilk test and a Mann Whitney test was performed. * p<0.05, Error bars = SD. Non-progressors N=47; Progressors N=28*

4.2.2 Lower iron loading is independently associated with greater progression in fibrotic ILD

To assess the likelihood of any associations of the clinical variables with the progression status, a multiple logistic regression was performed. The model used was:

$$Progression\ (1) \sim Intercept\ + Golde\ Score + UNCvsIPF + Age\ at\ time\ of\ BAL\ +\ \%\ predicted\ VC\ at\ time\ of\ BAL + sex + smoking\ (3cat)$$

Table 4.2.2-1 - Summary of the parameter estimates of the variables and the relevant p values.

Variable	Estimate (Odds ratio)	95% CI (profile likelihood)	P value	P value summary
UNCvsIPF [1]	1.19	0.39 to 3.70	0.76	ns
Age	1.11	1.03 to 1.22	0.02	*
Golde Score	0.98	0.97 to 0.99	0.04	*
% predicted FVC	0.98	0.95 to 1.0	0.28	ns
Sex [1]	0.94	0.31 to 2.88	0.91	ns
Smoking (Ex)	0.54	0.12 to 2.19	0.40	ns
Smoking (Current)	0.30	0.05 to 1.57	0.17	ns

Table 4.2.2-1 shows the summary of the estimates and statistical analysis from the multiple logistic regression. Lower Golde score had a very small but significant estimated higher risk of disease progression. Higher age also had small but significant estimated higher risk. The percentage predicted FVC at time of BAL, which was shown to be statistically different between these cohorts, did not significantly associate to increased risk of progression in multivariate analysis. Figure 4.2.2.1 displays these results in a forest plot form.

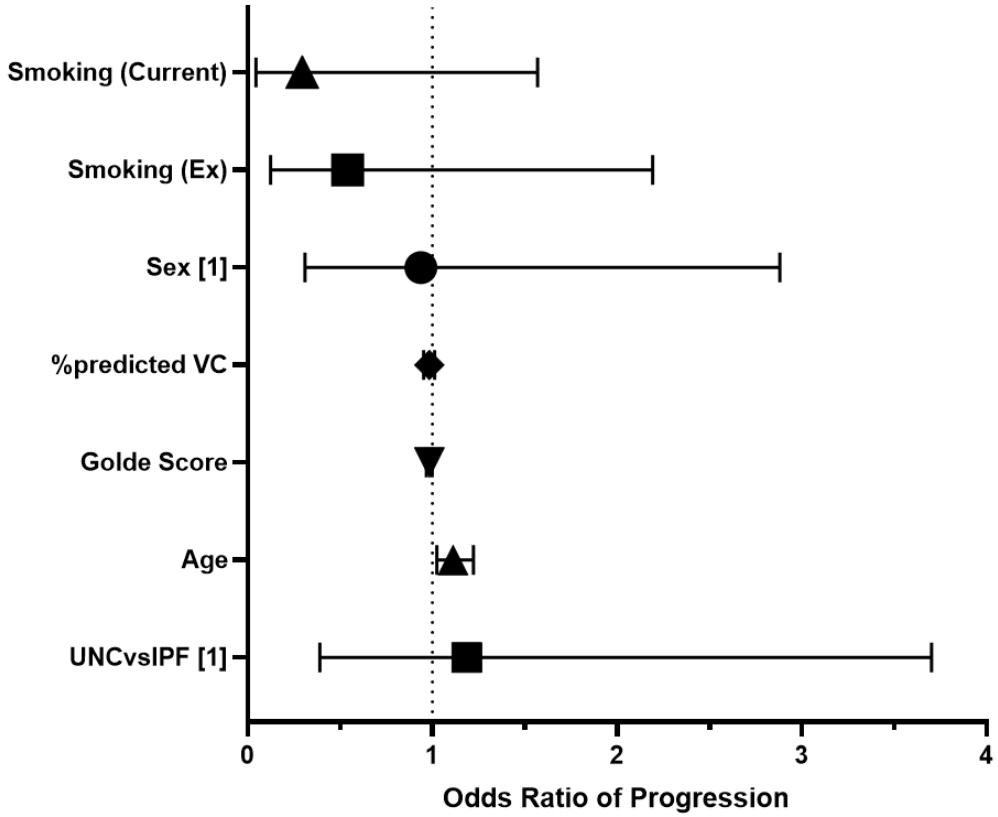

Figure 4.2.2.1 – Forest plot showing odds ratio estimates and 95% confidence intervals for each variable. The only significant associations with progression were age and Golde Score.

4.2.3 RNAseq analysis of progressors vs non-progressors

RNAseq was performed in archived whole BAL cell pellets for fibrotic ILD progressors (N=4) and non-progressors (N=6). When comparing these two groups with a statistical threshold adjusted for multiple testing using the false discovery rate of FDR-adjusted P<0.1, no differentially expressed genes were identified suggesting no significant differences between transcriptomes.

Adopting a more relaxed statistical approach such as unadjusted p-value threshold of P<0.05 greatly increases the risks of false discoveries. The next three subsections discuss the differentially expressed genes (DEGs) between these two groups with this unadjusted P-value threshold, recognising the need for caution when interpreting individual gene expression differences.

4.2.3.1 Differentially Expressed Genes and their effect

Out of 18716 genes identified, 615 genes had an unadjusted P-value of P<0.05. A volcano plot (as -log10 transformed p-values) against the magnitude of fold change (log2(fold change)) is shown in Figure 4.2.3.1. Overall, 215 genes were upregulated in progressors compared to non-progressors (188 genes above 1.3x; 57 genes above 2x) and 400 were downregulated in the same comparison (383 gene by at least 1.3x; 290 genes by at least 2x). In the volcano plot 3 genes with both a significant P-value and a larger fold change were arbitrarily selected, based on a literature search.

gstm1 encodes the Glutathione S-Transferase enzyme that enables the addition of glutathione, a potent antioxidant, to compounds that could cause oxidative stress. In this cohort of patients, *gstm1*is down-regulated in

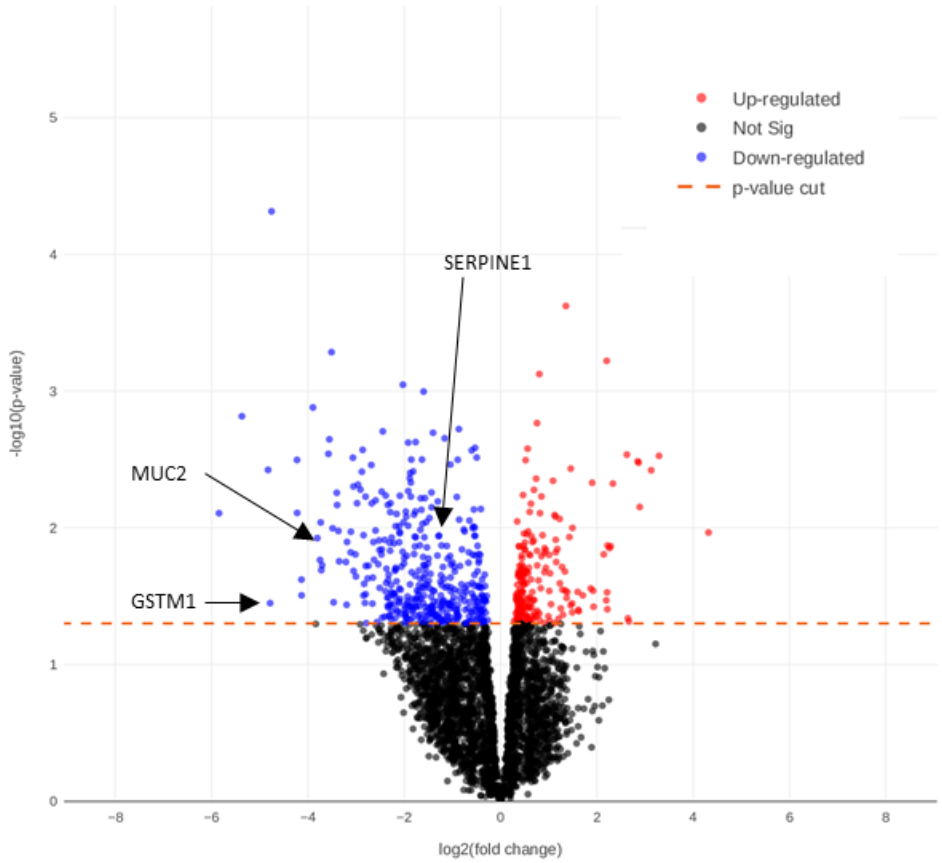

Figure 4.2.3.1 - Volcano plot showing significant (-log10 transformed p-values) against magnitude (log2(fold change)). Genes that are significant are above the orange line and are in blue if downregulated and red if they are upregulated in progressors over non-progressors.

progressors (FC=-27.56; P=0.036). No other genes in the same family had a P-value <0.05.

serpine1 is downregulated in progressors (FC=-2.425; P=0.011). It encodes the plasminogen activator inhibitor 1 (PAI-1). This protein has been shown to be increased in lung fibrotic diseases and relevant murine models, as it inhibits the plasminogen activators (in particular t-PA and uPA) which degrade ECM, and its inhibition supresses pulmonary fibrosis[255,256].

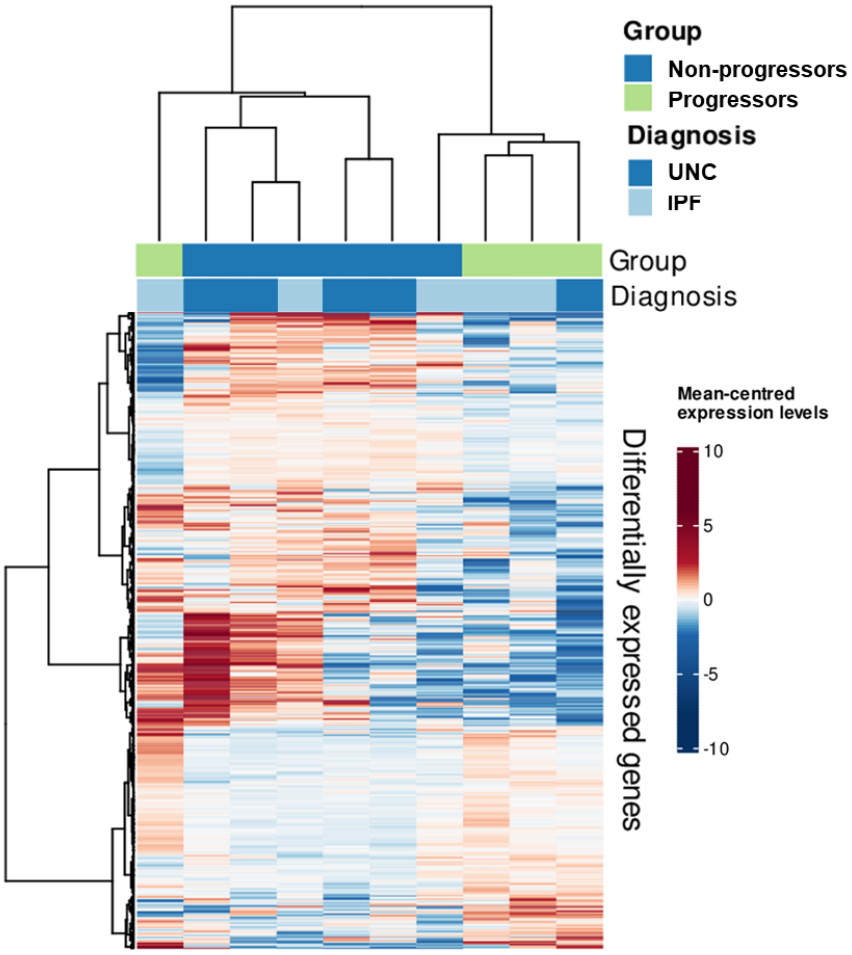

Figure 4.2.3.2 – Heatmap showing gene intensity per sample relative to the average level across the comparison of progressors and non-progressors samples. Individual genes were shown on the y-axis, and samples on the X-axis. Red and blue corresponds to the mean-centered expression levels, high and low respectively. A maximum of 1000 features were shown and chosen at random. An overall good clustering based on progression was shown, except for two patients' samples that are grouped incorrectly. When considering feature clusters, 2 clusters are upregulated, and 3 clusters of genes are downregulated in progressors over non-progressors.

Finally, *muc2* is a gene encoding a secreted gel-forming mucin in the lungs and it was shown to be downregulated in progressors compared to non-progressors by fold-change (FC) = -13.30 (P=0.0091). *muc21*, a gene encoding a transmembrane mucin, was shown to be downregulated in progressors (FC = -4.77; P=0.041) compared to non-progressors and was the only other mucin with a P<0.05 in this comparison[257]. *muc1*, gene encoding KL-6 which serum expression has been associated with progression of disease[35], is not significantly downregulated at the transcriptome level in progressors with a P=0.054 (FC=-2.88).

The heatmap (Figure 4.2.3.2) shows some clustering between the progressors and non-progressors genes. There is one patient from each group that incorrectly clustered with the other progression status. The progressor that clusters with the non-progressors had a very different transcriptome that does not group well with either, making it an outlier. The fingerprint of progression through the dendograms suggests that there are 3 main separate clusters of genes that are downregulated and 2 that are upregulated in progressors over non-progressors. Although this heatmap clusters progression well, samples based on their diagnosis are not well separated. This suggests that IPF and UNC fibrotic disease, when clustered based on progression, are not stratified well.

4.2.3.2 Functional analysis: Reactome pathways and Gene Ontology terms

Functional analysis was performed to identify any Reactome pathways or Gene Ontology (GO) terms that were enriched in DEGs. For the Reactome pathways a bubble plot of enriched pathways is shown in Figure 4.2.3.3. The signal transduction pathway was significantly enriched in non-progressors over progressors (Z=-0.4068; P=4.52x10^{-5}). Oppositely, the interferon α/β signalling is enriched in the progressors compared to the non-progressors (Z-score=0.7293; P= 0.0155). Many of the pathways significantly enriched in the non-progressors are related to erythrocytes, suggesting a possible infiltration of erythrocytes in the samples, further discussed later. Table 4.2.3-3 summarises the top 10 pathways.

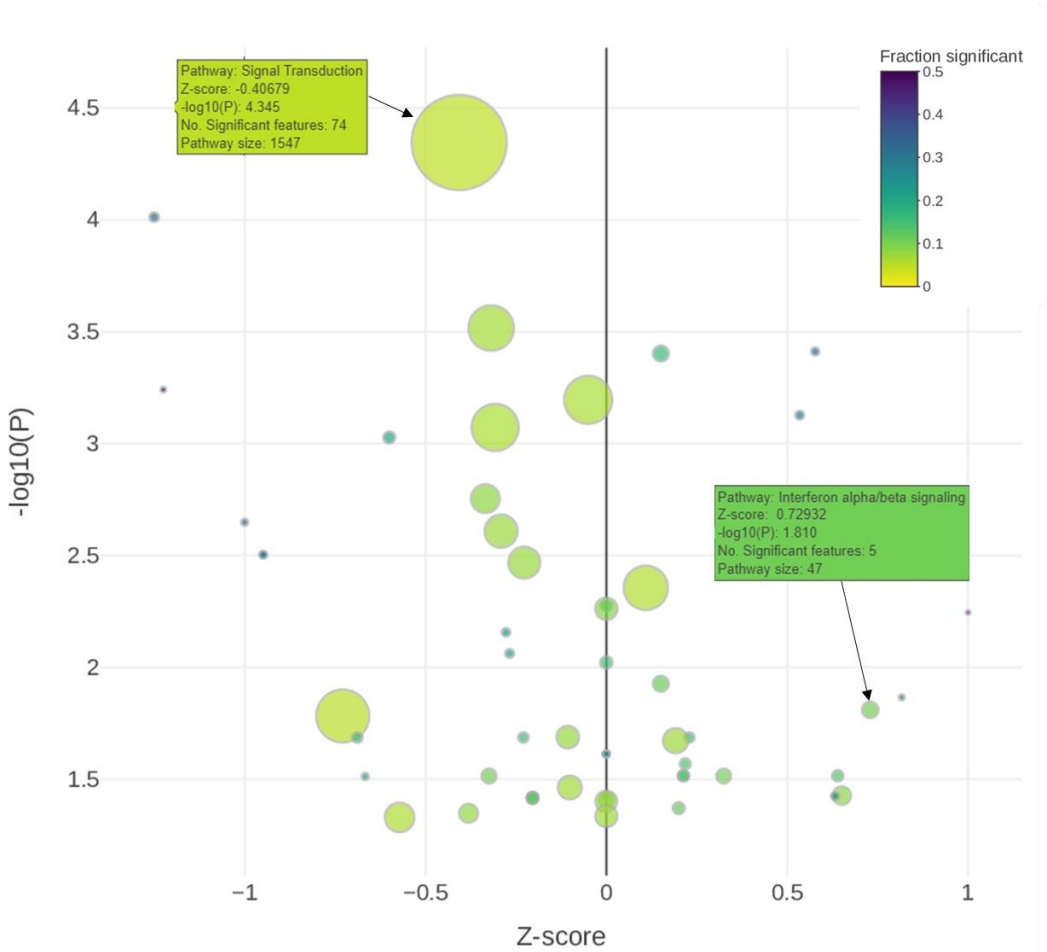

Figure 4.2.3.3 – Bubble plot of enriched Reactome pathways with enrichment Z-score, which considers number of significantly up- and down-regulated genes in the pathway, on the X-axis and -log10(p-value) on the y-axis. Only the top 50 pathways are displayed, and all enriched pathways have a p-value of P<0.05. The size of the bubble represents size of pathway and colour represents the fraction of genes that were significant.

Table 4.2.3-1 – Details of the top 10 Reactome pathways identified as significantly different in progressors compared to non-progressors. S is the number of significantly differentially expressed genes within than the pathway; N is the total number of genes in that pathway; odds ratio (OR) is calculated as the number of significant genes observed over what was expected. P value was calculated through a hypergeometric test and then corrected for tests over multiple pathways through a Benjamin-Hochberg procedure to reach a P-adjusted value.

ID	Name	S	N	S/N (%)	OR	Z-score	P	P (adj.)
R-HSA-162582	Signal Transduction	74	1547	4.783	1.825	-0.407	4.52E-05	0.018
R-HSA-420499	Class C/3 (Metabotropic glutamate/pheromone receptors)	5	16	31.250	14.283	-1.250	9.73E-05	0.020
R-HSA-388396	GPCR downstream signalling	24	355	6.761	2.382	-0.318	3.05E-04	0.032
R-HSA-203615	eNOS activation	4	12	33.333	15.645	0.577	3.88E-04	0.032
R-HSA-3000178	ECM proteoglycans	7	44	15.909	5.978	0.151	3.96E-04	0.032
R-HSA-1247673	Erythrocytes take up oxygen and release carbon dioxide	3	6	50.000	31.167	-1.225	5.74E-04	0.037
R-HSA-109582	Hemostasis	25	396	6.313	2.211	-0.050	6.38E-04	0.037
R-HSA-202131	Metabolism of nitric oxide: eNOS activation and regulation	4	14	28.571	12.512	0.535	7.47E-04	0.038
R-HSA-372790	Signalling by GPCR	24	381	6.299	2.199	-0.307	8.47E-04	0.038
R-HSA-8941326	RUNX2 regulates bone development	5	25	20.000	7.845	-0.600	9.39E-04	0.038

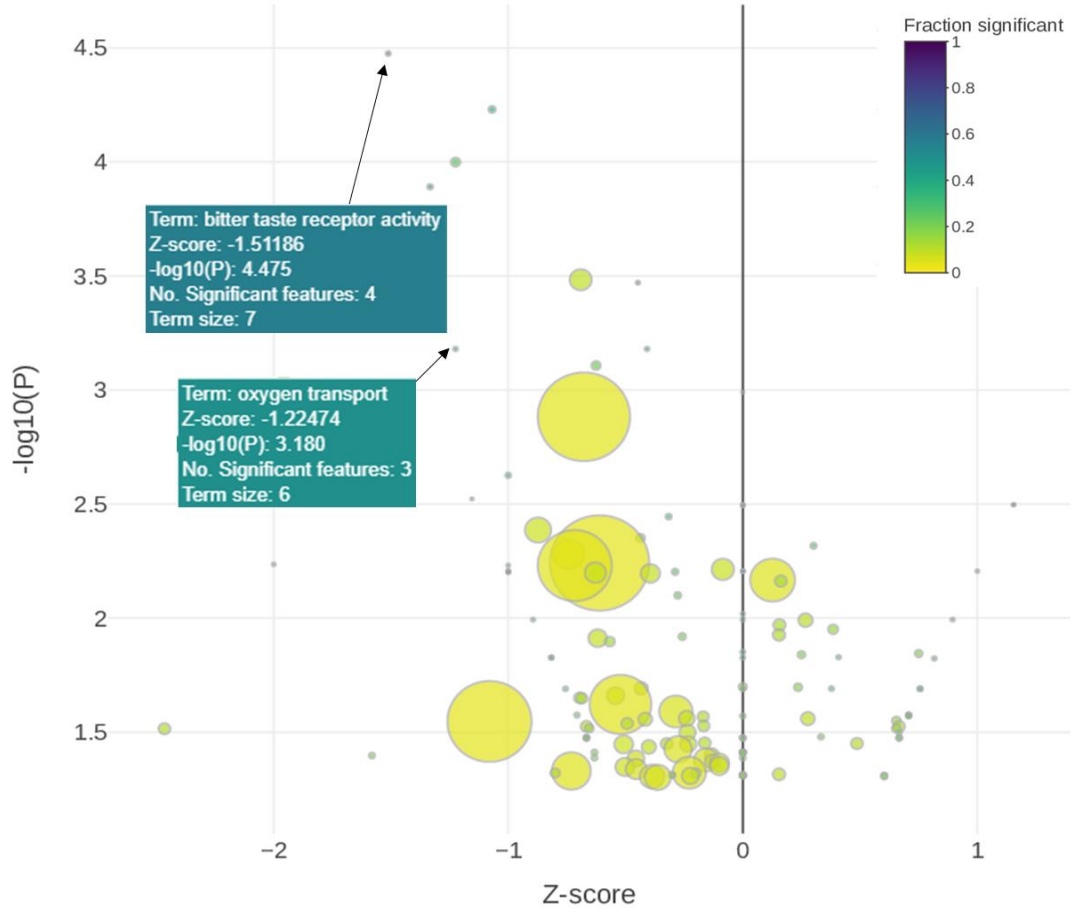

Figure 4.2.3.4 - Bubble plot of enriched GO Terms with enrichment Z-score, which considers number of significantly up- and down-regulated genes in the pathway, on the X-axis and -log10(p-value) on the y-axis. Only the top 50 pathways are displayed which have at least 2 significant genes, and all enriched pathways have a p-value of P<0.05. The size of the bubble represents size of GO term and colour represents the fraction of genes that were significant.

When analysing the GO terms enrichment, “oxygen transport” terms, associated with genes involved with haemoglobin directly, were significantly enriched in the same non-progressive group (Z-score=-1.225; $P=6.603x10^{4}$) (Figure 4.2.3.4). The main genes involved in these pathways are HBA1, HBA2 and SLC4A4.

The most significant GO term that is enriched in this group, shown to be down-regulated in progressors over non-progressors, is the “bitter taste receptor activity” term (Z-score=-1.512; $P=3.346x10^{5}$ and with an adjusted P-value=0.062). They will be discussed further in the discussion section. The top 10 GO-terms that were identified through the analysis are in Table 4.2.3-2.

Table 4.2.3-2 – Details of the top 10 GO terms identified as significantly different in progressors compared to non-progressors. S is the number of significantly differentially expressed genes within than the pathway; N is the total number of genes in that pathway; odds ratio (OR) is calculated as the number of significant genes observed over what was expected. P value was calculated through a hypergeometric test and then corrected for tests over multiple pathways through a Benjamini-Hochberg procedure to reach a P-adjusted value. Ontology abbreviations: BP – biological process; CC – cellular component; MF – molecular function.

Ontology	Name	S	N	S/N (%)	OR	Z-score	P	P (adj.)
MF	bitter taste receptor activity	4	7	57.14	40.786	-1.512	3.35E-05	0.062
BP	detection of chemical stimulus involved in sensory perception	5	14	35.71	16.546	-1.069	5.88E-05	0.062
BP	bicarbonate transport	6	24	25.00	9.929	-1.225	1.00E-04	0.068
BP	detection of chemical stimulus involved in sensory perception of bitter taste	4	9	44.44	23.721	-1.333	1.28E-04	0.068
MF	G protein-coupled receptor activity	13	134	9.70	3.368	-0.691	3.28E-04	0.119
BP	negative regulation of dendritic cell differentiation	3	5	60.00	44.361	-0.447	3.38E-04	0.119
BP	oxygen transport	3	6	50.00	29.571	-1.225	6.60E-04	0.174
BP	L-fructose catabolic process	3	6	50.00	29.571	-0.408	6.60E-04	0.174
BP	sensory perception of taste	5	23	21.74	8.250	-0.626	7.81E-04	0.183
MF	dimethylargininase activity	2	2	100.00	Inf	0.000	1.02E-03	0.190

4.2.3.3 Iron and macrophage genes

In the previous chapter, some genes associated with iron or macrophage polarisation were assessed through qPCR. These genes were therefore pulled

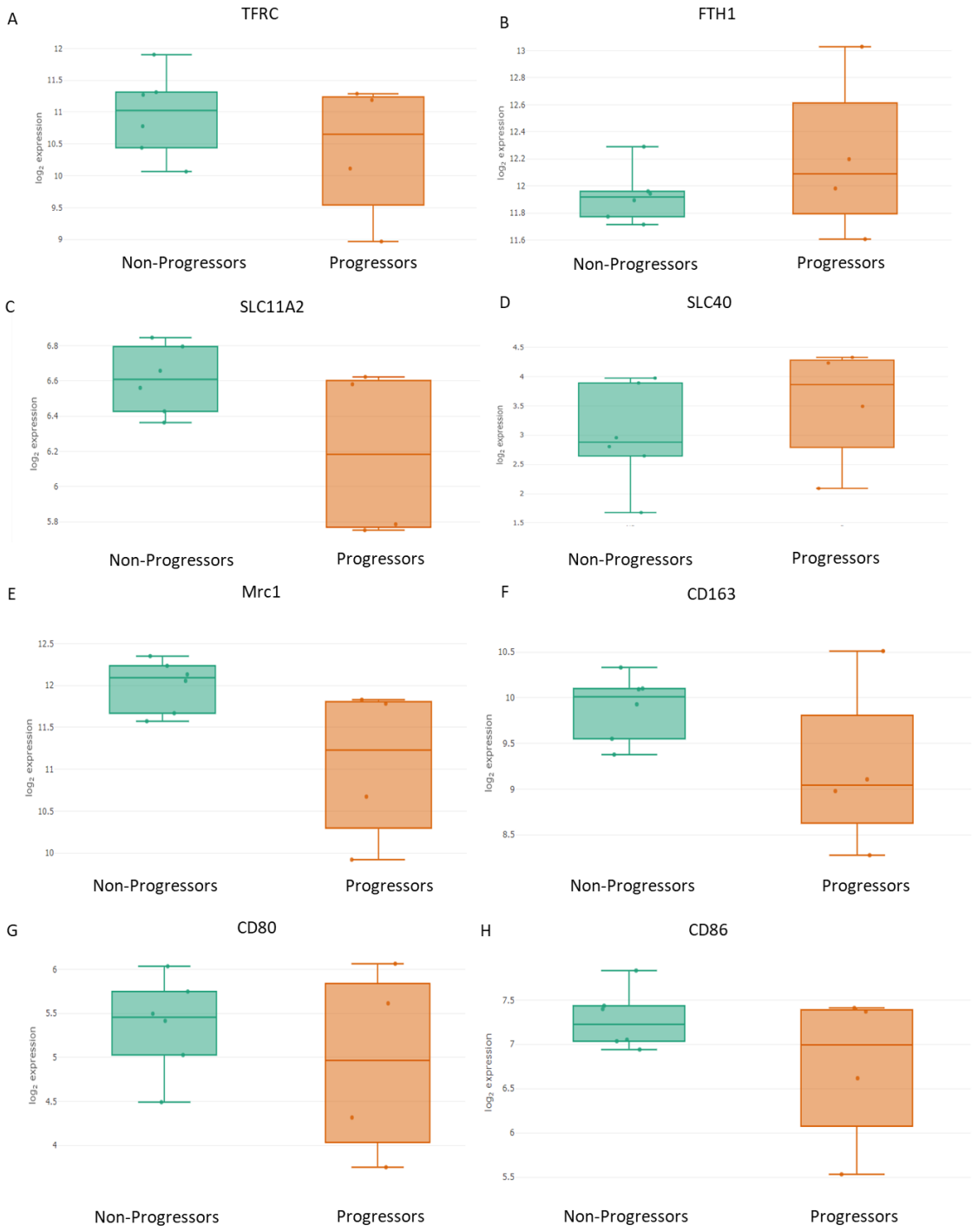

Figure 4.2.3.5 – Box plots of relevant genes expression (log2 expression) previously tested by qPCR in different cohorts, showing no differences across these genes between these patients. In particular (A) TFRC (transferrin receptor); (B) FTH1 (ferritin heavy chain; (C) SLC11A2 (divalent metal transporter 1 – DMT1); (D) SLC40 (ferroportin); (E) MRC1 (CD206); (F) CD163; (G) CD80; (H) CD86. Relevant p value and fold changes are shown in the next table.

out of the RNAseq results to assess any differences in progression. None of these genes resulted significant with the unadjusted P<0.05 value. This suggests there were no differences at the transcriptomic level for these genes. This was summarised in Figure 4.2.3.5, showing box-plots with these genes. Table 4.2.3-3 shows the fold changes and p-values for these genes. The only gene that nearly reached significance (with an unadjusted p-value of 0.0526) was FTH1, encoding the ferritin heavy chain. Expression of this gene was 1.672 times higher in progressors over non-progressors.

Table 4.2.3-3 – Summary of fold changes and P-values of the genes of interest previously analysed

Fig. Label	Gene	FC	Log2(FC)	P	P(adj)
A	TFRC	1.556	0.638	0.252	0.999
B	FTH1	1.672	0.742	0.053	0.790
C	SLC11A2	-1.140	-0.190	0.477	0.999
D	SLC40	2.693	1.429	0.075	0.863
E	Mrc1	1.444	0.530	0.221	0.999
F	CD163	1.903	0.928	0.110	0.946
G	CD80	-1.140	-0.189	0.748	0.999
H	CD86	1.319	0.399	0.286	0.999

4.3 Discussion

Research on fibrotic ILD progression and macrophages is limited. Previous studies have implicated the iron receptor CD71 on alveolar macrophages with progression with higher CD71 expression were associated with reduced survival[175]. High levels of CD71 are normally associated with highly proliferating cells, such as cancer cells, and this is associated with the role of iron in DNA synthesis and general metabolism[246–248].

The overall aim of this chapter was therefore to characterise further alveolar macrophages from fibrotic ILD patients with the hypothesis that higher Golde

score was associated with progression and expression of iron-regulatory genes were differential expressed between progressors and non-progressors.

4.3.1 Macrophage and iron phenotype in progression

In this cohort of fibrotic ILD patients, Golde score was shown to be significantly higher in alveolar macrophages of non-progressors patients compared to progressors, thus rejecting the hypothesis. This suggests that the iron loading observed through Prussian blue was likely to not be linked to the observation of high CD71 in progressors. Analysis of the proportion of CD71 negative cells in these two groups may have aided in understanding the underlying mechanism[112]. Through RNAseq, the genes that were shown in the previous chapter to be different between diseases, were assessed singularly between the two groups. However, none were significantly different, even at the FRD-unadjusted P-value. Similarly, when looking at the genes involved in the transcription of some established M1-like and M2-like markers, no differences were observed. These results suggest that the alveolar macrophages of these two groups are similar and that the increase in iron is unlikely to be associated with changes in transcriptome levels of relevant genes.

When analysing the functional pathways and terms enriched through RNAseq, although no pathways are differentially enriched with an adjusted P value, some pathways are significantly enriched in one group over the other when using an unadjusted $P<0.05$. Interestingly some of the ones enriched in non-progressors were related with erythrocyte and haemoglobin. The cell pellets were red blood cell lysed before RNA extraction so either this step was not thorough enough, or the macrophages may be expressing these receptors due to erythrophagocytosis which has been shown previously[258]. This could also suggest that the iron loading is due to this pathway occurring in the alveolar space. However, differences in this pathway are not observed in all genes involved, such as HMOX1 or HBB. One of the associated enriched GO terms was “oxygen transport”, which has previously shown to implicate hypoxia in the pathogenesis of pulmonary fibrosis[259]. However, none of the other genes involved in the hypoxic pathway were differentially expressed in this cohort.

The lack of overall pathways changes and the fact that an unadjusted P-value is used throughout this analysis, suggests that these changes are merely a speculation and overall inconclusive.

A multiple logistic regression was carried out to identify any variables that could be associated with the likelihood of progression. The only two variables that were shown to be associated significantly with progression were older age and a lower iron level. However, their effect, especially Golde score, was very small and likely to not have a significant impact at the clinical level.

4.3.2 Transcriptome phenotype associated with progression

Overall, no significant differences were observed between the two small groups when considering a FDR adjusted P-value>0.1. When using more relaxed statistical threshold of unadjusted P<0.05 was used and 615 genes fitting this lower threshold were identified. Out of these genes, 215 were upregulated and 400 downregulated in progressors.

Selected genes were highlighted based on their fold-change, unadjusted P-value and through a literature search. The use of a relaxed unadjusted P-value means that the changes observed are speculative and hypothesis-generating, requiring validation.

GSMT1 was shown to be downregulated in the non-progressors group in this cohort, however the link with lung fibrosis is not clear. Previous studies have shown that this enzyme is upregulated in fibrosis and its inhibition leads to attenuation of fibrosis in mice and in cellular models[260,261]. This is in contrast to the idea that antioxidant effects are positive in an inflammatory context. Noticeably the rest of the gene family was not differentially expressed suggesting that this observed fold change may be due to false-discovery rate.

SERPINE1, which is downregulated in progressors, encodes PAI-1, which has been shown to be upregulated in lung fibrosis. It inhibits proteins that are involved in the degradation of ECM, thus fibrosis[255,256,262,263]. Its transcriptome upregulation in non-progressors compared to progressors is therefore

surprising as the opposite would have been expected, with the latter group having a worse outcome.

The mucin family has previously been implicated in IPF. In particular a promoter polymorphism in MUC5B, a secreted mucin, has been shown to be associated with IPF risk[19]. In this study, MUC2 and MUC21 were both shown to be downregulated in progressors compared to non-progressors with an unadjusted P-value <0.05. The functions of these mucins in the fibrotic lungs is unknown.

Studies assessing progression in ILD from multiple aetiologies, identified pro-fibrotic factors that are associated with progressive PF, such as PDGFα/β, MMP-2, MMP-7 and IFNα/β[39,264,265]. These were not significantly different between the two cohorts here discussed, by themselves. However, when assessing the data through functional analysis, thus through identifying relevant Reactome pathways enriched, the interferon α/β signalling pathway, was significantly enriched in progressors over non-progressors. No genes involved in the telomere shortening pathways, a factor known to increase risk of IPF, were shown to be different between these two groups[42].

A heatmap was able to cluster the two progression groups quite well, except for one patient in each group clustering with the wrong group. This suggests some outliers that could be skewing the results significance. The diagnosis was not well clustered in this heatmap. This could suggest that fibrotic UNC and IPF are not significantly different at the transcriptome level. It cannot be excluded that the heterogeneity of these diseases will however influence the observed differences within the groups.

The main pathways and GO Terms identified through functional analysis were related to erythrocytes as discussed previously. Another GO-term that seems to be enriched in non-progressors is the bitter taste receptor activity. Although they have not been identified in IPF, these receptors have been previously studied in the context of other respiratory diseases, such as in asthma, where agonists have been shown to act as potent bronchodilators with therapeutic effects[266,267]. Although the relationship with IPF is unclear, the increase levels

of the transcriptome for these receptors in non-progressors may suggest a link with improved lung function tests.

As aforementioned these are speculation on these observations and care needs to be taken when thinking at future experiments and significance in disease. RNAseq on alveolar macrophages may be appropriate at identifying new targets for IPF but requires a larger dataset and further validation.

4.4 Limitations

The sample sizes were small and were determined by the availability of adequate samples and not by predetermined power calculation. The lack of significance could be linked to the small number of samples tested in a heterogeneous group of patients from different diagnostic groups. A comparison with control patients may have identified differences between the two groups compared to healthy state, possibly highlighting key components of disease progression. The RNAseq was performed on whole BAL cell pellets and not sorted alveolar macrophage which is a significant limitation when interpreting AM-specific gene expression. Further work could aim at isolating alveolar macrophages specifically through FACS sorting and sequencing. The classification of progressors versus non-progressors (mainly according to FVC decline) was based on validated data but it is still an insensitive measure of ‘progression’.

Further studies, both by increasing the number of patients involved, but also by validating these findings and inquiring on possible changes between timepoints, may help improving the current characterisation of progressive fibrosis. In particular, efforts could focus on other types of cells, such as epithelial cells or fibroblasts, or on characterisation of BAL fluid, as cytokines signatures may identify differences between groups. It is also possible that the alveolar macrophages exist in a very heterogeneous population that therefore skews the result by producing noise. FACS sorting specific populations and assessing them singularly may identify key players in progression.

4.5 Conclusions

This study shows that lower Golde score and older age are independently associated with progression, but the effect is very weak. The RNAseq analysis showed that there are no significant differences between progressors and non-progressors when considering an FDR-adjusted P<0.01 value.

4.6 Appendix

4.6.1 Appendix 4.6.1

Demographics of the non-progressors and progressors. No statistical differences were observed between the two groups. The samples were tested for normality and a Mann-Whitney test performed.

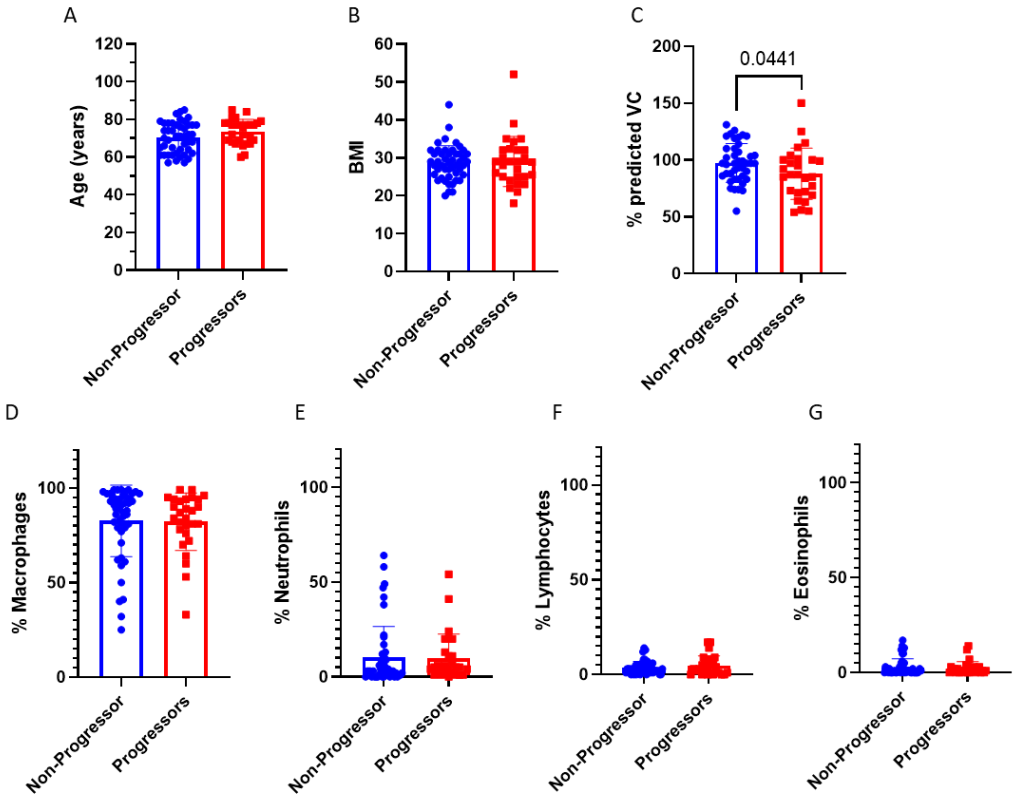

4.6.2 Appendix 4.6.2

The Kaplan Meier curves of progressor and non-progressor cohorts if the 4 patients that died were excluded showed still significant stratification based on definition of progression >10% decrease in FVC within a year. Median Survival for progressors was of 5.78 years; non-progressors for 6.21 years; (HR=1.878; 95% CI 0.747 to 4.719; P=0.03)

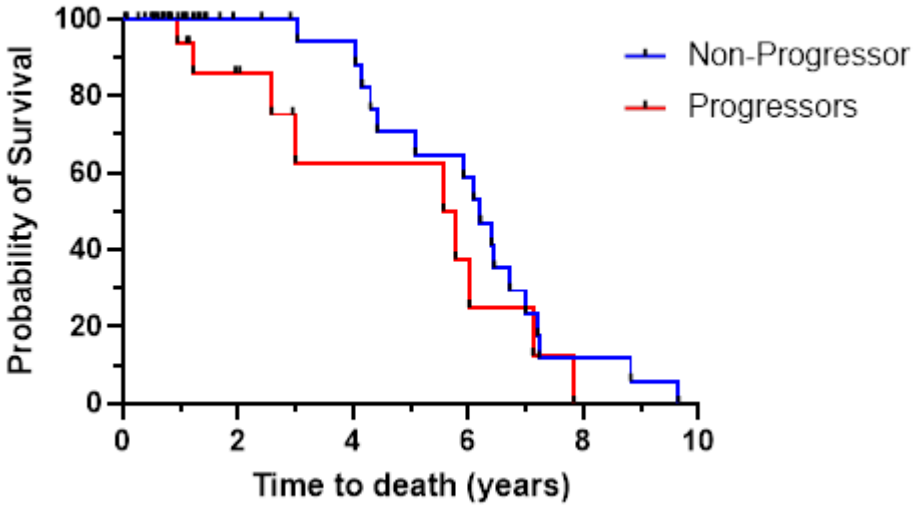

Chapter 5 - Ferroptosis in Macrophages

5.1 Introduction

Ferroptosis is an iron-dependent regulated form of cell death that is caused by an increase in ROS associated with lipid peroxidation and changes in iron and glutamate metabolism. In Chapter 3, iron loading was found to be associated with the presence of lung fibrosis independent of other clinical variables. Despite high iron content, these cells remain viable leading to the overarching hypothesis of this chapter that macrophages are less sensitive to ferroptosis than other cell types.

To study this, GPX4 inhibition through RSL3 and iron-loading studies were performed to induce ferroptosis in two macrophage-like cell lines and the cancerous epithelial cell line HT29 that has previously been shown to be sensitive to ferroptosis[220]. HT29 cells are epithelial-like cells derived from colon adenocarcinoma. RAW 264.7 are a murine macrophage-like cell line. THP1 cells are a human monocytic cell line that grows in suspension which can then be differentiated into macrophages by the addition of PMA.

There is no single marker that is known to identify ferroptosis: cell viability (and exclusion of other causes of cell death), generation of ROS, inhibition of GPX4 and CD71 upregulation have been described as markers of ferroptosis[183,206,268].

The hallmark of ferroptosis is a reduction in viability caused by known ferroptosis inducers such as RSL3. To study viability Propidium Iodide (PI), a red-fluorescent nuclear counterstain, which is not permeable to live cells and binds non-specifically to DNA, was used as a marker of late-stage cell death. This was used in combination with Annexin V (AnxV), a protein that binds to phosphatidylserine in a Ca^{2+}-dependent manner and is a conventional marker of apoptosis.

The ferroptosis-associated increase in reactive oxygen species is caused by either the inhibition of GPX4, leading to the peroxidation of polyunsaturated fatty acids (PUFA), or by Fenton reactions fuelled by the increase in iron. Many

compounds can be used to detect ROS in live cells including dichlorodihydrofluorescein diacetate (H_2DCFDA or DCFDA), which is a reduced form of fluorescein. Upon interaction with ROS, the acetate groups are cleaved, and the non-fluorescent form (H_2DCFDA) is converted to the highly fluorescent 2'7'-dichlorofluorescein (DCF)[269]. The intensity of fluorescence can be tracked through flow cytometry, plate readers or imaging. Liproxstatin-1 is an antioxidant that quenches ROS and is conventionally used to rescue viability in ferroptosis assays.

A more recently described potential marker of ferroptosis is the transferrin receptor (CD71). CD71 antibodies were shown to stain ferroptotic cells, preferentially over apoptotic cells, and this was reduced by the co-treatment with ferrostatin-1, another radical-trapping antioxidant[206]. As discussed in previous chapters, CD71 protein expression was also upregulated in the progressor group of IPF patients studied previously which provides a plausible link between ferroptosis and IPF.

In the studies herein, ferroptosis was induced in cells through i) GPX4 inhibition by RSL3 and ii) pre-treatment with iron in the form of Ferric Ammonium Sulphate (FAS).

Aims and Hypothesis

The overarching hypothesis of this chapter is that macrophages are relatively resistant to ferroptosis compared to HT29 cells.

Aim 1 – To induce and rescue ferroptosis through RSL3 and LIP-1 respectively in macrophage- and HT29 cell lines

Hypothesis 1 – Macrophage-like cell lines are relatively resistant to induction and rescue of ferroptosis compared to HT29

Aim 2 – To determine the relative contribution of ferroptotic versus apoptotic cell death with RSL3 treatment.

Hypothesis 2 – RSL3 induced cell death is not through apoptosis

Aim 3 – To assay ROS, CD71 and GPX4 in macrophages and HT29 cells treated with RSL3 and LIP-1

Hypothesis 3 – ROS, CD71 and GPX4 are differentially modulated in macrophages treated with RSL3 and LIP1 compared with HT29 cells

Aim 4 – To induced ferroptosis with iron-loading in macrophages and HT29 cells

Hypothesis 4 – Iron loading is better tolerated in the macrophage-like cell line compared with HT29 cells

5.2 Results

5.2.1 Macrophage-like cell lines are relatively resistant to RSL3 induction and rescue of ferroptosis compared with HT29

HT29 have been shown to be sensitive to RSL3-induced ferroptosis with LIP1 rescue[220]. Through flow cytometry single cells were gated and viability was assessed using different concentrations of RSL3, with and without LIP1, and at different timepoints. PI staining was used to measure cytotoxicity in single cells. As shown in Figure 5.2.1.1, LIP1 alone did not affect media-treated cells viability at any timepoint. When RSL3 is added at 10μM a PI positive HT29 population was formed (Figure 5.2.1.2A).

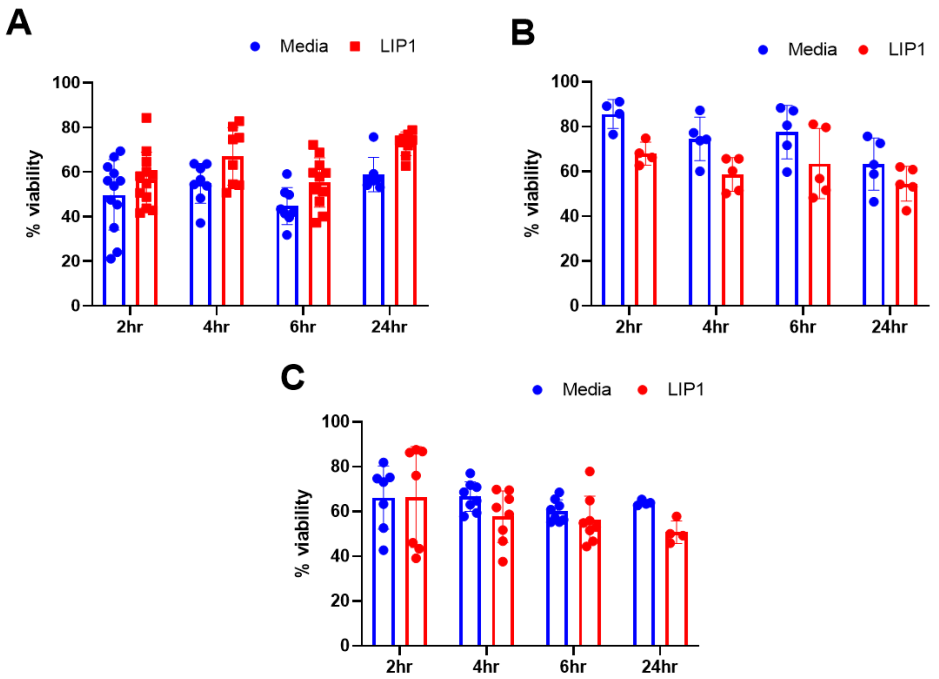

*Figure 5.2.1.1 - Cell viability is not affected by LIP1 treatment over time in (A) HT29, (B) RAW and (C) THP1 cells. Samples were tested for normality with a Shapiro-Wilk test and a 2-way Anova with a Sidak's multiple comparisons test was performed. * p<0.05, ** p<0.01, *** p<0.001. Error bars = SD. N=8*

HT29 cells were then treated at different timepoints with RSL3 at different concentrations and in the presence of LIP1 at 1μM (Figure 5.2.1.2B-C). There was a significant reduction in viability with RSL3 treatment at all concentrations

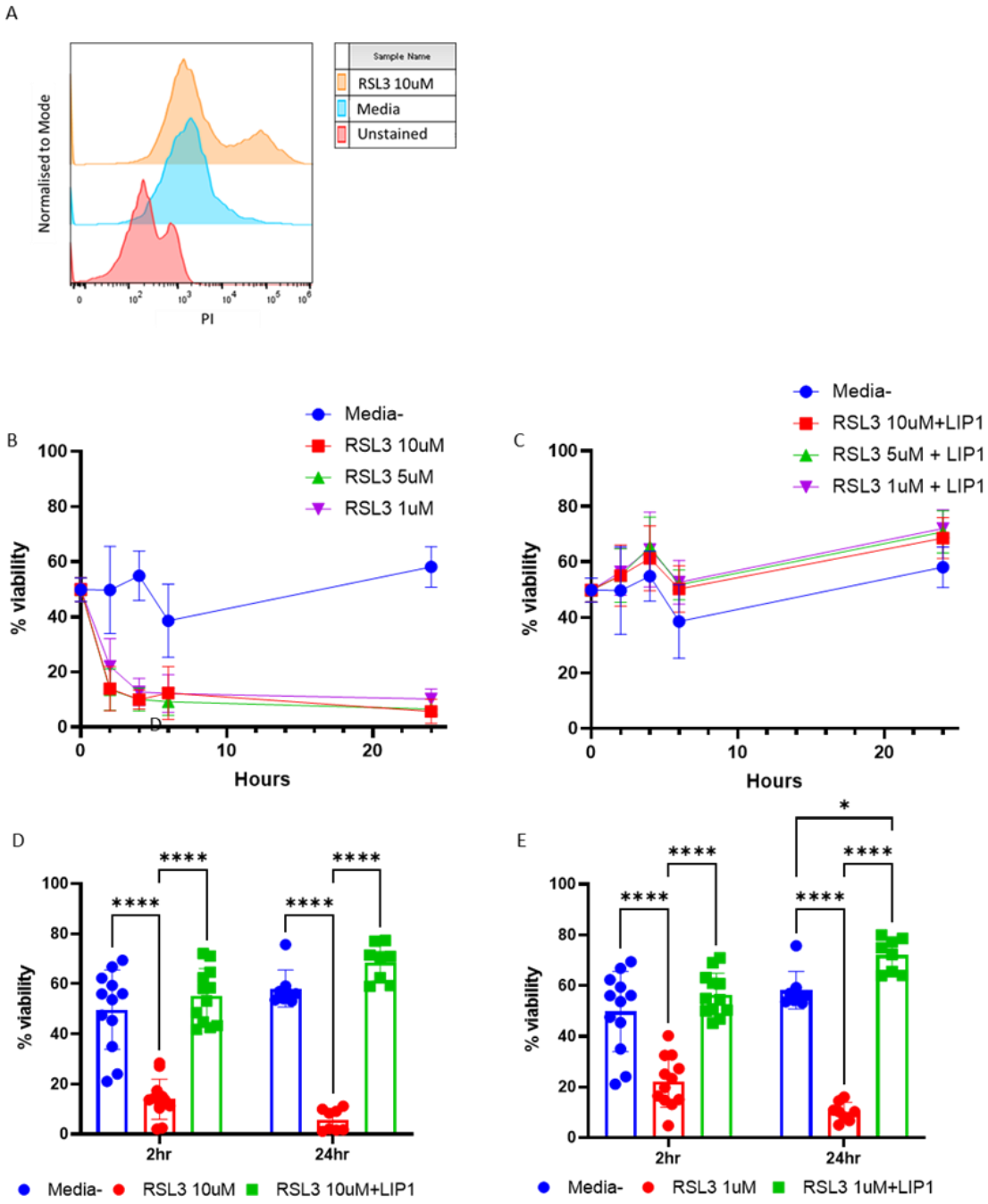

*Figure 5.2.1.2 - Induction and rescue of ferroptosis in HT29 cells. A – Flow histograms showing difference between unstained samples, media and a RSL3 10μM sample stained with PI. B – Time course of the viability showing the samples treated with media compared to samples treated with RSL3. C– Time course of the viability showing the samples treated with media compared to samples treated with RSL3 together with LIP1 at 1μM, showing a rescue in viability. D –Viability was significantly decreased compared to media when 10μM was used both at 2 and 24 hours. It was also significantly rescued to media levels when LIP1 is added to 10μM RSL3. E – Viability was significantly decreased compared to media when 1μM is used both at 2 and 24 hours. It was also significantly rescued to media levels when LIP1 was added to 10μM RSL3. Samples were tested for normality with a Shapiro-Wilk test and a 2-way Anova with a Tukey's multiple comparisons test was performed. * p<0.05, ** p<0.01, *** p<0.001. Error bars = SD. N=12*

compared to untreated cells (media alone) (Appendix 5.6.1). RSL3 significantly affected viability as soon as 2 hours after treatment and this was maintained to 24 hours (Figure 5.2.1.2B-D-E). LIP1 significantly rescued this reduction in viability (Figure 5.2.1.2C-D-E). There was no RSL3 dose response at the doses used. Statistical analysis for all timepoints and doses was performed (Appendix 5.6.1).

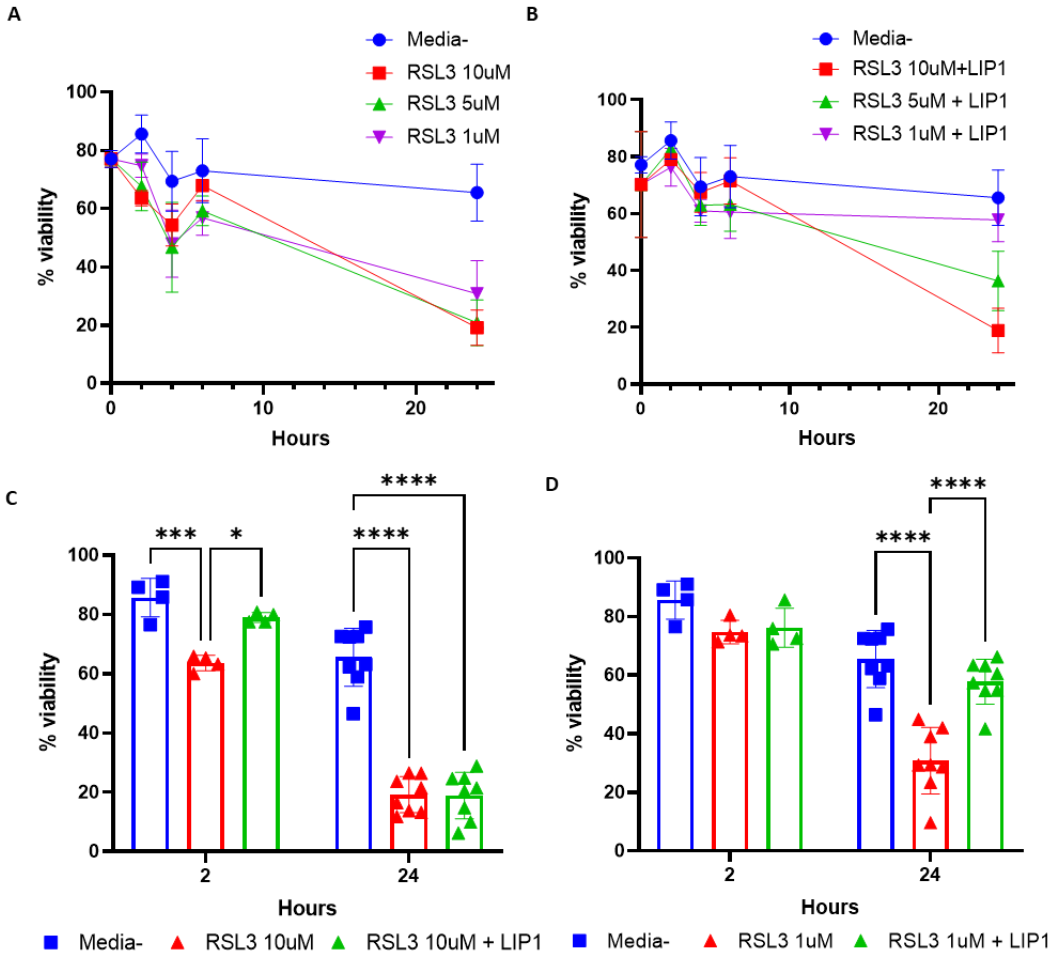

*Figure 5.2.1.3 - Induction and rescue of ferroptosis in RAW cells. A – Time course of the viability showing the samples treated with media compared to samples treated with RSL3. B– Time course of the viability showing the samples treated with media compared to samples treated with RSL3 together with LIP1, showing a rescue in viability. C –Viability was significantly decreased compared to media when 10μM was used following a 24-hours incubation. It was not significantly rescued to media levels when LIP1 was added to 10μM RSL3. D – Viability was significantly decreased compared to media when 1μM was incubated for 24 hours and it was significantly rescued at media levels at this concentration and timepoint. Samples were tested for normality with a Shapiro-Wilk test and a 2-way Anova, with Tukey's multiple comparison test was performed. * p<0.05, ** p<0.01, *** p<0.001 **** p<0.0001. Error bars = SD. N=4/9*

Figure 5.2.1.3A-C-D shows the effect of RSL3 on RAW cells over time. There was a significant reduction in viability at 2 hours but not as great as in HT29 cells. At 24 hours there was a significant reduction in viability associated with RSL3 treatment. This was rescued by LIP1 only at the lowest dose (1μM) of RSL3 (Figure 5.2.1.3B and D). This suggests RAW cells are relatively resistant

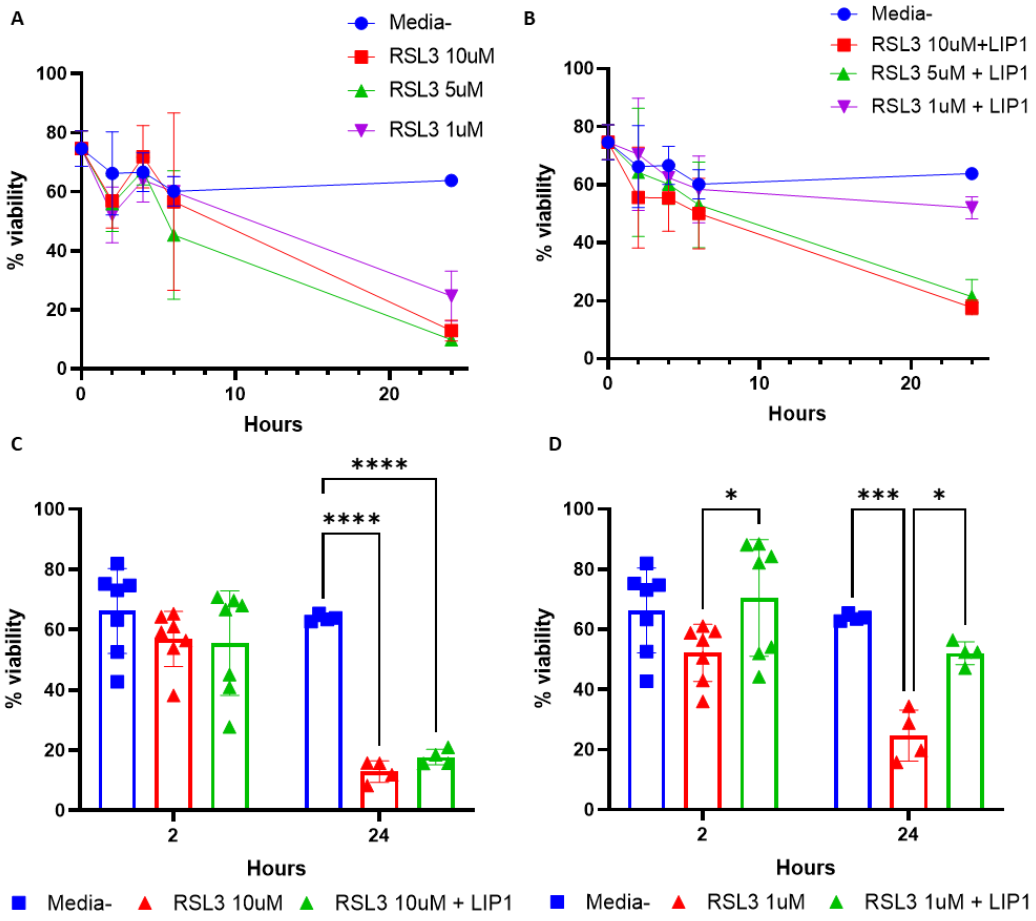

*Figure 5.2.1.4 - Induction and rescue of ferroptosis in PMA-treated THP1 cells. A – Time course of the viability showing the samples treated with media compared to samples treated with RSL3. B– Time course of the viability showing the samples treated with media compared to samples treated with RSL3 together with LIP1, showing a rescue in viability. C –Viability was significantly decreased compared to media when 10μM was used following a 24-hours incubation. It was not significantly rescued to media levels when LIP1 was added to 10μM RSL3. D – Viability was significantly decreased compared to media when the cells were incubated with 1μM RSL3 for 24 hours and it was significantly rescued at media levels at this concentration and timepoint. Samples were tested for normality with a Shapiro-Wilk test and a 2-way Anova, with Tukey's multiple comparison test was performed. * p<0.05, ** p<0.01, *** p<0.001. Error bars = SD. N=9*

to ferroptosis compared to HT29 cells. Statistical analysis for all timepoints and doses was performed (Appendix 5.6.1).

In PMA-treated THP1 cells, at 24 hours at all three concentrations of RSL3 there was a significant reduction of viability compared to media only (Figure 5.2.1.4A-C-D and Appendix 5.6.1) and this was only rescued at the 1μM concentration when LIP1 is present (Figure 5.2.1.4B and Figure 5.2.1.4D). Although ferroptosis was induced by 10μM RSL3 at late timepoints, this was not rescued by LIP1, similarly to RAW cells (Figure 5.2.1.4C). The same pattern is shown at 5μM (Appendix 5.6.1).

Figure 5.2.1.5 shows the percentage change in viability observed from media when RSL3 is added, thus summarising the results from these three cell lines. Overall, these results suggest RAW and THP-1 cells are relatively resistant to ferroptosis induction compared to HT29 cells.

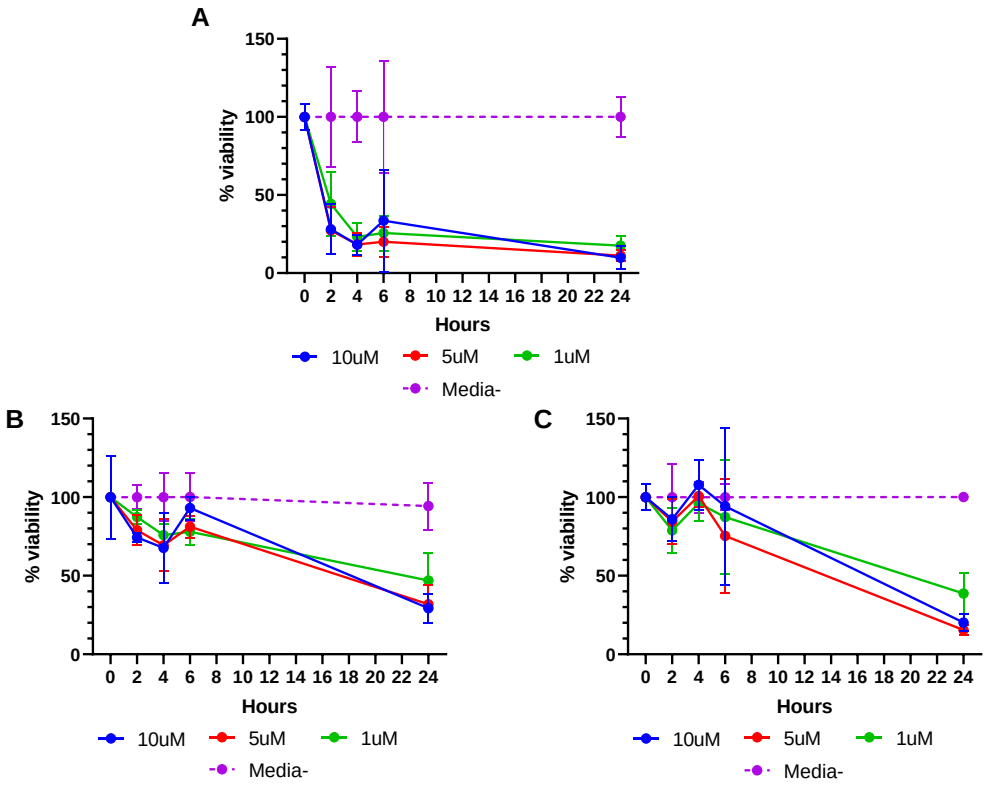

Figure 5.2.1.5 - Percentage change decrease in viability over time when RSL3 is added at different concentrations compared to media showing a greater reduction in viability (over 2 fold change) in HT29 (A) over RAW (B) and PMA-differentiated THP1 cells.

To understand this difference, it was hypothesised that macrophages and HT29 cells have different levels of baseline iron-loading, and this may affect sensitivity to ferroptosis. To address this, cells were stained with Prussian blue (Figure 5.2.1.6). In all three cell lines there was no Prussian blue staining, either in control medium or when treated with RSL3 for 2 hours, suggesting that the change in iron when ferroptosis is pharmacologically induced is below the limit of detection of Prussian blue (Figure 5.2.1.6). At 10μM RSL3 treatment all cell-lines had noticeably shrunk in volume when compared to media treated cells, a typical characteristic of ferroptotic cells[190]. These changes were observed in the macrophage-like cell lines, even if the reduction in viability was not clear, especially in THP1.

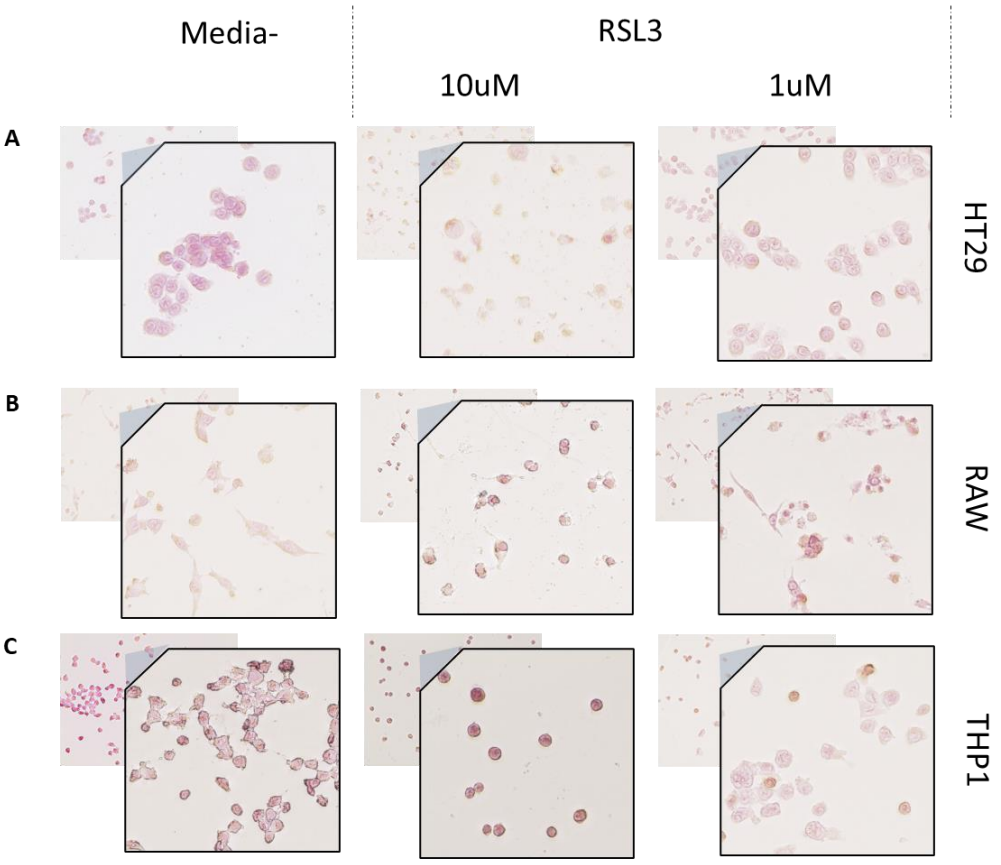

Figure 5.2.1.6 - Prussian blue staining with (A) HT29, (B) RAW, (C) THP1 treated with RSL3 at two different concentrations.

5.2.2 RSL3 causes both apoptosis and ferroptosis in THP1 cell but not in HT29 or RAW cells

The RSL3-induced viability experiments suggested that RLS3 significantly reduced viability in HT29 cells by over two-fold change compared to control, and that macrophages were relatively resistant to RSL3 at early timepoints. By 24 hrs, all cell lines showed low viability (more than 2-fold change from control) at least at higher doses of RSL3. To interrogate whether the cell death observed was indeed ferroptosis and not another form of regulated cell death, apoptosis was assayed by AnxV staining. All cells that were AnxV positive but PI negative, thus excluding cells that were already at later stages of death,

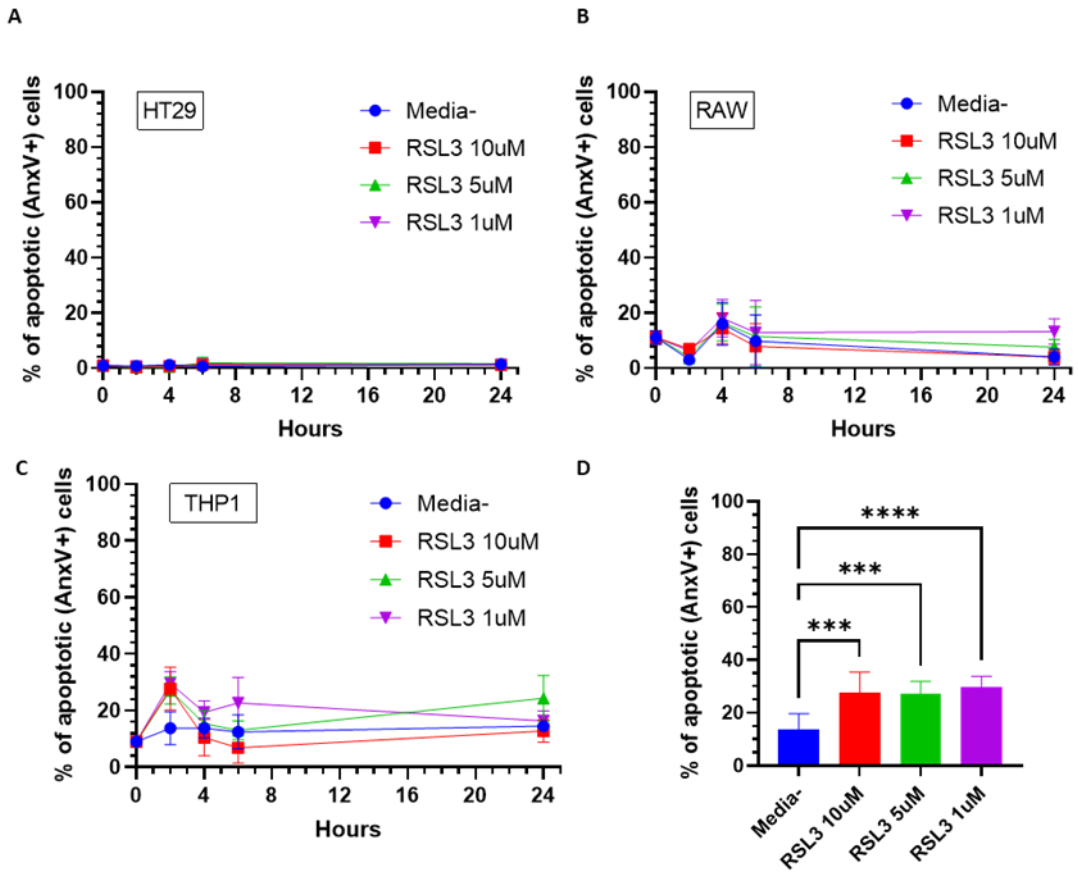

*Figure 5.2.2.1 - Apoptosis level in RSL3 treated cells compared to media. A – Percentage of apoptotic cells (AnxV+) cells following RSL3 treatments in HT29 cells. B – Percentage of apoptotic cells (AnxV+) cells following RSL3 treatments in RAW cells. C – Percentage of apoptotic cells (AnxV+) cells following RSL3 treatments in PMA-treated THP1 cells. D – Graph showing significant difference between THP1 cells at 2 hours following either media or RSL3 treatments. Samples were tested for normality with a Shapiro-Wilk test and a One-way ANOVA performed. * p<0.05, ** p<0.01, *** p<0.001. Error bars = SD.*

were assessed at different timepoints and when different concentrations of RSL3 were added.

HT29 (Figure 5.2.2.1A) had the lowest percentage of apoptotic cells, between 0-3% of single cells. RAW and THP1-differentiated cells had a much higher percentage of apoptotic cells, with about 20% of single cells being only AnxV positive (Figure 5.2.2.1B-C). In both RAW and HT29 cell lines the percentages

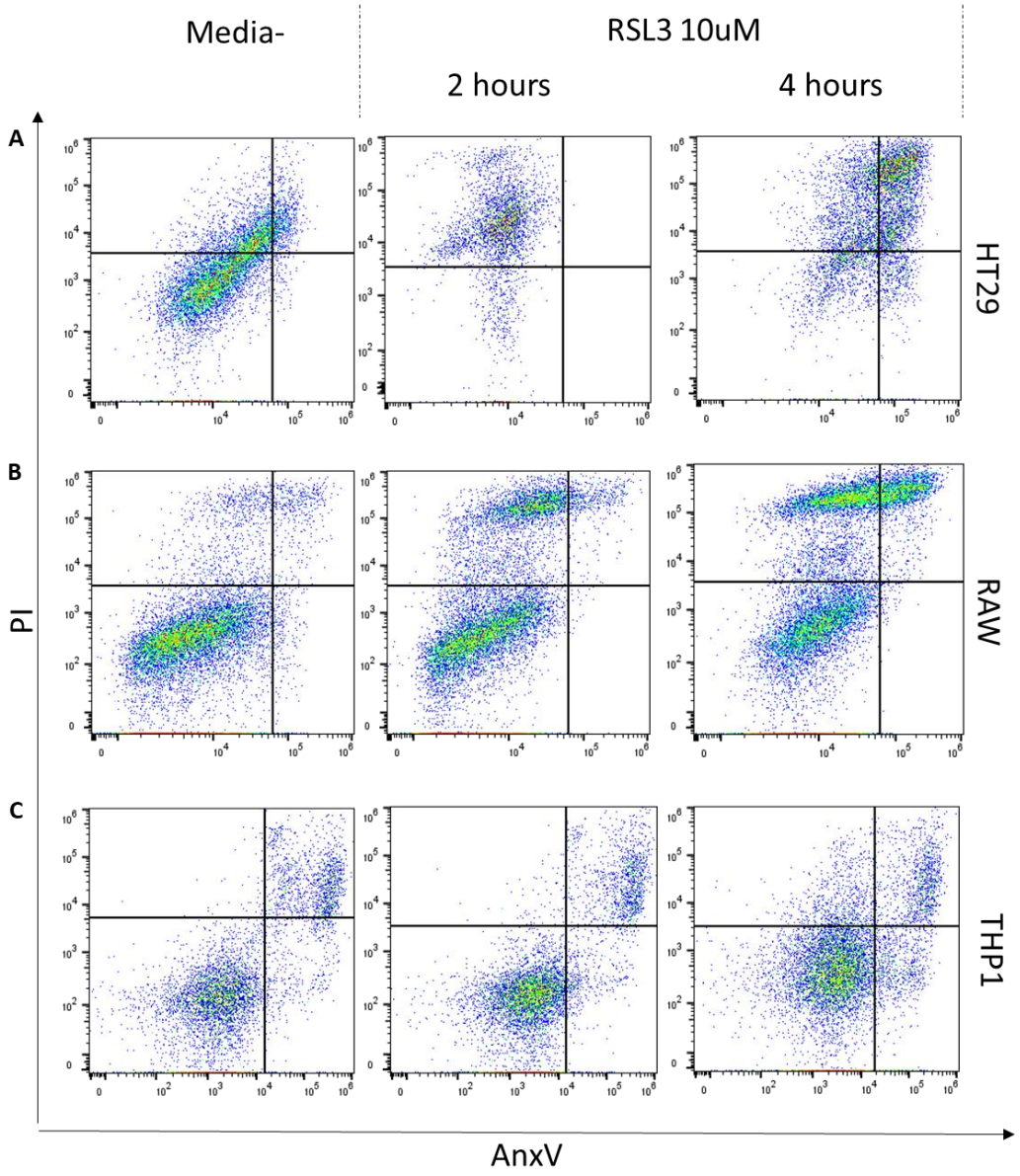

Figure 5.2.2.2 - Flow plots for the cell lines showing AnxV-PI quadrants following treatment with either media or with RSL3 10μM at two different timepoints. A – HT29 showed a shift towards the PI+ quadrants over time with a small percentage of AnxV+ cells initially. The cells seemed to acquire AnxV+ staining mostly after PI staining. B – RAW cells became PI+ following RSL3 treatment and acquired AnxV positivity increasingly over time. C- THP1 seemed to become firstly AnxV+ then acquire PI staining as well over time.

of apoptotic cells are consistent over time and seemed independent of RSL3 concentration. Indeed, the apoptosis present with treatments is comparable to media-only treated cells. This suggests that the reduction in viability observed when these cells are treated with RSL3 is not apoptosis and is therefore likely to be the previously described ferroptosis. In contrast PMA-treated THP1 cells, showed significant apoptosis at 2 hours compared to media (Figure 5.2.2.1D) (mean percentage of apoptotic cells ± SD in media: 13.83 ± 5.89% compared to 27.73 ±7.63% in 10μM RSL3 at 2 hours). This apoptotic population is dominant at early timepoints, with fewer PI+ cells. At later time-points, this relationship is progressively inverted, with the PI+ population becoming dominant.

The levels of staining with AnxV and PI were temporally very different between cell lines. Figure 5.2.2.2 shows the different cell lines following treatment with either media or 10μM RSL3 at 2 and 4 hours. Firstly, all cell lines show a significant level of PI+ cells at baseline in the media condition. Noticeably for HT29 there is an initial PI staining, followed by a slight increase in co-staining with AnxV. When RSL3 is added, the cells tend to be stained by PI firstly and then an increase in AnxV is observed, suggesting that PI+ cells are ferroptotic (Figure 5.2.2.2A). With RAW cells there is a clear shift upwards towards PI+ cells, with some cells also expressing AnxV. This pattern is increased over time when treated with RSL3 confirming ferroptosis (Figure 5.2.2.2B). Finally, THP1 cells seem to follow an initial AnxV+ apoptotic phenotype, to then become co-stained with AnxV-PI and thus entering a late-stage death (Figure 5.2.2.2C). This increase in apoptotic cells in THP1, could be associated just with the modality of death that THP1 undergo normally. As time progresses when treated with RSL3, a dominant PI+ population is formed, showing most cells being at a late-stage cell death. Although some apoptosis is induced in both HT29 and RAW cells independently from RSL3, the apoptotic population in THP1 cells is dominant, especially at early timepoints. These results suggest that the different cells undergo different types of death both at baseline and with RSL3 treatment. RSL3 induces ferroptosis in HT29 and RAW cells but induces both apoptosis and ferroptosis in differentiated-THP1 cells. For this

latter group at later timepoints, the increase in ferroptotic cells (PI+) is mostly associated with AnxV+PI+ cells. The percentage of different cells state across

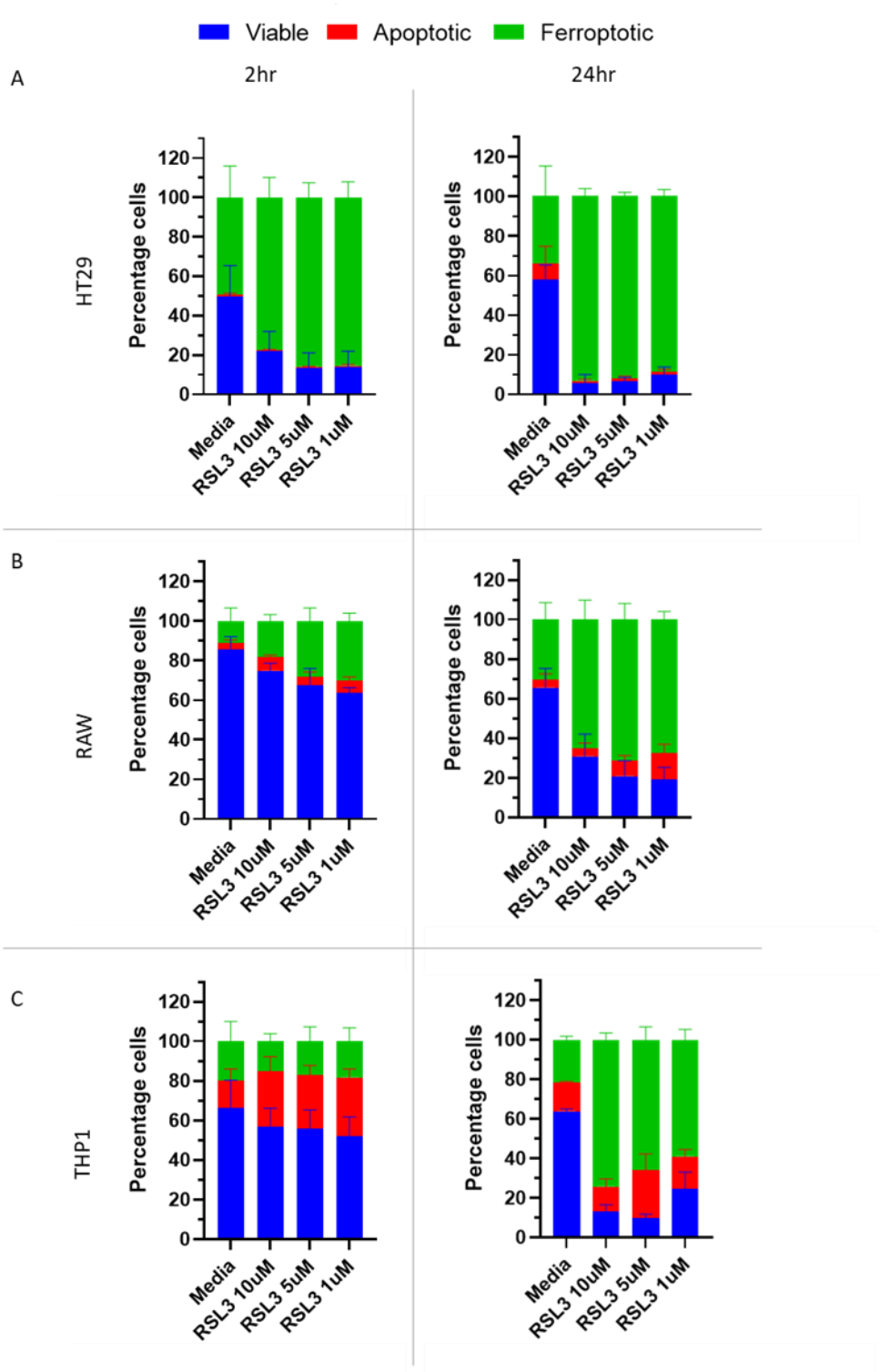

Figure 5.2.2.3 – Summary of the proportions of live, apoptotic and ferroptotic cells in (A) HT29, (B) RAW and (C) THP1.

the three different cell lines is shown in Figure 5.2.2.3, summarising the results hereby discussed. The full timecourse data are shown in Appendix 5.6.2.

5.2.3 RSL3-induced ferroptosis leads to ROS increase at different timepoints and at different levels.

To further elucidate the viability results observed in the previous section, ROS production was assessed through the measurement of fluorescent intensity of DCFDA. The baseline fluorescence intensity of the different cell lines was significantly different between the HT29 and the two macrophage-like cell lines (Figure 5.2.3.1A). To compensate for these baseline differences, each timepoint was normalised to the relevant average of the media-only treated

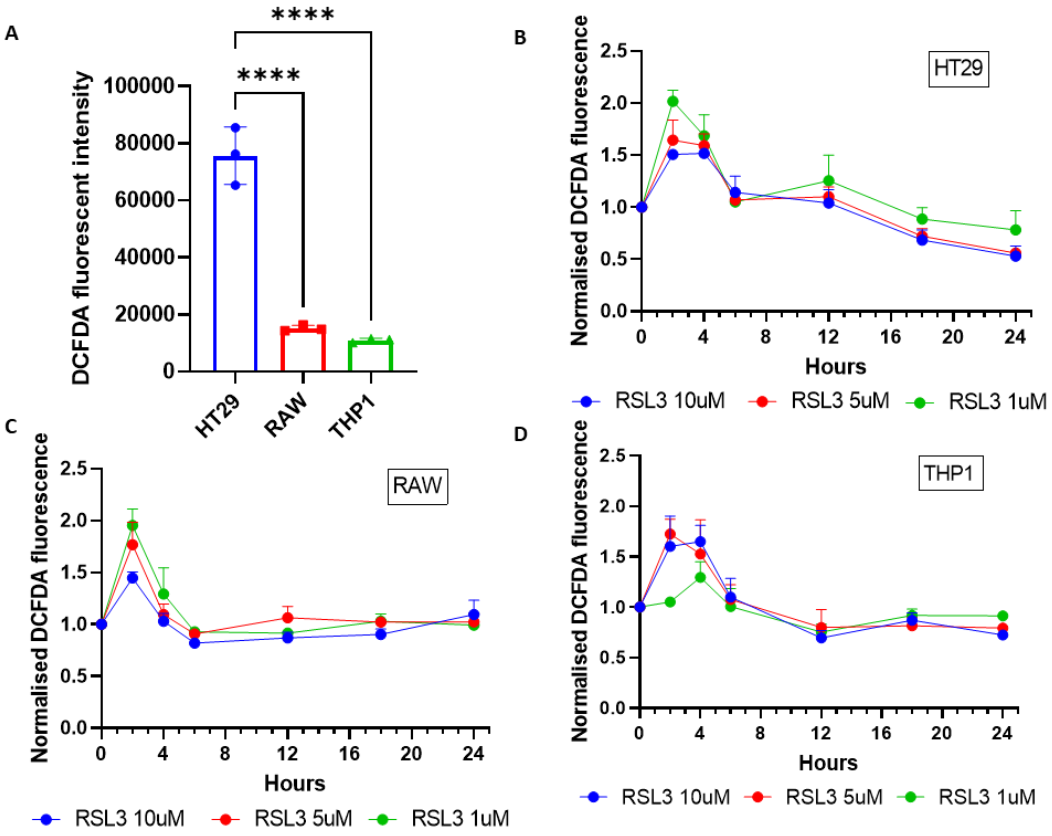

*Figure 5.2.3.1 - ROS detection following RSL3 treatments. A – Graph comparing the different cells lines' baseline ROS through DCFDA fluorescent intensity, showing a higher baseline in HT29 compared to both RAW and THP1 cells. The cells were tested for normality through a Shapiro-Wilkinson test and an Ordinary one-way ANOVA performed. B – Time course showing media-normalised change in ROS when different concentrations of RSL3 were added to HT29 cells. C – Time course showing media-normalised change in ROS when different concentrations of RSL3 were added to RAW cells. D – Time course showing media-normalised change in ROS when different concentrations of RSL3 were added to PMA-differentiated THP1 cells. Samples were tested for normality with a Shapiro-Wilk test and a one-way ANOVA performed. * p<0.05, ** p<0.01, *** p<0.001. Error bars = SD; N=3.*

cells. All cell lines have 1.5-2 fold increase in ROS production 2 hours following RSL3 addition at all concentrations (Figure 5.2.3.1B-C-D). After this initial spike, ROS production decreases and returns at baseline or below, probably due to the reduction in viability of the cells.

In HT29 cells, the lowest concentration of RSL3 (1µM) induces the largest fold-change at 2-hours compared to the higher concentrations (Figure 5.2.3.2A). A similar trend is observed in RAW cells (Figure 5.2.3.2B), but not in THP1 (Figure 5.2.3.2C). This might be due to the abrupt reduction of viability at the higher concentrations, leading to consequent less production. At the lower concentration, the cells are not dying as fast and will therefore continue reacting to RSL3. For HT29 and THP1 this increase in ROS is sustained at 4 hours as well, whereas there is a decrease at the same timepoint in RAW cells.

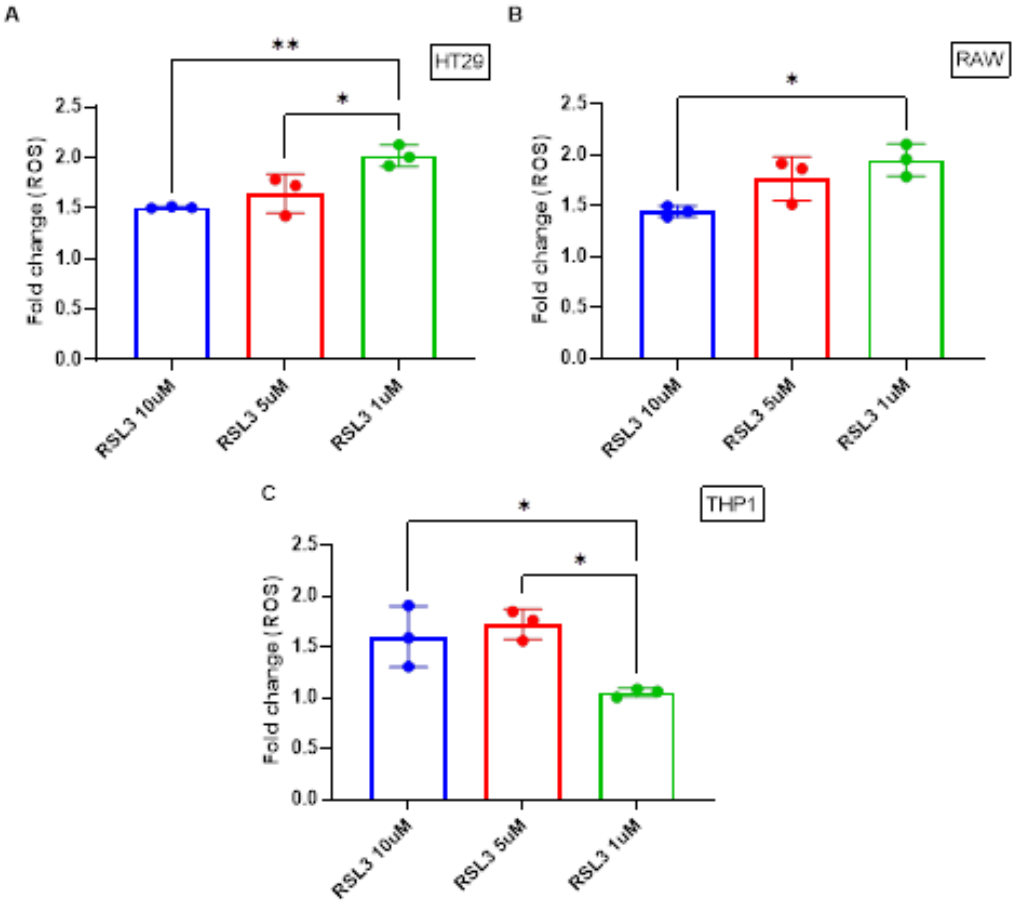

*Figure 5.2.3.2 - Fold change to untreated in ROS at the 2-hour timepoint for HT29 (A), RAW (B) and PMA-treated THP1 (C) cells. Samples were tested for normality with a Shapiro-Wilk test and a One-way ANOVA performed. * p<0.05, ** p<0.01, *** p<0.001. Error bars = SD. N=3*

When LIP1 is added the ROS levels are decreased to media levels for all three cell lines (Figure 5.2.3.3A-B-C). This indicates that the viability rescuing observed previously is indeed due to the radical trapping role of LIP1. HT29

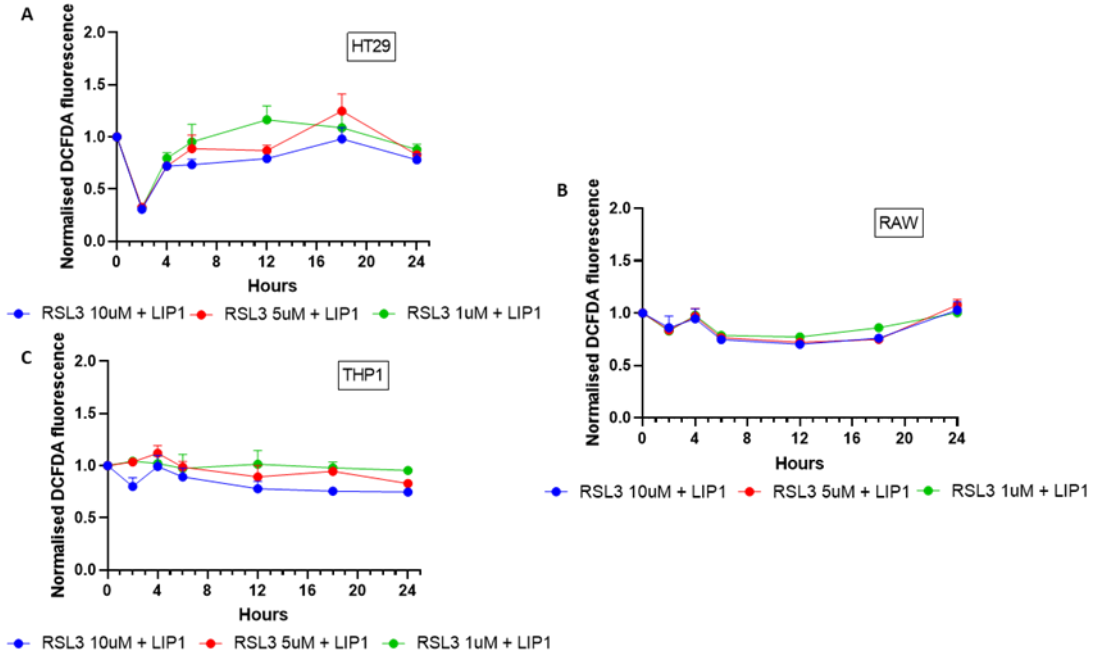

Figure 5.2.3.3 - ROS detection following RSL3 with LIP1 treatments. A – Time course showing media-normalised change in ROS when different concentrations of RSL3 with 1μM LIP1 were added to HT29 cells.B – Time course showing media-normalised change in ROS when different concentrations of RSL3 with 1μM LIP1 were added to RAW cells. D – Time course showing media-normalised change in ROS when different concentrations of RSL3 with 1μM LIP1 were added to PMA-differentiated THP1 cells. Error bars = SD. N=3

ROS levels reduction when LIP1 is present (Figure 5.2.3.3A) is not as clear as the other two cell lines (Figure 5.2.3.3B-C). Indeed, there is more variation and both fold-increases and decreases are observed. This may be due to the originally high fluorescence intensity which gives a larger range for normalisation and thus increased sensitivity to changes. When looking at the effect of LIP1 on media alone, no significant differences are observed in RAW cells (Figure 5.2.3.4B) and THP1 cells (Figure 5.2.3.4B), suggesting that the level of ROS is already at baseline when untreated. However, when looking at the HT29 cells (Figure 5.2.3.4C), a significant decrease is observed at the 2 hour timepoint, similarly to the decrease observed when also treated with RSL3, thus suggesting that HT29 may have a chelatable level of ROS at baseline.

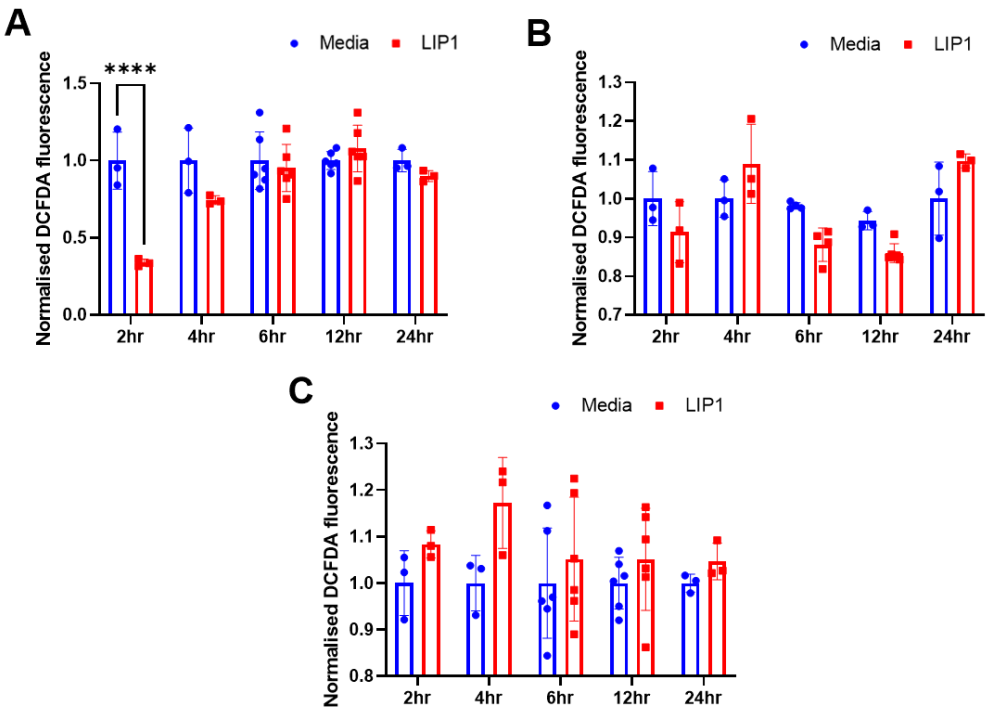

*Figure 5.2.3.4 – Baseline ROS levels are overall not significantly affected by the addition of LIP1 in (A) HT29, (B) RAW and (C) THP1 cells. A significant decrease is observed at the 2-hour timepoint for HT29 cells suggesting a chelatable level of ROS at baseline. Samples were tested for normality with a Shapiro-Wilk test and a 2-way Anova with a Sidak's multiple comparisons test was performed. * p<0.05, ** p<0.01, *** p<0.001. Error bars = SD. N=8*

5.2.4 CD71 is not consistently expressed when ferroptosis is induced.

CD71 (*TfR1*) was recently identified as a marker of ferroptosis[206]. The three different cell lines were assessed for CD71 protein and gene expression after RSL3 and LIP1 treatments. In HT29 cells no changes in *TfR1* mRNA levels were observed suggesting that the transferrin receptor was not affected at the gene level following RSL3 treatment (Figure 5.2.4.2A). The expression levels of the receptor were therefore assessed by flow cytometry. The antibody unspecific binding was tested by using a matching isotype and comparing it to the unstained and stained sample (Figure 5.2.4.1B). HT29 cells were observed to have a CD71 positive and a CD71 negative population. It was first interrogated whether these two distinct populations differ over time and whether the addition of RSL3 as a ferroptosis inducer, would impact the CD71+ population. In the control media-treated sample, there was a significant

reduction in frequency of CD71+ between the early timepoints and the 24-hour timepoint (Figure 5.2.4.1C). This reduction was observed with the RSL3 treated samples as well, with the 10μM and 5μM samples decreasing the most, and remaining below the media-treated samples. These results seem to partially mirror the reduction in viability observed in Figure 5.2.1.2. However, the proportion of CD71+ cells in the 1μM treated cells remained high in contrast with the reduction in viability previously observed. LIP1 treated samples maintained high levels of CD71 positive cells, comparable to media at all timepoints (Figure 5.2.4.1D).

The geometric mean of CD71, both for the CD71 positive cells alone but also for all single cells (thus considering both the CD71 positive and negative populations), showed similar concentration dependent trends (Figure 5.2.4.2A-B). At 2 hours the levels of CD71 expression of the 1μM treated

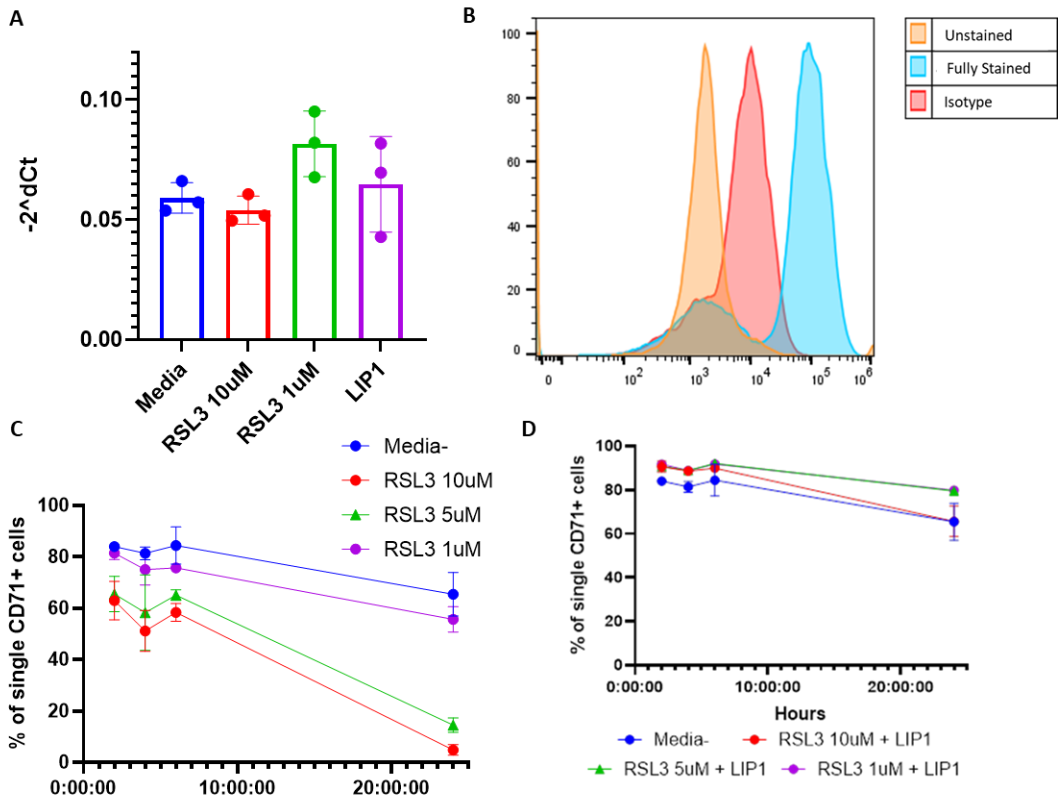

Figure 5.2.4.1 - HT29 and CD71 expression. A – There was no significant difference in the transferrin receptor mRNA between treatments. B – Flow histogram showing difference between unstained, stained and isotype in HT29 cells. C – Time course showing the percentage of CD71+ cells with the different treatments over time. D – Time course showing changes in CD71+ cells percentage when RSL3 is added with LIP1.Error bars = SD; N=3

samples is significantly higher than the media sample only when looking at the CD71 positive cells, and not when looking at the single cells (thus considering the CD71- population as well) (Figure 5.2.4.2C). This may suggest that the CD71+ cells increased expression of CD71 when ferroptosis is induced through lower concentrations of RSL3, even though the proportion of CD71+ cells did not vary compared to media at 2 hours (Figure 5.2.4.2D and Figure 5.2.4.1C). This was not observed at the higher concentrations at the time-point studied. CD71 is also a marker of proliferation[250,270,271] and therefore the abrupt reduction in viability at high concentrations of RSL3 may impact the overall expression of CD71 as well as the frequency of CD71 positive cells. This could

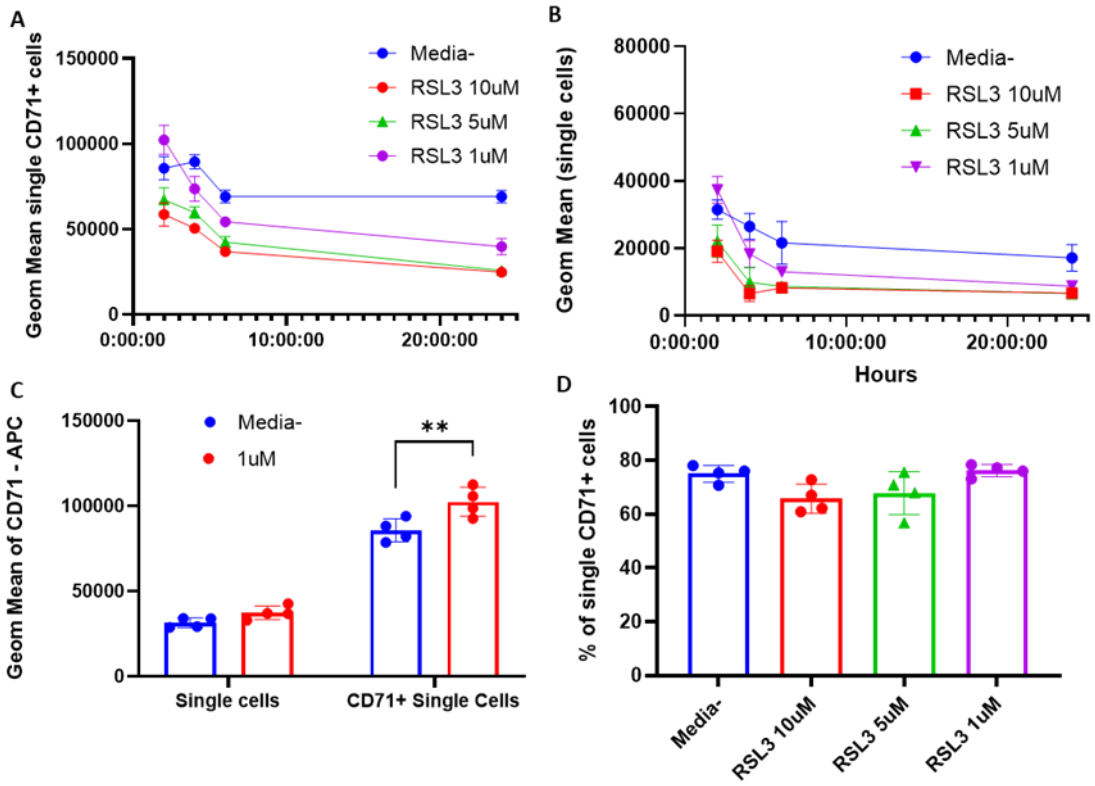

*Figure 5.2.4.2 – CD71 expression in HT29 cells. A – Time course showing the geometric mean of CD71+ cells with the different treatments over time. B – Time course showing the geometric mean for CD71 (APC) of single cells with the different treatments over time. C – Plot comparing the geometric mean of CD71 in media and in 1μM RSL3 treatment at 2 hours between single cells and between CD71+ single cells., suggesting an increase in CD71 when ferroptosis was induced at low concentration of RSL3 in CD71+ cells. D – Proportion of CD71+ single cells at 2 hours at different concentrations of RSL3. The cells were tested for Normality was tested with a Shapiro-Wilk test and a 2-way ANOVA (C) with Tukey's multiple comparison test or a one-way ANOVA (D), performed. * p<0.05, ** p<0.01, *** p<0.001. Error bars = SD. N=3/4*

also suggest that the reduction in viability observed earlier could have been at different stages depending on concentration of RSL3 used.

In RAW cells, specificity of the antibody was assessed with an isotype (Figure 5.2.4.3A). A more distinct difference was observed between fully stained and the isotype compared to HT29. A CD71 negative population was not observed in RAW cells.

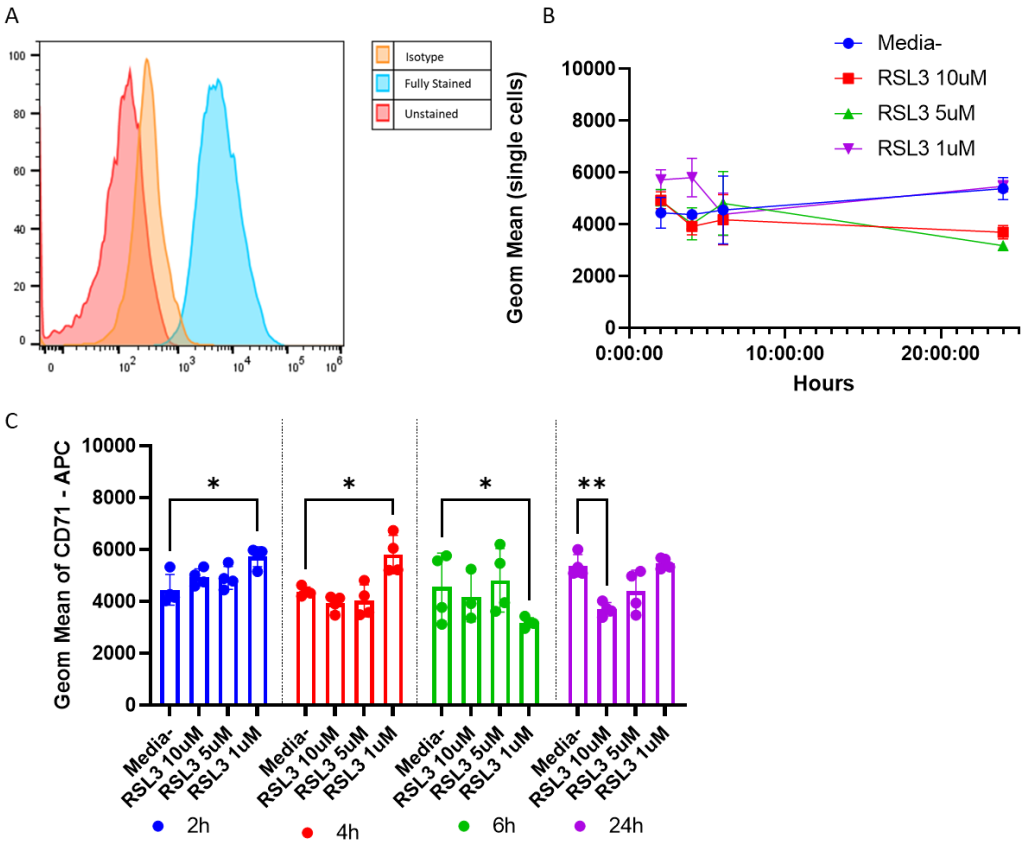

*Figure 5.2.4.3 - RAW cells CD71 expression. A - Flow histogram showing difference between unstained, stained and isotype in RAW cells. B – Time course showing the geometric mean for CD71 (APC) of single cells with the different treatments over time. C – Graph showing differences in CD71 geometric mean between time points and treatments with RSL3. There is an increase of CD71 compared to media at 2 and 4 hours when RAW cells were treated with 1μM of RLS3. Normality was tested through a Shapiro-Wilk test and a 2-way ANOVA, with Tukey's multiple comparison test, performed comparing treatments to media. * p<0.05, ** p<0.01, *** p<0.001. Error bars = SD. N=4*

At late stages, the RSL3 treatments follow similar trends compared to HT29, with the two treatments at 5μM and 10μM decreasing CD71 expression over time, whereas in control and 1μM RSL3 CD71 expression remained relatively high (Figure 5.2.4.3B). Observing the different timepoints singularly (Figure 5.2.4.3C), the higher concentration of RSL3 did not result in significantly higher

CD71 expression compared to media. Similarly, to HT29, and highlighted by the higher albeit non-significant level at the early timepoint, the increase in CD71 caused by ferroptosis might have been earlier than 2 hours in and was therefore missed. At the lowest concentration of RSL3 (1μM), CD71 expression was significantly different to control at early timepoints (2 and 4 hours) but not at late timepoints (6 and 24 hours). This reinforces the possibility of being able to observe CD71 increase at earlier timepoints for other concentrations.

In THP-1 cells, to assess specificity an isotype was used as control and the cells were incubated with an Fc block. To optimise the protocol the cells were either incubated with the Fc block (1:500) for 10 minutes on ice prior to staining or the Fc block was added at the same concentration together with the antibody, which was then left to stain for 30 minutes on ice. However, neither of the methods were very effective at blocking unspecific binding. As shown in Figure 5.2.4.4, the isotype histogram overlaps the fully stained one for both

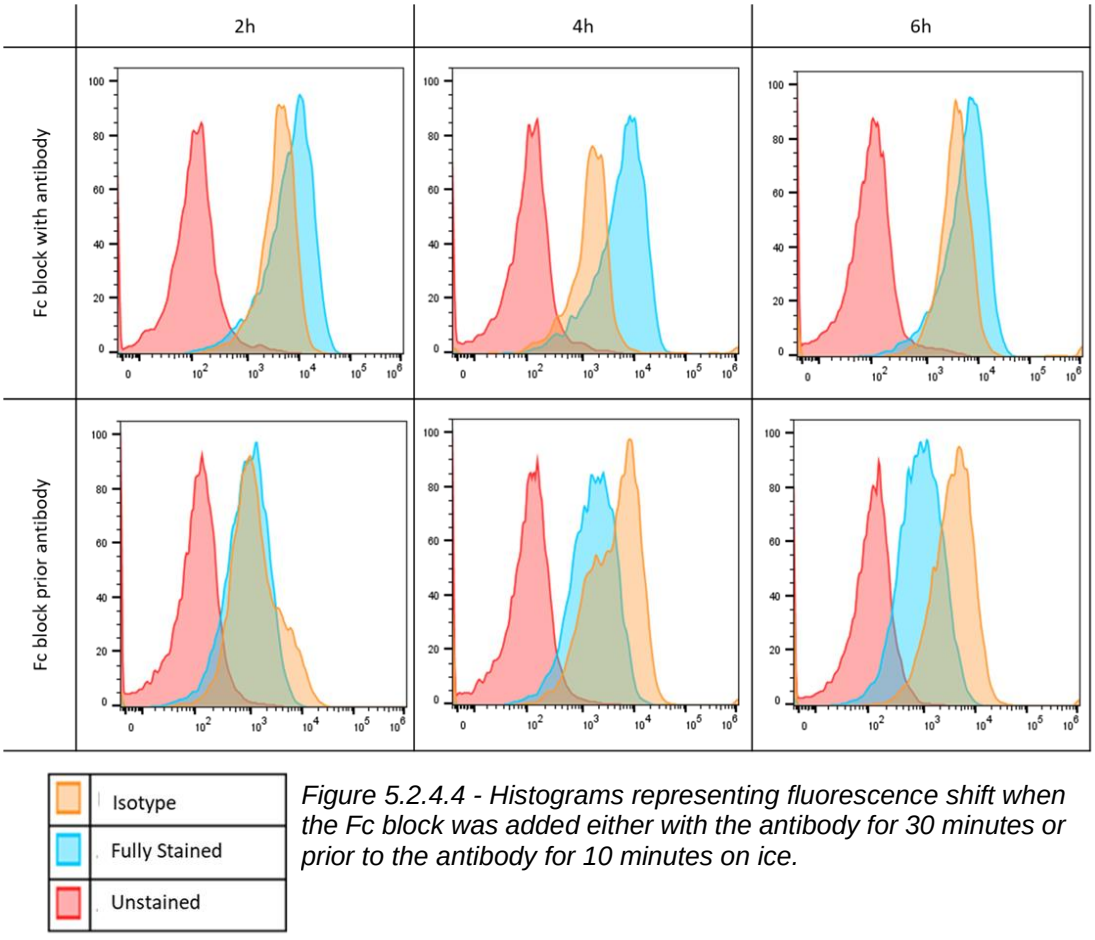

Figure 5.2.4.4 - Histograms representing fluorescence shift when the Fc block was added either with the antibody for 30 minutes or prior to the antibody for 10 minutes on ice.

methods, with a slight improvement when looking at the method that involved incubating the Fc block together with the antibody. This method seems to perform better at later timepoints. No analysis was therefore performed on these samples.

5.2.5 RSL3 treatment results in increased GSH in RAW cells

RSL3 is a GPX4 inhibitor that is thought to bind directly to the active site of the enzyme and block its ability to catalyse the conversion of two molecules of glutathione (GSH) into glutathione disulphide (GSSG), its oxidised form. Attempts to assess GPX4 activity with RSL3 treatment through a specific assay were unsuccessful. Therefore, the GPX4's substrate, GSH was measured with a colorimetric commercial assay, anticipating an increase in GSH accumulation following enzyme inhibition.

In HT29 there was an abolition in GSH levels with RSL3 compared to media which was rescued LIP1 treatment (Figure 5.2.5.1A). The likely explanation for this was reduced viability in these cells at 2 hours.

In RAW cells, which are relatively resistant to RSL3 induced death, RSL3 at 1uM had no effect on GSH. However, treatment with 10μM of RSL3, showed no significant changes of GSH compared to media (12.35 μM vs 7.67 μM;

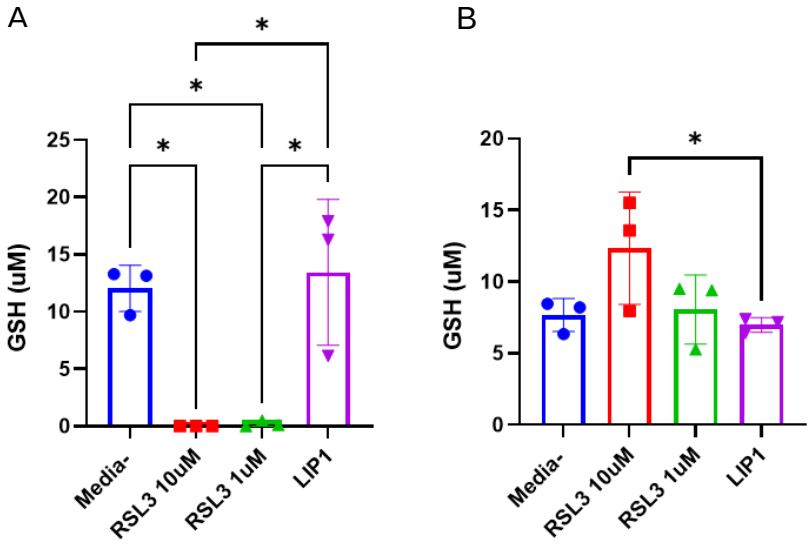

*Figure 5.2.5.1 – Quantification of GSH levels following two hours of RSL3 treatment in (A) HT29 and (B) RAW cells. Samples were tested for normality and a 2way ANOVA with Tukey's multiple comparison test performed * p<0.05, ** p<0.01, *** p<0.001. Error bars = SD N=3*

P=0.0636), which was rescued with LIP1 (12.35 µM vs 6.99 µM, P=0.0368) (Figure 5.2.5.1B). This implies RSL3 may be inhibiting GPX4 resulting in accumulating GSH.

5.2.6 FAS treatment causes an increase in cell death (mostly ferroptosis) at all timepoints with or without RSL3

One of the key components of ferroptosis is an increase in intracellular iron which generates ROS production and death. Alveolar macrophages from lung fibrosis patients were observed to have high iron load. HT29, RAW and THP-1 cells were therefore incubated with Ferric Ammonium Sulphate (FAS 200µM) for two hours before fixing and staining with Prussian Blue, as previously carried out in patient samples. The following data describes viability changes firstly when iron is added alone, and then when RSL3 is added following iron pre-treatment.

Viability was assessed by incubating cells with FAS (200µM) for two hours and then replacing supernatant with fresh medium. Compared to control, HT29 cells exhibited a significant reduction in viability immediately following the 2-hour incubation with FAS (0 hours). This reduction in relative reduced viability was sustained throughout the 24 hours, at which timepoint viability increases in both controls and FAS treated cells suggesting cell proliferation. (Figure 5.2.6.1A). Apoptosis was very low in HT29 cells (<2%) and was not increased with FAS treatment, implying cell death was through ferroptosis. RAW cells (Figure 5.2.6.1B) exhibited a significant and consistent reduction in viability over time with iron. At 2-hours, there was an increase in apoptotic cells in the iron-loading condition compared to no iron, suggesting that iron predominantly induces apoptosis rather than ferroptosis at this time-point. At the 4-hour timepoint and beyond, the significant reduction is viability is mostly non-apoptotic suggesting ferroptosis and/or secondary necrosis of previously apoptotic cells. In PMA-treated THP1 cells (Figure 5.2.6.1C) the decrease in viability associated with FAS treatment was significant but not as great as in the other cell lines. FAS pre-treatment did not induce apoptosis. In contrast to HT29 and RAW cells, THP-1 cells did not show any reduction in viability at 0

hours (2 hours-post treatment with FAS) implying relative insensitivity to FAS-induced ferroptosis and apoptosis.

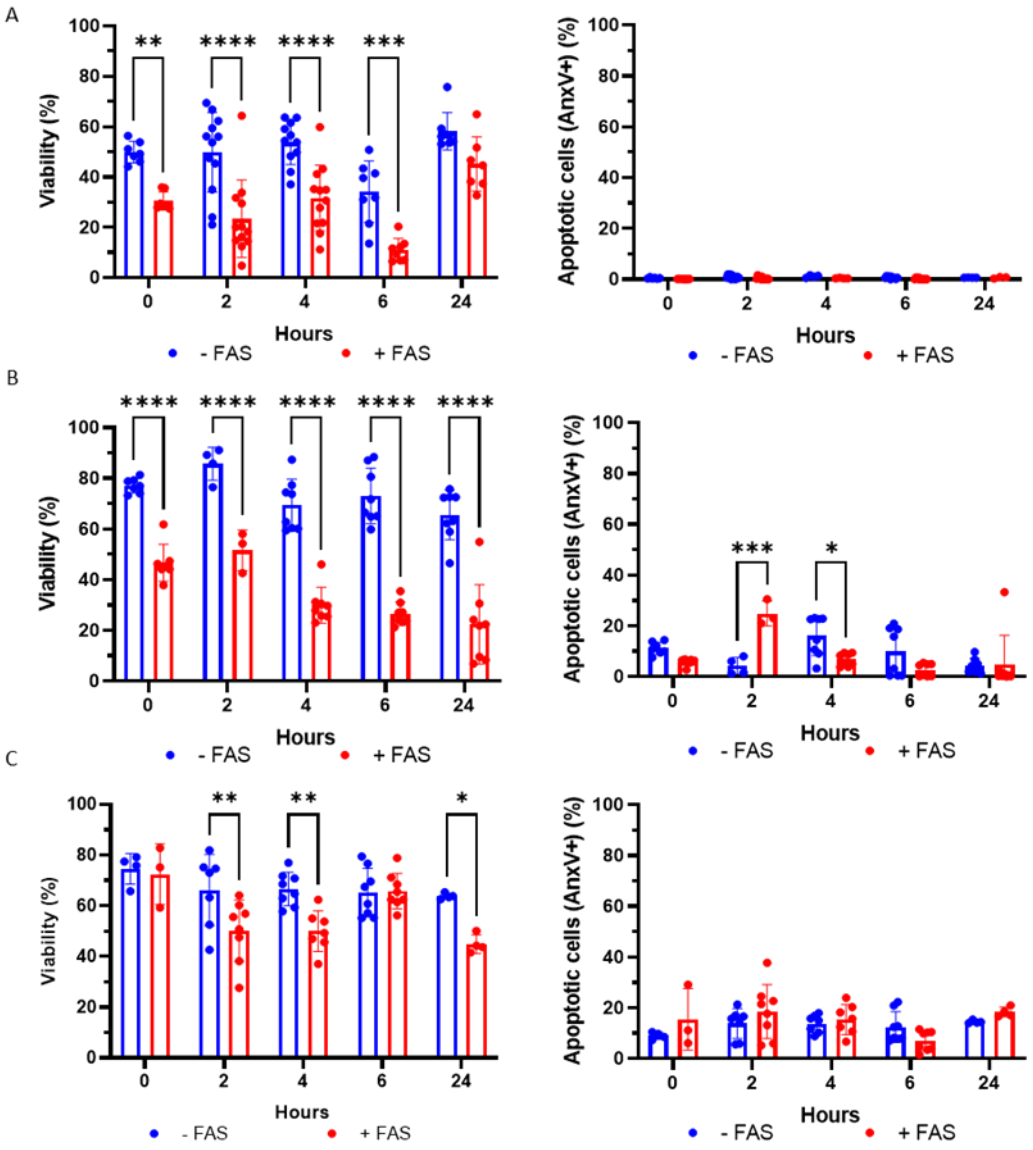

*Figure 5.2.6.1 - Viability and apoptosis in cells treated with or without FAS. Cells were incubated with FAS 200μm for 2 hours and then washed and fresh medium added. A – HT29 showed a significant decrease in viability with FAS treatment at all timepoints except at 24 hours, where possible proliferation increased the viability of both conditions. Apoptosis remained low for both conditions at all timepoints. B – In RAW cells the viability of FAS-treated cells was significantly lower than non-treated cells at all timepoints. Apoptosis was increased at 2 hours with FAS treatment. C – PMA-treated THP1 had a significant reduction in viability with FAS treatment at 2, 4 and 24 hours but the reduction is less than HT29 or RAW cells. FAS did not induce significant apoptosis in THP1 cells. All samples were tested for normality and a 2way ANOVA, with Tukey's multiple comparison test, carried out. * p<0.05, ** p<0.01, *** p<0.001. Error bars = SD N=3/5.*

Overall, 4 hours following iron treatment, THP1 have the highest mean viability (50.04% ± 8.04%SD) compared to RAW cells (29.94% ±7.07% SD) and HT29 (31.64% ±13.07%SD). The percentage change when iron is added compared to control at the same timepoint is significantly less in THP1 cells (-23.23% ± 16.28% SD) compared to the other two cell lines (HT29: -49.98% ± 13.70% SD, P=0.047; RAW: -56.37% ± 10.09% SD, P=0.004) (Figure 5.2.6.2) .This suggests that the human macrophage-like cell line is relatively insensitive to iron and the murine macrophage is more sensitive than HT29 cells.

Next, RSL3 was added to samples that were pre-treated with iron (200 um for 2 hours). Figure 5.2.6.3 shows the percentage of cells that are viable, apoptotic or ferroptotic (PI+) at the 2- and 24-hour timepoint. This compares the changes

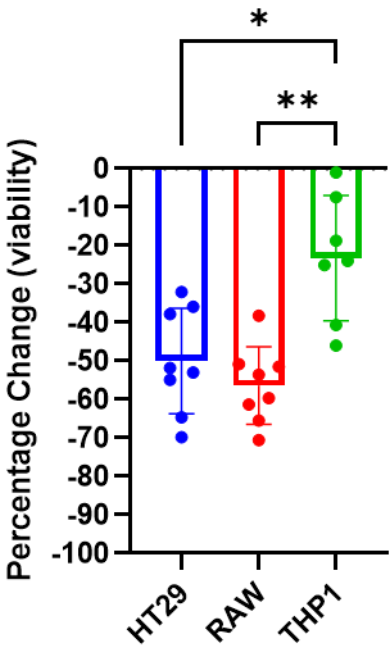

*Figure 5.2.6.2 – Percentage change in viability when iron is added compared to media in the three cell lines (4 hours), showing that THP1 cells were the least affected by the addition of iron compared to RAW and HT29 cells. Samples were tested for normality and a Kruskal Wallis test carried out. * p<0.05, ** p<0.01. Error bars = SD N=6/7.*

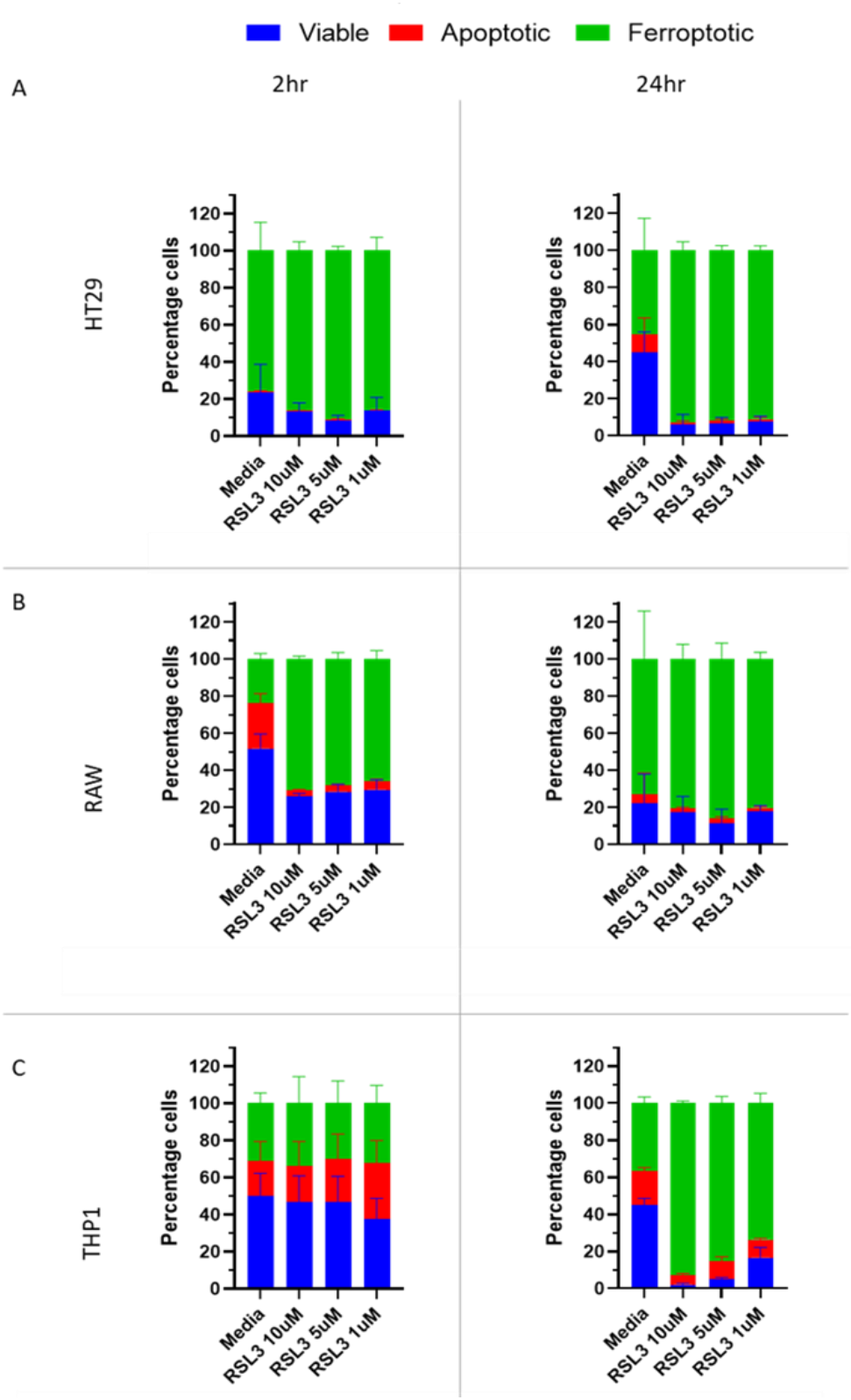

Figure 5.2.6.3 – Proportion of viable (AnxV-PI-), apoptotic (AnxV+PI-) and ferroptotic (PI+) cells in (A) HT29, (B) RAW and (C) THP1 cells treated with RSL3 2 and 24-hours following iron 200uM for 2 hours pre-treatment. Minimal apoptosis is observed in HT29 and RAW cells compared to THP1 cells which exhibit greater proportion of apoptotic cells following both treatment with iron alone and in combination with RSL3

of viability following iron treatment whether they are also treated with RSL3 or just with media, thus suggesting the sensitivity to the two different treatments. Figure 5.2.6.4 complements this figure by showing the statistical comparisons for the cells with either 5uM RSL3 treatment, iron or both treatments together. Complete time courses for both figures are shown in Appendix 5.6.3.

In HT29, although iron alone induces significant cell death at early timepoints, these cells seem more sensitive to RSL3 as this reduction in viability consistently maintained by RSL3 over time compared to iron (Figure 5.2.6.4A).

When RAW cells are treated with both iron and RSL3 a significant decrease compared to the two conditions alone at the 2-hour timepoint is shown. However, this is lost over the other timepoints (Figure 5.2.6.4B and Figure 5.2.6.4B). Indeed, treatment with iron alone is able to decrease viability similarly to when iron is used in addition to RSL3 at later stages. These results

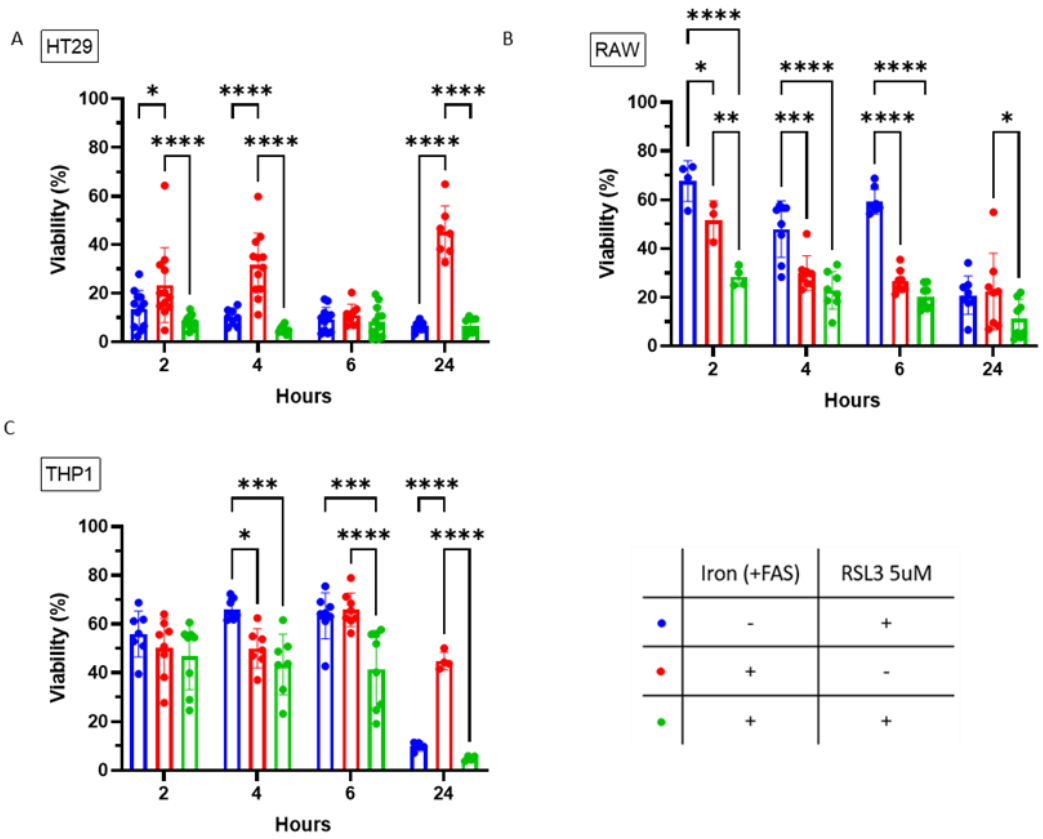

*Figure 5.2.6.4 - Viability in HT29 (A), RAW (B) and PMA-polarised THP1 (C) for RSL3 5 μM treatment following incubation with media or iron (FAS 200μM), or both. Data was tested for normality and a 2way ANOVA with Tukey's multiple comparison test was performed. * p<0.05, ** p<0.01, *** p<0.001. Error bars = SD N=6/7.*

suggests that the addition of both treatments leads to a faster decrease in viability, which is then equalised by iron alone at later timepoints. Iron seems to therefore drive more effective ferroptosis compared to RSL3 overall and that the action of RSL3 may be important only at early stages when in combination with iron.

THP1 cells overall were not affected by iron treatment (or RSL3) at early timepoints where an increase in apoptosis is observed in all conditions (Figure 5.2.6.3C) and remains unchanged at the 24-hour timepoint in iron alone, suggesting a very slow cell death (Figure 5.2.6.4C). These cells seem to be more sensitive to both treatments only at the 6-hour timepoint, whereas at the 4-hour timepoint iron seems to drive the reduction in viability (Figure 5.2.6.4C). However, at the later timepoint of 24-hour RSL3 is the treatment responsible for the reduction to below 10%. Therefore, THP1 sensitivity to treatments is somewhat time dependent. These results suggest different sensitivity to the two treatments and different mechanisms and timings involved between the cell lines.

5.2.7 FAS treatment leads to an increase in ROS with and without RSL3

To further investigate the role of FAS in inducing cell death through ferroptosis reactive oxygen species were measured as before and normalised to the media alone for each timepoint. Figure 5.2.7.1 shows the effect of FAS on ROS, with RSL3 (10μM) treatment as a comparator. In HT29, there was a 1.5-fold increase in ROS at 2 hours following iron and this was similar to RSL3 treatment (Figure 5.2.7.1A). In RAW cells (Figure 5.2.7.1B) FAS treatment increased ROS up to a 5-fold and was seen to be a much more potent inducer of ROS than RSL3. THP1 cells showed a 3.5-fold increase in ROS compared to untreated cells within 4 hours and this was more than was observed in RSL3 treatment. These results suggest that FAS potently induces ROS in these macrophage cell lines but THP-1 cells in particular are relatively resistant to FAS-induced ferroptosis compared with HT29 cells, consistent with the observations with RSL3 treatment.

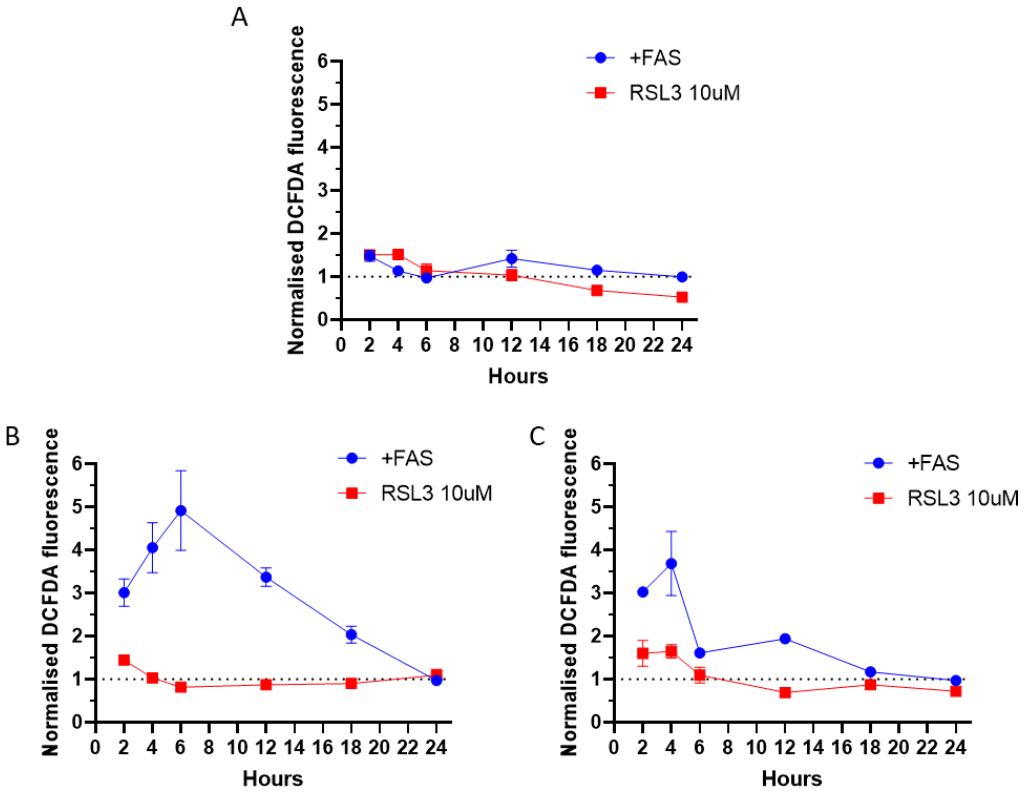

Figure 5.2.7.1 - ROS production following treatment with iron in different conditions, normalised to media with no iron, in HT29 (A), RAW (B), THP1 (C). The relevant RSL3 (10μM) with no iron loading data is shown for comparison. Error bars = SD N=3/6

To investigate the effect of FAS and RSL3 on ROS production, the combination of iron with RSL3 treatment was assessed compared to media that was pre-treated. These samples are all normalised to media without iron. Full statistical analysis and time courses are shown in Appendix 5.6.4, but the focus of Figure 5.2.7.2 is on the early timepoints as those are the most relevant for ROS production. In all three cell lines the combination of treatments leads to a significant but relative increase in ROS production compared to cells in media that were pre-treated with iron. It does not clearly reflect on the reduction of viability in macrophages possibly suggesting multiple mechanisms involved with ferroptosis following iron loading.

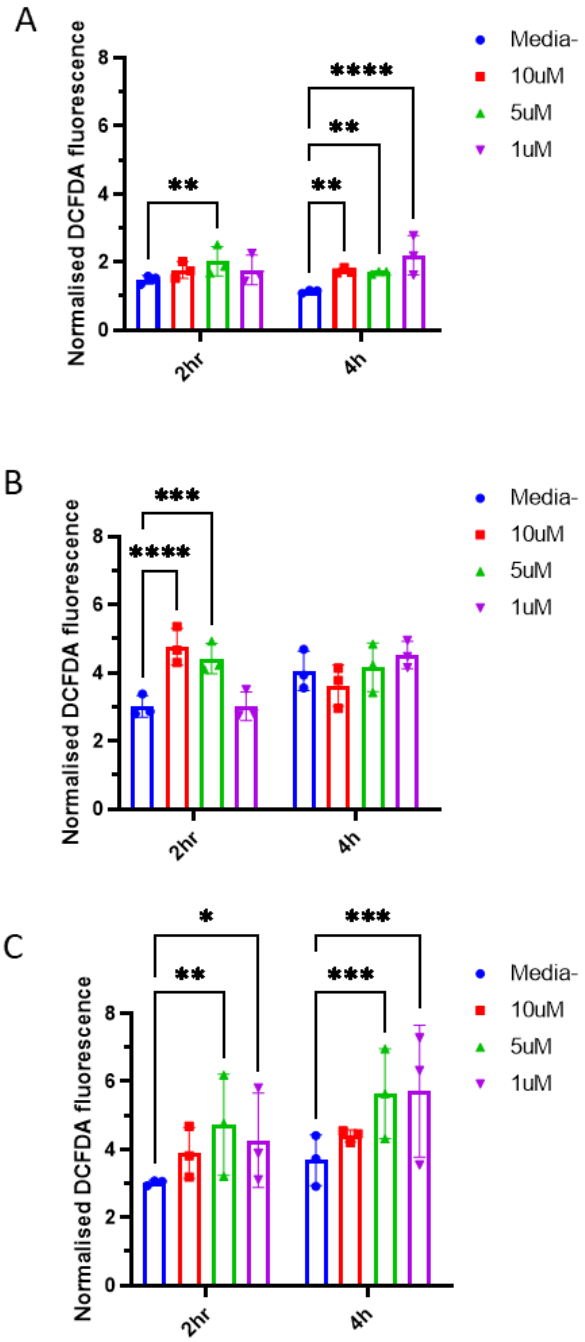

*Figure 5.2.7.2 - ROS production at 2 and 4 hours in HT29 (A), RAW (B) or THP-1 (C) cells were pre-treated with iron and then treated with different concentrations of RSL3 or media. Data was tested for normality and a 2way ANOVA with Tukey's multiple comparison test was performed. * p<0.05, ** p<0.01, *** p<0.001. Error bars = SD N=3.*

This suggests that both macrophage-like cells lines increase ROS production when iron is added with or without RSL3, and it is higher when compared to

HT29 cells. As aforementioned, HT29 have a higher baseline level of ROS compared to THP1 and RAW cells (Fig5.2.2.1A). This could be interpreted as HT29 cells exhibiting the maximum tolerable ROS concentrations over which cell death occurs, or that macrophagic lines are able to tolerate a wider range of ROS levels. Moreover, the low level of ROS in HT29 could also be linked to the low level of viability of the cells at all timepoints following iron loading (Fig.5.2.6.2A). If the measurement of ROS were taken also at the 0-hour timepoint, thus straight after incubation with iron or media, it would have shown whether the increase in ROS would have occurred during that time.

5.2.8 Viability following FAS treatment is rescued by LIP1 in HT29, but not in macrophages.

To further define the role of FAS induced ROS generation and ferroptosis, the effect of LIP1 was tested. Full time courses and statistical analysis is shown in Appendix 5.6.5.

In HT29 cells pre-treated with iron, LIP1 reduced ROS to the same levels present in the media alone (Figure 5.2.8.1A). This is consistent with the absence of significant ROS production observed previously. At 2 hours the LIP1-treated sample had a significant lower level of ROS compared to the two media samples. No differences were observed at 24 hours, possibly due to the reduction in viability. LIP1 addition to iron-treated cells, at 2 hours leads to a significant increase in viability compared to iron-treated media samples and achieves similar levels of viability to just media treated cells (Figure 5.2.8.1B). At 24 hours viability is increased in all conditions, probably due to proliferation. A statistically significant difference in viability is only observed between iron treated samples.

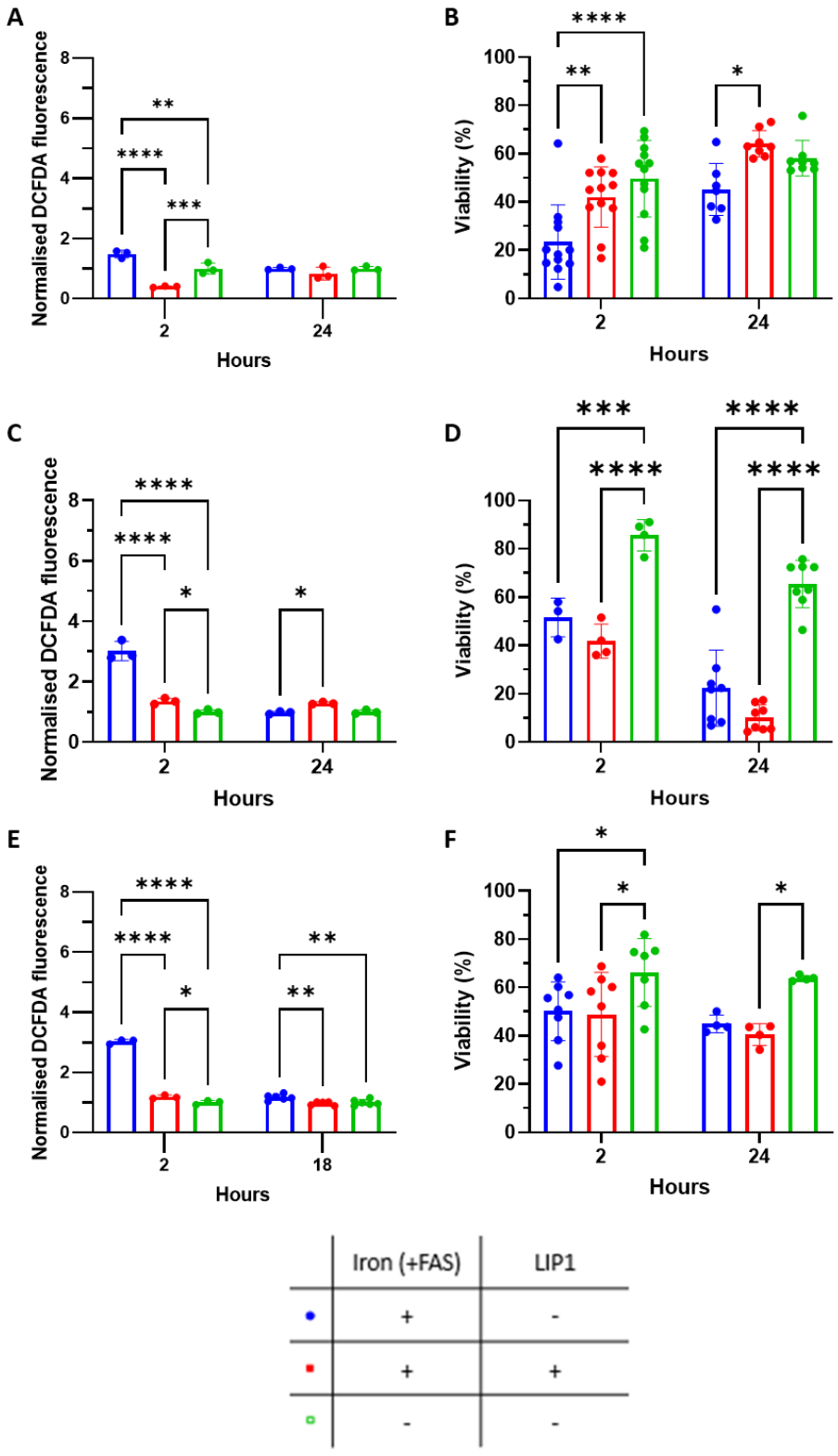

*Figure 5.2.8.1 – Effect of LIP1 on iron loaded cells on normalised ROS production and viability respectively, for HT29 (A-B), RAW (C-D) and PMA-polarised THP1 (E-F), compared to media with and without iron. The samples were tested for normality and a 2way ANOVA, with Tukey's multiple comparison test, performed. * p<0.05, ** p<0.01, *** p<0.001. Error bars = SD N=3/8.*

In RAW cells, the level of ROS was significantly lowered to non-iron treated levels by LIP1 when iron was present for all timepoints except 2 hours, where the levels are however consistently low (Figure 5.2.8.1C). Although the ROS increase seems to be kept under control by LIP1, viability was significantly lower than the non-iron treated samples, but not significantly different from the other iron treated sample at both timepoints (Figure 5.2.8.1D). This suggests that it was indeed the iron treatment that caused this reduction in viability and may cause this through a mechanism that does not depend solely on reactive oxygen species.

Similarly, to RAW cells, LIP1-treated iron-loaded THP1 cells had a significant decrease in ROS levels when compared to iron-loaded media-treated THP1. The level was comparable to the non-iron treated cells (Figure 5.2.8.1E). However, when looking at the viability, LIP1 does not rescue viability to non-iron treated cell levels at any timepoint (Figure 5.2.8.1F). This suggests a different iron-induced death mechanism that is not strictly linked to ROS production and may be common to all macrophages.

5.2.9 Expression of CD71 in RAW cells in response to iron is more pronounced compared to HT29 cells.

To elucidate further the effect of iron loading on the cells, CD71 was assessed as previously, in iron treated cells and compared to media at different timepoints.

Observing the geometric mean of CD71 in HT29 single cells, there was no difference between the treatment with iron (+FAS) and the treatment without (-FAS) at any timepoint (Figure 5.2.9.1A). However as shown previously in Figure 5.2.4.2, HT29 show a CD71 negative population that could skew mean expression. There was a significant increase in CD71 positive single cell frequency at the 24-hour timepoint. However, the overall frequency of CD71 positive cells at 24 hours was lower than the other timepoints (Figure 5.2.9.1B). This increase at late stages was not reflected in the CD71 positive cells' geometric mean. At the 2-hour timepoint a significant increase in CD71

geometric mean was shown following iron treatment, but no other significant differences were noted (Figure 5.2.9.1C).

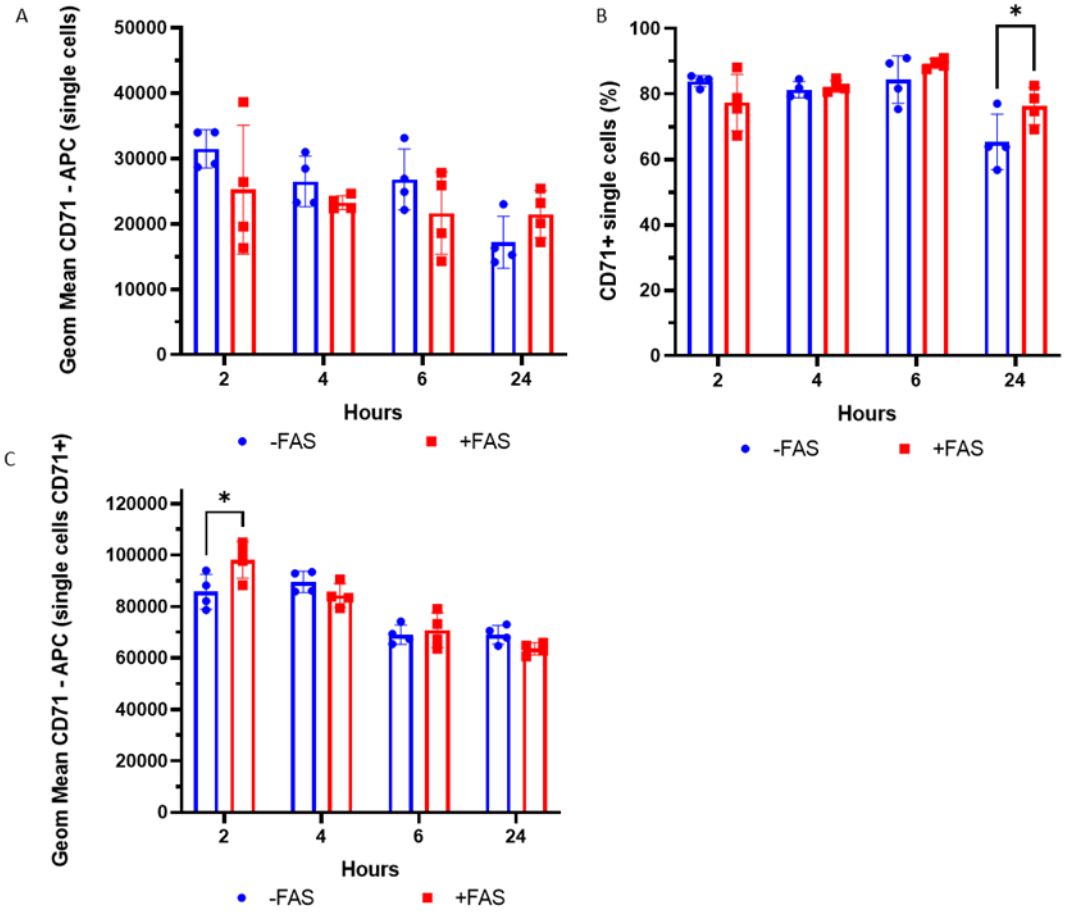

*Figure 5.2.9.1 - Assessment of CD71 in HT29 cells. (A) Geometric mean of CD71 in single cells. (B) Frequency of CD71 positive cells. (C) Geometric mean of CD71 in single CD71 positive cells. Samples were tested for normality and a 2way ANOVA, with Tukey's multiple comparison test, performed. * p<0.05, ** p<0.01, *** p<0.001. Error bars = SD N=4.*

RAW cells do not have a CD71 negative population and therefore the geometric mean of CD71 was measured on single cells. Overall, there was a statistically significant increase in CD71 with iron treatment (+FAS) compared to non-iron (-FAS). By 24 hours, this difference was not apparent anymore, which could be associated to reduced viability (Figure 5.2.9.2). This shows that RAW cells increase the levels of transferrin receptor which has the known function of iron-uptake and could explain the increase in ROS levels at those timepoints (Figure 5.2.7.1).

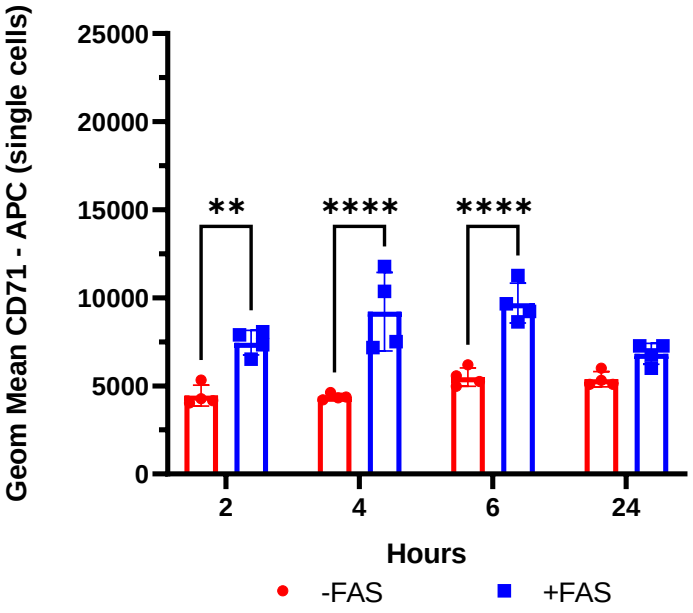

*Figure 5.2.9.2 - CD71 expression in RAW cells following no iron (-FAS) or iron loading (+FAS). The samples were tested for normality and a 2way ANOVA, with Tukey's multiple comparison test, performed. * p<0.05, ** p<0.01, *** p<0.001. Error bars = SD N=4.*

5.2.10 RSL3 causes a reduction in viability in alveolar macrophages at 24 hours

To establish if RSL3 ferroptosis and apoptosis is seen in alveolar macrophages, BAL-derived fresh alveolar macrophages from patients with IPF were selected by adhesion and then treated with two concentrations of RSL3 and LIP1 at 1µM. Due to the limited number of samples and cells, the viability assessment was prioritised for 2 and 24 hours. No differences were observed at the 2-hour timepoint (Figure 5.2.10.1A). There was a significant reduction in viability observed at 24 hours compared to the media treated cells (Figure

5.2.10.1B). This reduction was observed to be concentration dependent: lower concentrations of RLS3 (1μM) led to less loss in viability compared to 10μM RLS3.

The decrease in viability was shown to be mostly associated with an increase in apoptosis (Figure 5.2.10.1B). This was significantly different in the 10μM RSL3-treated cells compared to the media-only treated cells (RSL3 10μM vs Media (mean ± SD): 72.37% ± 5.29% vs 13.97% ± 6.60%; P=0.001). The gating strategy is presented in Appendix 5.6.6.

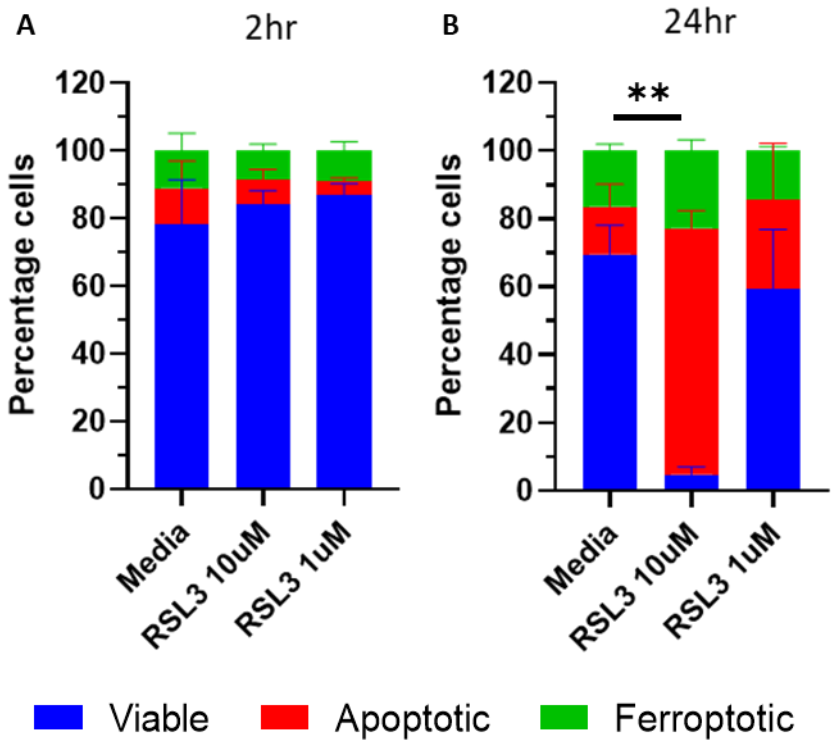

*Figure 5.2.10.1 – Summary of viable, apoptotic and ferroptotic BAL cells following RSL3 treatment at (A) 2 hours and (B) 24 hours. No statistically significant differences were observed at 2 hours, but some differences were observed at the 24-hour timepoint. The percentage of apoptotic cells was significantly higher in the 10μM RSL3 group compared to media. A Dunnett's multiple comparisons test was carried out. * p<0.05, ** p<0.01, *** p<0.001, ****p< <0.0001. Error bars=SD N=3*

5.3 Discussion

The overarching aim in these experiments was to test the hypothesis that macrophages are relatively resistant to ferroptosis, following the observation that alveolar macrophages from patients with lung fibrosis exhibit high iron content. The cells' ability to undergo this regulated form of cell death was tested with RSL3, a GPX4-inhibitor which has previously been shown to

specifically induce ferroptosis, and with exogenous iron. Viability, ROS production, apoptosis and CD71 increase were all assessed to evaluate ferroptosis and LIP-1, a ROS quencher was used to evaluate rescue of ferroptosis. The main finding was that the macrophages used in this study were relatively resistant to ferroptosis compared to HT29 cells. The data also showed RSL3 induces both apoptosis and ferroptosis in macrophages, particularly THP-1 cells.

5.3.1 Viability reduction through ferroptosis

Both macrophage cell lines and HT29 cells showed some degree of reduction in viability when treated with RSL3 or FAS.

HT29 sensitivity to ferroptosis through RSL3 induction has previously been described in the context of colorectal cancer[220]. These investigators have shown sensitivity to ferroptosis especially at higher concentrations of RSL3 (5-10μM) and following at least 24 hours of incubation. Through the experiments discussed in this chapter, HT29 were confirmed to be sensitive to ferroptosis. Indeed, even at low concentrations of RSL3 (1μM) there was a 70% reduction in viability compared to media within 2 hours of treatment, which is much faster and more significantly than in the study described in Sui et al. This reduction was significantly rescued with LIP1.

There are few previous studies of ferroptosis in macrophages. A study has demonstrated different degrees of sensitivity between polarisation-states of murine macrophages and microglia, but these were not compared to another cell type[272]. Overall, the experiments in this study confirmed that macrophage-like cell lines can undergo RSL3-induced ferroptosis, but they are relatively insensitive compared with HT29 cells.

Specific morphological changes are associated with ferroptosis such as shrinkage and increased membrane density of mitochondria[184,219]. These were not detectable through the brightfield imaging carried out in this study. Imaging through high resolution electron microscopy may have aided in identifying mitochondria-related changes but these changes are not specific to ferroptosis. A reduction in cell size, normally associated with non-apoptotic cell

death, was observed in these cell lines at early timepoints but was not formally assessed.

Mechanistically RSL3 treatment has been shown to increase intra-cellular iron but Prussian blue staining lacks sensitivity to measure these changes[220]. Sui et al., (2019) assessed relative change in iron through calcein-AM fluorescence before and after an iron chelator was added. Other studies used commercially available assays to assess iron levels[207,218,273]. Other sensitive techniques used in this thesis, such as specific iron-sensitive probes or ICP-MS, could have been used to detect these changes in this study. Clearly macrophage cell lines used in the RSL3 experiments did not resemble the alveolar macrophages from patients, which have significant staining through Prussian blue especially those derived from IPF patients.

Treatment with iron was carried out to determine iron-induced ferroptosis sensitivity. In HT29 this caused a significant reduction in viability compared to media alone at 4 hours. This suggested a sensitivity to iron loading, but not as great as with RSL3. This reduction in viability was significantly rescued by LIP1 at most timepoints confirming a ROS-dependent mechanism. Treatment with iron showed a consistent reduction in viability in RAW cells but PMA-differentiated THP1 viability was only significantly reduced at early timepoints. At 4 hours, the percentage change reduction in viability in PMA-differentiated THP1 was of 23.23%, compared to 49.98% in HT29 and 56.37% in RAW macrophages. This iron-dependent cell death was not rescued when LIP1 was added in both macrophage cell lines, suggesting that the cell death does not only rely on ROS accumulation or that the cells were irreversibly overwhelmed by the increase in ROS. The changes in ROS are discussed later. The data suggests that THP1-derived macrophages may be more resistant to iron compared to the other cell lines. A study using bone-marrow derived macrophage (BMDM) showed a 60% reduction in viability when FAS was added for 48 hours, and this was comparable to the reduction observed in hepatocytes[274]. In this study the ferroptosis inhibitor ferrostatin-1, was used and demonstrated a significant rescue of viability when iron was added.

HT29 cells had low baseline viability (49%), which could influence the further viability changes when iron is added. This low baseline level of viability may be linked to the high proliferation rate of this cell line and the confluency of the cells. Indeed, although RAW and HT29 were plated at the same density 24-hours prior treatments, the HT29 may have adhered covering a wider surface area, thus leading to over-confluency and cell death over time.

The cell lines were also treated with iron and RSL3 together to understand the effect of both treatments. This has not been previously shown in the literature and was carried out to mimic more closely the BAL-derived macrophages which are rich in iron. The RSL3 concentration discussed here was 5μM as it was the mid concentration tested. HT29 were particularly sensitive to RSL3, and iron did not further influence viability. RAW cells were overall more sensitive to iron than to RSL3, as the viability was significantly reduced in iron treated cells over RSL3 (5μM) cells. THP1 sensitivity to the two treatments is time-dependent, with the cells being more sensitive to iron early and to RSL3 at later time-points. This is similar to alveolar macrophages that are already iron-rich, where viability with RSL3 is unchanged at 2 hours, but significantly reduced at 24 hours.

5.3.2 Apoptosis and ferroptosis

At early time-points, the distinction between what is apoptosis and what is ferroptosis can be determined through appropriate staining. However, at later time-points it is possible that secondary death from apoptosis plays a role in the reduction in viability at late timepoints. The relative contribution of secondary necrosis versus ferroptosis at late timepoints (24 hours) cannot be readily determined in these studies.

In addition to ferroptosis, inhibition of GPX4 is implicated in various programmed cell death pathways such as apoptosis[275], necroptosis[276] and pyroptosis[277], the latter two being mostly studied through genetic knockouts and not pharmacological inhibition. To assess whether the addition of RSL3 leads to apoptosis as well as ferroptosis, the cells were stained for Annexin V and PI. The AnxV+PI- cells were considered apoptotic cells. HT29 and RAW

cells were shown to have a very small percentage of apoptotic cells which did not significantly change from media levels, suggesting that any apoptosis shown was not due to RSL3 treatment. However, RSL3 caused a significant level of apoptosis in differentiated THP1 cells especially at early timepoints, with about 20-30% of the reduction of viability associated with AnxV+PI- cells and about 10-15% with PI+ cells. This study does not explain whether this is due to the mode of cell death of THP1 in general or whether this is specific to RSL3 treatment, but the flow cytometry plots showed different pattern of cell death across the three cell lines, with THP1 plots suggesting a shift first towards apoptosis followed by late-stage death. This was not observed for HT29 and RAW, which showed an upward shift towards the PI+ population.

When cells were treated with iron, there were no significant differences compared to no-iron in HT29 and THP1. The observed differences in apoptosis in RAW cells, at 2 and 4 hours timepoints were inconclusive. Apoptosis in all cell lines represented less than half the dead cells, suggesting that iron does not reduce viability through apoptosis. This might suggest that there are two mechanisms of iron-dependent cell death which might differ between the two cell lines.

Further studies could be carried out by using apoptosis inhibitors together with RSL3 or iron treatment to assess whether the cells would still undergo significant ferroptosis. Other forms of cell death could also have been excluded by using specific inhibitors, such as Z-VAD-FMK for apoptosis.

5.3.3 GPX4-inhibition and ferroptosis

Attempts were made to assay GPX4 following RSL3 to verify the mode of action of RSL3. GPX4 has been shown to be downregulated at the protein level in the presence of RSL3, thus the level of substrate and products should change accordingly[200,220]. This is however controversial due to the different susceptibility of cells to ferroptosis induction, leading to different concentrations of RSL3 used and the timepoints analysed. This was observed in this study as well. Indeed, in HT29 cells an increase in GSH was not observed, probably due to the prominent reduction in viability at early

timepoints. In RAW cells there was an increase in GSH when 10μM RSL3 was added, suggesting inhibition of GPX4 and consequently accumulation of GSH. It also suggests a different timeline of GSH metabolism compared to the faster-proliferating HT29. Other concentrations and timepoints could have been used to understand its relationship, as well as assessing the protein level of GPX4.

Although not directly inhibiting GPX4, iron loading showed a reduction in GPX4 expression in an study of embryos, but GSH levels were not assayed [278]. The effect of iron on GSH or GPX4 was not carried out in this study.

5.3.4 ROS and ferroptosis

One of the hallmarks of ferroptosis is increase in ROS species, which then leads to the reduction in viability. To elucidate this further, ROS levels with and without RSL3 treatment were studied.

Firstly, when looking at the ROS levels at baseline, HT29 have a much higher level compared to the two macrophage-like cell lines. However, when RSL3 was added at different concentrations the increased in ROS, normalised to media, between cell lines was similar. Indeed, all cell lines had a 1.5-2-fold increase in ROS compared to media following an incubation with RSL3 for 2-4 hours. This increase was then subdued for the remaining time course, which could be a result of the reduction in viability.

When LIP is added in addition to RSL3, the effect of RSL3 on ROS production is completely attenuated in all cell lines. In the macrophage cell lines, although there is death and rescue observed at certain timepoints and concentrations, this is not as consistently observed as with HT29 cells.

These results suggest that macrophages are less sensitive to changes in ROS than HT29. This could be linked to the inflammatory nature of these cells compared to the HT29. Indeed, macrophages and other phagocytes are known to being able to regulate and achieve self-protection against oxidative stress, which is at points a necessary mechanism for an effective inflammatory response. An oxidative burst, which is not unique to macrophages, involves a production of ROS which is essential to kill bacteria by oxidative stress directly,

or by activating other non-oxidative microbicidal effectors[279–281]. Following this acute phase of inflammation, the macrophages enter a resolution stage where they undergo a lipid mediator switch, producing specialised pro-resolving mediators[282]. HT29 do not seem to be as resistant to ROS increase as macrophages, but macrophages may become “exhausted” at later timepoints, which leads to a ROS-independent cell death.

The effect of the addition of iron on ROS was also assessed in the different cell lines, as iron-interaction is more clinically relevant than pharmacological treatment. In HT29 the change in ROS when iron was added was not significantly different from the RSL3 treatment. In contrast both macrophage-like cell lines showed a significantly greater increase in ROS with iron compared to RSL3 10μM. This observation does not correlate clearly with the reduction in viability, as neither macrophage cell lines are rescued following LIP, even if ROS are decreased to media level. This could be linked again to the inflammatory nature of macrophages. Uptake of iron by macrophages is observed in a pro-inflammatory environment when pathogens are present, so to limit iron availability needed for replication[116,128]. ROS production then acts as a signalling molecule to develop a pro-inflammatory response against the pathogens. However iron-induced ROS can become damaging if the system is overwhelmed, leading to irreversible cytotoxicity[283].

In all three cell lines, iron with RSL3 led to an increase of ROS, especially at early timepoints, compared to not-iron treated cells. The differences between cell lines may be linked to the changes in viability, as the lowest levels of ROS were observed in HT29 which undergo ferroptosis at early timepoints. Oppositely, THP1 had the highest level of ROS, which was not clearly linked to a reduction in viability.

Overall, this relative sensitivity to iron when it comes to ROS production for the macrophage cell lines may be linked to their role in immunity. Macrophages are highly heterogeneous and adapt to their environment. Some macrophage-phenotype are specialised in iron recycling, particularly M2-like macrophages, and M1-like macrophages tend to store iron to limit its access to

pathogens[113,116]. This plasticity is achieved by differential expression of receptors. A better characterisation of the macrophages is necessary, not only by analysing receptors expression, but also through functional assays. This may elucidate further the effect of iron and whether the loss in viability following iron loading is associated with specific protective mechanism rather than an overwhelming of ROS. For example, chronic iron loading has been shown to impair bacterial killing by blocking lysosomal acidification in pro-inflammatory macrophages[115], whereas HO-1, the heme-degrading enzyme is elevated in M2-like macrophages, leading to an increased production of anti-inflammatory cytokines[284]. Analysis of their killing ability and their cytokine production would have completed the picture further.

5.3.5 CD71 and ferroptosis

The only receptor that has been shown to be a marker of ferroptosis is CD71, the transferrin receptor[206]. It was shown that cells treated with 1μM RSL3 had a significant higher expression of CD71 after 4 hours, compared to cells treated with media. As HT29, RAW and THP1 were not used in this paper, the level of CD71 was assessed through flow cytometry for different concentrations of RSL3 and at different timepoints. Although Fc block was used in different ways, THP1 cells did not achieve significant staining against the control isotype and are therefore not discussed. Comparing HT29 and RAW cells however is not very straightforward. Indeed, HT29 present a CD71 negative population, whereas RAW cells are overall CD71 positive. The cells are also derived from two different species, increasing the level of complexity of the comparison.

For both HT29 and RAW cells, only the lowest concentration of RSL3 led to an increase in CD71 in CD71+ cells at early timepoints. This could be associated with the more prominent reduction in viability at higher concentrations and at later timepoints.

When iron is added to HT29, an increase in CD71 levels is observed at 2 hours when considering CD71+ cells. RAW cells on the other hand have a significantly higher level of CD71 when treated with iron compared to no iron at most timepoints, similarly to the 1μM RSL3 results (all but the 24-hour one).

However, the increase in the presence of iron is greater, suggesting that the role of CD71 as an iron receptor may be more important than its role as a marker of ferroptosis. This increase may also be linked directly with the higher level of ROS observed in this cell line compared to the HT29, if iron entered the cell bound to transferrin.

5.3.6 Differences and similarities between RAW, THP1 and alveolar macs

RAWs, THP1 and BAL-derived alveolar macrophages behave differently when their ability to undergo RSL3 or iron-induced ferroptosis is assessed. In contrast to the observations with RSL3, RAW cells exhibit large increases in ROS and are as susceptible to cell death with iron treatment as HT29 cells, although a proportion of this death is due to apoptosis. THP1 cells remain relatively resistant to iron-associated death despite exhibiting high levels of ROS with iron treatment compared with RSL3. This latter phenotype may be analogous to alveolar macrophages that exhibit high iron content but remain functionally viable. However, even in alveolar macrophages, RSL3 10uM caused cell death at 24 hrs. This cell death was not rescued by LIP1 and seemed mostly through apoptosis not ferroptosis.

Due to limited availability of fresh alveolar macrophages, these experiments were in small numbers of patients and would benefit from increased sample size. Apoptosis inhibitors could be used to check whether RSL3-induced ferroptotic cell death could be caused in these clinically relevant samples, thus confirming whether this is just a transient state of ferroptosis in this primary cell. RSL3 does not lead to an increase in apoptosis in RAW cells, suggesting a different mode of cell death following RSL3 treatment between the two cell lines.

Studies on proliferation rate and its effect on ferroptosis induction could have also helped elucidate some differences between these cells. Indeed, differentiated THP1 and BAL-derived AM are both not very proliferative, whereas RAW cells are a non-differentiated cancer cell line which is highly

proliferative. This could have an impact on the metabolism of the cells and consequent time-dependent changes following treatments.

When focusing on the macrophage-like cell lines, differences can be explained by two main reasons. Firstly, the origin of the cells as RAW cells are murine macrophages and THP1 are of human origin. Secondly, RAW cells are proliferating cells that require splitting and adhere in basal conditions. Whereas THP1 are monocyte-like cells in suspension, which are PMA treated to become differentiated and less-proliferating. Senescent cells were found to be more resistant to ferroptosis, thus a proliferation marker could have been used to compare the two macrophagic cell lines[285]. A full characterisation of these cells, by studying their receptors expression, or a polarisation study, thus treating the cells with cytokine leading to either a pro-inflammatory or anti-inflammatory characterisation, would have ensured phenotypical similarity between these cells.

Noticeably, not only polarisation of macrophages may lead to different ROS-sensitivity, but the different levels of ROS may lead to different macrophage phenotypes. In the literature ROS seem to promote an anti-inflammatory polarisation, characterised by an increased arginase-1 activity, leading to a reduction in ROS[286,287]. Interaction with apoptotic bodies leads anti-inflammatory macrophages to an instability of NADPH oxidase Nox2 mRNA, which leads to further defects in ROS production[288]. This loss of NADPH oxidase has also been shown to have implications in diseases like diabetes[289]. Nevertheless, the production of ROS, following RSL3 treatment, is very quick (2-4 hours) which may suggest that the changes in macrophage phenotype may only be significant at later stages. A characterisation of key phenotypic receptors, such as CD163 and CD86, at different timepoints following RSL3, could have clarified any possible changes, both across the two lines, but also within the same one.

5.3.7 RSL3 and iron-induced ferroptosis

Although RSL3 and iron-induced ferroptosis should have overlapping mechanisms, both involving an increase in ROS which leads to cell death, they seem to induce different levels of ferroptosis depending on the cell of interest. The impact of the treatments on the different cell lines is summarised in Table 5.3.7-1. Overall, HT29 are more sensitive to ferroptosis than macrophages. In particular, HT29 are more sensitive to RSL3 compared to iron, but macrophages are more sensitive to iron rather than RSL3.

Table 5.3.7-1 – Table summarising the effect of the RSL3 and FAS treatments on the different cell lines.

Treatment:	**RSL3**			**FAS**		
Cell line:	**HT29**	**RAW**	**THP1**	**HT29**	**RAW**	**THP1**
Sensitivity to treatments leading to changes in:						
Ferroptosis	High	Medium	Low	High	High	Low
Rescue with LIP1	Yes	Partial	Partial	Yes	No	No
Apoptosis	No	Low	High	No	No	No
ROS	High	High	High	Low	High	High

RSL3 leads to a similar increase in ROS for all three cell lines, where over 1.5-fold change to media is observed for all three concentrations of RSL3. However, this does not correlate to reduction in cell viability, as a 70% reduction is observed in HT29 but only a 10-20% decrease is observed in macrophages within 6 hours. Viability is lost in macrophages later at 24 hours, with a 70% decrease achieved.

In contrast, iron treatment causes a greater increase in ROS in macrophages, which is not observed in HT29. Although this 3.5-4-fold increase is observed in macrophages, cell death is not correlated clearly, suggesting that

macrophages are less sensitive to ROS increase compared to HT29. As discussed previously, this is probably linked to their immunological role.

RSL3 induced ferroptosis seems to cause a significant level of apoptosis in THP1 at early timepoints, which is then substituted by the PI+ population. Low levels of apoptosis are observed with RSL3 treatments in the other cell lines. Iron treatment does not cause any significant changes in apoptosis levels in all cell lines, at all timepoints.

5.4 Limitations

The first limitation is the lack of a specific and consistent marker for ferroptosis across cell lines. To determine ferroptosis a combination of viability, exclusion of apoptosis, ROS production and CD71 levels were used, all hallmarks of this relatively novel pathway. CD71 expression was not consistent, possibly due to the timings and concentrations of drugs used, in contrast to other studies[206]. Ferroptosis is not the only pathway that incurs death following an increase in ROS[290,291]. Apoptosis was excluded by staining with Annexin V but other markers of apoptosis including caspase activation were not assayed. Further studies could have been carried out by inhibiting apoptosis chemically, by for example a pan-caspase inhibitors such as QVD-OPh[292]. Necroptosis could have been excluded by the use of necrostatin-1 or Oxa12[293,294].

The source of ROS is also important to the resulting cell death. Ferroptosis involves the oxidation of PUFA by intracellular ROS. Mitochondrial ROS can cause oxidative stress leading to late stage necrosis, but they are also involved cell death signalling in the initiation phase of apoptosis[295]. Although ferroptosis is induced by general inhibition of GPX4 and consequent production of ROS, studies have shown that mitochondrial rescue was able to prevent RSL3-induced cell death, highlighting the importance of the mitochondria in this form of cell death[296]. Studying macrophages' mitochondria and their ROS production may not only characterise ferroptosis induction further, but also elucidate the sensitivity to iron in the cell lines, and the incongruent observations in clinical samples. A study of the peroxidation of PUFAs focusing

on the enzymes concentrations and activity, such as phosphorylase kinase G2, and the hydroperoxides levels involved, could have also highlighted mechanisms involved in the different cell lines[297].

It was hypothesised that the GPX4 substrate level would accumulate following ferroptosis induction by RSL3, in contrast with observed reduction due to cysteine starvation through erastin induction[298]. However, GSH levels were not clearly changed in HT29 and RAW cells, a significant increase compared to LIP1 treated cells was observed in the latter cell type. Further optimisation with a sub-lethal dose of RSL3 in all three cell lines would elucidate this relationship further.

Another factor that could have been assessed to determine ferroptosis would have been the iron levels. Although this was attempted with Prussian blue, this was not sensitive for small changes in iron to be observed. ICP-MS or an iron probe, such as TRX-puro, could have been used to assess these differences[299].

Changes in morphology could have been observed. In contrast to other form of cell death, ferroptosis is characterised by increased mitochondrial membrane density and an overall cell volume shrinkage, the latter clearly visible in the Prussian blue staining of cells[190].

Another limitation, previously discussed, is the polarisation of macrophages. This could have ensured that the macrophages were more clinically relevant. Moreover, a comparison between polarisations sensitivity to ferroptosis could have identified differences between types, with the hypothesis being that M2-like macrophages, thus more similar to the iron-loaded fibrotic alveolar macrophages were less sensitive to ferroptosis than M1-like, pro-inflammatory macrophages.

Finally, the more technical limitation is related to the confluency and numbers of cells used. The three different cell lines have different proliferation rates and different adhesion characteristics. The number of cells plated was optimised for each cell line, but the confluency was inherently different. A study by Wu et

al., (2019) showed that intercellular interactions (as well as intracellular NF2-YAP signalling) affected ferroptotic death. Indeed, in HCT116, a human colon cancer cell which represents a different extent of differentiation to HT29, higher cell confluence led to ferroptotic resistance[300].

5.5 Conclusions

RAW and THP-1 macrophages were relatively resistant to ferroptosis compared to HT29 cells. RSL3 and iron generate ROS in macrophages and induce both ferroptosis and, particularly in THP-1 cells, apoptosis.

5.6 Appendix

5.6.1 Appendix 5.6.1

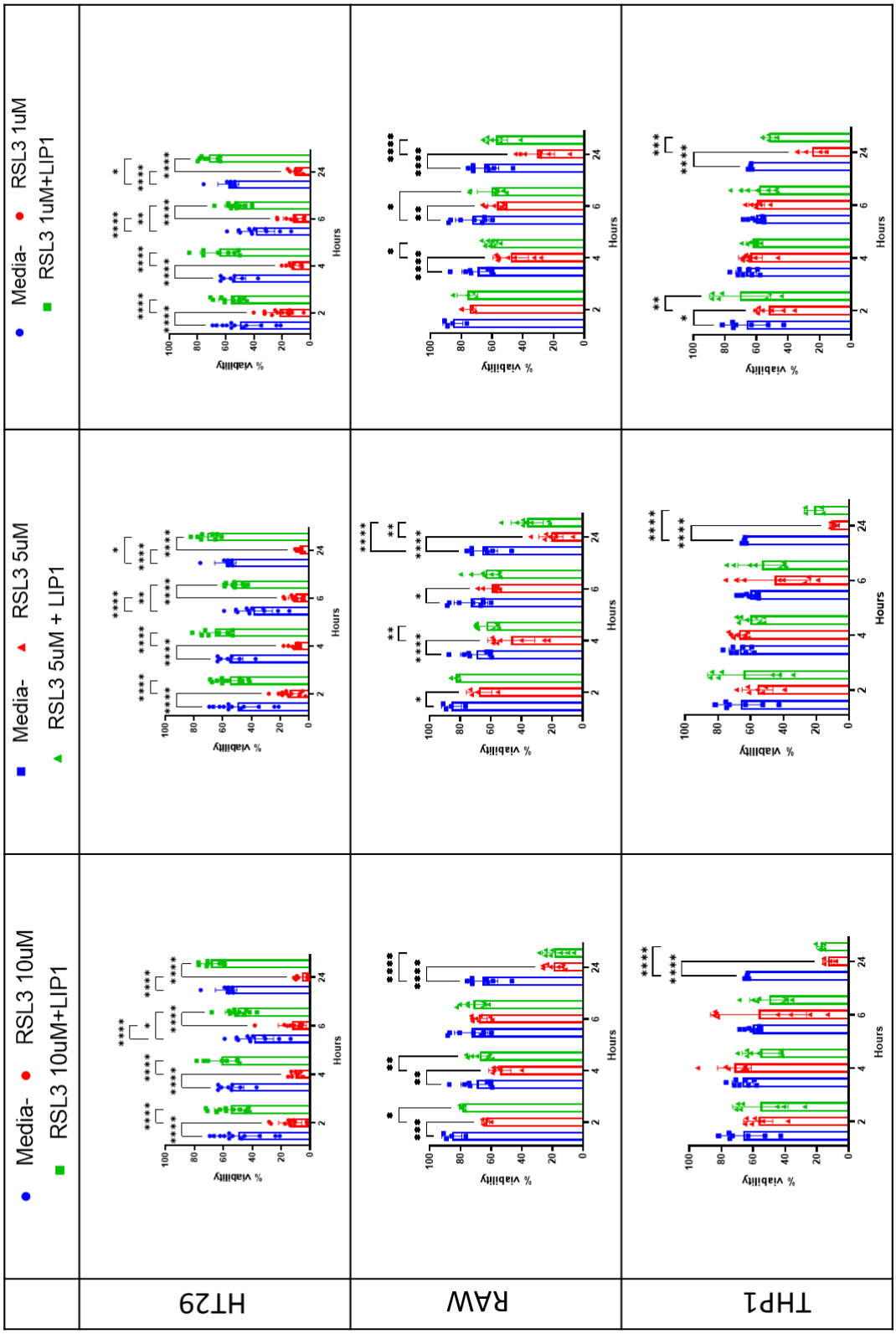

5.6.2 Appendix 5.6.2

Graphs showing percentage of viable, apoptotic and late stage (A) HT29, (B) RAW and (C) THP1 cells over time following treatment with either media or RSL3.

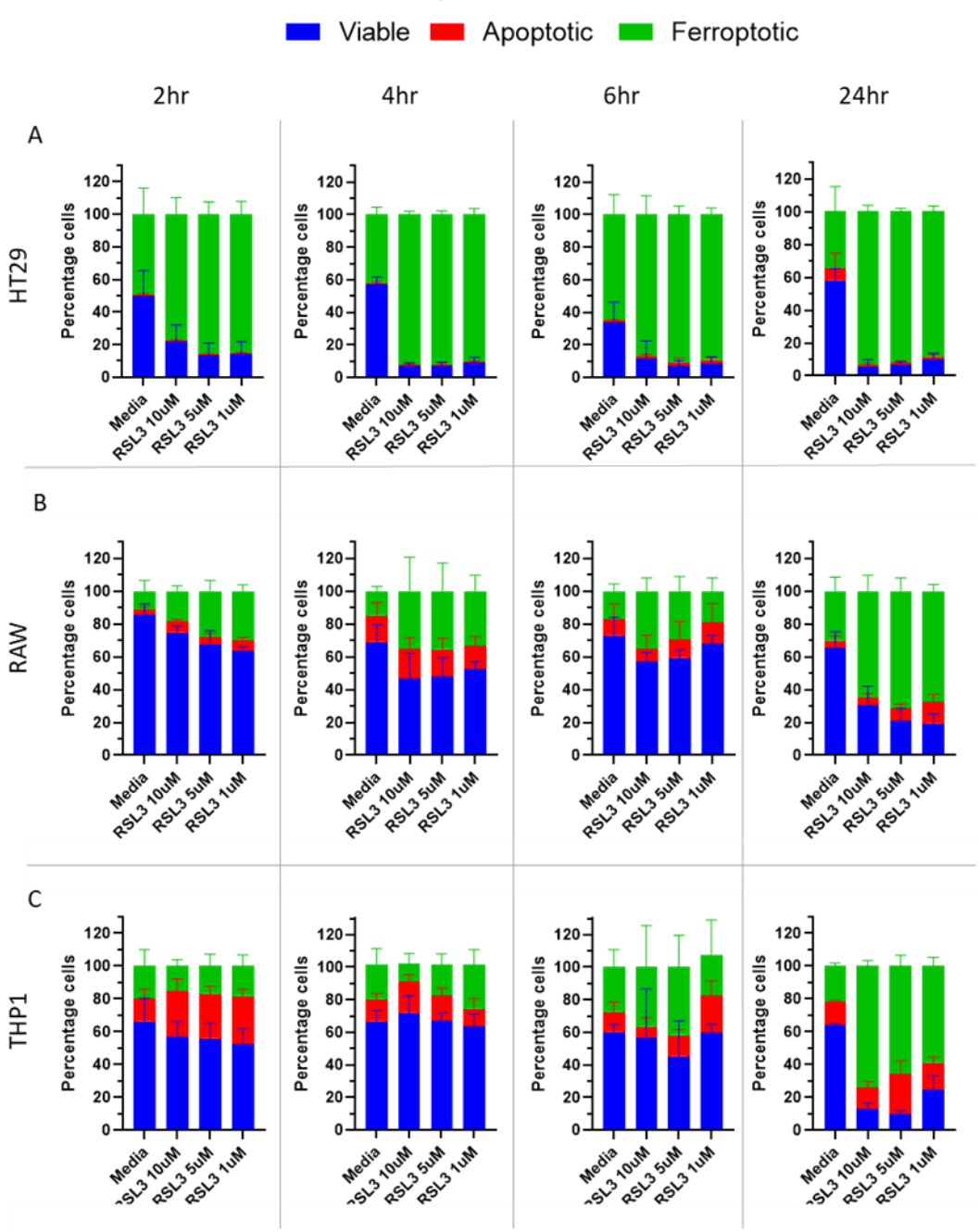

5.6.3 Appendix 5.6.3

Graphs showing percentage of viable, apoptotic and ferroptotic of (A) HT29, (B) RAW and (C) THP1 cells pre-treated with iron and then with either media or RSL3 at different concentrations.

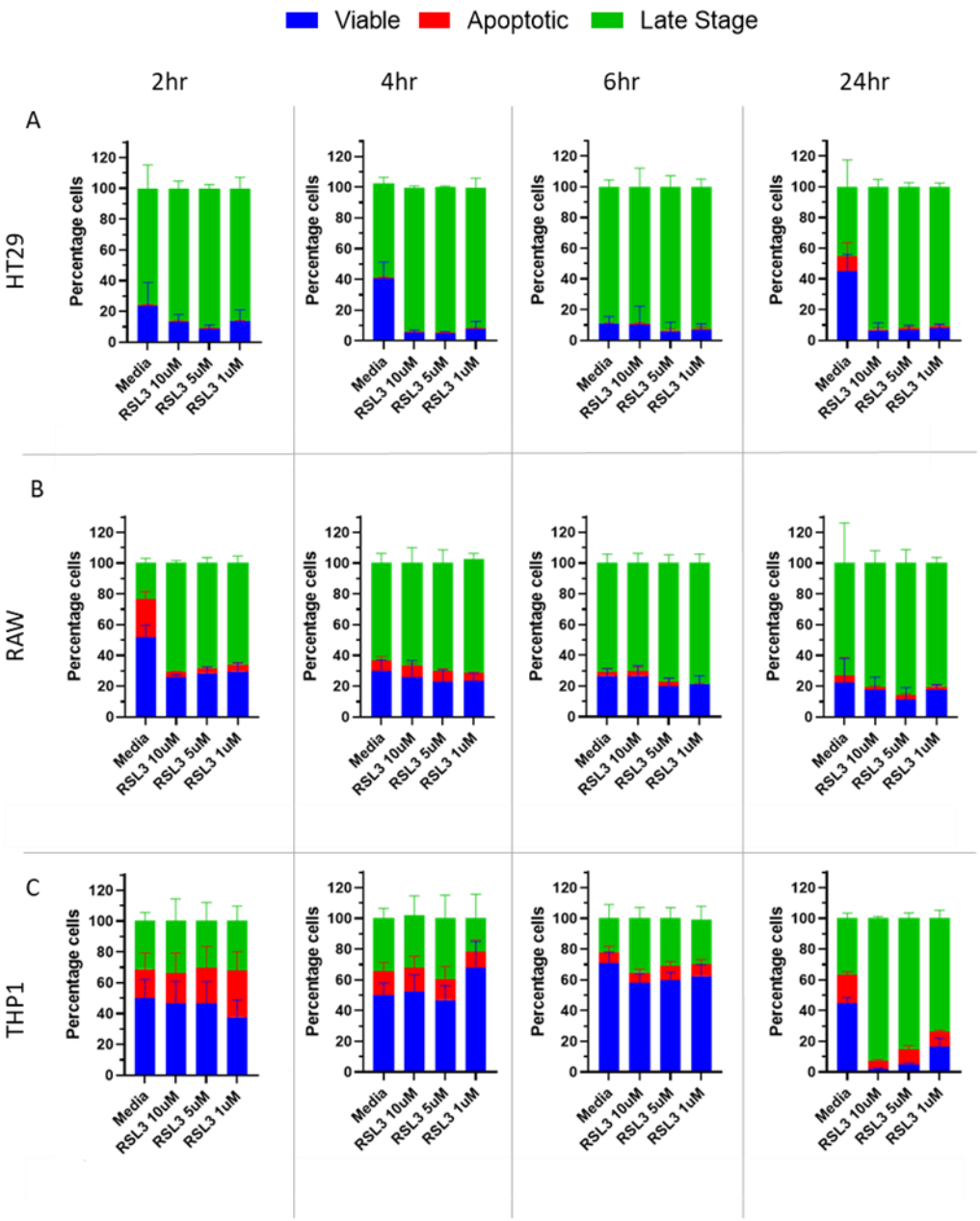

Completed timecourses showing statistical differences between only iron, RSL3 and the combination of treatments.

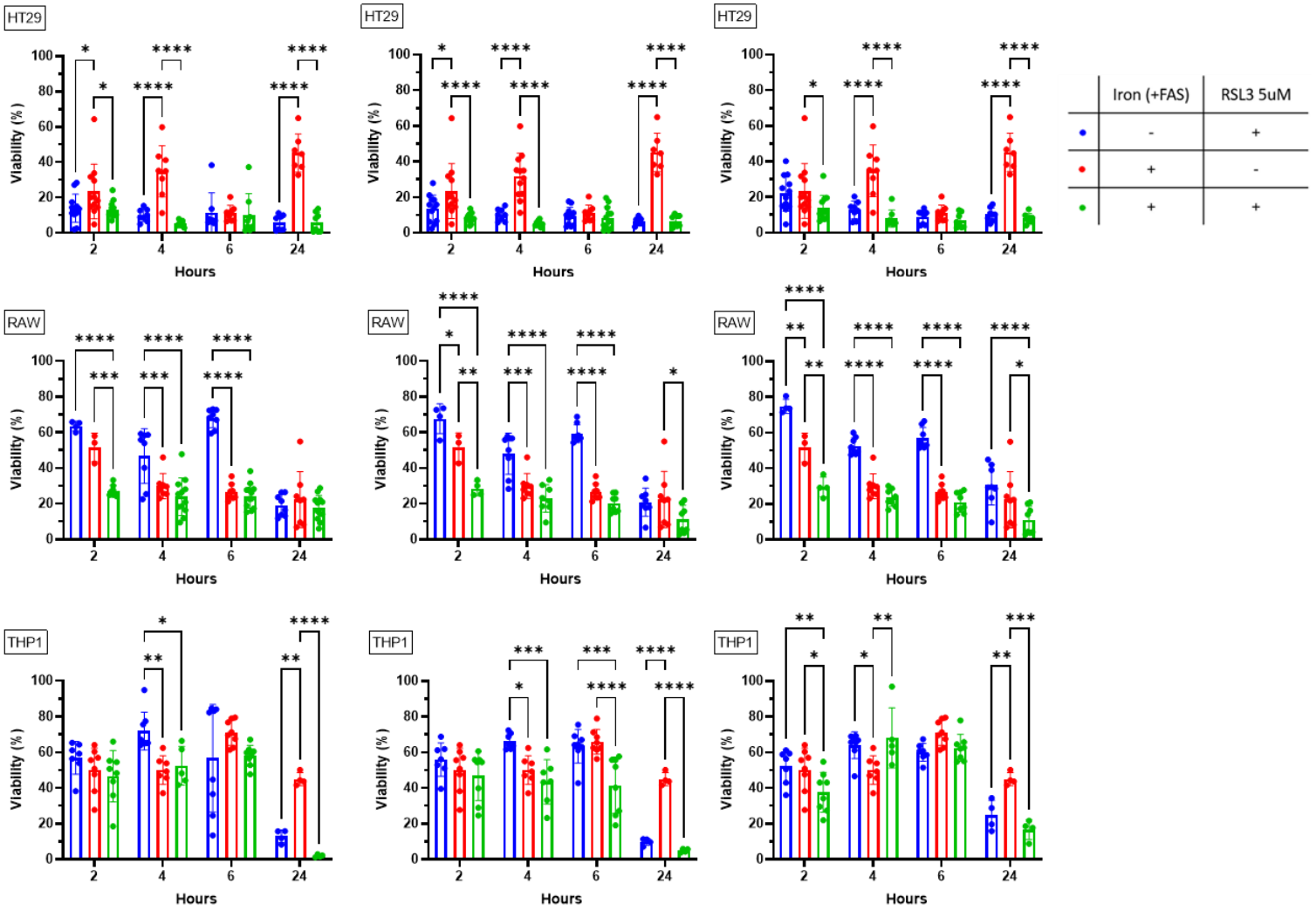
HT29
RAW
THP1
Viability (%)
Hours
2
4
6
24
Iron (+FAS)
RSL3 5uM
-
+

5.6.4 Appendix 5.6.4

Cells were treated with iron for 2 hours and then with either media or RSL3 at different concentrations for different timepoints in (A) HT29, (B) RAW and (C) THP1 cells. Graphs show ROS levels normalised to media (with no iron).

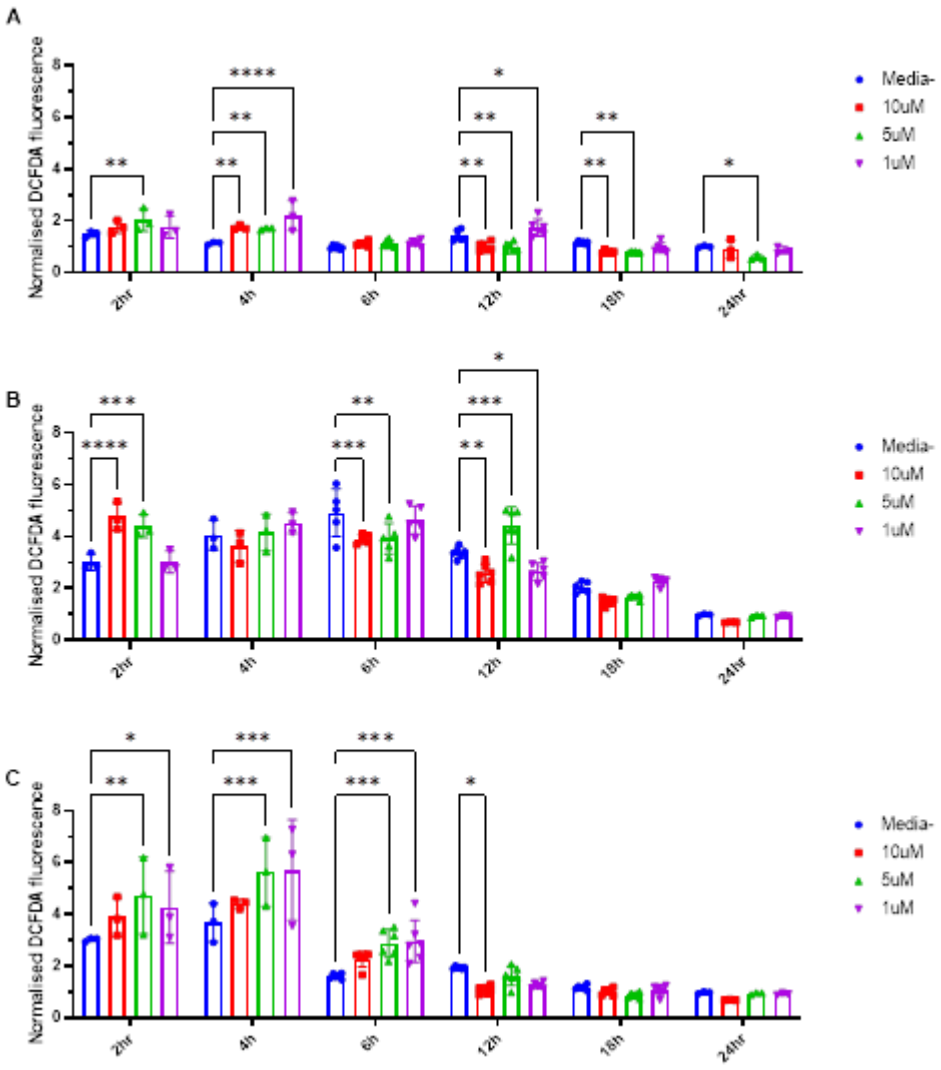

5.6.5 Appendix 5.6.5

Complete timecourses for the different cell lines when treatment of iron is compared to iron+LIP1 or no iron.

HT29

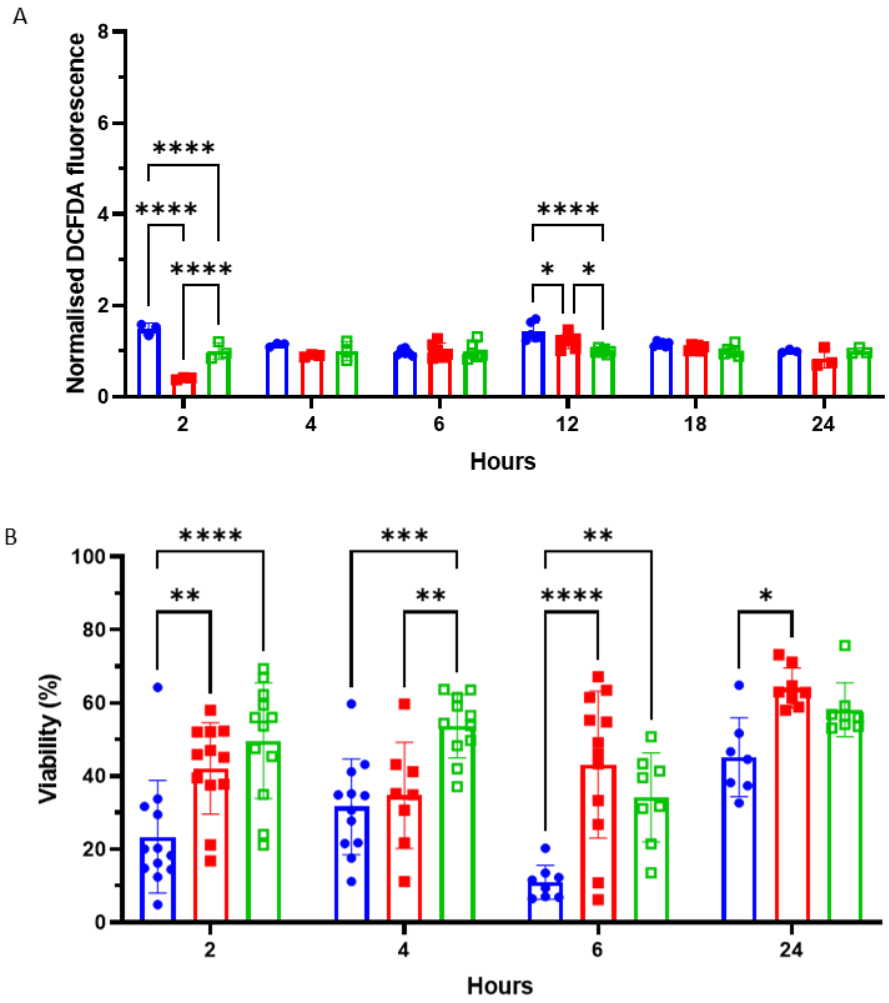

*Effect of LIP1 on iron loaded HT29 cells on ROS production (A) and viability (B), compared to media with and without iron. The samples were tested for normality and a 2way ANOVA, with Tukey's multiple comparison test, performed. * p<0.05, ** p<0.01, *** p<0.001. Error bars = SD.*

RAW

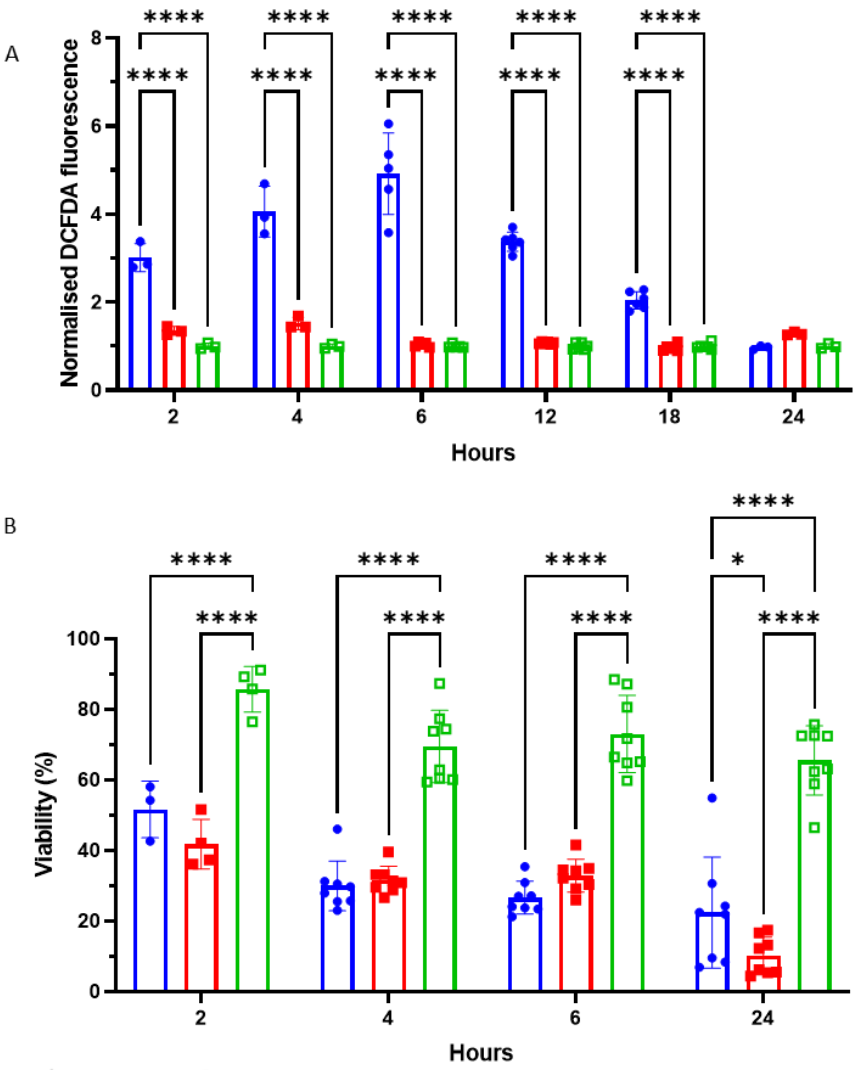

*Effect of LIP1 on iron loaded RAW cells on ROS production (A) and viability (B), compared to media with and without iron. The samples were tested for normality and a 2way ANOVA, with Tukey's multiple comparison test, performed. * p<0.05, ** p<0.01, *** p<0.001. Error bars = SD.*

THP1

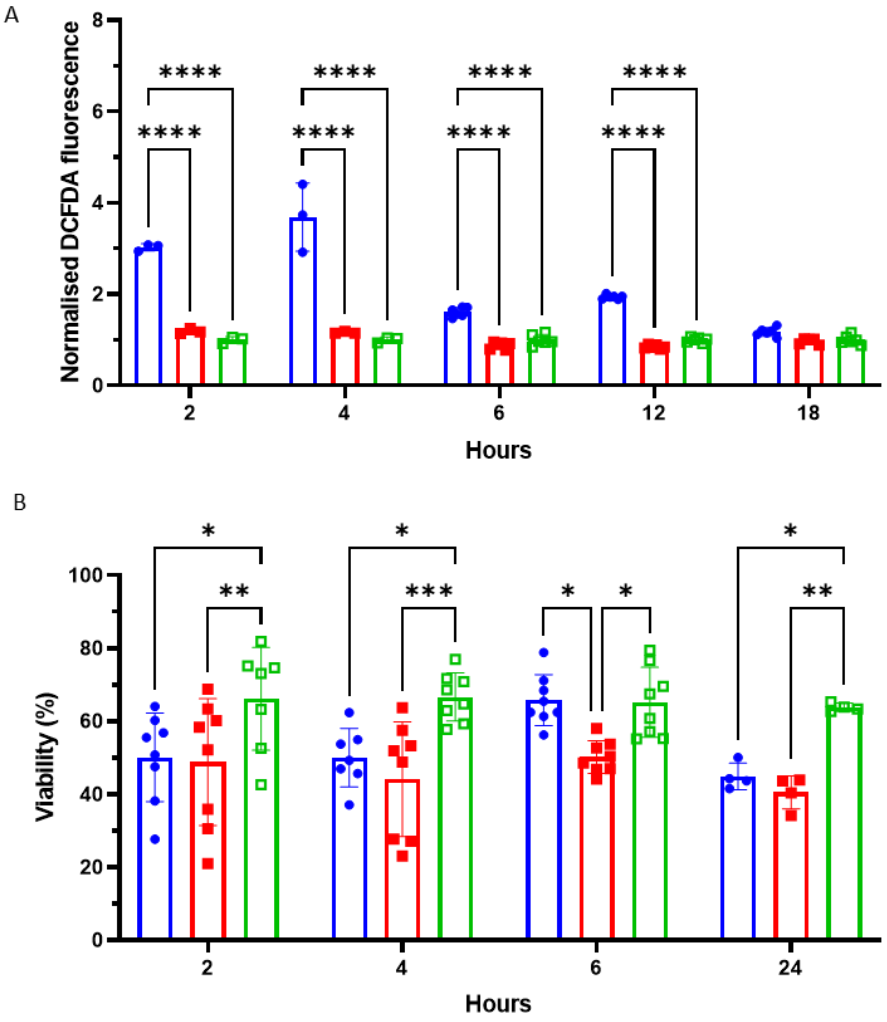

	Iron (+FAS)	LIP1
●	+	-
■	+	+
▫	-	-

*Effect of LIP1 on iron loaded THP1 cells on ROS production (A) and viability (B), compared to media with and without iron. The samples were tested for normality and a 2way ANOVA, with Tukey's multiple comparison test, performed. * p<0.05, ** p<0.01, *** p<0.001. Error bars = SD.*

5.6.6 Appendix 5.6.6

Gating strategy for BAL cells showing identification of single cells and AnxV/PI quadrants strategy identifying viable, apoptotic and late stage necrotic cells.

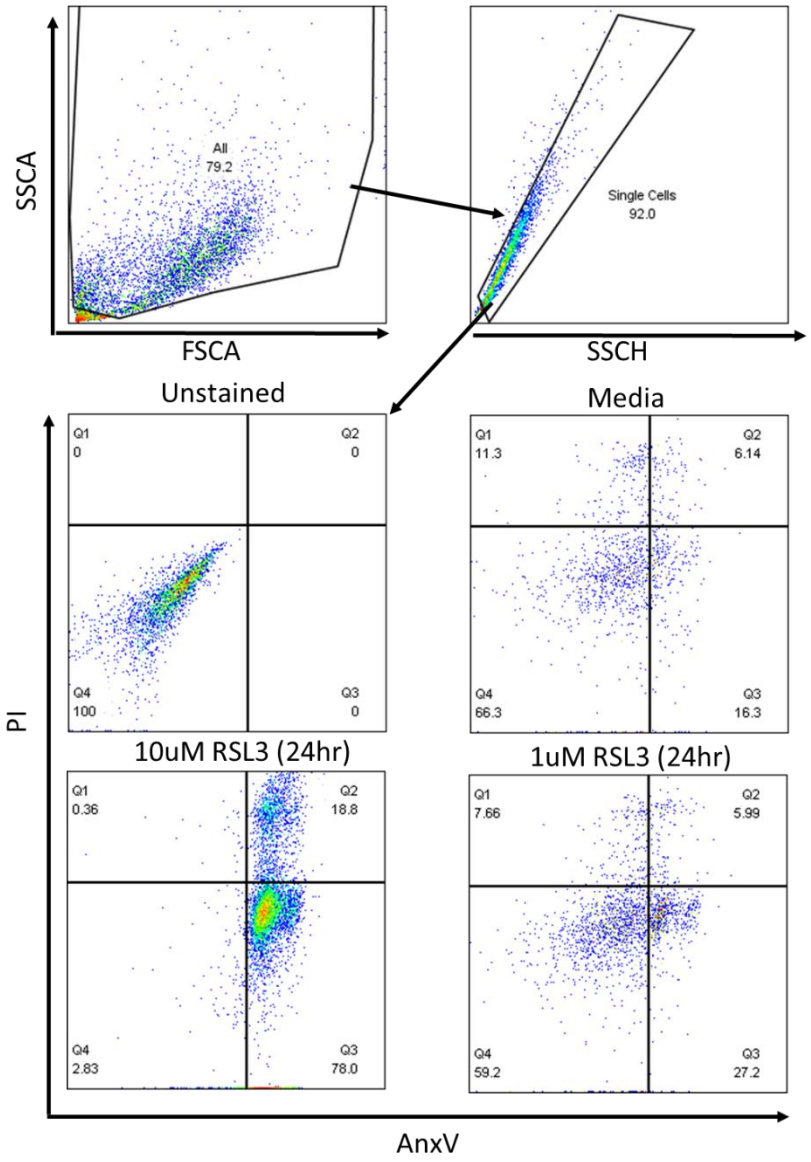

Chapter 6 - Discussion and Conclusion

6.1 Summary

This thesis showed that increased iron loading in alveolar macrophages, determined by Golde score, is independently associated with the presence of fibrosis. Additionally, this increased iron level is also associated with IPF diagnosis over a diagnosis of unclassifiable fibrotic ILD. Some differences in alveolar macrophages between these two diseases were identified through qPCR, with IPF relatively presenting an iron exporting phenotype.

Golde score was not associated with disease progression and indeed higher scores had an independent but weak association with non-progression. No FDR-adjusted significant differences ($P<0.1$) were identified at the transcriptomic level between progressors and non-progressors.

Iron loading in cells has been shown to lead to ferroptosis. However, the alveolar macrophages in fibrotic ILD, which are loaded with iron, are viable. Induction of ferroptosis through RSL3 or exogenous iron showed relative insensitivity in two macrophage cell lines, compared to HT29, an epithelial cell line. In human macrophages (both PMA-differentiated THP1 and patient-derived), RSL3 treatment led to both ferroptosis and apoptosis. Exogenous iron led to greater increase in ROS in macrophages compared to HT29, but this did not result in reduced viability, reflecting the ability of macrophages to handle increased ROS levels.

6.2 Iron and ILD

The role of iron in lung disease pathology has been a topic of interest in recent years. The transferrin receptor (CD71) and increased iron in alveolar macrophages have both been implicated in pulmonary fibrosis pathogenesis. BAL-derived alveolar macrophages from pulmonary fibrosis patients and murine models have indeed been shown to have an overall increased CD71 expression associated with higher iron, while displaying an altered phenotype in disease[111]. IPF patients derived BAL cells have also shown an increased iron-dependent ROS generation compared to control, which is associated with

a pro-inflammatory, tissue remodelling and angiogenic phenotype[110]. Another study has identified a CD71 negative macrophage population in IPF, representing approximately 6% of all airway macrophages, and linked it to worse prognosis[112]. This population was also defined by an increase in classical monocyte activation marker, CD14, suggesting that it was indeed monocyte derived. Previous studies in the Hirani lab have also been able to stratify progression through the CD71+ population when considering a high and low expression level[175]. Increased progression of ILD, thus worse prognosis, was associated with a higher expression of CD71. The CD71 negative population was not considered in these studies.

In this thesis, iron loading was shown to be associated with fibrosis independently of other clinically relevant variables. It was also independently associated with an IPF diagnosis over an UNC one. Although some differences are shown in macrophage phenotype, with IPF alveolar macrophages showing an iron exporting phenotype, further studies at the protein and functional level may have aided in improving this characterisation. The difference in iron levels between fibrotic and non-fibrotic ILD is a novel finding.

Levels of iron and expression of associated proteins have been linked to different macrophage polarisations, in turn associated with different roles in wound healing[233,301]. Understanding if iron loading in alveolar macrophages is associated with a pro-fibrotic or protective phenotype, may help clarify the role of macrophages in fibrosis pathogenesis and identify therapeutic avenues. CD71+ macrophages have been shown to exhibit a phenotype that is plausibly protective in fibrosis (with a reduced Mmp9 and increased Timp1) with CD71 negative cells showing a pro-fibrotic phenotype[111,112]. In the bleomycin model, the iron chelator DFO led to a decrease in the CD71 positive population and an improvement of lung fibrosis, in contrast with the protective role attributed to CD71+ cells[111]. However, DFO has been shown to have antioxidant properties and is able to activate the hypoxia-inducible factor signalling pathway as well, which could lead to suppression of pathological features[302,303]. The use of DFO in this context highlights the complexity of iron metabolism in pulmonary fibrosis and the need for further studies.

Another study using the anti-fungal clioquinol, which acts as an iron chelator, showed inactivation of fibroblasts leading to attenuation of bleomycin-induced PF[304]. In IPF compared to control patients, Pantopoulous et al. (2008), identified an increase in allelic variants of the HFE gene, which resulting protein normally leads to the inhibition of the transferrin receptor and degradation of ferroportin[305]. This was also associated with an increased iron-dependent ROS generation, possibly triggering microscopic injury leading to fibrosis as previously identified[306]. Antioxidants are able to dampen this exaggerated ROS production and it is one of the mechanisms that Pirfenidone, one of the two drugs approved for IPF, is thought to act through[307,308]. Although patients with HFE mutations are likely to develop liver fibrosis, lung fibrosis is not observed. This is likely to be linked to the high levels of iron and overall role of the liver when it comes to iron metabolism. Indeed, HFE mutations are known to hamper hepcidin release by hepatocytes, leading to inadequate inhibition of ferroportin and overall increase of iron[309]. HFE knockouts in murine models however lead to increased iron and fibrosis in the lungs[111]. Current knowledge and understanding of the relationship between iron, macrophages and fibrosis therefore remain controversial and unclear.

When looking at progression of pulmonary fibrosis in this study, iron loading was significantly higher in non-progressors compared to progressors. Lower Golde score was associated with progression independent of any other variables, but the associated risk was very small. BAL cells transcriptome between progressors and non-progressors and iron-regulatory genes were not significantly different in this small study. As iron loading was independently associated with IPF and fibrosis, and they in turn are associated with a worse prognosis compared with non-fibrotic ILDs, an increased iron load would have been expected to be linked to worse prognosis (and progression). These observations require a larger sample size, ideally with an independent validation cohort before firm conclusions can be drawn.

6.2.1 Iron detection methods

Iron detection can be carried out through different techniques but is highly dependent on the nature of the sample. It can be carried out directly, through iron-sensitive probes or staining, or indirectly, using chelators or assessing changes in relevant genes. In this study four different methods were tested to directly assess levels of iron, summarised in Table 6.2.1-1.

Prussian blue is a histochemical stain that uses a semi-quantitative method to assess the levels of iron in cells, the Golde Score. This is based on a subjective scoring of the cells, which validity was demonstrated in this study by assessing it across slides of the same patient on different days. The main reason this was used as the baseline for iron assessment in patient samples is due to the ability of carrying this out systematically on historical samples, with a high success rate and clear results.

TRX-puro (from the Spangler lab) was used on fixed cells which were previously incubated with the probe. Following immunohistochemistry these could be imaged and analysed with high-throughput microscope. Although the method was relatively complex and lengthy compared to the other three iron detection methods, the results were sensitive and specific to the cells of interest. The analysis software, Columbus, can be used to identify features of interest in the cells. Nevertheless, the probe incubation and staining protocol limits the ability to use this routinely.

FIP-1 on the other hand is a fluorescent probe which can only be used in live cells and is very quick acting. It can then be either directly imaged or assessed through flow cytometry, leading to a high-throughput and quantitative result. This has the potential to be used in vivo.

ICP-MS is an analytical method that can be used on frozen cells and fluids, such as BAL fluid. This form of mass spectrometry is used to detect trace elements and therefore gives a very accurate measurement of iron levels within the cells. This was however used on BAL cells aliquots, thus containing other inflammatory cells as well as macrophages. Selection of alveolar

macrophages prior freezing may have improved the characterisation of these aliquots.

Table 6.2.1-1 - Comparison between different methods of iron detection

	Prussian Blue	**ICP-MS**	**TRX-Puro**	**FIP-1**
Type	Fixed cells (historical)	Frozen cells BALf	Fixed cells	Live cells
Iron state	Fe^{3+}	Fe^{2+}/ Fe^{3+}	Fe^{2+}	Fe^{2+}
Applications	Brightfield Imaging		Fluorescence Imaging	Fluorescence Imaging, Flow Cytometry
Sensitivity	Semi-quantitative	Very high	High throughput	High throughput
Translatable	No	No	No	Yes
Time	1 hour	2 hours	6 hours	<1 hour

Iron exists in two states: the ferrous state (Fe^{2+}) and the ferric state (Fe^{3+}). Prussian blue detects Fe^{3+}, whereas the two probes detect Fe^{2+}. ICP-MS detects iron as a whole (^{56}Fe) thus assessing both states. Although this will influence the levels of iron detected in the cell, labile iron continuously switches between the two states based on the pH and oxidising condition of the cell. Iron can be bound to proteins in both forms: transferrin binds ferrous iron, ferritin binds ferric iron, and heme can bind both forms. Due to iron ions instability and the different levels of proteins, iron levels alone may not be enough to understand the iron-state of the cell. Therefore, comparing these techniques, as well as assessing the proteins expression, is key to gather a better picture of the cellular iron metabolism.

6.2.2 Ferroptosis and ILD

Ferroptosis is an iron-dependent form of regulated cell-death[181]. It involves an increase of iron which causes an increase in ROS and associated oxidative stress, leading to cell death. In this study, it was hypothesised that macrophages, which have been shown to have an increased iron loading in pulmonary fibrosis, are resistant to ferroptosis thus remaining viable in the

alveolar space. This could lead to the macrophages being malfunctional in vivo and lead to fibrosis development.

In this study, it was demonstrated that macrophages can undergo ferroptosis but are less sensitive to its induction compared to HT29, an epithelial cell line. RSL3 is a GPX4 inhibitor that has been shown to induce ferroptosis in different cell lines. This inhibition blocks the enzyme's ability to use the potent antioxidant GSH to protect cells against lipid peroxidation. This leads to an increased ROS and consequent death. Increased oxidative burden has been associated in IPF and a reduction in sputum and plasma GSH has been shown[310]. The relative amount of ROS in alveolar macrophages in ILD has not been determined and could improve the characterisation of ferroptosis in these cells.

When RSL3 is used on PMA-differentiated THP1 cells, this led to both ferroptosis and apoptosis (defined as AnxV+PI- cells), and was not clearly rescued by LIP1, an established antioxidant able to rescue viability following ferroptosis induction. This increase in apoptosis was also shown in BAL cells following RSL3 treatment. In the initial studies of ferroptosis using erastin, apoptosis was excluded through the identification of different morphological, biochemical and genetic features. Other studies have shown AnxV+ staining in Jurkat cells following RSL3 treatment. Exposure of phosphatidylserine has been shown in other forms of cell deaths, such as necroptosis, and therefore it should not be used alone to define apoptosis[311,312]. Using apoptosis inhibitors and other morphological and biochemical markers of apoptosis, may have elucidated whether the macrophages were indeed undergoing apoptosis rather than ferroptosis.

Loading the cells with iron (FAS) led to a significant increase in ROS production by macrophages, which was not as striking in HT29 cells. Although this led to a significant reduction in viability in both HT29 and RAW cells, this was not as clear in THP1-derived macrophages. As discussed previously, this is likely to be linked to the ability of macrophages to regulate and withstand high levels of oxidative stress, for example during an oxidative burst during

inflammation[279,313]. Different macrophage phenotypes have been shown to have differential sensitivity to ferroptosis[313]. A better characterisation of the macrophage phenotypes involved in fibrosis development, but also their level of GPX4 and associated activity, may help understand their role in different diseases.

The differences observed between macrophages are likely to be linked to their proliferation rate as well. Indeed, RAW macrophages are highly proliferative, whereas, once differentiated with PMA, THP1 cells are less so. This is linked to a slower metabolism, which can have an impact on how the cell handles iron and compounds. Different rates of proliferation can lead to different degrees of confluency in vitro. Confluency and cell density, a process regulated by the Hippo-YAP/TAZ pathways, has been shown to be a key determinant of ferroptosis sensitivity in cell lines[314]. Some efforts were carried out to characterise this pathway in these cell lines but were unsuccessful.

6.3 Future directions

Most of the cellular characterisation of the macrophage results was carried out through qPCR. Limited understanding of the protein characterisation and functionality of these cells has been demonstrated. Indeed, polarisation of macrophages may have an impact on iron loading and ferroptosis sensitivity. Future studies should focus on characterising these further through flow cytometry, western blotting, and assays such as phagocytosis or autophagy assays. Using supernatants and BAL fluid to demonstrate further functions and molecular signatures would also improve the context of these findings.

BAL-derived cells were not readily available and therefore validation of techniques and experiments was limited. Experiments could have been carried out to characterise progression further. Increasing the RNAseq numbers, while also considering the different diagnosis and control samples, may have identified significant DEGs, which could have then been tested and validated further.

Using sensitive iron probes in live cells may have helped elucidating changes following ferroptosis induction and understand the role of iron further. Optimisation and experiments looking at iron chelators and the effect that these have on the induction of ferroptosis, both in cell lines and primary cells, may help understand the role of iron in the production of key cytokines and pathogenesis. Other ferroptosis inducers, such as erastin, as well as other cell deaths inhibitors, such as zVAD-fmk or Nec-1, and high-resolution imaging, would have clarified what kind of death the cells are undergoing.

Studies focusing on other cellular features of ferroptosis may help understanding this further. For example, studying the changes observed during the oxidation of polyunsaturated fatty acid-containing phospholipids may have identified differences between macrophages linked to their sensitivity. Thorough assessment of iron metabolism could have also aided in understanding the iron loading but lack of cell viability reduction[314].

When comparing cell lines, cell proliferation rate was not considered. This is likely to have an impact on overall metabolism (thus sensitivity to drugs and iron turnover) but also to levels of confluency in vitro, which was shown to play a role in ferroptosis sensitivity.

Finally, there is no single markers available to detect ferroptosis in cells and therefore a combination of markers and cellular changes were used. Ideally future studies will identify a key marker that can be used to detect ferroptosis independently.

Chapter 7 - References

1. Wallis A, Spinks K. The diagnosis and management of interstitial lung. *BMJ*. 2015;2072(May):1-12. doi:10.1136/bmj.h2072

2. Zhang L, Wang Y, Wu G, Xiong W, Gu W, Wang C-Y. Macrophages: friend or foe in idiopathic pulmonary fibrosis? *Respir Res*. 2018;19(170):10. doi:10.1186/s12931-018-0864-2

3. Cairo G, Recalcati S. Iron-regulatory proteins: molecular biology and pathophysiological implications. *Expert Rev Mol Med*. 2007;9(33):1-13. doi:10.1017/S1462399407000531

4. Jung M, Mertens C, Brüne B. Macrophage iron homeostasis and polarization in the context of cancer. *Immunobiology*. 2015;220(2):295-304. doi:10.1016/j.imbio.2014.09.011

5. Ali K, Kim RY, Brown AC, et al. Crucial role for lung iron level and regulation in the pathogenesis and severity of asthma. *Eur Respir J*. 2020;5(4). http://dx.doi.org/10.1183/13993003.01340-2019

6. Do Van B, Gouel F, Jonneaux A, et al. Ferroptosis, a newly characterized form of cell death in Parkinson's disease that is regulated by PKC. *Neurobiol Dis*. 2016;94:169-178. doi:10.1016/j.nbd.2016.05.011

7. Guiney SJ, Adlard PA, Bush AI, Finkelstein DI, Ayton S. Ferroptosis and cell death mechanisms in Parkinson's disease. *Neurochem Int*. 2017;104(June 2018):34-48. doi:10.1016/j.neuint.2017.01.004

8. Linkermann A, Skouta R, Himmerkus N, et al. Synchronized renal tubular cell death involves ferroptosis. *Proc Natl Acad Sci U S A*. 2014;111(47):16836-16841. doi:10.1073/pnas.1415518111

9. Chen L, Hambright WS, Na R, Ran Q. Ablation of the ferroptosis inhibitor glutathione peroxidase 4 in neurons results in rapid motor neuron degeneration and paralysis. *J Biol Chem*. 2015;290(47):28097-28106. doi:10.1074/jbc.M115.680090

10. Yoshida M, Minagawa S, Araya J, et al. Involvement of cigarette smoke-induced epithelial cell ferroptosis in COPD pathogenesis. *Nat Commun*. 2019;10(1):1-14. doi:10.1038/s41467-019-10991-7

11. Raghu G, Remy-Jardin M, Myers JL, et al. Diagnosis of idiopathic pulmonary fibrosis An Official ATS/ERS/JRS/ALAT Clinical practice guideline. *Am J Respir Crit Care Med*. 2018;198(5):e44-e68. doi:10.1164/rccm.201807-1255ST

12. Travis WD, Costabel U, Hansell DM, et al. An official American Thoracic Society/European Respiratory Society statement: Update of the international multidisciplinary classification of the idiopathic interstitial pneumonias. *Am J Respir Crit Care Med*. 2013;188(6):733-748. doi:10.1164/rccm.201308-1483ST

13. Raghu G, Collard HR, Egan JJ, et al. An Official ATS / ERS / JRS / ALAT Statement : Idiopathic Pulmonary Fibrosis : Evidence-based Guidelines for Diagnosis and Management. 2011;183:788-824. doi:10.1164/rccm.2009-040GL

14. Lynch DA, Sverzellati N, Travis WD, et al. Diagnostic criteria for idiopathic pulmonary fibrosis: a Fleischner Society White Paper. *Lancet Respir Med*. 2018;6(2):138-153. doi:10.1016/S2213-2600(17)30433-2

15. Ryerson CJ, Urbania TH, Richeldi L, et al. Prevalence and prognosis of unclassifiable interstitial lung disease. *Eur Respir J*. 2013;42(3):750-757. doi:10.1183/09031936.00131912

16. British Lung Foundation. Idiopathic pulmonary fibrosis statistics. Published 2016. Accessed July 2, 2020. https://statistics.blf.org.uk/pulmonary-fibrosis?cmp_id=1486409450&adg_id=61541973990&kwd=%2Bipf%2Bstatistics&device=c&gclid=CjwKCAjwi_b3BRAGEiwAemPNUya91uQZRWGh2HzTYu2kTOHcxvonwP3pE0I2sj7bWYgRumQLmYU-BBoCuPMQAvD_BwE

17. Boon K, Bailey NW, Yang J, et al. Molecular Phenotypes Distinguish Patients with Relatively Stable from Progressive Idiopathic Pulmonary Fibrosis (IPF). 2009;4(4). doi:10.1371/journal.pone.0005134

18. Schwartz DA, Fossen DSVAN, Davis CS, et al. Determinants of Progression in Idiopathic Pulmonary Fibrosis. 1994;149:444-449.

19. Seibold M, Wise A, Speer M, et al. A Common MUC5B Promoter Polymorphism and Pulmonary Fibrosis. *N Engl J Med*. 2011;364(16):1503-1512.

20. Allen RJ, Porte J, Braybrooke R, et al. Genetic variants associated with susceptibility to idiopathic pulmonary fibrosis in people of European ancestry: a genome-wide association study. *Lancet Respir Med*. 2017;5(11):869-880. doi:10.1016/S2213-2600(17)30387-9

21. Lorenzo-Salazar JM, Ma S-F, Jou J, et al. Novel idiopathic pulmonary fibrosis susceptibility variants revealed by deep sequencing. doi:10.1183/23120541.00071-2019

22. Raghu G, Rochwerg B, Zhang Y, et al. An Official ATS / ERS / JRS / ALAT Clinical Practice Guideline : Treatment of Idiopathic Pulmonary Fibrosis An Update of the 2011 Clinical Practice Guideline. *Am Thorac Soc*. 2015;192:3-19. doi:10.1164/rccm.201506-1063ST

23. Ley B, Collard HR, King TE. Clinical Course and Prediction of Survival in Idiopathic Pulmonary Fibrosis. (3). doi:10.1164/rccm.201006-0894CI

24. Margaritopoulos G, Vasarmidi E, Antoniou K. Pirfenidone in the treatment of idiopathic pulmonary fibrosis: an evidence-based review of its place in therapy. *Core Evid*. 2016;Volume 11:11-22. doi:10.2147/CE.S76549

25. Hajari Case A, Johnson P. Clinical use of nintedanib in patients with idiopathic pulmonary fibrosis. *BMJ Open Respir Res*. 2017;4(1):1-8. doi:10.1136/bmjresp-2017-000192

26. Hughes G, Toellner H, Morris H, Leonard C, Chaudhuri N. Real World Experiences: Pirfenidone and Nintedanib are Effective and Well Tolerated Treatments for Idiopathic Pulmonary Fibrosis. *J Clin Med*. 2016;5(9):78. doi:10.3390/jcm5090078

27. Nasser M, Larrieu S, Si-Mohamed S, et al. Progressive fibrosing interstitial lung disease: a clinical cohort (the PROGRESS study). *Eur Respir J*. 2021;57(2002718). doi:10.1183/13993003.02718-2020

28. Ley B, Ryerson CJ, Vittinghoff E, et al. A multidimensional index and staging system for idiopathic pulmonary fibrosis. *Ann Intern Med*. 2012;156(10):684-695. doi:10.7326/0003-4819-156-10-201205150-00004

29. Wells AU, Desai SR, Rubens MB, et al. Idiopathic Pulmonary Fibrosis A Composite Physiologic Index Derived from Disease Extent Observed by Computed Tomography. doi:10.1164/rccm.2111053

30. Collard HR, King TE, Bartelson BB, Vourlekis JS, Schwarz MI, Brown KK. Changes in Clinical and Physiologic Variables Predict Survival in Idiopathic Pulmonary Fibrosis. Published online 2003. doi:10.1164/rccm.200211-1311OC

31. Raghu G, Collard HR, Anstrom KJ, et al. Idiopathic pulmonary fibrosis: Clinically meaningful primary endpoints in phase 3 clinical trials. *Am J Respir Crit Care Med*. 2012;185(10):1044-1048. doi:10.1164/rccm.201201-0006PP

32. Prasse A, Probst C, Bargagli E, et al. Serum CC-chemokine ligand 18 concentration predicts outcome in idiopathic pulmonary fibrosis. *Am J Respir Crit Care Med*. 2009;179(8):717-723. doi:10.1164/rccm.200808-1201OC

33. Kinder BW, Brown KK, McCormack FX, et al. Serum surfactant protein-A is a strong predictor of early mortality in idiopathic pulmonary fibrosis. *Chest*. 2009;135(6):1557-1563. doi:10.1378/chest.08-2209

34. Korthagen NM, Van Moorsel CHM, Barlo NP, et al. Serum and BALF YKL-40 levels are predictors of survival in idiopathic pulmonary fibrosis. *Respir Med*. 2011;105(1):106-113. doi:10.1016/j.rmed.2010.09.012

35. Yokoyama A, Kondo K, Nakajima M, et al. Prognostic value of circulating KL-6 in idiopathic pulmonary fibrosis. *Respirology*. 2006;11(2):164-168. doi:10.1111/J.1440-1843.2006.00834.X

36. Benyamine A, Heim X, Resseguier N, et al. Elevated serum Krebs von den Lungen-6 in systemic sclerosis: a marker of lung fibrosis and severity of the disease. *Rheumatol Int*. 2018;38(5):813-819. doi:10.1007/s00296-018-3987-3

37. Rosas IO, Richards TJ, Konishi K, et al. MMP1 and MMP7 as potential peripheral blood biomarkers in idiopathic pulmonary fibrosis. *PLoS Med*. 2008;5(4):0623-0633. doi:10.1371/JOURNAL.PMED.0050093

38. Richards TJ, Kaminski N, Baribaud F, et al. Peripheral blood proteins predict mortality in idiopathic pulmonary fibrosis. *Am J Respir Crit Care Med*. 2012;185(1):67-76. doi:10.1164/rccm.201101-0058OC

39. Bauer Y, White ES, de Bernard S, et al. MMP-7 is a predictive biomarker of disease progression in patients with idiopathic pulmonary fibrosis. *ERJ Open Res*. 2017;3(1). doi:10.1183/23120541.00074-2016

40. Armanios MY, Chen JJ-L, Cogan JD, et al. Telomerase Mutations in Families with Idiopathic Pulmonary Fibrosis. *N Engl J Med*. 2007;356(13):1317-1326. doi:10.1056/NEJMOA066157/SUPPL_FILE/NEJM_ARMANIOS_1317SA1.PDF

41. Stuart BD, Lee JS, Kozlitina J, et al. Effect of telomere length on survival in patients with idiopathic pulmonary fibrosis: an observational cohort study with independent validation. *Lancet Respir Med*. 2014;2(7):557-565. doi:10.1016/S2213-2600(14)70124-9

42. Duckworth A, Gibbons MA, Allen RJ, et al. Telomere length and risk of idiopathic pulmonary fibrosis and chronic obstructive pulmonary disease: a mendelian randomisation study. *Lancet Respir Med*. 2021;9(3):285-294. doi:10.1016/S2213-2600(20)30364-7

43. Schafer MJ, White TA, Iijima K, et al. Cellular senescence mediates fibrotic pulmonary disease. *Nat Commun*. Published online 2017. doi:10.1038/ncomms14532

44. Aoshiba K, Tsuji T, Nagai A. Bleomycin induces cellular senescence in alveolar epithelial cells. *Eur Respir J*. 2003;22(3):436-443. doi:10.1183/09031936.03.00011903

45. Aoshiba K, Tsuji T, Kameyama S, et al. Senescence-associated secretory phenotype in a mouse model of bleomycin-induced lung injury. *Exp Toxicol Pathol*. 2013;65(7-8):1053-1062. doi:10.1016/J.ETP.2013.04.001

46. DePianto DJ, Vander Heiden JA, Morshead KB, et al. Molecular mapping of interstitial lung disease reveals a phenotypically distinct senescent basal epithelial cell population. *JCI Insight*. 2021;6(8). doi:10.1172/JCI.INSIGHT.143626

47. Hashimoto M, Asai A, Kawagishi H, et al. Elimination of p19 ARF-expressing cells enhances pulmonary function in mice. *JCI insight*. 2016;1(12). doi:10.1172/JCI.INSIGHT.87732

48. Adamson IYR, Bowden DH. The pathogenesis of bleomycin induced pulmonary fibrosis in mice. *Am J Pathol*. 1974;77(2):185-198.

49. Walters DM, Kleeberger SR. Mouse models of bleomycin-induced pulmonary fibrosis. *Curr Protoc Pharmacol*. 2008;(SUPPL. 40):1-17. doi:10.1002/0471141755.ph0546s40

50. Moore BB, Hogaboam CM. Murine models of pulmonary fibrosis. *Am J Physiol - Lung Cell Mol Physiol*. 2008;294(2):152-160. doi:10.1152/ajplung.00313.2007

51. Moore BB, Lawson WE, Oury TD, Sisson TH, Raghavendran K, Hogaboam CM. Animal models of fibrotic lung disease. *Am J Respir Cell Mol Biol*. 2013;49(2):167-179. doi:10.1165/rcmb.2013-0094TR

52. Allawzi A, Elajaili H, Redente EF, Nozik-Grayck E. Oxidative toxicology of bleomycin: Role of the extracellular redox environment. *Curr Opin Toxicol*. 2019;13:68-73. doi:10.1016/j.cotox.2018.08.001

53. Teixeira KC, Soares FS, Rocha LGC, et al. Attenuation of bleomycin-induced lung injury and oxidative stress by N-acetylcysteine plus deferoxamine. *Pulm Pharmacol Ther*. 2008;21(2):309-316. doi:10.1016/j.pupt.2007.07.006

54. Scotton CJ, Chambers RC. Bleomycin revisited: Towards a more representative model of IPF? *Am J Physiol - Lung Cell Mol Physiol*. 2010;299(4):439-441. doi:10.1152/ajplung.00258.2010

55. Gibbons MA, MacKinnon AC, Ramachandran P, et al. Ly6Chi monocytes direct alternatively activated profibrotic macrophage regulation of lung fibrosis. *Am J Respir Crit Care Med*. 2011;184(5):569-581. doi:10.1164/rccm.201010-1719OC

56. Scotton CJ, Hayes B, Alexander R, et al. Ex vivo micro-computed tomography analysis of bleomycin-induced lung fibrosis for preclinical drug evaluation. *Eur Respir J*. 2013;42(6):1633-1645. doi:10.1183/09031936.00182412

57. Degryse AL, Tanjore H, Xu XC, et al. Repetitive intratracheal bleomycin models several features of idiopathic pulmonary fibrosis. *Am J Physiol - Lung Cell Mol Physiol*. 2010;299(4):442-452. doi:10.1152/ajplung.00026.2010

58. Limjunyawong N, Mitzner W, Horton MR. A mouse model of chronic idiopathic pulmonary fibrosis. *Physiol Rep*. 2014;2(2):e00249. doi:10.1002/phy2.249

59. The Idiopathic Pulmonary Fibrosis Clinical, Research Network. Prednisone, Azathioprine, and N-Acetylcysteine for Pulmonary Fibrosis. *N Engl J Med*. 2012;366:1968-1977.

60. Selman M, King Jr T, Pardo A. Prevailing and Evolving Hypotheses about Its Pathogenesis and Implications for Therapy. *Ann Intern Med*. 2001;(2).

61. Byrne AJ, Maher TM, Lloyd CM. Pulmonary Macrophages: A New

Therapeutic Pathway in Fibrosing Lung Disease? *Trends Mol Med*. 2016;22(4):303-316. doi:10.1016/j.molmed.2016.02.004

62. Khalil N, Bereznay O, Sporn M, Greenberg AH. Macrophage Production of Transforming Growth Factor Beta and Fibroblast Collagen Synthesis in Chronic Pulmonary Inflammation. *J Exp Med*. 1989;170(September):727-737.

63. Murray LA, Chen Q, Kramer MS, et al. TGF-beta driven lung fibrosis is macrophage dependent and blocked by Serum amyloid P. *Int J Biochem Cell Biol*. 2011;43(1):154-162. doi:10.1016/j.biocel.2010.10.013

64. Korfei M, Ruppert C, Mahavadi P, et al. Epithelial endoplasmic reticulum stress and apoptosis in sporadic idiopathic pulmonary fibrosis. *Am J Respir Crit Care Med*. 2008;178(8):838-846. doi:10.1164/rccm.200802-313OC

65. Gunther A, Korfei M, Mahavadi P, Beck D Von Der, Ruppert C, Markart P. Unravelling the progressice pathophysiology of idiopathic pulmonary fibrosis. *Eur Respir Rev*. 2012;21(124):152-160. doi:10.1183/09059180.00001012

66. García-Sancho C, Buendía-Roldán I, Fernández-Plata MR, et al. Familial pulmonary fibrosis is the strongest risk factor for idiopathic pulmonary fibrosis. *Respir Med*. 2011;105(12):1902-1907. doi:10.1016/j.rmed.2011.08.022

67. Adams TS, Schupp JC, Poli S, et al. Single-cell RNA-seq reveals ectopic and aberrant lung-resident cell populations in idiopathic pulmonary fibrosis. *Sci Adv*. 2020;6(28). doi:10.1126/sciadv.aba1983

68. Xu Y, Mizuno T, Sridharan A, et al. Single-cell RNA sequencing identifies diverse roles of epithelial cells in idiopathic pulmonary fibrosis. *JCI Insight*. 2016;1(20). doi:10.1172/JCI.INSIGHT.90558

69. Kim KK, Kugler MC, Wolters PJ, et al. Alveolar epithelial cell mesenchymal transition develops in vivo during pulmonary fibrosis and is regulated by the extracellular matrix. *PNAS*. 2006;103(35):13180-13185. www.pnas.orgcgidoi10.1073pnas.0605669103

70. Selman M, Pardo A. Idiopathic pulmonary fibrosis: An epithelial/fibroblastic cross-talk disorder. *Respir Res*. 2001;3:1-8. doi:10.1186/rr175

71. Selman M, Pardo A. Role of Epithelial Cells in Idiopathic Pulmonary Fibrosis From Innocent Targets to Serial Killers. 2006;3:364-372. doi:10.1513/pats.200601-003TK

72. Plataki M, Koutsopoulos A V., Darivianaki K, Delides G, Siafakas NM, Bouros D. Expression of apoptotic and antiapoptotic markers in epithelial cells in idiopathic pulmonary fibrosis. *Chest*. 2005;127(1):266-274. doi:10.1378/chest.127.1.266

73. Cui Y, Robertson J, Maharaj S, et al. Oxidative stress contributes to the induction and persistence of TGF-β1 induced pulmonary fibrosis. *Int J Biochem Cell Biol*. 2011;43(8):1122-1133. doi:10.1016/j.biocel.2011.04.005

74. Zhu L, Fu X, Chen X, Han X, Dong P. M2 macrophages induce EMT through the TGF-β/Smad2 signaling pathway. *Cell Biol Int*. 2017;41(9):960-968. doi:10.1002/cbin.10788

75. Byrne AJ, Maher TM, Lloyd CM. Pulmonary Macrophages : A New Therapeutic Pathway in Fibrosing Lung Disease ? *Trends Mol Med*. 2016;22(4):303-316. doi:10.1016/j.molmed.2016.02.004

76. Schyns J, Bai Q, Ruscitti C, et al. Non-classical tissue monocytes and two functionally distinct populations of interstitial macrophages populate the mouse lung. *Nat Commun*. 2019;10(1). doi:10.1038/s41467-019-11843-0

77. Schneider C, Nobs SP, Kurrer M, Rehrauer H, Thiele C, Kopf M. Induction of the nuclear receptor PPAR-γ 3 by the cytokine GM-CSF is critical for the differentiation of fetal monocytes into alveolar macrophages. *Nat Immunol*. 2014;15(11):1026-1037. doi:10.1038/ni.3005

78. Guilliams M, De Kleer I, Henri S, et al. Alveolar macrophages develop from fetal monocytes that differentiate into long-lived cells in the first week of life via GM-CSF. *J Exp Med*. 2013;210(10):1977-1992. doi:10.1084/jem.20131199

79. Tate MD, Pickett DL, van Rooijen N, Brooks AG, Reading PC. Critical Role of Airway Macrophages in Modulating Disease Severity during Influenza Virus Infection of Mice. *J Virol*. 2010;84(15):7569-7580. doi:10.1128/jvi.00291-10

80. Hussell T, Bell TJ. Alveolar macrophages: Plasticity in a tissue-specific context. *Nat Rev Immunol*. 2014;14(2):81-93. doi:10.1038/nri3600

81. Herold S, Steinmueller M, Von Wulffen W, et al. Lung epithelial apoptosis in influenza virus pneumonia: The role of macrophage-expressed TNF-related apoptosis-inducing ligand. *J Exp Med*. 2008;205(13):3065-3077. doi:10.1084/jem.20080201

82. Martinez FO, Gordon S. The M1 and M2 paradigm of macrophage activation: time for reassessment. *F1000Prime Rep*. 2014;6(March):1-13. doi:10.12703/P6-13

83. Murray PJ, Allen JE, Biswas SK, et al. Macrophage Activation and Polarization: Nomenclature and Experimental Guidelines. *Immunity*. 2014;41(1):14-20. doi:10.1016/j.immuni.2014.06.008

84. Schupp JC, Binder H, Jäger B, et al. Macrophage Activation in Acute Exacerbation of Idiopathic Pulmonary Fibrosis. *PLoS One*. 2015;10(1):1-11. doi:10.1371/journal.pone.0116775

85. Collard HR, Moore BB, Flaherty KR, et al. Acute Exacerbations of Idiopathic Pulmonary Fibrosis. *Fernando J Martinez*. 2007;24.

86. Juarez MM, Chan AL, Norris AG, Morrissey BM, Albertson TE. Acute exacerbation of idiopathic pulmonary fibrosis-A review of current and novel pharmacotherapies. *J Thorac Dis*. 2015;7(3):499-519. doi:10.3978/J.ISSN.2072-1439.2015.01.17

87. Bargagli E, Prasse A, Olivieri C, Muller-Quernheim J, Rottoli P. Macrophage-derived biomarkers of idiopathic pulmonary fibrosis. *Pulm Med*. 2011;2011. doi:10.1155/2011/717130

88. Madsen DH, Leonard D, Masedunskas A, et al. M2-like macrophages are responsible for collagen degradation through a mannose receptor-mediated pathway. *J Cell Biol*. 2013;202(6):951-966. doi:10.1083/jcb.201301081

89. Rohani MG, McMahan RS, Razumova M V., et al. MMP-10 Regulates Collagenolytic Activity of Alternatively Activated Resident Macrophages. *J Invest Dermatol*. 2015;135(10):2377-2384. doi:10.1038/jid.2015.167

90. Nouno T, Okamoto M, Ohnishi K, et al. Elevation of pulmonary CD163 + and CD204 + macrophages is associated with the clinical course of idiopathic pulmonary fibrosis patients. *J Thorac Dis*. 2019;11(9):4005-4017. doi:10.21037/jtd.2019.09.03

91. Graversen JH, Madsen M, Moestrup SK. CD163: A signal receptor scavenging haptoglobin-hemoglobin complexes from plasma. *Int J Biochem Cell Biol*. 2002;34(4):309-314. doi:10.1016/S1357-2725(01)00144-3

92. Sulahian TH, Högger P, Wahner AE, et al. Human monocytes express CD163, which is upregulated by IL-10 and identical to p155. *Cytokine*. 2000;12(9):1312-1321. doi:10.1006/cyto.2000.0720

93. Raggi F, Pelassa S, Pierobon D, et al. Regulation of Human Macrophage M1–M2 Polarization Balance by Hypoxia and the Triggering Receptor Expressed on Myeloid Cells-1. *Front Immunol*. 2017;0(SEP):1097. doi:10.3389/FIMMU.2017.01097

94. Parker D. CD80/CD86 signaling contributes to the proinflammatory response ofStaphylococcus aureus in the airway. *Cytokine*. 2018;107:130. doi:10.1016/J.CYTO.2018.01.016

95. Julià A, Bonafonte-Pardàs I, Gómez A, et al. Targeting of the CD80/86 proinflammatory axis as a therapeutic strategy to prevent severe COVID-19. *Sci Reports 2021 111*. 2021;11(1):1-14. doi:10.1038/s41598-021-90797-0

96. Misharin A V, Morales-Nebreda L, Mutlu GM, Budinger GR, Perlman H. Flow cytometric analysis of macrophages and dendritic cell subsets in the mouse lung. *Am J Respir Cell Mol Biol*. 2013;49(4):503-510. doi:10.1165/rcmb.2013-0086MA

97. Misharin A V, Morales-Nebreda L, Reyfman PA, et al. Monocyte-derived alveolar macrophages drive lung fibrosis and persist in the lung over the life span. *J Exp Med*. Published online 2017:1-18. doi:10.1084/jem.20162152

98. Aran D, Looney AP, Liu L, et al. Reference-based analysis of lung single-cell sequencing reveals a transitional profibrotic macrophage. *Nat Immunol*. 2019;20(2):163-172. doi:10.1038/s41590-018-0276-y

99. Gibbons MA, MacKinnon AC, Ramachandran P, et al. Ly6Chimonocytes direct alternatively activated profibrotic macrophage regulation of lung fibrosis. *Am J Respir Crit Care Med*. 2011;184(5):569-581. doi:10.1164/rccm.201010-1719OC

100. Young LR, Gulleman PM, Short CW, et al. Epithelial-macrophage interactions determine pulmonary fibrosis susceptibility in Hermansky-Pudlak syndrome. *JCI Insight*. 2016;1(17):1-15. doi:10.1172/jci.insight.88947

101. Zhou Y, Peng H, Sun H, et al. Chitinase 3-Like 1 Suppresses Injury and Promotes Fibroproliferative Responses in Mammalian Lung Fibrosis. *Sci Transl Med*. 2014;6(240):240ra76-240ra76. doi:10.1126/scitranslmed.3007096

102. Desai O, Winkler J, Minasyan M, Herzog EL. The role of immune and inflammatory cells in idiopathic pulmonary fibrosis. *Front Med*. 2018;5(43). doi:10.3389/fmed.2018.00043

103. Morimoto K, Janssen WJ, Terada M. Defective efferocytosis by alveolar macrophages in IPF patients. *Respir Med*. 2012;106(12):1800-1803. doi:10.1016/j.rmed.2012.08.020

104. Kim MS, Baek AR, Lee JH, et al. IL-37 Attenuates Lung Fibrosis by Inducing Autophagy and Regulating TGF-β1 Production in Mice. *J Immunol*. 2019;203(8):2265-2275. doi:10.4049/jimmunol.1801515

105. Li Y, Gao Q, Xu K, et al. Interleukin-37 Attenuates Bleomycin-Induced Pulmonary Inflammation and Fibrosis in Mice. *Inflammation*. 2018;41(5):1772-1779. doi:10.1007/s10753-018-0820-9

106. Reyfman PA, Walter JM, Joshi N, et al. Single-Cell Transcriptomic Analysis of Human Lung Provides Insights into the Pathobiology of Pulmonary Fibrosis. *Am J Respir Crit Care Med*. 2019;199:1517-1536. doi:10.1164/rccm.201712-2410OC

107. Lishnevsky M, Young LC, Woods SJ, et al. Microhemorrhage is an early event in the pulmonary fibrotic disease of PECAM-1 deficient FVB/n mice. *Exp Mol Pathol*. 2014;97(1):128-136. doi:10.1016/j.yexmp.2014.06.008

108. Colombat M, Mal H, Groussard O, et al. Pulmonary vascular lesions in end-stage idiopathic pulmonary fibrosis: histopathologic study on lung explant specimens and correlations with pulmonary hemodynamics.

Hum Pathol. 2007;38(1):60-65. doi:10.1016/j.humpath.2006.06.007

109. Kim J. The Role of Iron Metabolism in Lung Inflammation and Injury. *J Allergy Ther*. 2012;01(S4). doi:10.4172/2155-6121.S4-004

110. Lee J, Arisi I, Puxeddu E, et al. Bronchoalveolar lavage (BAL) cells in idiopathic pulmonary fibrosis express a complex pro-inflammatory, pro-repair, angiogenic activation pattern, likely associated with macrophage iron accumulation. *PLoS One*. 2018;13(4):1-15. doi:10.1371/journal.pone.0194803

111. Ali MK, Kim RY, Brown AC, et al. Critical role for iron accumulation in the pathogenesis of fibrotic lung disease. *J Pathol*. 2020;251(1):49-62. doi:10.1002/PATH.5401

112. Allden SJ, Ogger PP, Ghai P, et al. The transferrin receptor CD71 delineates functionally distinct airway macrophage subsets during idiopathic pulmonary fibrosis. *Am J Respir Crit Care Med*. 2019;200(2):209-219. doi:10.1164/rccm.201809-1775OC

113. Soares MP, Hamza I. Macrophages and Iron Metabolism. *Immunity*. 2016;44(3):492-504. doi:10.1016/j.immuni.2016.02.016

114. Vidal SM, Pinner E, Lepage P, Gauthier S, Gros P. Natural resistance to intracellular infections: Nramp1 encodes a membrane phosphoglycoprotein absent in macrophages from susceptible (Nramp1 D169) mouse strains. *J Immunol*. 1996;157(8):3559-3568. Accessed May 14, 2020. http://www.ncbi.nlm.nih.gov/pubmed/8871656

115. Kao JK, Wang SC, Ho LW, et al. Chronic iron overload results in impaired bacterial killing of THP-1 derived macrophage through the inhibition of lysosomal acidification. *PLoS One*. 2016;11(5):1-16. doi:10.1371/journal.pone.0156713

116. Recalcati S, Locati M, Marini A, et al. Differential regulation of iron homeostasis during human macrophage polarized activation. *Eur J Immunol*. 2010;40(3):824-835. doi:10.1002/eji.200939889

117. Corna G, Campana L, Pignatti E, et al. Polarization dictates iron handling by inflammatory and alternatively activated macrophages. *Haematologica*. 2010;95(11):1814-1822. doi:10.3324/haematol.2010.023879

118. Johnson DC, Dean DR, Smith AD, Johnson MK. Structure, Function, and Formation of Biological Iron-Sulfur Clusters. *Annu Rev Biochem*. 2005;74(1):247-281. doi:10.1146/annurev.biochem.74.082803.133518

119. Andrews NC. Iron homeostasis: insights from genetics and animal models. *Nat Rev Genet*. 2000;1(December):208-217. doi:10.1038/35042073

120. Korolnek T, Hamza I. Macrophages and iron trafficking at the birth and death of red cells. *Blood Spotlight*. 2018;125(19):2893-2898.

doi:10.1182/blood-2014-12-567776.BLOOD

121. Andrews NC. Iron homeostasis: insights from genetics and animal models. *Nat Rev Genet*. 2000;1. Accessed April 29, 2020. www.nature.com/reviews/genetics

122. Gunshin H, Mackenzie B, Berger U V., et al. Cloning and characterization of a mammalian proton-coupled metal-ion transporter. *Nature*. 1997;388(6641):482-488. doi:10.1038/41343

123. Pigeon C, Ilyin G, Courselaud B, et al. A New Mouse Liver-specific Gene, Encoding a Protein Homologous to Human Antimicrobial Peptide Hepcidin, Is Overexpressed during Iron Overload. *J Biol Chem*. 2001;276(11):7811-7819. doi:10.1074/jbc.M008923200

124. Nicolas G, Bennoun M, Devaux I, et al. Lack of hepcidin gene expression and severe tissue iron overload in upstream stimulatory factor 2 (USF2) knockout mice. *PNAS*. 2001;98(15):8780-8785. doi:10.1073/pnas.151179498

125. Nicolas G, Bennoun M, Porteu A, et al. Severe iron deficiency anemia in transgenic mice expressing liver hepcidin. *Proc Natl Acad Sci U S A*. 2002;99(7):4596-4601. doi:10.1073/pnas.072632499

126. Lesbordes-Brion JC, Viatte L, Bennoun M, et al. Targeted disruption of the hepcidin 1 gene results in severe hemochromatosis. *Blood*. 2006;108(4):1402-1405. doi:10.1182/blood-2006-02-003376

127. Park CH, Valore E V., Waring AJ, Ganz T. Hepcidin, a Urinary Antimicrobial Peptide Synthesized in the Liver. *J Biol Chem*. 2001;276(11):7806-7810. doi:10.1074/jbc.M008922200

128. Schmidt PJ. Regulation of Iron Metabolism by Hepcidin under Conditions of Inflammation *. *J Biol Chem*. 2015;290(31):18975-18983. doi:10.1074/jbc.R115.650150

129. Nemeth E, Tuttle M, Powelson J, et al. Hepcidin Regulates Cellular Iron Efflux by Binding to Ferroportin and Inducing Its Internalization. *Science (80-)*. 2004;306(5704):2090-2093. doi:10.1126/science.1104742

130. Hentze MW, Muckenthaler MU, Galy B, Camaschella C. Two to Tango: Regulation of Mammalian Iron Metabolism. *Cell*. 2010;142(1):24-38. doi:10.1016/j.cell.2010.06.028

131. Mladenka P, Hrdina R, Hübl M, Simůnek T. The fate of iron in the organism and its regulatory pathways. *Acta Medica (Hradec Kralove)*. 2005;48(3-4):127-135. doi:10.14712/18059694.2018.40

132. Eisenstein RS. Discovery of the Ceruloplasmin Homologue Hephaestin: New Insight into the Copper/Iron Connection. *Nutr Rev*. 2000;58(1):22-26. doi:10.1111/j.1753-4887.2000.tb01821.x

133. Ganz T, Nemeth E. Iron homeostasis in host defence and inflammation. *Nat Publ Gr*. Published online 2015. doi:10.1038/nri3863

134. Donovan A, Lima CA, Pinkus JL, et al. The iron exporter ferroportin/Slc40a1 is essential for iron homeostasis. *Cell Metab*. 2005;1(3):191-200. doi:10.1016/j.cmet.2005.01.003

135. Schmidt PJ, Toran PT, Giannetti AM, Bjorkman PJ, Andrews NC. The Transferrin Receptor Modulates Hfe-Dependent Regulation of Hepcidin Expression. *Cell Metab*. 2008;7(3):205-214. doi:10.1016/j.cmet.2007.11.016

136. Donovan A, Lima CA, Pinkus JL, et al. The iron exporter ferroportin/Slc40a1 is essential for iron homeostasis. *Cell Metab*. 2005;1(3):191-200. doi:10.1016/j.cmet.2005.01.003

137. Sangiuolo F, Puxeddu E, Pezzuto G, et al. HFE gene variants and iron-induced oxygen radical generation in idiopathic pulmonary fibrosis. *Eur Respir J*. 2015;45(2):483-490. doi:10.1183/09031936.00104814

138. Kondo H, Saito K, Grasso JP, Aisen P. Iron metabolism in the erythrophagocytosing Kupffer cell. *Hepatology*. 1988;8(1):32-38. doi:10.1002/hep.1840080108

139. Zhang V, Nemeth E, Kim A. Iron in lung pathology. *Pharmaceuticals*. 2019;12(1):1-11. doi:10.3390/ph12010030

140. Poss KD, Tonegawa S. Heme oxygenase 1 is required for mammalian iron reutilization. *Proc Natl Acad Sci U S A*. 1997;94(20):10919-10924. doi:10.1073/pnas.94.20.10919

141. Bianchi L, Tacchini L, Cairo G. HIF-1-mediated activation of transferrin receptor gene transcription by iron chelation. *Nucleic Acids Res*. 1999;27(21):4223-4227. doi:10.1093/NAR/27.21.4223

142. Recalcati S, Minotti G, Cairo G. Iron regulatory proteins: From molecular mechanisms to drug development. *Antioxidants Redox Signal*. 2010;13(10):1593-1616. doi:10.1089/ars.2009.2983

143. McMahon HT, Boucrot E. Molecular mechanism and physiological functions of clathrin-mediated endocytosis. *Nat Rev Mol Cell Biol 2011 128*. 2011;12(8):517-533. doi:10.1038/nrm3151

144. Lim JE, Jin O, Bennett C, et al. A mutation in Sec15l1 causes anemia in hemoglobin deficit (hbd) mice. 2005;37. doi:10.1038/ng1659

145. Li F, Liu CF, Xu YZ, et al. Neonatal lethality and recycling defect of transferrin receptor in mice with Syntaxin12/13 disruption. *Protein Cell*. 2019;10(1):67-71. doi:10.1007/s13238-018-0519-6

146. Chen C, Garcia-Santos D, Ishikawa Y, et al. Snx3 regulates recycling of the transferrin receptor and iron assimilation. Published online 2013. doi:10.1016/j.cmet.2013.01.013

147. Dautry Varsat A, Ciechanover A, Lodish HF. pH and the recycling of transferrin during receptor-mediated endocytosis. *Proc Natl Acad Sci U S A*. 1983;80(8 I):2258-2262. doi:10.1073/pnas.80.8.2258

148. Ohgami RS, Campagna DR, Greer EL, et al. Identification of a ferrireductase required for efficient transferrin-dependent iron uptake in erythroid cells. *Nat Genet*. 2005;37(11):1264-1269. doi:10.1038/ng1658

149. Shi H, Bencze KZ, Stemmler TL, Philpott CC. A cytosolic iron chaperone that delivers iron to ferritin. *Science (80-)*. 2008;320(5880):1207-1210. doi:10.1126/science.1157643

150. Frey AG, Nandal A, Park JH, et al. Iron chaperones PCBP1 and PCBP2 mediate the metallation of the dinuclear iron enzyme deoxyhypusine hydroxylase. *Proc Natl Acad Sci U S A*. 2014;111(22):8031-8036. doi:10.1073/pnas.1402732111

151. Leidgens S, Bullough KZ, Shi H, et al. Each member of the poly-r(C)-binding protein 1 (PCBP) family exhibits iron chaperone activity toward ferritin. *J Biol Chem*. 2013;288(24):17791-17802. doi:10.1074/jbc.M113.460253

152. Arosio P, Levi S. Ferritin, iron homeostasis, and oxidative damage. *Free Radic Biol Med*. 2002;33(4):457-463. doi:10.1016/S0891-5849(02)00842-0

153. Mancias JD, Wang X, Gygi SP, Harper JW, Kimmelman AC. Quantitative proteomics identifies NCOA4 as the cargo receptor mediating ferritinophagy. *Nature*. 2014;508(7498):105-109. doi:10.1038/nature13148

154. Mancias JD, Vaites LP, Nissim S, et al. Ferritinophagy via NCOA4 is required for erythropoiesis and is regulated by iron dependent HERC2-mediated proteolysis. *Elife*. 2015;4(OCTOBER2015):1-19. doi:10.7554/eLife.10308

155. Yanatori I, Richardson DR, Imada K, Kishi F. Iron export through the transporter ferroportin 1 is modulated by the iron chaperone PCBP2. *J Biol Chem*. 2016;291(33):17303-17318. doi:10.1074/jbc.M116.721936

156. Gammella E, Lomoriello IS, Conte A, et al. Unconventional endocytosis and trafficking of transferrin receptor induced by iron. *Mol Biol Cell*. 2021;32(2):98-108. doi:10.1091/MBC.E20-02-0129

157. Levy JE, Jin O, Fujiwara Y, Kuo F, Andrews NC. Transferrin receptor is necessary for development of erythrocytes and the nervous system. *Nat Genet*. 1999;21(4):396-399. doi:10.1038/7727

158. Oudit GY, Trivieri MG, Khaper N, Liu PP, Backx PH. Role of L-type Ca2+ channels in iron transport and iron-overload cardiomyopathy. *J Mol Med*. 2006;84(5):349-364. doi:10.1007/s00109-005-0029-x

159. Liuzzi JP, Aydemir F, Nam H, Knutson MD, Cousins RJ. *Zip14 (Slc39a14) Mediates Non-Transferrin-Bound Iron Uptake into Cells*.; 2006. Accessed April 30, 2020. www.pnas.orgcgidoi10.1073pnas.0606424103

160. Kristiansen M, Graversen JH, Jacobsen C, et al. Identification of the haemoglobin scavenger receptor. *Nature*. 2001;409(6817):198-201. doi:10.1038/35051594

161. Guetta J, Strauss M, Levy NS, Fahoum L, Levy AP. Haptoglobin genotype modulates the balance of Th1/Th2 cytokines produced by macrophages exposed to free hemoglobin. *Atherosclerosis*. 2007;191(1):48-53. doi:10.1016/j.atherosclerosis.2006.04.032

162. Nicolas G, Chauvet C, Viatte L, et al. The gene encoding the iron regulatory peptide hepcidin is regulated by anemia, hypoxia, and inflammation. *J Clin Invest*. 2002;110(7):1037-1044. doi:10.1172/jci15686

163. Andriopoulos B, Corradini E, Xia Y, et al. BMP6 is a key endogenous regulator of hepcidin expression and iron metabolism. *Nat Genet*. 2009;41(4):482-487. doi:10.1038/ng.335

164. Wrighting DM, Andrews NC. Interleukin-6 induces hepcidin expression through STAT3. *Blood*. 2006;108(9):3204-3209. doi:10.1182/blood-2006-06-027631

165. Wilkinson N, Pantopoulos K. The IRP/IRE system in vivo: Insights from mouse models. *Front Pharmacol*. 2014;5 JUL(July):1-15. doi:10.3389/fphar.2014.00176

166. Muckenthaler MU, Galy B, Hentze MW. Systemic Iron Homeostasis and the Iron-Responsive Element/Iron-Regulatory Protein (IRE/IRP) Regulatory Network. *Annu Rev Nutr*. 2008;28(1):197-213. doi:10.1146/annurev.nutr.28.061807.155521

167. Camaschella C, Campanella A, De Falco L, et al. The human counterpart of zebrafish shiraz shows sideroblastic-like microcytic anemia and iron overload. *Blood*. 2007;110(4):1353-1358. doi:10.1182/blood-2007-02-072520

168. Zhou H, Yang J, Li D, et al. Association of IREB2 and CHRNA3/5 polymorphisms with COPD and COPD-related phenotypes in a Chinese Han population. *J Hum Genet*. 2012;57(11):738-746. doi:10.1038/jhg.2012.104

169. Coon KD, Siegel AM, Yee SJ, et al. Preliminary demonstration of an allelic association of the IREB2 gene with Alzheimer's disease. *J Alzheimer's Dis*. 2006;9(3):225-233. doi:10.3233/JAD-2006-9301

170. Hansen HM, Xiao Y, Rice T, et al. Fine mapping of chromosome 15q25.1 lung cancer susceptibility in African-Americans. *Hum Mol Genet*. 2010;19(18):3652-3661. doi:10.1093/hmg/ddq268

171. Pantopoulos K, Hentze MW. Activation of iron regulatory protein-1 by oxidative stress in vitro. *Proc Natl Acad Sci U S A*. 1998;95(18):10559-10563. doi:10.1073/pnas.95.18.10559

172. Puxeddu E, Comandini A, Cavalli F, et al. Iron laden macrophages in idiopathic pulmonary fibrosis: The telltale of occult alveolar hemorrhage? *Pulm Pharmacol Ther*. 2014;28(1):35-40. doi:10.1016/j.pupt.2013.12.002

173. Maldonado F, Parambil JG, Yi ES, Decker PA, Ryu JH. Haemosiderin-laden macrophages in the bronchoalveolar lavage fluid of patients with diffuse alveolar damage. *Eur Respir J*. 2009;33(6):1361-1366. doi:10.1183/09031936.00119108

174. Ali MK, Kim RY, Brown AC, et al. Critical role for iron accumulation in the pathogenesis of fibrotic lung disease. *J Pathol*. 2020;251(March):49-62. doi:10.1002/path.5401

175. Nicol L, Brittna M, Marwick J, et al. Identification of alveolar macrophage phenotypes predictive of disease progression in idiopathic pulmonary fibrosis. *QJM - An Int J Med*. 2016;0:2016.

176. Brittan M, Barr LC, Anderson N, et al. Functional characterisation of human pulmonary monocyte-like cells in lipopolysaccharide-mediated acute lung inflammation. *J Inflamm (United Kingdom)*. 2014;11(1):1-7. doi:10.1186/1476-9255-11-9

177. Sahoo SK, Crisponi G. Recent advances on iron(III) selective fluorescent probes with possible applications in bioimaging. *Molecules*. 2019;24(18). doi:10.3390/molecules24183267

178. Chen Y-C, Oses-Prieto JA, Pope LE, Burlingame AL, Dixon SJ, Renslo AR. Reactivity-Based Probe of the Iron(II)-Dependent Interactome Identifies New Cellular Modulators of Ferroptosis. *J Am Chem Soc*. Published online 2020. doi:10.1021/jacs.0c06709

179. Aron AT, Loehr MO, Bogena J, Chang CJ. An Endoperoxide Reactivity-Based FRET Probe for Ratiometric Fluorescence Imaging of Labile Iron Pools in Living Cells. *J Am Chem Soc*. 2016;138(43):14338-14346. doi:10.1021/jacs.6b08016

180. Golde DW, Drew WL, Klein HZ, Finley TN, Cline MJ. Occult Pulmonary Haemorrhage in Leukaemia. *Br Med J*. 1975;2(April):166-168.

181. Dixon SJ, Lemberg KM, Lamprecht MR, et al. Ferroptosis: An iron-dependent form of nonapoptotic cell death. *Cell*. 2012;149(5):1060-1072. doi:10.1016/j.cell.2012.03.042

182. Vigil D, Cherfils J, Rossman KL, Der CJ. Ras superfamily GEFs and GAPs: validated and tractable targets for cancer therapy? *Nat Rev Cancer*. 2010;10(12):842-857. doi:10.1038/nrc2960

183. Cao JY, Dixon SJ. Mechanisms of ferroptosis. *Cell Mol Life Sci*. 2016;73(11-12):2195-2209. doi:10.1007/s00018-016-2194-1

184. Li J, Cao F, Yin H, et al. Ferroptosis : past , present and future. *Cell Death Dis*. 2020;11(88). doi:10.1038/s41419-020-2298-2

185. Friedmann Angeli JP, Schneider M, Proneth B, et al. Inactivation of the ferroptosis regulator Gpx4 triggers acute renal failure in mice. *Nat Cell Biol*. 2014;16(12):1180-1191. doi:10.1038/ncb3064

186. Yang WS, Kim KJ, Gaschler MM, Patel M, Shchepinov MS, Stockwell BR. Peroxidation of polyunsaturated fatty acids by lipoxygenases drives ferroptosis. *Proc Natl Acad Sci U S A*. 2016;113(34):E4966-E4975. doi:10.1073/pnas.1603244113

187. Doll S, Conrad M. Iron and ferroptosis: A still ill-defined liaison. *IUBMB Life*. 2017;69(6):423-434. doi:10.1002/iub.1616

188. Abeysinghe RD, Roberts PJ, Cooper CE, Maclean KH, Hider RC, Porter JB. *The Environment of the Lipoxygenase Iron Binding Site Explored with Novel Hydroxypyridinone Iron Chelators**.; 1996. Accessed April 28, 2020. http://www.jbc.org/

189. Doll S, Proneth B, Tyurina YY, et al. ACSL4 dictates ferroptosis sensitivity by shaping cellular lipid composition. *Nat Chem Biol*. 2017;13(1):91-98. doi:10.1038/nchembio.2239

190. Dixon SJ, Lemberg KM, Lamprecht MR, et al. Ferroptosis: An iron-dependent form of nonapoptotic cell death. *Cell*. 2012;149(5):1060-1072. doi:10.1016/j.cell.2012.03.042

191. Wu G, Fang Y-Z, Yang S, Lupton JR, Turner ND. Glutathione Metabolism and Its Implications for Health. *J Nutr*. 2004;134(3):489-492. doi:10.1093/jn/134.3.489

192. Lu SC. Glutathione Synthesis. Published online 2012. doi:10.1016/j.bbagen.2012.09.008

193. Thomas JP, Girotti AW. Photooxidation of cell membranes in the presence of hematoporphyrin derivative: reactivity of phospholipid and cholesterol hydroperoxides with glutathione peroxidase. *Biochim Biophys Acta (BBA)/Lipids Lipid Metab*. 1988;962(3):297-307. doi:10.1016/0005-2760(88)90259-7

194. Dixon SJ. Ferroptosis: bug or feature? *Immunol Rev*. 2017;277(1):150-157. doi:10.1111/imr.12533

195. Gao M, Monian P, Quadri N, Ramasamy R, Jiang X. Glutaminolysis and Transferrin Regulate Ferroptosis. *Mol Cell*. 2015;59(2):298-308. doi:10.1016/j.molcel.2015.06.011

196. Yang WS, Stockwell BR. Synthetic Lethal Screening Identifies Compounds Activating Iron-Dependent, Nonapoptotic Cell Death in Oncogenic-RAS-Harboring Cancer Cells. *Chem Biol*. 2008;15(3):234-245. doi:10.1016/j.chembiol.2008.02.010

197. DeBerardinis RJ, Lum JJ, Hatzivassiliou G, Thompson CB. The Biology of Cancer: Metabolic Reprogramming Fuels Cell Growth and Proliferation. *Cell Metab*. 2008;7(1):11-20.

doi:10.1016/j.cmet.2007.10.002

198. Hu W, Zhang C, Wu R, Sun Y, Levine A, Feng Z. Glutaminase 2, a novel p53 target gene regulating energy metabolism and antioxidant function. *Proc Natl Acad Sci U S A*. 2010;107(16):7455-7460. doi:10.1073/pnas.1001006107

199. Wang H, Liu C, Zhao Y, Gao G. Mitochondria regulation in ferroptosis. *Eur J Cell Biol*. 2020;99(1):151058. doi:10.1016/j.ejcb.2019.151058

200. Kagan valerian, Mao G, Qu F, et al. Oxidized arachidonic and adrenic pes navigate cells to ferroptosis. *Nat Chem Biol* |. 2017;13. doi:10.1038/nCHeMBIO.2238

201. Shibata Y, Id HY, Higashikawa K, Miyamoto N, Kuge Y. Erastin, a ferroptosis-inducing agent, sensitized cancer cells to X-ray irradiation via glutathione starvation in vitro and in vivo. *PLoS One*. Published online 2019. doi:10.1371/journal.pone.0225931

202. Yu X, Long YC. Crosstalk between cystine and glutathione is critical for the regulation of amino acid signaling pathways and ferroptosis OPEN. *Nat Publ Gr*. Published online 2016. doi:10.1038/srep30033

203. Yang WS, Sriramaratnam R, Welsch ME, et al. Regulation of ferroptotic cancer cell death by GPX4. *Cell*. 2014;156(1-2):317-331. doi:10.1016/J.CELL.2013.12.010/ATTACHMENT/B36F8D87-D7D3-4A20-B351-3EF61F734BC3/MMC6.XLSX

204. Shah R, Shchepinov MS, Pratt DA. Resolving the Role of Lipoxygenases in the Initiation and Execution of Ferroptosis. *ACS Cent Sci*. 2018;4(3):387-396. doi:10.1021/acscentsci.7b00589

205. Wenzel SE, Tyurina YY, Zhao J, et al. PEBP1 Wardens Ferroptosis by Enabling Lipoxygenase Generation of Lipid Death Signals. *Cell*. 2017;171(3):628-641.e26. doi:10.1016/j.cell.2017.09.044

206. Feng H, Schorpp K, Jin J, et al. Transferrin Receptor Is a Specific Ferroptosis Marker. *Cell Rep*. 2020;30(10):3411-3423.e7. doi:10.1016/j.celrep.2020.02.049

207. Hou W, Xie Y, Song X, et al. Autophagy promotes ferroptosis by degradation of ferritin. *Autophagy*. 2016;12(8):1425-1428. doi:10.1080/15548627.2016.1187366

208. Gao H, Bai Y, Jia Y, et al. Ferroptosis is a lysosomal cell death process. *Biochem Biophys Res Commun*. 2018;503(3):1550-1556. doi:10.1016/j.bbrc.2018.07.078

209. Brown CW, Amante JJ, Chhoy P, et al. Prominin2 Drives Ferroptosis Resistance by Stimulating Iron Export. *Dev Cell*. 2019;51(5):575-586.e4. doi:10.1016/j.devcel.2019.10.007

210. Chen GQ, Benthani FA, Wu J, Liang D, Bian ZX, Jiang X. Artemisinin compounds sensitize cancer cells to ferroptosis by regulating iron

homeostasis. *Cell Death Differ*. 2020;27(1):242-254. doi:10.1038/s41418-019-0352-3

211. Wortmann M, Schneider M, Pircher J, et al. Combined deficiency in glutathione peroxidase 4 and vitamin e causes multiorgan thrombus formation and early death in mice. *Circ Res*. 2013;113(4):408-417. doi:10.1161/CIRCRESAHA.113.279984

212. Matsushita M, Freigang S, Schneider C, Conrad M, Bornkamm GW, Kopf M. T cell lipid peroxidation induces ferroptosis and prevents immunity to infection. *J Exp Med*. 2015;212(4):555-568. doi:10.1084/JEM.20140857

213. Zilka O, Shah R, Li B, et al. On the Mechanism of Cytoprotection by Ferrostatin-1 and Liproxstatin-1 and the Role of Lipid Peroxidation in Ferroptotic Cell Death. Published online 2017. doi:10.1021/acscentsci.7b00028

214. Krainz T, Gaschler MM, Lim C, Sacher JR, Stockwell BR, Wipf P. A Mitochondrial-Targeted Nitroxide Is a Potent Inhibitor of Ferroptosis. Published online 2016. doi:10.1021/acscentsci.6b00199

215. Haidasz EA, Meng D, Amorati R, et al. Acid Is Key to the Radical-Trapping Antioxidant Activity of Nitroxides. Published online 2016. doi:10.1021/jacs.6b00677

216. Xu Y, Li X, Cheng Y, Yang M, Wang R. Inhibition of ACSL4 attenuates ferroptotic damage after pulmonary ischemia-reperfusion. *FASEB J*. 2020;34(12):16262-16275. doi:10.1096/FJ.202001758R

217. Chen J, Yang L, Geng L, et al. Inhibition of Acyl-CoA Synthetase Long-Chain Family Member 4 Facilitates Neurological Recovery After Stroke by Regulation Ferroptosis. *Front Cell Neurosci*. 2021;15:93. doi:10.3389/FNCEL.2021.632354/BIBTEX

218. Yao X, Zhang Y, Hao J, et al. Deferoxamine promotes recovery of traumatic spinal cord injury by inhibiting ferroptosis. *Neural Regen Res*. 2019;14(3):532-541. doi:10.4103/1673-5374.245480

219. Chen X, Comish PB, Tang D, Kang R. Characteristics and Biomarkers of Ferroptosis. *Front Cell Dev Biol*. 2021;9(January):1-9. doi:10.3389/fcell.2021.637162

220. Sui X, Zhang R, Liu S, Duan T, Zhai L. RSL3 Drives Ferroptosis Through GPX4 Inactivation and ROS Production in Colorectal Cancer. *Front Pharmacol*. 2018;9(November):1-8. doi:10.3389/fphar.2018.01371

221. Li X, Duan L, Yuan S, Zhuang X, Qiao T, He J. Ferroptosis inhibitor alleviates Radiation-induced lung fibrosis (RILF) via down-regulation of TGF-β1. *J Inflamm (United Kingdom)*. 2019;16(1):1-10. doi:10.1186/s12950-019-0216-0

222. Bocchino M, Agnese S, Fagone E, et al. Reactive oxygen species are

required for maintenance and differentiation of primary lung fibroblasts in idiopathic pulmonary fibrosis. *PLoS One*. 2010;5(11). doi:10.1371/journal.pone.0014003

223. Spangler B, Morgan CW, Fontaine SD, et al. A reactivity-based probe of the intracellular labile ferrous iron pool. *Nat Chem Biol*. 2016;12(9):680-685. doi:10.1038/nchembio.2116

224. Wilschefski SC, Baxter MR. Inductively Coupled Plasma Mass Spectrometry: Introduction to Analytical Aspects. *Clin Biochem Rev*. 2019;40(3):115. doi:10.33176/AACB-19-00024

225. Alber A, Howie SEM, Wallace WAH, Hirani N. The role of macrophages in healing the wounded lung. *Int J Exp Pathol*. 2012;93(4):243. doi:10.1111/J.1365-2613.2012.00833.X

226. Borthwick LA, Barron L, Hart KM, et al. Macrophages are critical to the maintenance of IL-13-dependent lung inflammation and fibrosis. *Mucosal Immunol 2016 91*. 2015;9(1):38-55. doi:10.1038/mi.2015.34

227. Mosser DM, Edwards JP. Exploring the full spectrum of macrophage activation. *Nat Rev Immunol*. 2008;8(12):958-969. doi:10.1038/nri2448

228. Martinez FO, Helming L, Gordon S. Alternative Activation of Macrophages: An Immunologic Functional Perspective. *http://dx.doi.org/101146/annurev.immunol021908132532*. 2009;27:451-483. doi:10.1146/ANNUREV.IMMUNOL.021908.132532

229. Desch AN, Gibbings SL, Goyal R, et al. Flow Cytometric Analysis of Mononuclear Phagocytes in Nondiseased Human Lung and Lung-Draining Lymph Nodes. *Am J Respir Crit Care Med*. 2016;193:614-626. doi:10.1164/rccm.201507-1376OC

230. Nouno T, Okamoto M, Ohnishi K, et al. Elevation of pulmonary CD163 + and CD204 + macrophages is associated with the clinical course of idiopathic pulmonary fibrosis patients. *J Thorac Dis*. 2019;11(9):4005-4017. doi:10.21037/jtd.2019.09.03

231. Garnier M, Gibelin A, Mailleux AA, et al. Macrophage Polarization Favors Epithelial Repair During Acute Respiratory Distress Syndrome. *Crit Care Med*. 2018;46(7):e692-e701. doi:10.1097/CCM.0000000000003150

232. Arora S, Dev K, Agarwal B, Das P, Syed A. Macrophages: Their role, activation and polarization in pulmonary diseases. Published online 2017. doi:10.1016/j.imbio.2017.11.001

233. Cairo G, Recalcati S, Mantovani A, Locati M. Iron trafficking and metabolism in macrophages: Contribution to the polarized phenotype. *Trends Immunol*. 2011;32(6):241-247. doi:10.1016/j.it.2011.03.007

234. Thompson AB, Bohling T, Heires A, Linder J, Rennard SI. Lower respiratory tract iron burden is increased in association with cigarette

smoking. *J Lab Clin Med*. 1991;117(6). doi:10.1016/0011-5029(84)90008-7

235. McGowan SE, Henley SA. Iron and ferritin contents and distribution in human alveolar macrophages. *J Lab Clin Med*. 1988;136(6):449-456. doi:10.1067/mlc.2000.110905

236. Zhang V, Nemeth E, Kim A. Lung iron overload does not exacerbate the fibrotic response to bleomycin in a mouse model of pulmonary fibrosis. *Am J Respir Cell Mol Biol*. 2020;63(5):713-716. doi:10.1165/RCMB.2020-0192LE

237. Waheed A, Grubb JH, Zhou XY, et al. Regulation of transferrin-mediated iron uptake by HFE, the protein defective in hereditary hemochromatosis. *Proc Natl Acad Sci U S A*. 2002;99(5):3117-3122. doi:10.1073/pnas.042701499

238. Gao J, Chen J, Kramer M, Tsukamoto H, Zhang AS, Enns CA. Interaction of the Hereditary Hemochromatosis Protein HFE with Transferrin Receptor 2 Is Required for Transferrin-Induced Hepcidin Expression. *Cell Metab*. 2009;9(3):217-227. doi:10.1016/j.cmet.2009.01.010

239. Pietrangelo A. Iron and the liver. *Liver Int*. 2016;36:116-123. doi:10.1111/LIV.13020

240. Loréal O, Deugnier Y, Moirand R, et al. Liver fibrosis in genetic hemochromatosis: Respective roles of iron and non-iron-related factors in 127 homozygous patients. *J Hepatol*. 1992;16(1):122-127. doi:10.1016/S0168-8278(05)80104-7

241. Mir MA. *Concept of Reverse Costimulation and Its Role in Diseases*.; 2015. doi:10.1016/b978-0-12-802585-7.00002-9

242. Nielsen MC, Hvidbjerg Gantzel R, Clària J, Trebicka J, Møller J, Grønbaek H. Macrophage Activation Markers, CD163 and CD206, in Acute-on-Chronic Liver Failure. *Cells*. 2020;9(1175). doi:10.3390/cells9051175

243. Ji WJ, Ma YQ, Zhou X, et al. Temporal and spatial characterization of mononuclear phagocytes in circulating, lung alveolar and interstitial compartments in a mouse model of bleomycin-induced pulmonary injury. *J Immunol Methods*. 2014;403(1-2):7-16. doi:10.1016/J.JIM.2013.11.012

244. Smith DR, Kunkel SL, Standiford TJ, et al. Increased interleukin-1 receptor antagonist in idiopathic pulmonary fibrosis. A compartmental analysis. *https://doi.org/101164/ajrccm15167767546*. 2012;151(6):1965-1973. doi:10.1164/AJRCCM.151.6.7767546

245. Pourcelot E, Lénon M, Mobilia N, et al. Iron for proliferation of cell lines and hematopoietic progenitors: Nailing down the intracellular functional iron concentration. *Biochim Biophys Acta - Mol Cell Res*.

2015;1853(7):1596-1605. doi:10.1016/J.BBAMCR.2015.03.009

246. Zhou L, Zhao B, Zhang L, et al. Alterations in Cellular Iron Metabolism Provide More Therapeutic Opportunities for Cancer. *Int J Mol Sci*. 2018;19(5). doi:10.3390/IJMS19051545

247. Ponka P. Iron and cell proliferation: another piece of the puzzle. *Blood*. 2004;104(9):2620-2621. doi:10.1182/BLOOD-2004-08-3212

248. Le NTV, Richardson DR. The role of iron in cell cycle progression and the proliferation of neoplastic cells. *Biochim Biophys Acta - Rev Cancer*. 2002;1603(1):31-46. doi:10.1016/S0304-419X(02)00068-9

249. Motamedi M, Xu L, Elahi S. Correlation of transferrin receptor (CD71) with Ki67 expression on stimulated human and mouse T cells: The kinetics of expression of T cell activation markers. *J Immunol Methods*. 2016;437:43-52. doi:10.1016/J.JIM.2016.08.002

250. Wei YY, Zhang XZ, Zhang F, et al. Expression of CD71 on cell proliferation in hematologic malignancy and its correlation with Ki-67. *Zhongguo Shi Yan Xue Ye Xue Za Zhi*. 2015;23(1):234-240. doi:10.7534/J.ISSN.1009-2137.2015.01.044

251. Ikeda Y, Ozono I, Tajima S, et al. Iron Chelation by Deferoxamine Prevents Renal Interstitial Fibrosis in Mice with Unilateral Ureteral Obstruction. *PLoS One*. 2014;9(2):e89355. doi:10.1371/JOURNAL.PONE.0089355

252. Montani D, Price LC, Dorfmuller P, et al. Pulmonary veno-occlusive disease. *Eur Respir J*. 2009;33. doi:10.1183/09031936.00090608

253. Latunde-Dada GO. Ferroptosis: Role of lipid peroxidation, iron and ferritinophagy. *Biochim Biophys Acta - Gen Subj*. 2017;1861(8):1893-1900. doi:10.1016/j.bbagen.2017.05.019

254. Cottin V, Hirani NA, Hotchkin DL, et al. Presentation, diagnosis and clinical course of the spectrum of progressive-fibrosing interstitial lung diseases REVIEW PROGRESSIVE-FIBROSING ILD. *Eur Respir J*. 2018;27. doi:10.1183/16000617.0076-2018

255. Marudamuthu AS, Shetty SK, Bhandary YP, et al. Plasminogen activator inhibitor-1 suppresses profibrotic responses in fibroblasts from fibrotic lungs. *J Biol Chem*. 2015;290(15):9428-9441. doi:10.1074/JBC.M114.601815

256. Senoo T, Hattori N, Tanimoto T, et al. Suppression of plasminogen activator inhibitor-1 by RNA interference attenuates pulmonary fibrosis. *Thorax*. 2010;65(4):334-340. doi:10.1136/THX.2009.119974

257. Ballester B, Milara J, Cortijo J. Mucins as a New Frontier in Pulmonary Fibrosis. *Clin Med (Northfield Il)*. 2019;8(1447). doi:10.3390/jcm8091447

258. Haschka D, Petzer V, Kocher F, et al. Classical and intermediate

monocytes scavenge non-transferrin-bound iron and damaged erythrocytes. *JCI Insight*. 2019;4(8). doi:10.1172/jci.insight.98867

259. Tzouvelekis A, Harokopos V, Paparountas T, et al. Comparative expression profiling in pulmonary fibrosis suggests a role of hypoxia-inducible factor-1?? in disease pathogenesis. *Am J Respir Crit Care Med*. 2007;176(11):1108-1119. doi:10.1164/rccm.200705-683OC

260. Mcmillan DH, Anathy V, Janssen-Heininger YMW. Attenuation of lung fibrosis in mice with a clinically relevant inhibitor of glutathione-S-transferase π. doi:10.1172/jci.insight.85717

261. He N, Bai S, Huang Y, et al. Evaluation of Glutathione S-Transferase Inhibition Effects on Idiopathic Pulmonary Fibrosis Therapy with a Near-Infrared Fluorescent Probe in Cell and Mice Models. *Anal Chem*. 2019;91(8):5424-5432. doi:10.1021/acs.analchem.9b00713

262. Sisson TH, Hanson KE, Subbotina N, Patwardhan A, Hattori N, Simon RH. Inducible lung-specific urokinase expression reduces fibrosis and mortality after lung injury in mice. *Am J Physiol Lung Cell Mol Physiol*. 2002;283(5). doi:10.1152/AJPLUNG.00049.2002

263. Hattori N, Mizuno S, Yoshida Y, et al. The Plasminogen Activation System Reduces Fibrosis in the Lung by a Hepatocyte Growth Factor-Dependent Mechanism. *Am J Pathol*. 2004;164(3):1091-1098. doi:10.1016/S0002-9440(10)63196-3

264. Hoffmann-Vold A-M, Weigt SS, Saggar R, et al. Endotype-phenotyping may predict a treatment response in progressive fibrosing interstitial lung disease. *EBioMedicine*. 2019;50:379-386. doi:10.1016/j.ebiom.2019.10.050

265. Christmann RB, Sampaio-Barros P, Stifano G, et al. Association of Interferon-and Transforming Growth Factor-Regulated Genes and Macrophage Activation With Systemic Sclerosis-Related Progressive Lung Fibrosis. *ARTHRITIS Rheumatol*. 2014;66(3):714-725. doi:10.1002/art.38288

266. Orsmark-Pietras C, James A, Konradsen JR, et al. Transcriptome analysis reveals upregulation of bitter taste receptors in severe asthmatics. *Eur Respir J*. 2013;42(1):65-78. doi:10.1183/09031936.00077712

267. Nayak AP, Shah SD, Michael J V., Deshpande DA. Bitter taste receptors for asthma therapeutics. *Front Physiol*. 2019;10(JUL):884. doi:10.3389/FPHYS.2019.00884/BIBTEX

268. Dixon SJ, Stockwell BR. The Hallmarks of Ferroptosis. *Annu Rev Cancer Biol*. 2018;3(1):35-54. doi:10.1146/annurev-cancerbio-030518-055844

269. Anker K, Erik P, Max I, Schulz A. Monitoring reactive oxygen species formation and localisation in living cells by use of the fluorescent probe

CM-H 2 DCFDA and confocal laser microscopy. Published online 2009:369-383. doi:10.1111/j.1399-3054.2009.01243.x

270. Dinh HQ, Eggert T, Meyer MA, et al. Coexpression of CD71 and CD117 Identifies an Early Unipotent Neutrophil Progenitor Population in Human Bone Marrow. *Immunity*. 2020;53(2):319-334.e6. doi:10.1016/J.IMMUNI.2020.07.017

271. El-Menshawy N, Abd-Aziz SM, Ebrahim MA, El-Malky N. Impact of cellular CD71 (transferrin receptor 1) expression in Egyptian acute leukemia: correlation with clinicopathologic features. *Comp Clin Path*. 2016;25. doi:10.1007/s00580-015-2213-x

272. Kapralov AA, Yang Q, Dar HH, et al. Redox lipid reprogramming commands susceptibility of macrophages and microglia to ferroptotic death. *Nat Chem Biol*. 2020;16:278-290. doi:10.1038/s41589-019-0462-8

273. Yao F, Cui X, Zhang Y, et al. Iron regulatory protein 1 promotes ferroptosis by sustaining cellular iron homeostasis in melanoma. *Oncol Lett*. 2021;22(3):1-12. doi:10.3892/OL.2021.12918/HTML

274. Wang H, An P, Xie E, et al. Characterization of ferroptosis in murine models of hemochromatosis. *Hepatology*. 2017;66(2):449-465. doi:10.1002/HEP.29117/SUPPINFO

275. Seiler A, Schneider M, Fö H, et al. Glutathione Peroxidase 4 Senses and Translates Oxidative Stress into 12/15-Lipoxygenase Dependent-and AIF-Mediated Cell Death. *Cell Metab*. 2008;8:237-248. doi:10.1016/j.cmet.2008.07.005

276. Canli O, Alankus YB, Grootjans S, et al. Glutathione peroxidase 4 prevents necroptosis in mouse erythroid precursors¨Ozge. Published online 2016. doi:10.1182/blood-2015-06

277. Kang R, Zeng L, Zhu S, et al. Lipid Peroxidation Drives Gasdermin D-Mediated Pyroptosis in Lethal Polymicrobial Sepsis. *Cell Host Microbe*. 2018;24:97-108. doi:10.1016/j.chom.2018.05.009

278. Li S, Zhou Y, Huang Q, et al. Iron overload in endometriosis peritoneal fluid induces early embryo ferroptosis mediated by HMOX1. *Cell Death Discov*. 2021;7(355). doi:10.1038/s41420-021-00751-2

279. Weigert A, Von Knethen A, Fuhrmann D, Dehne N, Brüne B. Redox-signals and macrophage biology. *Mol Aspects Med*. 2018;63. doi:10.1016/j.mam.2018.01.003

280. Huang J, Canadien V, Lam GY, et al. Activation of antibacterial autophagy by NADPH oxidases. *PNAS*. 2009;106(15). www.pnas.org/cgi/content/full/

281. Piattini F, Matsushita M, Muri J, et al. Differential sensitivity of inflammatory macrophages and alternatively activated macrophages to

ferroptosis. *Eur J Immunol*. 2021;51(10):2417-2429. doi:10.1002/eji.202049114

282. Virág L, Jaén RI, Regdon Z, Boscá L, Prieto P. Self-defense of macrophages against oxidative injury: Fighting for their own survival. *Redox Biol*. Published online 2019. doi:10.1016/j.redox.2019.101261

283. Gammella E, Recalcati S, Cairo G. Dual Role of ROS as Signal and Stress Agents: Iron Tips the Balance in favor of Toxic Effects. *Oxid Med Cell Longev*. 2016;2016. doi:10.1155/2016/8629024

284. Orozco LD, Kapturczak MH, Barajas B, et al. Heme Oxygenase-1 Expression in Macrophages Plays a Beneficial Role in Atherosclerosis. Published online 2007. doi:10.1161/CIRCRESAHA.107.151720

285. Masaldan S, Clatworthy SAS, Gamell C, et al. Iron accumulation in senescent cells is coupled with impaired ferritinophagy and inhibition of ferroptosis. *Redox Biol*. 2018;14(August 2017):100-115. doi:10.1016/j.redox.2017.08.015

286. Zhang Y, Choksi S, Chen K, Pobezinskaya Y, Linnoila I, Liu Z-G. ROS play a critical role in the differentiation of alternatively activated macrophages and the occurrence of tumor-associated macrophages. *Nat Publ Gr*. 2013;23(7):898-914. doi:10.1038/cr.2013.75

287. Balce DR, Li B, Allan ERO, Rybicka JM, Krohn RM, Yates RM. Alternative activation of macrophages by IL-4 enhances the proteolytic capacity of their phagosomes through synergistic mechanisms. Published online 2011. doi:10.1182/blood-2011-01-328906

288. Kuchler L, Giegerich AK, Sha LK, et al. SYNCRIP-Dependent Nox2 mRNA Destabilization Impairs ROS Formation in M2-Polarized Macrophages. doi:10.1089/ars.2013.5760

289. Padgett LE, Burg AR, Lei W, Tse HM. Loss of NADPH Oxidase-Derived Superoxide Skews Macrophage Phenotypes to Delay Type 1 Diabetes. *Diabetes*. 2015;64. doi:10.2337/db14-0929

290. Fiers W, Beyaert R, Declercq W, Vandenabeele P. More than one way to die: apoptosis, necrosis and reactive oxygen damage. *Nature*. Published online 2000.

291. Morgan MJ, Morgan MJ, Kim Y, Liu Z. TNF α and reactive oxygen species in necrotic cell death. Published online 2008:343-349. doi:10.1038/cr.2008.31

292. Caserta TM, Smith AN, Gultice AD, Reedy MA, Brown TL. Q-VD-OPh , a broad spectrum caspase inhibitor with potent antiapoptotic properties. 2003;8(4):345-352.

293. Degterev A, Huang Z, Boyce M, et al. Chemical inhibitor of nonapoptotic cell death with therapeutic potential for ischemic brain injury. 2005;1(2). doi:10.1038/nchembio711

294. Oliveira SR, Dion PA, Gaspar MM, et al. Discovery of a Necroptosis Inhibitor Improving Dopaminergic Neuronal Loss after MPTP Exposure in Mice. Published online 2021.

295. Fleury C, Mignotte B, Vayssière J. Mitochondrial reactive oxygen species in cell death signaling. 2002;84:131-141.

296. Jelinek A, Heyder L, Daude M, Plessner M, Krippner S. Free Radical Biology and Medicine Mitochondrial rescue prevents glutathione peroxidase-dependent ferroptosis. *Free Radic Biol Med*. 2018;117(December 2017):45-57. doi:10.1016/j.freeradbiomed.2018.01.019

297. Yang WS, Kim KJ, Gaschler MM, Patel M, Shchepinov MS, Stockwell BR. Peroxidation of polyunsaturated fatty acids by lipoxygenases drives ferroptosis. *Proc Natl Acad Sci U S A*. 2016;113(34):E4966-E4975. doi:10.1073/pnas.1603244113

298. Yang WS, Sriramaratnam R, Welsch ME, et al. Regulation of ferroptotic cancer cell death by GPX4. *Cell*. 2014;156(1-2):317-331. doi:10.1016/j.cell.2013.12.010

299. Ma Y, Abbate V, Hider RC. Iron-sensitive fluorescent probes: monitoring intracellular iron pools. *Metallomics*. 2015;7(2):212-222. doi:10.1039/C4MT00214H

300. Wu J, Minikes A, Gao M, et al. Intercellular interaction dictates cancer cell ferroptosis via NF2–YAP signalling. *Nature*. Published online 2019. doi:10.1038/s41586-019-1426-6

301. A.D.T.G. Wagener F, Scharstuhl A, M. Tyrrell R, et al. The Heme-Heme Oxygenase System in Wound Healing; Implications for Scar Formation. *Curr Drug Targets*. 2012;11(12):1571-1585. doi:10.2174/1389450111009011571

302. Chen Y, Gao S, Yan Y, Qian J, Chen H. Aerosolized deferoxamine administration in mouse model of bronchopulmonary dysplasia improve pulmonary development. *Am J Transl Res*. 2018;10(1):325-332.

303. Goodwin J, Choi H, Hsieh MH, et al. Targeting Hypoxia-Inducible Factor-1α/Pyruvate Dehydrogenase Kinase 1 Axis by Dichloroacetate Suppresses Bleomycin-induced Pulmonary Fibrosis. *Am J Respir Cell Mol Biol*. 2018;58(2):216-231. doi:10.1165/RCMB.2016-0186OC

304. Zhu Y, Chang J, Tan K, et al. Clioquinol Attenuates Pulmonary Fibrosis through Inactivation of Fibroblasts via Iron Chelation. *Cell Mol Biol*. 2021;65(2):189-200. doi:10.1165/rcmb

305. Pantopoulous K. Function of the hemochromatosis protein HFE: Lessons from animal models. *World J Gastroenterol*. 2008;7(14). doi:10.3748/wjg.14.6893

306. Cantin AM, North SL, Fells GA, Hubbard RC, Crystal RG. Oxidant-

mediated epithelial cell injury in idiopathic pulmonary fibrosis. Oxidant-mediated Epithelial Cell Injury in Idiopathic Pulmonary Fibrosis. *J Clin Invest*. 1987;79(6):1665-1673. doi:10.1172/JCI113005

307. Salazar-Montes A, Ruiz-Corro L, López-Reyes A, Castrejón-Gómez E, Armendáriz-Borunda J. Potent antioxidant role of Pirfenidone in experimental cirrhosis. *Eur J Pharmacol*. 2008;595(1-3):69-77. doi:10.1016/J.EJPHAR.2008.06.110

308. Azuma A, Nukiwa T, Tsuboi E, et al. Double-blind, placebo-controlled trial of pirfenidone in patients with idiopathic pulmonary fibrosis. *Am J Respir Crit Care Med*. 2005;171(9):1040-1047. doi:10.1164/RCCM.200404-571OC

309. Canavesi E, Alfieri C, Pelusi S, Valenti L. Hepcidin and HFE protein: Iron metabolism as a target for the anemia of chronic kidney disease? *World J Nephrol*. 2012;1(6):166-176. doi:10.5527/wjn.v1.i6.166

310. Beeh KM, Beier J, Haas IC, Kornmann O, Micke P, Buhl R. Glutathione deficiency of the lower respiratory tract in patients with idiopathic pulmonary fibrosis. *Eur Respir J2*. 2002;19:1119-1123. doi:10.1183/09031936.02.00262402

311. Zargarian S, Shlomovitz I, Erlich Z, et al. Phosphatidylserine externalization, “necroptotic bodies” release, and phagocytosis during necroptosis. *PLOS Biol*. 2017;15(6):e2002711. doi:10.1371/JOURNAL.PBIO.2002711

312. Shlomovitz I, Speir M, Gerlic M. Flipping the dogma-phosphatidylserine in non-apoptotic cell death. *Cell Commun Signal*. 2019;17(139). doi:10.1186/s12964-019-0437-0

313. Piattini F, Matsushita M, Muri J, et al. Differential sensitivity of inflammatory macrophages and alternatively activated macrophages to ferroptosis. *Eur J Immunol*. 2021;51(10):2417-2429. doi:10.1002/EJI.202049114

314. Yang WH, Ding CKC, Sun T, et al. The Hippo Pathway Effector TAZ Regulates Ferroptosis in Renal Cell Carcinoma. *Cell Rep*. 2019;28(10):2501-2508.e4. doi:10.1016/j.celrep.2019.07.107